VNIVERSITAT DE VALÈNCIA

Phenomenology of Non-Standard Neutrino Interactions

Francisco Javier Escrihuela Ferrándiz

Departament de Física Teòrica

Tesi Doctoral

Director: **Prof. José Wagner Furtado Valle**
Co-Director: **Prof. Omar Gustavo Miranda Romagnoli**
Co-Directora: **Dra. María Amparo Tórtola Baixauli**

2016

Certificat

Prof. José W. Furtado Valle, professor d'investigació del IFIC, centre mixt del CSIC i de la Universitat de València,
Dra. María Amparo Tórtola Baixauli, investigadora Ramón y Cajal de la Universitat de València,
Prof. Omar Gustavo Miranda Romagnoli, professor d'investigació del CINVESTAV de Mèxic D.F.,

CERTIFIQUEN:

Que la present memòria, "Phenomenology of Non-Standard Neutrino Interaccions", ha estat realitzada sota la seva direcció al Departament de Física Teòrica de la Universitat de València per Francisco Javier Escrihuela Ferrándiz, i que constitueix la seva tesi doctoral per optar al grau de Doctor en Física.

Perquè així conste, en compliment de la legislació vigent, presenten al Departament de Física Teòrica de la Universitat de València la referida Tesi doctoral, i signen el present certificat.

Prof. José W. Furtado Valle

Dra. María Amparo Tórtola Baixauli

Prof. Omar Gustavo Miranda Romagnoli

Agraïments

M'agradaria expressar la més sincera gratitud a tots aquells que han fet possible la realització d'aquesta tesi.

En primer lloc a la meva família científica composada principalment pels meus directors de tesi: José W. Furtado Valle, María Amparo Tórtola Baixauli i Omar G. Miranda Romagnoli, vosaltres sabeu ben bé que aquest treball no haguera eixit mai endavant sense vosaltres, i es "quasi" més vostre que meu. Gràcies José per haver-me donat la oportunitat de treballar amb tu en les condicions tan especials que m'envoltaven; sempre m'he sentit recolzat i m'has animat a seguir endavant. Gràcies Mariam perquè sempre has estat ahí, disposada a ajudar-me amb paciència i dedicació, sempre atenta a les meves necessitats. Gràcies Omar pel teu tracte personal; m'has fet sentir com part de la família i has sigut peça fonamental en la consecució d'aquesta tesi, bé que ho saps. De tots tres m'emporte una nova forma de vore la Física i una estima incondicional pels neutrins.

Dins d'aquesta família científica estan també tots els membres del AHEP, encapçalats per Martin i Sergio; sempre m'heu fet sentir com a casa. Voldria agrair també l'hospitalitat que sempre m'ha brindat el CINVESTAV de Mèxic D.F, en especial a Àlex, Félix, Estela, Ricardo i Blanca; i a la meva família mexicana, Luz, Gustavo i Lupita. Entre tots m'heu fet els estius mexicans molt càlids i interessants.

Deixant a banda la Física m'agradaria agrair, per descomptat, a la meva família. Als meus pares Paco i Maria, per donar-me una gran educació, suport incondicional i amor durant tots els dies de la meva vida. Sempre esteu ahí. Als meus germans Mariam i Víctor, perquè no seria el que sóc si no els haguera tingut sempre al meu costat. Moltes gràcies als meus cunyats David i Ana, i als meus nebodets David i Lucía, per donar-li calor i alegria a la meva vida.

Vull mostrar també el meu agraïment als meus amics, perquè amb el vostre... "¡a ver cuándo acabas!" o "tómate unas birras para despejarte", m'heu donat forces per seguir endavant. Gràcies a Pablo, Pepe B., José Alberto, Francis, Josemi, Jose, Ricard, Antonio, Galera, Olaya, Pepe Ll., Joan, Gabi, Juan, Álex, Jorge, Jaumet, Abuelo... Espere no

deixar-me ningun... Gràcies també als companys de treball, que quan m'han vist aclaparat m'han fet la vida més fàcil: Carles, J. Antonio, Maria, Marisa, Ródenas, H.Ana...

I l'últim però, això sí, el més especial agraïment és per a la meva dona Ana. La teva paciència amb mi no té límits. Sempre tens una paraula d'alè i un somriure a la cara. La vida sense tu no tindria sentit.

Gràcies a tots! Aquesta tesi és un poc de tots vosaltres.

I want to thank Conacyt (Mexico) because part of this work has been supported by Conacyt grant 166639.

Preface

Today neutrino physics is in a privileged position within the fascinating field of particle physics. From the discovery of neutrino oscillations by Super-Kamiokande [1] in 1998, the door to physics beyond the Standard Model (SM in what follows) has been opened. This fact implies that neutrinos have to be massive [2] in opposition to the Standard Model assumption. However, this is not a surprise completely, but it was already hinted from theoretical and experimental observations in the two decades prior to the discovery of the oscillatory phenomenon:

- In principle, it is not necessary to introduce neutrino masses in the Standard Model. Nevertheless, this is not a characteristic arising from a gauge symmetry (as in the photon case) but it is chosen for simplicity, avoiding, for instance, to introduce the right-handed neutrino.

- Most of the unification models incorporate neutrino masses.

- The experimentally observed deficit of the atmospheric and solar neutrino fluxes could be explained by the phenomenon of neutrino oscillations, mechanism that requires neutrino mass and mixing.

As a consequence of this new path opened by neutrinos, one may observe processes forbidden in the Standard Model [3]:

- Neutrino oscillations imply neutrino mixing; therefore the generational lepton numbers are not valid as a global symmetry. Decays with lepton flavor violation (LFV) are possible, as for example:

  - $\mu \to e\,\gamma$,
  - $\tau \to e\,\gamma$,
  - $\mu \to 3e$.

- If neutrinos are Majorana particles,neutrinoless double beta decay ($0\nu\beta\beta$) and other processes with lepton number violation could occur. Until such historic observation is made, the debate about the nature of neutrinos as Dirac or Majorana particles will be open.

- Cosmology is sensitive to massive neutrinos, which may affect the cosmic microwave background and other cosmological observables.

- The neutrino, as a massive particle, could decay:

  - $\nu_\alpha \to \nu_{\alpha'}\,\gamma$,
  - $\nu_\alpha \to \nu_{\alpha'}\,\nu_{\alpha''}\nu_{\alpha'''}$, where three neutrinos are produced in the final state. These could be the same kind of neutrino or not.
  - $\nu_\alpha \to \nu_{\alpha'}\,J$, where J is a majoron [1].

As we have already mentioned, none of the phenomena described in the above paragraphs is foreseen in the SM. Therefore models beyond SM are required to introduce neutrino mass and they may imply new interactions with matter: Non-Standard Interactions (NSI in what follows). In this thesis we study some of these new interactions from a phenomenological point of view. To achieve it, we will use data from several neutrino experiments, obtaining extra information on NSI stemming from a combined analysis of them. For this purpose the thesis is organized as follows:

- **Chapter 1**: We begin with a review of the most important characteristics of neutrinos in the Standard Model. Along with them, we will also present other properties of beyond the SM neutrinos, such as neutrino mass and neutrino oscillations.

- **Chapter 2**: In this chapter we will give an introduction to NSI, explaining their appearance and main features. Along with this generic explanation, we will discuss models where NSI appear spontaneously and their influence on neutrino oscillation probabilities and experiments.

- **Chapter 3**: The main goal of this chapter is to show that, although playing a secondary role, NSI still have an influence on the solution of the solar neutrino problem. We will combine solar, reactor and accelerator data, in order to get limits on parameters which determine the NSI strength.

[1] The majoron J is a Goldstone boson which appears in models with spontaneous breaking of the lepton number [4].

- **Chapter 4**: In this part of the thesis we will get limits on NSI parameters involved in muon-neutrino interactions with quarks. For this purpose, we will use the results from a NUTeV reanalysis performed by two collaborations, along with data coming from accelerator and atmospheric neutrino experiments.

- **Chapter 5**: The non-unitarity of the light neutrino mixing matrix is the simplest example of NSI. In this chapter we will describe a formalism which will allow us to work easily with models where more than three neutrinos are considered (as seesaw models), separating the new physics and the standard one. We will finish this chapter compiling experimental results on heavy and light neutrino couplings.

- **Chapter 6**: At last, we will finish the thesis presenting our conclusions and future prospects.

I hope this thesis is of interest to the reader, then all the enthusiasm and effort put into it will be rewarded.

Prefaci

La física de neutrins es troba avuí en dia en una posició privilegiada dins d'un camp tan apassionant com és el de la físca de partícules. Des del descobriment de les oscil·lacions de neutrins per part de Super-Kamiokande [1] a l'any 1998, la porta de la física més enllà del Model Estàndar (SM a partir d'ara) ha sigut oberta. Aquest fet implica que els neutrins han de ser massius [2] en contraposició al que suposa el Model Estàndard. No obstant, açò no és una sorpresa completament, sinó que ja venia sent apuntada a partir d'observacions teòriques i experimentals en les dues dècades prèvies al descobriment del fenomen oscil·latori:

- En principi, no és necessari introduir la massa del neutrí al Model Estàndard. Però aquesta no és una característica que sorgeixi degut a una simetria (com és el cas del fotó), sinó que s'elegeix per simplicitat, evitant, per exemple, introduir el neutrídret.

- La gran majoria de models d'unificació requerixen la presència de la massa del neutrí.

- El dèficit observat experimentalment en els fluxos de neutrins solars i atmosfèrics podria ser explicat pel fenomen d'oscil·lacions de neutrins, mecanisme que requereix l'existència de la massa dels neutrins i la mescla entre ells.

Com a conseqüència d'aquest nou camí obert pels neutrins, es podrien observar processos que es troben prohibits al Model Estàndard [5]:

- Les oscil·lacions de neutrins impliquen la mescla dels tres estats d'aquests; per tant els nombres leptònics generacionals no seran vàlids com a simetries globals i es podrien observar desintegracions on es viole el nombre de sabor leptònic (LFV):

  - $\mu \to e\,\gamma$,
  - $\tau \to e\,\gamma$,

  - $\mu \to 3e$.

- Si els neutrins són partícules de Majorana, la desintegració doble beta sense neutrins ($0\nu\beta\beta$) i altres processos on es viole el nombre leptònic podrien observar-se. Fins que tal observació històrica es produïsca, el debat sobre la natura dels neutrins com a partícules de Dirac o Majorana, continuarà obert.

- La cosmologia és sensible a l'existència de neutrins massius, els quals poden afectar al fons còsmic de microones i a altres observables cosmològics.

- El neutrí, com a partícula massiva, podria desintegrar-se:

  - $\nu_\alpha \to \nu_{\alpha'}\, \gamma$,
  - $\nu_\alpha \to \nu_{\alpha'}\, \nu_{\alpha''} \nu_{\alpha'''}$, on tres neutrins són produïts a l'estat final. Aquests podrien ser del mateix tipus o no,
  - $\nu_\alpha \to \nu_{\alpha'}\, J$, on J és un majoron [2].

Com ja hem mencionat, cap dels fenòmens descrits en els paràgrafs anteriors es troba contemplat al Model Estàndard. Per tant, models més enllà del Model Estàndard són necessaris per a introduir la massa del neutrins, podent implicar l'existència de noves interaccions amb la matèria: les Interaccions No Estàndard (NSI a partir d'ara). En aquesta tesi estudiarem algunes d'aquestes noves interaccions des d'un punt de vista fenomenològic. Per aconseguir-ho, utilitzarem les dades de diferent experiments de neutrins, obtenint així una major informació sobre les NSI a partir d'un anàlisi combinat d'aquestes. Per a aquest propòsit, la tesi s'organitza de la següent forma:

- **Capítol 1**: Iniciarem el nostre treball amb una revisió de les característiques més importants dels neutrins dins del Model Estàndard. Junt amb aquestes, es presentaran també altres propietats més enllà del SM, com són la massa i les oscil·lacions de neutrins.

- **Capítol 2**: En aquest capítol realitzarem una introducció a les NSI, explicant la seva aparició a la teoria i les seves principals característiques. Junt amb aquesta explicació genèrica, discutirem els models on apareixen de forma espontània i la seva influència sobre les probabilitats d'oscil·lació de neutrins i els experiments.

[2] El majoron J és un bosó de Goldstone que apareix en models on la ruptura del nombre leptònic és espontània [4].

- **Capítol 3**: El principal objectiu d'aquest capítol és mostrar que, encara que jugant un paper secundari, les NSI encara tenen influència en la solució del problema dels neutrins solars. Combinarem les dades d'experiments solars, reactor i accelerador, per així obtindre límits dels paràmetres que determinen la força d'aquestes NSI.

- **Capítol 4**: En aquesta part de la tesi obtindrem cotes als paràmetres de NSI implicats en interaccions del neutrí muònic amb quarks. Per a aquest comès utilitzarem els resultats de la reanàlisis de NuTeV realitzats per dues col·laboracions en cojunt amb dades d'experiments d'accelerador i d'atmosfèrics.

- **Capítol 5**: La no unitarietat de la matriu de mescla dels neutrins lleugers és l'exemple més simple de NSI. En aquest capítol descriurem un formalisme que ens permetrà treballar de forma senzilla amb models que consideren més de tres neutrins (com els models seesaw), separant nova física d'aquella que és estàndard. Acabarem aquest capítol fent una recopilació dels resultats experimentals de l'acoblament d'un neutrí pesat amb un altre lleuger.

- **Capítol 6**: Finalment, per acabar la tesi presentarem les nostres conclusions i perspectives a futur.

Espere que aquesta tesi siga de l'interés del lector, d'aquesta forma tot el treball, il·lusió i esforç posats en ella seran recompensats.

List of publications

This thesis is based on the following publications carried out with the supervisors of the thesis and several collaborators:

- F. J. Escrihuela, O. G. Miranda, M. A. Tórtola and J. W. F. Valle,

  "Constraining nonstandard neutrino-quark interactions with solar, reactor and accelerator data".

  Phys. Rev. D **80**, 105009 (2009), arXiv:0907.2630 [hep-ph].

- F. J. Escrihuela, O. G. Miranda, M. Tórtola and J. W. F. Valle,

  "Global constraints on muon-neutrino non-standard interactions".

  Phys. Rev. D **83**, 093002 (2011), arXiv:1103.1366 [hep-ph].

- F. J. Escrihuela, D. V. Forero, O. G. Miranda, M. Tórtola and J. W. F. Valle,

  "On the description of non-unitary neutrino mixing".

  Phys. Rev. D **92**, 053009 (2015), arXiv:1503.08879 [hep-ph].

The results of these works were presented in several conferences and they have been published as proceedings:

- F. J. Escrihuela, O. G. Miranda, M. A. Tórtola and J. W. F. Valle,

  "Constraining nonstandard neutrino-quark interactions with solar, reactor and accelerator data".

  J. Phys. Conf. Ser. **259**, 012091 (2010).

  Talk presented at PASCOS 2010, Valencia (Spain).

- F. J. Escrihuela,

  "Status of neutrino-quark NSI parameters".

J. Phys. Conf. Ser. **375**, 042046 (2012).

Talk presented at TAUP 2011, Munich (Germany).

- F. J. Escrihuela,

  "Analysis of non-standard neutrino-quark interactions".

  AIP Conf. Proc. **1420**, 97 (2012).

  Talk presented at EAV 2011, CINVESTAV, Mexico City (Mexico).

- F. J. Escrihuela,

  "Constraining right-handed neutrinos".

  Conference: C14-07-02, arXiv:1505.01097 [hep-ph].

  Talk presented at ICHEP 2014, Valencia (Spain).

Contents

Chapter 1

Neutrinos in the Standard Model and beyond

The Standard Model of particles is the most successful theory describing the interactions of elementary particles. This quantum field theory describes the strong, weak and electromagnetic interactions of elementary particles using the following components summarized in Table 1.1:

- **Fermions**, which are particles with spin $\frac{1}{2}$. They are classified into three families:
  - **First family**: Up and down quarks, electron and electron-neutrino. These are the components of the ordinary matter.
  - **Second family**: Charm and strange quarks, muon and muon-neutrino.
  - **Third family**: Top and bottom quarks, tau and tau-neutrino.
- **Gauge bosons**, correspond to particles with spin 1, responsible for carrying the three interactions mentioned above:
  - **Photon**: It is the gauge boson of the electromagnetic interaction. It is a massless particle.
  - **W^+, W^- and Z^0**: These particles mediate the weak interaction, W^+ and W^- for charged-current weak interactions and Z^0 for neutral-current weak interactions. Unlike photons and gluons, these particles have a mass.
  - **Gluon**: This gauge boson mediates strong interactions between quarks. As the photon, it is a massless particle.

Table 1.1: Standard Model components.

Fermions	**First family**	**Second family**	**Third family**
Quarks	u (up)	c (charm)	t (top)
	d (down)	s (strange)	b (bottom)
Leptons	ν_e (electron-neutrino)	ν_μ (muon-neutrino)	ν_τ (tau-neutrino)
	e (electron)	μ (muon)	τ (tau)
	Electromagnetism	**Weak**	**Strong**
Boson	γ (photon)	W^+, W^- and Z^0	$\mathcal{A}^C$ (gluon)
	Higgs boson		

- **Higgs boson**: This particle is the last ingredient in the Standard Model of particles. It is responsible for the mass of particles and interacts with them through the so-called Higgs mechanism. It is a particle with spin 0, and a mass of $m_H \approx 125\,GeV$.

This model is supported by a large number of experimental results, as for example [6]:

- Particle predictions: W, Z, gluons, top quark, charm quark...
- Couplings constants to Z^0 gauge boson in $e^-e^+ \to \bar{f}f$ processes.
- Branching ratio in $Z^0 \to \bar{f}f$, $W^- \to \bar{\nu}_l l$ and $W^- \to \bar{u}_i d_j$.
- Leptonic universality.
- Z invisible decay width $Z^0 \to \nu_\alpha\, \bar{\nu}_\alpha$.
- Higgs boson.
- ...

However, despite this great success, there are several open questions which have not been answered yet:

- The mechanism which generates neutrino masses.
- Baryonic asymmetry of the Universe.

- Dark matter nature.
- The violation of CP symmetry in the leptonic sector.
- Neutrino nature, Dirac or Majorana?.
- The neutrino mass hierarchy problem.
- Proton stability.
- ....

Finding solutions to these problems has led to the proposal of "new physics" beyond the Standard Model. Neutrinos are an important motivation for physics beyond the Standard Model, as we will see in this thesis.

1.1 Brief description of the Standard Model

The Standard Model is a gauge theory mathematically described by the local symmetry group $SU(3)_C \times SU(2)_L \times U(1)_Y$:

- $SU(3)_C$ stands for the description of strong interaction through the color quantum number. This symmetry group has eight generators which correspond to the eight gluons that mediate the strong force.
- $SU(2)_L$ represents the weak interaction whose local symmetry is the weak isospin. Only left-handed particles with weak isospin $I = \frac{1}{2}$ couple to weak bosons. As this symmetry group has three generators, the number of gauge bosons is three too, W^+, W^- and Z^0 as we have seen above.
- $U(1)_Y$ is the symmetry group for the electromagnetic interaction. In this case, the local symmetry is the hypercharge (Y), having only one generator which is related with the photon, the unique gauge boson related to this group.

With these ingredients, Sheldon Glashow, Abdus Salam and Steven Weinberg were able to unify the weak and electromagnetic interaction in the so-called *electroweak interaction*. This interaction is described by the $SU(2)_L \times U(1)_Y$ symmetry group, having four gauge bosons, three corresponding to the three generators of $SU(2)_L$, W^i, and one gauge boson coming from the electromagnetic $U(1)_Y$ group, B. After spontaneous symmetry

breaking, the usual gauge bosons, W^+, W^-, Z^0 and γ, which mediate the electroweak interaction, arise as a combination of the first ones.

On the other hand, strong interaction cannot be combined with other force, that is why $SU(3)_C$ is studied separately of $SU(2)_L \times U(1)_Y$.

Now, we will take a quick look of the mathematical description of each group, focusing mainly on the description of the electroweak interaction, related, among others, with neutrinos.

1.1.1 Electroweak theory

The electroweak model is described by the $SU(2)_L \times U(1)_Y$ group. $SU(2)_L$ is the group of weak isospin (I), which is a quantum number assigned only to left-handed quarks and leptons of each generation. This violates parity symmetry giving rise to a V-A theory. Keeping this in mind, the leptons can be grouped into doublets of chiral left-handed fields and singlets of right-handed fields, as we show in Table 1.2.

As we have said before, the $SU(2)_L$ has three generators denoted by

$$I_k = \frac{1}{2}\sigma_k \,, \tag{1.1}$$

where k goes from 1 to 3 and σ_k are the isospin version of the Pauli matrices:

$$\sigma_1 = \begin{pmatrix} 0 & 1 \\ 1 & 0 \end{pmatrix}, \qquad \sigma_2 = \begin{pmatrix} 0 & -i \\ i & 0 \end{pmatrix}, \qquad \sigma_3 = \begin{pmatrix} 1 & 0 \\ 0 & -1 \end{pmatrix}. \tag{1.2}$$

These generators satisfy the angular momentum commutation relations, as spin does:

$$[I_k, I_j] = i\epsilon_{kjl} I_l \,. \tag{1.3}$$

Besides $SU(2)_L$, we find the symmetry group $U(1)_Y$ which is known as the weak hypercharge group and its generator is the weak hypercharge Y. This operator relates the weak isospin I_3 with the charge operator Q through the Gell-Mann-Nishijima relation:

$$Q = I_3 + \frac{Y}{2} \,. \tag{1.4}$$

This expression illustrates the unification of weak and electromagnetic interactions.

Once we have the basic ingredients of electroweak theory, we are going to study the lagrangian of the model. For this purpose and for simplicity, we will take into account

Table 1.2: Quantum numbers of leptons and quarks.

		I	**I_3**	**Y**	**Q**
Lepton Doublet	$L_L = \begin{pmatrix} \nu_{eL} \\ e_L \end{pmatrix}$	1/2	$\begin{matrix} 1/2 \\ -1/2 \end{matrix}$	-1	$\begin{matrix} 0 \\ -1 \end{matrix}$
Lepton Singlet	e_R	0	0	-2	-1
Quark Doublet	$Q_L = \begin{pmatrix} u_L \\ d_L \end{pmatrix}$	1/2	$\begin{matrix} 1/2 \\ -1/2 \end{matrix}$	1/3	$\begin{matrix} 2/3 \\ -1/3 \end{matrix}$
Quark Singlet	$\begin{matrix} u_R \\ d_R \end{matrix}$	0	0	$\begin{matrix} 4/3 \\ -2/3 \end{matrix}$	$\begin{matrix} 2/3 \\ -1/3 \end{matrix}$

only the first generation leptons (e_L, ν_{eL} and e_R) considering them as massless particles [1]; we begin our discussion assuming that leptons have no couplings with electroweak gauge bosons. With these conditions, the lagrangian for these free Dirac fields can be written as

$$\mathcal{L} = (\bar{\nu}_{eL}, \bar{e}_L)(i\gamma^\mu \partial_\mu) \begin{pmatrix} \nu_{eL} \\ e_L \end{pmatrix} + \bar{e}_R i\gamma^\mu \partial_\mu e_R \,. \tag{1.5}$$

Note that we have respected the doublet-singlet notation. This lagrangian is not invariant under weak isospin transformations [2], but we can introduce gauge vector fields to compensate it. As we said before, we find three vectors fields in $SU(2)_L$ as generators of the symmetry group, $W^i{}_\mu$ (with $i = 1, 2, 3$). Including these fields, the lagrangian becomes

$$\mathcal{L} = \frac{1}{2} Tr(W_{\mu\rho} W^{\mu\rho}) + (\bar{\nu}_{eL}, \bar{e}_L) i\gamma^\mu (\partial_\mu + igW_\mu) \begin{pmatrix} \nu_{eL} \\ e_L \end{pmatrix} + \bar{e}_R i\gamma^\mu \partial_\mu e_R \,. \tag{1.6}$$

The gauge bosons W^Q have electromagnetic charge and they are defined as a linear

[1] We know from neutrino oscillations that the neutrino is a massive particle in the $SU(2)_L \times U(1)_Y$ description of the electroweak theory. But, in order to simplify the discussion, here the neutrino is chosen without mass and only left-handed.

[2] Weak isospin transformations can be considered as space rotations of a vector.

combination of $W^i{}_\mu$ as:

$$\begin{aligned} W^+_\mu &= \frac{1}{\sqrt{2}}(W^1_\mu - iW^2_\mu)\,, \\ W^-_\mu &= \frac{1}{\sqrt{2}}(W^1_\mu + iW^2_\mu)\,, \\ W^0_\mu &= W^3_\mu\,. \end{aligned} \tag{1.7}$$

Introducing these fields in Eq. (1.6), we obtain the following lagrangian for the lepton-boson coupling term,

$$\begin{aligned} \mathcal{L} &= -g(\bar{\nu}_{eL}, \bar{e}_L)\gamma^\mu W_\mu \frac{\sigma}{2}\begin{pmatrix} \nu_{eL} \\ e_L \end{pmatrix} \\ &= -g(\bar{\nu}_{eL}, \bar{e}_L)\gamma^\mu \frac{1}{2}\begin{pmatrix} W^0_\mu & \sqrt{2}\,W^+_\mu \\ \sqrt{2}\,W^-_\mu & -W^0_\mu \end{pmatrix}\begin{pmatrix} \nu_{eL} \\ e_L \end{pmatrix} \\ &= -\frac{g}{2}\left[W^0_\mu(\bar{\nu}_{eL}\gamma^\mu\nu_{eL} - \bar{e}_L\gamma^\mu e_L) + \sqrt{2}\,W^+_\mu\bar{\nu}_{eL}\gamma^\mu e_L + \sqrt{2}\,W^-_\mu\bar{e}_L\gamma^\mu\nu_{eL}\right], \end{aligned} \tag{1.8}$$

where σ are the Pauli matrices in Eq. (1.2) and the weak isospin components are defined as $I_k = \frac{1}{2}\sigma_k$. We can rewrite Eq. (1.8) in a more usual form using the left-chirality projector γ^5 [3],

$$\bar{\psi}_L\gamma^\mu\psi_L = \frac{1}{2}\bar{\psi}\gamma^\mu(1-\gamma^5)\psi\,, \tag{1.9}$$

giving rise to

$$\begin{aligned} \mathcal{L} &= -\frac{g}{4}\Big[W^0_\mu(\bar{\nu}_e\gamma^\mu(1-\gamma^5)\nu_e - \bar{e}\gamma^\mu(1-\gamma^5)e) + \sqrt{2}\,W^+_\mu\bar{\nu}_e\gamma^\mu(1-\gamma^5)e \\ &+ \sqrt{2}\,W^-_\mu\bar{e}\gamma^\mu(1-\gamma^5)\nu_e\Big]\,. \end{aligned} \tag{1.10}$$

As we can see from the equations above, only left-handed leptons interact with weak gauge bosons, as expected.

Since we are talking about electroweak interaction, one extra-component must be introduced in the lagrangian, electromagnetism. We could think that W^0_μ is associated with the photon, but this is not possible because W^0_μ and the photon have different couplings. Therefore, the electromagnetic interaction is inserted in the lagrangian through the hypercharge group $U(1)_Y$, where, as we have said in Eq. (1.4), charge and isospin are related. In this group, the vector field is B_μ with the corresponding coupling constant g'.

[3] It is defined in Sec. 1.2.2.

Both neutral vector fields combine as

$$Z_\mu = \frac{1}{\sqrt{g^2+g'^2}}\left(gW_\mu^0 - g'B_\mu\right), \tag{1.11}$$

$$A_\mu = \frac{1}{\sqrt{g^2+g'^2}}\left(g'W_\mu^0 + gB_\mu\right), \tag{1.12}$$

leading to gauge bosons of weak neutral-current and electromagnetism respectively. Defining the weak mixing angle θ_W in terms of the coupling constants g and g',

$$\sin\theta_W = \frac{g'}{\sqrt{g^2+g'^2}}, \qquad \cos\theta_W = \frac{g}{\sqrt{g^2+g'^2}}, \tag{1.13}$$

the expressions above, Eqs. (1.11) and (1.12), are simplified as

$$Z_\mu = \cos\theta_W W_\mu^0 - \sin\theta_W B_\mu, \tag{1.14}$$

$$A_\mu = \sin\theta_W W_\mu^0 + \cos\theta_W B_\mu. \tag{1.15}$$

Replacing Z_μ and A_μ in Eq. (1.8), it results in

$$\begin{aligned}\mathcal{L} &= -\frac{g}{\sqrt{2}}\left(W_\mu^+ \bar{\nu}_{eL}\gamma^\mu e_L + W_\mu^- \bar{e}_L\gamma^\mu \nu_{eL}\right) \\ &- \sqrt{g^2+g'^2}Z_\mu\left[\frac{1}{2}\bar{\nu}_{eL}\gamma^\mu\nu_{eL} - \frac{1}{2}\bar{e}_L\gamma^\mu e_L + \sin^2\theta_W\left(\bar{e}_L\gamma^\mu e_L + \bar{e}_R\gamma^\mu e_R\right)\right] \\ &+ \frac{gg'}{\sqrt{g^2+g'^2}}A_\mu\left(\bar{e}_L\gamma^\mu e_L + \bar{e}_R\gamma^\mu e_R\right),\end{aligned} \tag{1.16}$$

where the vector field A_μ is only coupled to charged leptons, so it can be associated with the photon, whereas $W_\mu^\pm$ and Z_μ represent the gauge bosons of weak charged-current and weak neutral-current respectively.

In order to relate the electromagnetism and weak interactions, along with the Eq. (1.4), we have

$$\frac{gg'}{\sqrt{g^2+g'^2}} = e, \tag{1.17}$$

which leads to the relation between the weak mixing angle and the electromagnetic charge:

$$\sin\theta_W = \frac{e}{g}. \tag{1.18}$$

Finally, we may write the complete lagrangian including electromagnetism, charged-

current and neutral-current weak interactions, respectively:

$$\mathcal{L} = -e\left\{A_\mu J^\mu_{em} + \frac{1}{\sqrt{2}\sin\theta_W}\left(W^+_\mu \bar{\nu}_{eL}\gamma^\mu e_L + W^-_\mu \bar{e}_L\gamma^\mu \nu_{eL}\right) + \frac{1}{\sin\theta_W\cos\theta_W} Z_\mu J^\mu_{NC}\right\}, \tag{1.19}$$

where

$$J^\mu_{em} = -\left(\bar{e}_L\gamma^\mu e_L + \bar{e}_R\gamma^\mu e_R\right) = -\bar{e}\gamma^\mu e\,, \tag{1.20}$$

$$J^\mu_{NC} = \frac{1}{2}\bar{\nu}_{eL}\gamma^\mu\nu_{eL} - \frac{1}{2}\bar{e}_L\gamma^\mu e_L - \sin^2\theta_W J^\mu_{em}\,. \tag{1.21}$$

1.1.2 A touch of QCD

For the sake of completeness, we just mention QCD which is described by the symmetric group $SU(3)_C$, as already stated. Quantum Chromodynamics is the gauge theory that describes the strong interaction between colored quarks and is mediated by eight gluons carrying color. The QCD lagrangian is [7]

$$\mathcal{L} = \sum_q \bar{\psi}_{q,a}(i\gamma^\mu\partial_\mu\delta_{ab} - g_s\gamma^\mu t^C_{ab}\mathcal{A}^C_\mu - m_q\delta_{ab})\psi_{q,b} - \frac{1}{4}F^A_{\mu\nu}F^{A\,\mu\nu}\,, \tag{1.22}$$

where

- γ^μ are the Dirac matrices,
- $\psi_{q,a}$ stand for quark-field spinors of mass m_q, with $a = 1, 2, 3$ which is the number of colors,
- $\mathcal{A}^C_\mu$ correspond to the gluon fields, where C goes from 1 to 8, the number of gluons in QCD,
- t^c_{ab} are the eight generators of $SU(3)_c$,
- g_s is the QCD coupling constant,
- $F^A_{\mu\nu} = \partial_\mu\mathcal{A}^A_\nu - \partial_\nu\mathcal{A}^A_\mu - g_s f_{ABC}\mathcal{A}^B_\mu\mathcal{A}^C_\nu$, with f_{ABC} as the structure constants of $SU(3)_C$.

1.2 Neutrinos in the Standard Model

Neutrinos are electrically neutral particles of spin $\frac{1}{2}$. There are three flavors of neutrinos in the SM, ν_e, ν_μ and ν_τ (Table 1.1), which are left-handed, being associated with a lepton

of each family as we saw in Sec. 1.1.1 (Table 1.2). We also find their three antiparticles, the antineutrinos $\bar{\nu}_e$, $\bar{\nu}_\mu$ and $\bar{\nu}_\tau$, which are right-handed particles. Right-handed neutrinos and left-handed antineutrinos have not been experimentally found, which corresponds to particles without mass in the Standard Model [4]. In the rest of the chapter, we are going to deepen slightly in neutrino properties in order to provide the reader a first insight into neutrino theory.

1.2.1 Origin and number of neutrinos

Neutrinos and antineutrinos are particles produced in several processes as, for instance:

- Nuclear $\beta^\pm$ decay,

$$\begin{aligned} A(Z,N) &\rightarrow A(Z+1,N-1) + e^- + \bar{\nu}_e\,, \\ A(Z,N) &\rightarrow A(Z-1,N+1) + e^+ + \nu_e\,. \end{aligned} \tag{1.23}$$

- Muon decays,

$$\begin{aligned} \mu^+ &\rightarrow e^+ + \bar{\nu}_\mu + \nu_e\,, \\ \mu^- &\rightarrow e^- + \nu_\mu + \bar{\nu}_e\,. \end{aligned} \tag{1.24}$$

- Pion decays,

$$\begin{aligned} \pi^+ &\rightarrow e^+ + \nu_e\,, \\ \pi^- &\rightarrow e^- + \bar{\nu}_e\,, \\ \pi^+ &\rightarrow \mu^+ + \nu_\mu\,, \\ \pi^- &\rightarrow \mu^- + \bar{\nu}_\mu\,. \end{aligned} \tag{1.25}$$

- Tau decays,

$$\begin{aligned} \tau^- &\rightarrow \mu^- + \bar{\nu}_\mu + \nu_\tau\,, \\ \tau^+ &\rightarrow \mu^+ + \nu_\mu + \bar{\nu}_\tau\,. \end{aligned} \tag{1.26}$$

[4] Particles require both chiralities to produce mass in the Standard Model, as we will see in Sec. 1.2.3.

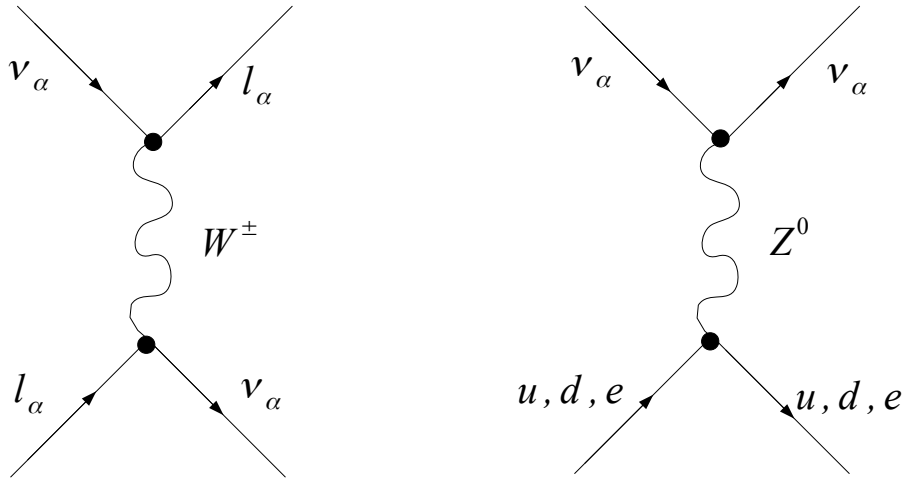

Figure 1.1: Neutrino weak interactions with leptons. The left diagram stands for charged-current weak interactions through $W^\pm$, whereas the right diagram represents neutral-current weak interactions mediated by Z^0.

- Solar neutrino production,

$$\begin{aligned} p^+ + p^+ &\rightarrow {}^2\mathrm{H} + e^+ + \nu_e\,, \\ p^+ + e^- + p^+ &\rightarrow {}^2\mathrm{H} + \nu_e\,, \\ {}^3\mathrm{He} + p^+ &\rightarrow {}^4\mathrm{He} + e^+ + \nu_e\,, \\ {}^7\mathrm{Be} + e^- &\rightarrow {}^2\mathrm{Li} + \nu_e\,, \\ {}^8\mathrm{B} &\rightarrow {}^8\mathrm{Be} + e^+ + \nu_e\,. \end{aligned} \tag{1.27}$$

Neutrinos interact with charged leptons through charged-current weak interactions, Fig. 1.1, coupling with bosons $W^\pm$ in reactions involving

$$W^\pm \rightarrow l^\pm_\alpha + \nu_\alpha(\bar{\nu}_\alpha)\,, \tag{1.28}$$

where α indicates the flavor of the lepton and the neutrino. Similarly, they also participate in processes mediated by the Z^0 boson, the so-called neutral-current weak interactions Fig. 1.1. These are elastic or quasi-elastic scattering processes and Z^0 decays,

$$Z^0 \rightarrow \nu_\alpha\,\bar{\nu}_\alpha\,. \tag{1.29}$$

Notice that these couplings were given before in Eqs. (1.16) and (1.19).

Following with the Z^0 decay, it allowed to determine the number of light neutrinos. Indeed, neutrinos from Z^0 are not detected directly, but the presence of neutrinos is known from the difference between the total decay width of the Z^0 boson and widths of visible particles after decaying,

$$\Gamma_{inv} = \Gamma_{tot} - \Gamma_{vis} = 499.0 \pm 1.5\,\text{MeV}\,. \tag{1.30}$$

This invisible width should correspond to the decay into a pair $\nu\bar{\nu}$ of any flavor. So, considering that the width of Z^0 decaying to one pair is $\Gamma_{\nu\bar{\nu}} = 167.2\,\text{MeV}$, we can translate this into the number of light active neutrinos species (with their corresponding antineutrinos) as [6, 8]

$$N_\nu = \frac{\Gamma_{inv}}{\Gamma_{\nu\bar{\nu}}} = 2.984 \pm 0.082\,, \tag{1.31}$$

almost three light neutrino flavors, as it is assumed in the Standard Model.

1.2.2 Chirality and helicity of neutrinos

In Quantum Field Theory, fermions can be described by four-component spinors ψ which obey the Dirac equation,

$$\left(i\gamma^\mu \frac{\partial}{\partial x^\mu} - m\right)\psi = 0\,, \tag{1.32}$$

where γ^μ are the Dirac matrices [5]

$$\gamma^0 = \begin{pmatrix} 0 & 1 \\ 1 & 0 \end{pmatrix}\,, \qquad \gamma^i = \begin{pmatrix} 0 & \sigma_i \\ -\sigma_i & 0 \end{pmatrix} \tag{1.33}$$

and σ_i are the Pauli matrices, given already in Eq. (1.2). We want to stress the importance of the combination of Dirac matrices in

$$\gamma_5 = i\gamma_0\gamma_1\gamma_2\gamma_3 = \begin{pmatrix} -1 & 0 \\ 0 & 1 \end{pmatrix}\,, \tag{1.34}$$

because, as we will see in the following lines, this matrix will give rise to the chirality operator.

Using the Eq. (1.32) and the Dirac matrices, taking into account that $\gamma_i = \gamma_0\gamma_5\sigma_i$; we obtain the Dirac equation in a convenient form in terms of γ_5, decoupled in two

[5] Other conventions of these matrices are also used in the literature.

expressions:

$$\left(i\frac{\partial}{\partial x^0}(1+\gamma_5)+i\sigma_i\frac{\partial}{\partial x_i}(1+\gamma_5)-m\gamma_0(1-\gamma_5)\right)\psi = 0\,, \tag{1.35}$$

$$\left(i\frac{\partial}{\partial x^0}(1-\gamma_5)-i\sigma_i\frac{\partial}{\partial x_i}(1-\gamma_5)-m\gamma_0(1+\gamma_5)\right)\psi = 0\,. \tag{1.36}$$

From the equations above, we can define two projection operators given by

$$P_L=\frac{1}{2}(1-\gamma_5)\,,\qquad P_R=\frac{1}{2}(1+\gamma_5)\,, \tag{1.37}$$

getting the left-handed and right-handed component of the fermion ψ as

$$\psi_L=P_L\psi,\qquad \psi_R=P_R\psi\qquad\text{and}\qquad P_L\psi_R=P_R\psi_L=0. \tag{1.38}$$

As we mentioned before, γ_5 plays a key role as a chirality operator

$$\gamma_5\psi_{L,R}=\mp\psi_{L,R}\,, \tag{1.39}$$

where ∓1 correspond to the chirality eigenvalues and $\psi_{L,R}$ are the chiral projections of ψ. Any spinor ψ can be written in terms of its projections as follows

$$\psi=(P_L+P_R)\psi=P_L\psi+P_R\psi=\psi_L+\psi_R\,. \tag{1.40}$$

Chirality is related with helicity, in such a way that, if a fermion ψ is a massless particle, both properties are the same. Now we will see it.

Combining Eqs. (1.35), (1.36) and (1.40), we may rewrite the Dirac equation in terms of left and right-handed components, obtaining:

$$\left(i\frac{\partial}{\partial x^0}-i\sigma_i\frac{\partial}{\partial x_i}\right)\psi_R = m\gamma_0\psi_L\,, \tag{1.41}$$

$$\left(i\frac{\partial}{\partial x^0}+i\sigma_i\frac{\partial}{\partial x_i}\right)\psi_L = m\gamma_0\psi_R\,. \tag{1.42}$$

In the case of vanishing mass, the equations can be rewritten as

$$i\frac{\partial}{\partial x^0}\psi_R = i\sigma_i\frac{\partial}{\partial x_i}\psi_R\,, \tag{1.43}$$

$$i\frac{\partial}{\partial x^0}\psi_L = -i\sigma_i\frac{\partial}{\partial x_i}\psi_L\,, \tag{1.44}$$

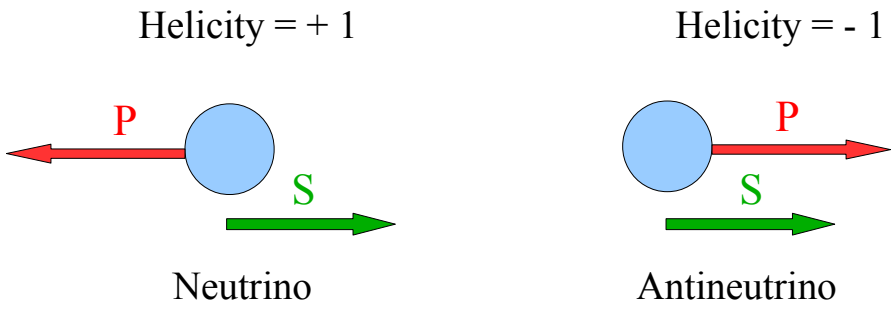

Figure 1.2: Helicity for neutrino and antineutrino, which is coincident with chirality in the Standard Model, where $m_\nu = 0$.

which are "equal" to the Schrödinger equation, with $x_0 = t$ and $\hbar = 1$. Using the definitions $E = i\frac{\partial}{\partial t}$ and $p_i = -i\frac{\partial}{\partial x_i}$, Eqs. (1.41) and (1.42) acquire a more compact form

$$E\psi_{L,R} = \pm\sigma_i p_i \psi_{L,R}\,. \tag{1.45}$$

This equation defines a new operator, the helicity $\hat{h}$, as

$$\hat{h} = \frac{\sigma \cdot \mathbf{p}}{|\mathbf{p}|}\,, \tag{1.46}$$

which is the projection of the spin over the linear momentum, as we may see in Fig. 1.2. Notice from Eq. (1.45) that ψ_L represents a spinor with $\hat{h} = +1$ for particles and $\hat{h} = -1$ for antiparticles. On the other hand, ψ_R stands for a spinor with helicity $\hat{h} = -1$ for particles and $\hat{h} = +1$ for antiparticles. Therefore, if we neglect the fermion mass, chirality and helicity are the same.

So that, we may affirm that, in the Standard Model, where the neutrino is a massless particle, the interacting neutrino is always left-handed, and therefore $\hat{h} = +1$,

$$\frac{1}{2}(1 - \gamma_5)\nu = \nu_L\,, \tag{1.47}$$

while the antineutrino is always right-handed, with $\hat{h} = -1$.

1.2.3 Massless neutrinos

As we will briefly discuss, in the Standard Model neutrinos are particles without mass and this fact is related with their chirality, studied in the previous section. From the Higgs mechanism, fermions acquire mass through their couplings to the Higgs field. The

resulting coupling is known as the Yukawa coupling. Here, we take the lagrangian for the first family of leptons for illustration:

$$\begin{aligned}
\mathcal{L} &= -\lambda_e \left[(\bar{\nu}_{eL}, \bar{e}_L)\, \phi_0\, e_R + \bar{e}_R\, \phi_0^\dagger \begin{pmatrix} \nu_{eL} \\ e_L \end{pmatrix} \right] \\
&= -\lambda_e \left[\bar{e}_L \frac{1}{\sqrt{2}} v e_R + \bar{e}_R \frac{1}{\sqrt{2}} v e_L \right] \\
&= -\lambda_e \frac{1}{\sqrt{2}} v \left(\bar{e}_L e_R + \bar{e}_R e_L \right) \\
&= -\lambda_e \frac{1}{\sqrt{2}} v \left(\bar{e} e \right) . \qquad (1.48)
\end{aligned}$$

As we can appreciate, only particles with both (left and right) chiralities couple to the Higgs boson and thus obtain their mass. In contrast, neutrinos remain massless because they do not couple to the Higgs field (no evidence of right-handed neutrino or left-handed antineutrino has been found). But neutrino mass is a reality, so mechanisms beyond the Standard Model are introduced to generate the neutrino mass, as we will see in the next section.

1.3 Massive neutrinos

In the Standard Model, neutrinos are taken as particles without mass. However, after the discovery of neutrino oscillations [1] (Sec. 1.5), the situation has changed and introducing neutrino masses is necessary. Nevertheless, the absolute value of the neutrino mass has not been measured yet, because only the mass differences between neutrinos and the mixing angles enter in neutrino oscillations.

Along with this, there are other mysteries that accompany neutrino masses, as the mechanism responsible for them and their small size compared with the rest of fermions. Answering these and other related questions has led people to develop many models in order to shed light on these mysteries. In what follows, we will discuss the neutrino mass, taking into account the particle nature (Dirac or Majorana), as well as the mechanism to originate it.

1.3.1 Dirac vs Majorana particles

Let us start considering the Dirac lagrangian for free particles:

$$\mathcal{L} = \bar{\psi} \left(i\gamma^\mu \partial_\mu - m \right) \psi \,, \qquad (1.49)$$

where the four-component Dirac spinor can be written in terms of two-component left-handed spinors χ and ξ as [3, 9],

$$\psi = \begin{pmatrix} \chi \\ i\sigma_2\xi^* \end{pmatrix} = \begin{pmatrix} \chi \\ \bar{\xi} \end{pmatrix} , \tag{1.50}$$

with σ_2 as one of the Pauli matrices defined in Eq. (1.2). Therefore, we may expand Eq. (1.49) in terms of two-component spinor (Eq. (1.50)) obtaining the following expression:

$$\begin{aligned} \mathcal{L} &= i\xi\sigma^\mu\partial_\mu\bar{\xi} + i\bar{\chi}\bar{\sigma}^\mu\partial_\mu\chi - m\left(\xi\chi + \bar{\chi}\bar{\xi}\right) \\ &= i\bar{\xi}\bar{\sigma}^\mu\partial_\mu\xi + i\bar{\chi}\bar{\sigma}^\mu\partial_\mu\chi - m\left(\xi\chi + \bar{\chi}\bar{\xi}\right) , \end{aligned} \tag{1.51}$$

where the following definitions of the Pauli matrices have been used [3],

$$\sigma^\mu \equiv (1, \vec{\sigma}) , \qquad \bar{\sigma}^\mu \equiv (1, -\vec{\sigma}) . \tag{1.52}$$

Notice that in Eq. (1.51) the first two terms represent the kinetic energy, while the last one stands for the Dirac mass term given by

$$\mathcal{L}_{m_D} = -m\left(\xi^T i\sigma_2\chi + \chi^\dagger i\sigma_2\xi^*\right) , \tag{1.53}$$

where we have used the condition $\bar{\psi} = \psi^\dagger\gamma^0$.

If we identify the two-component spinors χ and ξ with the chiral-components of some field ψ [3, 9],

$$\psi = \begin{pmatrix} \psi_L \\ \psi_R \end{pmatrix} = \begin{pmatrix} \chi \\ \bar{\xi} \end{pmatrix} , \tag{1.54}$$

we see that both chiralities (left and right) are necessary in order to produce a Dirac mass term, as it can be observed from Eq. (1.53). But as we already mentioned in Sec. 1.2.2, the SM only includes left-handed neutrinos $\nu_L \equiv \chi$, avoiding the right-handed component, and right-handed antineutrinos ν_R^c, avoiding the left-handed component in this case. As a consequence, neutrinos remain massless in the SM, as we have discussed in Sec. 1.2.3.

Note that one can rewrite the two-component spinors in Eq. (1.50) as

$$\chi = \frac{1}{\sqrt{2}}(\rho_1 + i\rho_2) , \qquad \xi = \frac{1}{\sqrt{2}}(\rho_1 - i\rho_2) , \tag{1.55}$$

so Eq. (1.51) becomes

$$\mathcal{L} = i \sum_{a=1}^{2} \bar{\rho}_a \bar{\sigma}^\mu \partial_\mu \rho_a - \frac{1}{2} m \sum_{a=1}^{2} \left(\rho_a \rho_a + \bar{\rho}_a \bar{\rho}_a \right) . \tag{1.56}$$

Each of these ρ fields by itself represents a Majorana particle:

$$\rho = \rho^c = C \bar{\rho}^T , \tag{1.57}$$

where C is defined as the charge conjugation operator, which connects a particle $p(x,t)$ with its antiparticle $\bar{p}(x,t)$ as [10–12]:

$$C|p(x,t)\rangle = \eta_c |\bar{p}(x,t)\rangle , \tag{1.58}$$

with $|\eta_c| = 1$. It can be defined explicitly as

$$C = \begin{pmatrix} -i\sigma_2 & 0 \\ 0 & i\sigma_2 \end{pmatrix} . \tag{1.59}$$

Hence, we can separate Eq. (1.56) in two pieces:

$$\mathcal{L} = i \bar{\rho}\, \bar{\sigma}^\mu \partial_\mu \, \rho - \frac{1}{2} m \left(\rho\rho + \bar{\rho}\bar{\rho} \right) , \tag{1.60}$$

getting the following Majorana mass term,

$$\mathcal{L}_{m_M} = -\frac{1}{2} m \left(\rho^T i\sigma_2 \rho + h.c. \right) . \tag{1.61}$$

From the whole discussion we can find that a four-component Dirac fermion is equivalent to two Majorana fermions of equal mass, represented by two-component spinors. Hence, the description with a two-component spinor is the most basic representation of a spin-1/2 fermion and we consider it more general in order to discuss the neutrino mass.

Using a four-component spinor description, we define a Majorana fermion as [3, 9]

$$\psi_M = \psi_M^c = C\, \bar{\psi}_M^T . \tag{1.62}$$

We can see from Eq. (1.62) that both two-component spinors are the same for a Majorana

particle [3, 9]:

$$\psi_M = \begin{pmatrix} \chi \\ i\sigma_2\chi* \end{pmatrix} = \begin{pmatrix} \chi \\ \bar{\chi} \end{pmatrix} . \tag{1.63}$$

Notice that only neutral particles could be described as Majorana.

1.3.2 Producing the neutrino mass

Since neutrinos are massless particles in the Standard Model, extra components have to be added in order to introduce the neutrino mass. If we want to produce massive neutrinos without extending the lepton sector, it is necessary to introduce a $SU(2)_L$ Higgs triplet [9], which is written in matrix form as

$$\Delta = \begin{pmatrix} \frac{\Delta^+}{\sqrt{2}} & \Delta^{++} \\ \Delta^0 & -\frac{\Delta^+}{\sqrt{2}} \end{pmatrix} . \tag{1.64}$$

This Higgs triplet will produce the following Yukawa terms in the weak lagrangian [9]:

$$-\frac{1}{2}\sum_{a,b} g_{ab} l_a^T C^{-1} i\sigma_2 \Delta l_b + h.c. , \tag{1.65}$$

where C is the charge conjugation operator, l represents the SM doublet (Table 1.1) and g_{ab} is the coupling constant. After spontaneous symmetry breaking, the Higgs triplet acquires a vacuum expected value (vev in what follows), generating a Majorana mass term as in Eq. (1.61). The following condition has to be verified by the Higgs triplet [13],

$$\langle \Delta^0 \rangle = -\mu_\Delta \frac{\langle \phi^0 \rangle^2}{M_\Delta^2} , \tag{1.66}$$

arising from the minimization of the scalar potential. As neutrino masses are proportional to $g_{ab}\langle \Delta^0 \rangle$, the smallness of neutrino mass will be conditioned by the Higgs triplet mass M_Δ.

Another way to generate neutrino masses is introducing extra components to the fermion sector of the SM. For instance, $SU(2)_L$ isosinglets, represented by left-handed spinor fields ρ_{La}, can be added producing Majorana mass terms such as [9]

$$-\sum_{a,b} g'_{ab} \rho_{La}^T C^{-1} \rho_{Lb} + h.c. \tag{1.67}$$

In addition, a Dirac mass term can be induced through the coupling between the SM

doublet l and the singlet ρ_L:

$$\sum_{a,b} g''_{ab} \bar{l}_a i\sigma_2 \phi^* C \bar{\rho}^T_{Lb} + h.c. \,, \tag{1.68}$$

with ϕ as the SM Higgs doublet.

In a very general model of neutrinos, we can find n neutrinos belonging to $SU(2)_L$ doublets and described by two-component spinors ρ_n, along with m extra neutrinos as $SU(2)_L$ singlets, ρ_m. The lagrangian of this model is a generalization of Eq. (1.60), which becomes

$$\mathcal{L} = \sum_{\alpha,\beta}^{n+m} i\bar{\rho}_\alpha \, \bar{\sigma}_\mu \partial^\mu \, \rho_\alpha - \frac{1}{2} \left(M_{\alpha\beta} \rho_\alpha \rho_\beta + h.c. \right) \,, \tag{1.69}$$

where α and β run from 1 to $n+m$. The mass matrix M is a symmetric [6] matrix that can be written in general as

$$M = \begin{pmatrix} M_L & M_D \\ M_D^T & M_R \end{pmatrix} \,. \tag{1.70}$$

Here, the $n \times n$ M_L submatrix comes from Eq. (1.65) where a Higgs triplet is present, the $m \times m$ M_R piece follows from Eq. (1.67) where extra $SU(2)_L$ isosinglets couple among them, and the M_D block stems from Eq. (1.68) as a consequence of the coupling between $SU(2)_L$ doublets and singlets.

In the most general case, when all the submatrices described above are present, models are called Type-I+II seesaw. But if the Higgs triplet is not present and $M_L = 0$, they will be named Type-I seesaw [7]. Finally, if a fermion triplet (T_F) is introduced as a mass messenger, we have the Type-III seesaw [14]. For a more detailed analysis on this topic, the reader should consult Refs. [3–5, 9, 12, 14] among others.

1.4 Neutrino mass models

The most popular mechanism to provide the neutrino mass is the *seesaw mechanism* [15]. Mainly it is based on the idea of generating the effective dimension-five operator $\mathcal{O}_5 = \lambda L\Phi L\Phi$ [16], Fig. 1.3 (where L represents a lepton doublet for each family and Φ is the SM scalar doublet), by the interchange of heavy particles, that could be fermions (Type-I and Type-III) or scalars (Type-II). This can be achieved in different ways, with several multiplet contents and different gauge groups. The mass of the messenger determines the

[6] The symmetry condition implies $M_{\alpha\beta} = M_{\beta\alpha}$.

[7] Notice that we are using the standard notation, but we can find different notation as in Ref. [9].

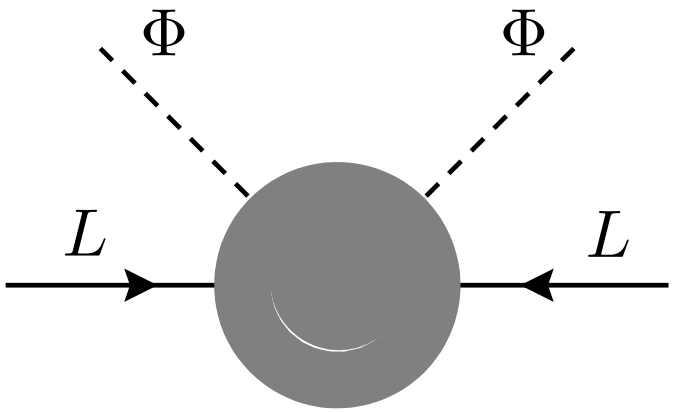

Figure 1.3: Dimension five operator which leads to the neutrino mass [16].

scale where the global lepton number symmetry is violated due to the presence of new physics:

$$m_\nu = \lambda_0 \frac{\langle \Phi \rangle^2}{M_X} \,, \tag{1.71}$$

with λ_0 as an unknown dimensionless constant.

The seesaw mechanism is an elegant way of, not only introducing neutrino masses, but also explaining its smallness, since as the mass of the intermediate particles increases, the neutrino mass decreases at fixed coupling. In this section we will review some significant examples of these models.

1.4.1 Type I+II seesaw

In a $(3 + 3)$ neutrino scheme [8], with three left-handed and three right-handed neutrinos represented by ν_L and N_L^c respectively, the seesaw mass matrix can be built as in Eq. (1.70) [9],

$$M_6 = \begin{pmatrix} M_L & M_D \\ M_D^T & M_R \end{pmatrix} . \tag{1.72}$$

It includes a $SU(2)$ triplet giving rise to the M_L mass term, a Higgs doublet leading to the Dirac mass term M_D and a gauge singlet identified with M_R. This seesaw mass matrix is diagonalized by a unitary matrix $U_{6\times6}$ producing six mass eigenstates,

$$U_{6\times6}^T \, M_6 \, U_{6\times6} = diag\left[m_i, M_i\right] \,, \tag{1.73}$$

[8]Note that a minimum of two right-handed neutrinos is needed in order to reproduce the observed light neutrino masses. Here the $(3 + 3)$ case is shown for illustration.

three for the light neutrinos m_i and three for the heavy leptons M_i. Explicitly, the light neutrino mass is given in a seesaw Type-I+II form by [4]

$$m_\nu = M_L - M_D M_R^{-1} M_D^T \,, \tag{1.74}$$

where the smallness of neutrino masses stems from assuming $M_R \gg M_D \gg M_L$.

It is easy to see that for a standard Type-I mechanism, the light neutrino mass becomes

$$m_\nu = -M_D M_R^{-1} M_D^T \,. \tag{1.75}$$

In order to explain briefly the origin of neutrino mass through seesaw schemes, we may rewrite the neutrino mass matrix as [17]

$$\mathcal{M}_\nu = \begin{pmatrix} Y_3 v_3 & Y_\nu \langle \Phi \rangle \\ Y_\nu^T \langle \Phi \rangle & M_R \end{pmatrix} \,, \tag{1.76}$$

where Y_3 and Y_ν are the Yukawa coupling submatrices (complex in general), and v_3 and $v_2 \equiv \langle \Phi \rangle$ are the Higgs triplet vev and the SM Higgs doublet vev respectively. In this scenario, the effective light neutrino mass is calculated from the equation [9]

$$m_\nu = Y_3 v_3 - Y_\nu M_R^{-1} Y_\nu^T \langle \Phi \rangle^2 \,. \tag{1.77}$$

1.4.2 Inverse seesaw

One of the most interesting properties of the seesaw mechanism is its versatility. In fact, new important features arise when the lepton sector is extended adding extra gauge singlets, N_L^c and S_L [18, 19], giving rise to a $(3 + 6)$ description. In this scheme, it is considered three light states and six heavy states, forming three pseudo-Dirac quasi-degenerate pairs. In the ν_L, N_L^c and S_L basis, the seesaw mass matrix is defined as

$$M_\nu = \begin{pmatrix} 0 & M_D & 0 \\ M_D^T & 0 & M \\ 0 & M^T & \mu \end{pmatrix} \,, \tag{1.78}$$

where M and μ are $SU(2)$ singlet complex mass matrices. Note that the $\nu_L - \nu_L$ and $N_L^c - N_L^c$ terms are neglected, as suggested in several string models [20], and lepton number

[9] The naturalness of the Yukawa coupling ($Y \sim 1$) would imply the need of a very massive neutral lepton as the messenger of the seesaw.

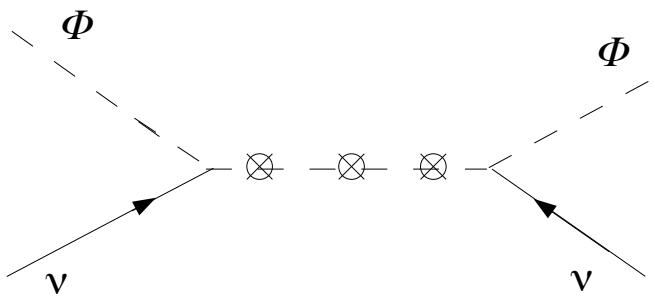

Figure 1.4: Inverse seesaw mechanism where N_L^c and S_L are included [18].

is broken only by the nonzero $\mu_{ij} S_i S_j$ mass terms.

This description belongs to the so-called *inverse seesaw mechanism*, where the masses of the three light neutrinos are defined, after the diagonalization [21], by

$$m_\nu = M_D (M^T)^{-1} \, \mu \, M^{-1} M_D^T \, . \tag{1.79}$$

Notice that, in contrast to the standard seesaw mechanism, the smallness of neutrino mass emerges from the tiny mass value arising from μ [10]. In fact, the following condition characterizes this scheme,

$$\mu \ll M_D \ll M \, . \tag{1.80}$$

This "inverse" behavior of μ induces the name inverse seesaw to this mechanism.

For the sake of clarity, again we can translate Eq. (1.78) in terms of Yukawa couplings and vevs in order to illustrate the mass generation [4, 18] as it can be seen in Fig. 1.4. We obtain

$$\mathcal{M}_\nu = \begin{pmatrix} 0 & Y_\nu \langle \Phi \rangle & 0 \\ Y_\nu^T \langle \Phi \rangle & 0 & M \\ 0 & M^T & \mu \end{pmatrix} \tag{1.81}$$

for the inverse seesaw mass matrix, Eq. (1.78). From this mass matrix, the light neutrino mass is expressed as

$$m_\nu = \langle \Phi \rangle^2 Y_\nu (M^T)^{-1} \, \mu \, M^{-1} Y_\nu^T \, . \tag{1.82}$$

[10] The neutrino mass disappears when $\mu \to 0$.

1.4.3 Linear seesaw

An alternative description of the seesaw mechanism arises from a $SO(10)$ unified model [22]. It is based on the same basis as inverse seesaw, ν_L, N_L^c and S_L, but the seesaw mass matrix obtained after the rupture of the extended gauge structure is

$$M_\nu = \begin{pmatrix} 0 & M_D & M_L \\ M_D^T & 0 & M_R \\ M_L^T & M_R^T & 0 \end{pmatrix} , \tag{1.83}$$

giving rise to the following effective neutrino mass:

$$m_\nu = M_D(M_L M_R^{-1})^T + (M_L M_R^{-1})M_D^T . \tag{1.84}$$

It is worth noting that if $M_L \to 0$, the three light neutrinos become massless, recovering the SM.

Again, in order to shed light to the origin of neutrino mass, we rewrite Eq. (1.83) as

$$\mathcal{M}_\nu = \begin{pmatrix} 0 & Y_\nu\langle\Phi\rangle & F\langle\chi_L\rangle \\ Y_\nu^T\langle\Phi\rangle & 0 & \tilde{F}\langle\chi_R\rangle \\ F^T\langle\chi_L\rangle & \tilde{F}^T\langle\chi_R\rangle & 0 \end{pmatrix} , \tag{1.85}$$

leading to the following light neutrino mass:

$$m_\nu \simeq \frac{\langle\Phi\rangle^2}{M_{unif}} \left[Y_\nu(F\tilde{F}^{-1})^T + (F\tilde{F}^{-1})Y_\nu^T \right] , \tag{1.86}$$

where M_{unif} indicates the unification scale and F and $\tilde{F}$ represent independent combinations of Yukawa coupling of S_L.

One can observe that Eqs. (1.84) and (1.86) are linear in the Yuakawa couplings of Dirac neutrinos. This is the reason why this description is called *linear seesaw*.

1.4.4 Left-right symmetric model

Left-right symmetric models are based on the $SU(3) \times SU(2)_L \times SU(2)_R \times U(1)_{B-L}$ structure and are characterized by the parity conservation of weak interactions. It implies that each left-handed fermion must have a right-handed partner, that is, ν_L and N_R for the neutrino sector. This scenario generates a seesaw mass matrix as in Eq. (1.72), with

the following expression in terms of Yukawa couplings and vacuum expected values:

$$\mathcal{M}_\nu = \begin{pmatrix} Y_L\langle\Delta_L\rangle & Y_\nu\langle\Phi\rangle \\ Y_\nu^T\langle\Phi\rangle & Y_R\langle\Delta_R\rangle \end{pmatrix} . \tag{1.87}$$

As in the previous models, the basis is defined by ν_L and N_L^c; $Y_{L,R}$ indicate the left-right Yukawa couplings and $\langle\Delta_{L,R}\rangle$ are the vevs producing the left-right Majorana mass terms.

The matrix $\mathcal{M}_\nu$ can be diagonalized using a perturbative method [17], getting the following expression for light neutrino masses:

$$m_\nu \approx Y_L\langle\Delta_L\rangle - Y_\nu Y_R^{-1} Y_\nu^T \frac{\langle\Phi\rangle^2}{\langle\Delta_R\rangle} . \tag{1.88}$$

It is important to reiterate that the main idea of these models is that the smallness of neutrino mass is induced through the exchange of a heavy singlet right-handed neutrino (Type-I) or a heavy scalar boson (Type-II).

1.4.5 Radiative models

Neutrino masses can be also produced as a consequence of radiative corrections [23]. For instance, in the Babu model they can appear at two-loop level [24] with this expression:

$$\mathcal{M}_\nu \sim \lambda_0 \left(\frac{1}{16\pi^2}\right)^2 f Y_l h Y_l f^T \frac{\langle\Phi\rangle^2}{(m_k)^2}\langle\sigma\rangle . \tag{1.89}$$

Here, it is introduced a doubly-charged scalar k^{++} that is much heavier than h^+, l indicates a charged lepton, f, h and Y_l represent the Yukawa couplings and $\langle\sigma\rangle$ is a vev of a $SU(3) \times SU(2) \times U(1)$ singlet [25].

More details can be found in Refs. [23–25].

1.4.6 Supersymmetry as origin of neutrino mass

Low-energy supersymmetry can generate neutrino masses [26] by means of the R-parity symmetry rupture, which produces lepton number violation. This could occur spontaneously thanks to an $SU(3) \times SU(2) \times U(1)$ singlet sneutrino, which yields a non zero vev [27–29]. The general expression related with this kind of models is given by the following approximation:

$$\mathcal{M}_\nu \sim \left(\frac{1}{16\pi^2}\right) \langle\Phi\rangle^2 \frac{A}{m_0} Y_d Y_d . \tag{1.90}$$

For an extensive description of supersymmetry as origin of neutrino mass, please see Refs. [30, 31].

1.5 Neutrino oscillations in vacuum

Neutrino oscillations are the most sensitive evidence of neutrino mass and, therefore, that physics beyond the Standard Model is needed. The idea of neutrino oscillations is very simple and was introduced by Pontecorvo in 1957 [32, 33].

Neutrinos are produced as flavor eigenstates as a result of charged-current weak interactions. The neutrino hamiltonian in this basis is not diagonal. This fact makes a difference between the flavor states, ν_e, ν_μ and ν_τ, and the mass states, ν_1, ν_2 and ν_3. Thus, since the flavor states are a combination of the mass states (Eq. (1.92)), the probability of finding a neutrino with the same flavor state that was created oscillates with time, because the mass states evolve as

$$|\nu_i(t)\rangle = e^{-iE_i t}|\nu_i(0)\rangle\,. \tag{1.91}$$

This phenomenon is called *neutrino oscillations*.

For their detection, let us consider, for instance, a pion beam decaying into a muon and a muon-neutrino ($\pi^\pm \to \mu^\pm + \nu_\mu(\bar{\nu}_\mu)$). Although only muon-neutrinos are produced initially, some electrons can be registered in the detector. This result is obtained because some muon-neutrinos have oscillated to electron-neutrinos producing electrons via charged-current weak interactions.

A similar phenomenon was detected by the Super-Kamiokande Collaboration in June of 1998 [1] when reported the muon-neutrino disappearance ($\nu_\mu \to \nu_\tau$) from their atmospheric neutrino data, providing the first evidence of neutrino oscillations [34]. In subsequent years, several experiments have evidenced the neutrino oscillation phenomenon as SNO [35, 36], which measured the solar neutral neutrino flux through neutral and charged-current weak interactions, establishing the conversion of electron-neutrinos into muon and tau-neutrinos, or KamLAND [37] that confirmed neutrino oscillations at the solar sector. Finally, the oscillations of atmospheric neutrinos were also confirmed at the long baseline accelerator experiments as K2K [38], T2K [39–41] and MINOS [42–44].

1.5.1 The neutrino oscillation probability in vacuum

Let us start considering that there are n flavor eigenstates, ν_α, which are connected with n mass eigenstates ν_i, through the relations [10, 12]

$$|\nu_\alpha\rangle = \sum_i U^*_{\alpha i}|\nu_i\rangle\,, \qquad |\nu_i\rangle = \sum_\alpha U_{\alpha i}|\nu_\alpha\rangle\,, \tag{1.92}$$

where greek indices represent flavor states and latin indices mass eigensates. U is the neutrino mixing matrix, also known as Maki-Nakagawa-Sakata (MNS) matrix for the three-neutrino case [11], and it satisfies the following properties:

$$U^\dagger U = 1\,, \qquad \sum_i U_{\alpha i}U^*_{\beta i} = \delta_{\alpha\beta}\,, \qquad \sum_\alpha U_{\alpha i}U^*_{\alpha j} = \delta_{ij}. \tag{1.93}$$

For the case of n active neutrinos, U is a $n \times n$ matrix characterized by $n(n-1)/2$ Euler angles and $n(n+1)/2$ phases. If we are considering Dirac neutrinos, the number of physical phases is $(n-1)(n-2)/2$, being responsible of CP violation in the lepton sector. However, if neutrinos have Majorana nature the matrix U contains $n(n-1)/2$ CP violation phases. Then, in general, the U matrix can be written as

$$U = VP, \tag{1.94}$$

where V is a matrix containing the Dirac phases, and P is a diagonal matrix including $(n-1)$ Majorana phases $(\beta_1, \beta_2, \beta_3, \ldots, \beta_{n-1})$ in the form

$$P = diag(1, e^{i\beta_1}, e^{i\beta_2}, ..., e^{i\beta_{n-1}})\,. \tag{1.95}$$

For example, with $n = 3$ (usual number of light active neutrinos) we find one Dirac phase and two Majorana phases, all three associated with CP violation.

Let us assume that a flavor state $|\nu_\alpha\rangle$ has been produced in $t = 0$. What is the probability of finding a neutrino in a flavor state $|\nu_\beta\rangle$ after a time t? We should follow the evolution of the system in order to answer this question. The initial state of the produced neutrino is

$$|\nu(x,0)\rangle = |\nu_\alpha\rangle = \sum_i U^*_{\alpha i}|\nu_i\rangle\,; \tag{1.96}$$

[11] An explicit expression of this matrix is given in Sec. 1.5.3 and Refs. [7, 9, 45].

and after evolving a time t,

$$|\nu(x,t)\rangle = \sum_i U^*_{\alpha i} e^{-iE_i t}|\nu_i\rangle = \sum_{i,\beta} U^*_{\alpha i} U_{\beta i} e^{ip_i x} e^{-iE_i t}|\nu_\beta\rangle\,, \tag{1.97}$$

where p_i is the momentum of the emitted neutrino and Eq. (1.92) has been used.

Therefore, the probability amplitude of finding a neutrino at a time t in the flavor state $|\nu_\beta\rangle$ is given by

$$A(\nu_\alpha \to \nu_\beta; t) = \langle\nu_\beta|\nu(x,t)\rangle = \sum_i U^*_{\alpha i} U_{\beta i} e^{ip_i x} e^{-iE_i t}\,. \tag{1.98}$$

Considering the emitted neutrino as a relativistic particle, $p_i \gg m_i$, we can do the following approximation,

$$E_i = \sqrt{m_i^2 + p_i^2} \simeq p_i + \frac{m_i^2}{2p_i} \simeq E + \frac{m_i^2}{2E}, \tag{1.99}$$

obtaining

$$A(\nu_\alpha \to \nu_\beta; t) = \sum_i U^*_{\alpha i} U_{\beta i} \exp\left(-i\frac{m_i^2}{2}\frac{L}{E}\right) = A(\nu_\alpha \to \nu_\beta; L)\,. \tag{1.100}$$

Here, it is considered $t \simeq x = L$ since relativistic neutrinos travel at nearly the speed of light, being L the distance to the detector [12]. From Eq. (1.100), we can find the expression for the transition probability [12]:

$$\begin{aligned} P_{\nu_\alpha \to \nu_\beta}(L,E) &= |A(\alpha \to \beta; t)|^2 = \sum_{i,j} U^*_{\alpha i} U_{\alpha j} U_{\beta i} U^*_{\beta j} e^{-i(E_j - E_i)t} \\ &= \sum_i |U^*_{\alpha i}|^2 |U_{\beta i}|^2 + 2\sum_{i>j} Re\left[U^*_{\alpha i} U_{\alpha j} U_{\beta i} U^*_{\beta j}\right] \exp\left(-i\frac{\Delta m^2_{ij} L}{2E}\right)\,, \end{aligned} \tag{1.101}$$

with the mass difference defined as

$$\Delta m^2_{ij} = m_i^2 - m_j^2. \tag{1.102}$$

At this point, we should do some remarks about the expression of the oscillation probability, Eq. (1.101):

- If $L \gg 2E/\Delta m^2_{ij}$, the oscillatory term is averaged giving rise to a constant conversion probability.

[12] Notice that we are using natural units, $\hbar = c = 1$.

- At least one mass splitting has to be different from zero, $\Delta m^2_{ij} \neq 0$, which implies that two neutrinos have to be massive in order to observe oscillations among three neutrinos.

- The mixing among neutrinos is necessary in order to have oscillations, so the off-diagonal elements of U must be different from zero.

- The oscillation probability is the same if we consider Dirac neutrinos or Majorana neutrinos. In particular, this means that we can not distinguish between Dirac and Majorana neutrinos by studying neutrino oscillations.

- From the unitarity of the matrix U, we have that

$$\sum_{\beta=e,\mu,\tau} P(\alpha \to \beta; t) = \sum_{\beta=e,\mu,\tau} P(\bar{\alpha} \to \bar{\beta}; t) = 1. \tag{1.103}$$

A more useful way to write the oscillation probability in Eq (1.101) is separating the real and imaginary parts of the product of matrices $\left[U^*_{\alpha i} U_{\alpha j} U_{\beta i} U^*_{\beta j}\right]$, through the unitarity condition

$$\sum_i |U_{\alpha i}|^2 |U_{\beta i}|^2 = \delta_{\alpha\beta} - 2 \sum_{i>j} Re\left[U^*_{\alpha i} U_{\alpha j} U_{\beta i} U^*_{\beta j}\right] . \tag{1.104}$$

From the above equation, we can rewrite the oscillation probability as

$$\begin{aligned} P_{\nu_\alpha \to \nu_\beta}(L,E) = \delta_{\alpha\beta} \quad &- \quad 2 \sum_{i>j} Re\left[U^*_{\alpha i} U_{\alpha j} U_{\beta i} U^*_{\beta j}\right] \left[1 - \cos\left(\frac{\Delta m^2_{ij} L}{2E}\right)\right] \\ &+ \quad 2 \sum_{i>j} Im\left[U^*_{\alpha i} U_{\alpha j} U_{\beta i} U^*_{\beta j}\right] \sin\left(\frac{\Delta m^2_{ij} L}{2E}\right). \end{aligned} \tag{1.105}$$

And using some simple algebra we get the most usual expression [10, 12]:

$$\begin{aligned} P_{\nu_\alpha \to \nu_\beta}(L,E) = \delta_{\alpha\beta} \quad &- \quad 4 \sum_{i>j} Re\left[U^*_{\alpha i} U_{\alpha j} U_{\beta i} U^*_{\beta j}\right] \sin^2\left(\frac{\Delta m^2_{ij} L}{4E}\right) \\ &+ \quad 2 \sum_{i>j} Im\left[U^*_{\alpha i} U_{\alpha j} U_{\beta i} U^*_{\beta j}\right] \sin\left(\frac{\Delta m^2_{ij} L}{2E}\right). \end{aligned} \tag{1.106}$$

Antineutrino oscillations

The derivation of the oscillation probability for antineutrinos is straightforward following the same steps as for neutrinos. In analogy with the neutrino case, we can define the

antineutrino flavor states as

$$|\bar{\nu}_\alpha\rangle = \sum_i U_{\alpha i}|\bar{\nu}_i\rangle\,. \tag{1.107}$$

If we use Eq. (1.107), we obtain the same expressions that in Eqs. (1.101), (1.105) or (1.106), only taking into account that $U_{\alpha j} \to U^*_{\alpha j}$ and $U_{\beta i} \to U^*_{\beta i}$,

$$\begin{aligned} P_{\bar{\nu}_\alpha\to\bar{\nu}_\beta}(L,E) = \delta_{\alpha\beta} \;&-\; 4\sum_{i>j} Re\left[U_{\alpha i}U^*_{\alpha j}U^*_{\beta i}U_{\beta j}\right]\,\sin^2\left(\frac{\Delta m^2_{ij}L}{4E}\right) \\ &+\; 2\sum_{i>j} Im\left[U_{\alpha i}U^*_{\alpha j}U^*_{\beta i}U_{\beta j}\right]\,\sin\left(\frac{\Delta m^2_{ij}L}{2E}\right). \end{aligned} \tag{1.108}$$

CP, T and CPT implications

The CP transformation interchanges neutrinos with positive helicity to antineutrinos with negative helicity, connecting the oscillation channels,

$$\nu_\alpha \to \nu_\beta \Longleftrightarrow \bar{\nu}_\alpha \to \bar{\nu}_\beta\,. \tag{1.109}$$

After this transformation we obtain Eq. (1.108) from Eq. (1.106). In general, the mixing matrix is complex and contains phases, which could lead to CP symmetry violation. Such violation can be measured in neutrino oscillation experiments as

$$A^{CP}_{\alpha\beta} = P_{\nu_\alpha\to\nu_\beta} - P_{\bar{\nu}_\alpha\to\bar{\nu}_\beta}\,. \tag{1.110}$$

On the other hand, the T symmetry interchanges the initial and final states of a given processes and therefore relates the oscillation channels,

$$\begin{aligned} \nu_\alpha \to \nu_\beta \;&\Longleftrightarrow\; \nu_\beta \to \nu_\alpha\,, \\ \bar{\nu}_\alpha \to \bar{\nu}_\beta \;&\Longleftrightarrow\; \bar{\nu}_\beta \to \bar{\nu}_\alpha\,. \end{aligned} \tag{1.111}$$

T symmetry violation can be also observed in neutrino oscillation experiments through the observables

$$\begin{aligned} A^T_{\alpha\beta} &= P_{\nu_\alpha\to\nu_\beta} - P_{\nu_\beta\to\nu_\alpha}\,, \\ \bar{A}^T_{\alpha\beta} &= P_{\bar{\nu}_\alpha\to\bar{\nu}_\beta} - P_{\bar{\nu}_\beta\to\bar{\nu}_\alpha}\,. \end{aligned} \tag{1.112}$$

Finally, if we apply both transformations at the same time, we get the CPT transfor-

mation,

$$\nu_\alpha \to \nu_\beta \Longleftrightarrow \bar{\nu}_\beta \to \bar{\nu}_\alpha \,, \tag{1.113}$$

which is expected to be conserved as an underlying principle of the Standard Model:

$$P_{\nu_\alpha \to \nu_\beta} = P_{\bar{\nu}_\beta \to \bar{\nu}_\alpha} \,. \tag{1.114}$$

1.5.2 Oscillations with two neutrinos

The most simple illustration of neutrino oscillations considers only two flavor states: ν_e and ν_μ for example, with their two corresponding mass states, ν_1 and ν_2. In this approximation, the mixing matrix U is a 2×2 matrix given by

$$U = \begin{pmatrix} \cos\theta & \sin\theta \\ -\sin\theta & \cos\theta \end{pmatrix} , \tag{1.115}$$

where θ is the mixing angle. From Eq. (1.106), we get the following expression for the oscillation probability in the appearance channel,

$$\begin{aligned} P(\nu_e \to \nu_\mu) &= P(\nu_\mu \to \nu_e) = P(\bar{\nu}_e \to \bar{\nu}_\mu) = P(\bar{\nu}_\mu \to \bar{\nu}_e) \\ &= \sin^2 2\theta \, \sin^2 \left(\frac{\Delta m^2 L}{4E} \right) , \end{aligned} \tag{1.116}$$

whereas for the disappearance channel we have the following survival probability,

$$P(\nu_e \to \nu_e) = 1 - P(\nu_e \to \nu_\mu) \,, \tag{1.117}$$

as we can derive from Eq. (1.103).

Sometimes, it is convenient to write the probability Eq. (1.116) in the following form:

$$P(\nu_\alpha \to \nu_\beta) = \sin^2 2\theta \, \sin^2 \left(1.27 \, \frac{\Delta m^2 L}{E} \right) , \tag{1.118}$$

where natural units have been used ($\hbar = c = 1$) and the 1.27 factor follows from the conversion of km into eV^{-1}, with Δm^2 and E given in eV^2 and GeV respectively.

At this point, we should do a reflexion: why is the study of the two-neutrino case useful if we know the existence of three neutrinos at least?

- The oscillation probability of two-neutrino case is much simpler than three neutrinos.

- Many experiments are not sensitive to all mass-splittings and mixing angles, so the data can be analyzed by considering the two-neutrino approximation, as we will see in Sec. 1.5.3.

1.5.3 Oscillations with three neutrinos

In this section, we will introduce the oscillation mechanism for three generations of neutrinos, the standard number of light active neutrinos. For this purpose, we start providing a parameterization for the lepton mixing matrix $U^{3\times3}$, considering it unitary [13]. It is a 3×3 matrix which can be written, using the Okubo's notation [46], as a product of three complex rotations:

$$\begin{pmatrix} 1 & 0 & 0 \\ 0 & c_{23} & e^{-i\phi_{23}}s_{23} \\ 0 & -e^{i\phi_{23}}s_{23} & c_{23} \end{pmatrix} \begin{pmatrix} c_{13} & 0 & e^{-i\phi_{13}}s_{13} \\ 0 & 1 & 0 \\ -e^{i\phi_{13}}s_{13} & 0 & c_{13} \end{pmatrix} \begin{pmatrix} c_{12} & e^{-i\phi_{12}}s_{12} & 0 \\ -e^{i\phi_{12}}s_{12} & c_{12} & 0 \\ 0 & 0 & 1 \end{pmatrix}, \tag{1.119}$$

where c_{ij} and s_{ij} represents $\cos\theta_{ij}$ and $\sin\theta_{ij}$ respectively. Eq. (1.119) leads to the symmetrical representation of the lepton mixing matrix [14] [9, 45]

$$\begin{pmatrix} c_{12}c_{13} & s_{12}c_{13}e^{-i\phi_{12}} & s_{13}e^{-i\phi_{13}} \\ -s_{12}c_{23}e^{i\phi_{12}} - c_{12}s_{23}s_{13}e^{-i(\phi_{23}-\phi_{13})} & c_{12}c_{23} - s_{12}s_{23}s_{13}e^{-i(\phi_{12}+\phi_{23}-\phi_{13})} & s_{23}c_{13}e^{-i\phi_{23}} \\ s_{12}s_{23}e^{i(\phi_{12}+\phi_{23})} - c_{12}c_{23}s_{13}e^{i\phi_{13}} & -c_{12}s_{23}e^{i\phi_{23}} - s_{12}c_{23}s_{13}e^{-i(\phi_{12}-\phi_{13})} & c_{23}c_{13} \end{pmatrix}. \tag{1.120}$$

This symmetric parameterization is equivalent to the PDG [7] description of U,

$$\begin{pmatrix} c_{12}c_{13} & s_{12}c_{13} & s_{13}e^{-i\delta} \\ -s_{12}c_{23} - c_{12}s_{23}s_{13}e^{i\delta} & c_{12}c_{23} - s_{12}s_{23}s_{13}e^{i\delta} & s_{23}c_{13} \\ s_{12}s_{23} - c_{12}c_{23}s_{13}e^{i\delta} & -c_{12}s_{23} - s_{12}c_{23}s_{13}e^{i\delta} & c_{23}c_{13} \end{pmatrix} \times \mathrm{diag}(1, e^{i\beta_1}, e^{i\beta_2}), \tag{1.121}$$

where δ is the Dirac CP violation phase and β_1 and β_2 are the phases associated to Majorana neutrinos. The connection between Eq. (1.120) and Eq. (1.121) is given by the

[13] This is not a general condition since in extended models, where more than 3 neutrinos are considered, the lepton mixing matrix involving three active neutrinos is not unitary, as we will see in chapter 5.

[14] We want to emphasize this parameterization of the lepton mixing matrix U because it will be used later in chapter 5, since it is more intuitive in order to work with more than three neutrinos.

following relation of phases:

$$\begin{aligned} \delta &= \phi_{13} - \phi_{12} - \phi_{23} \\ \beta_1 &= \phi_{12} \\ \beta_2 &= \phi_{12} + \phi_{23} \end{aligned} \tag{1.122}$$

Although the mixing matrix has been written in Eq. (1.120) using all physical phases ϕ_{ij}, only one combination of them can be observed in neutrino oscillation experiments [45]:

$$I_{123} = \phi_{12} + \phi_{23} - \phi_{13} = -\delta\,. \tag{1.123}$$

Obtaining the expression of the neutrino oscillation probability in the case of three families is straightforward from Eq. (1.106), taking into account that latin indices go from 1 to 3, and there are only two independent mass-splittings, Δm^2_{21} and Δm^2_{31}. With these considerations we finally get:

$$\begin{aligned} P(\nu_\alpha \to \nu_\beta) = \delta_{\alpha\beta} \;&-\; 4 \sum_{i>j=1}^{3} Re\left[U^*_{\alpha i} U_{\alpha j} U_{\beta i} U^*_{\beta j}\right] \sin^2\left(\frac{\Delta m^2_{ij} L}{4E}\right) \\ &+\; 2 \sum_{i>j=1}^{3} Im\left[U^*_{\alpha i} U_{\alpha j} U_{\beta i} U^*_{\beta j}\right] \sin\left(\frac{\Delta m^2_{ij} L}{2E}\right)\,. \end{aligned} \tag{1.124}$$

This is the most general expression of the neutrino oscillation probability in vacuum for three generations. But in particular, we can reduce this expression to a case of two-neutrino flavors, as we commented in Sec. 1.5.2. For instance, for some atmospheric, reactor and accelerator neutrino experiments we can assume that

$$\frac{\Delta m^2_{21}}{2E} L \ll 1\,, \tag{1.125}$$

giving rise to a two-neutrino probability [47]:

$$P_{\nu_\alpha \to \nu_\beta}(L, E) = 4 |U_{\alpha 3}|^2 |U_{\beta 3}|^2 \sin^2\left(\frac{\Delta m^2_{31}}{4E} L\right)\,. \tag{1.126}$$

For the sake of completeness, we consider another limiting case concerning solar neutrinos and long baseline reactor experiments (as KamLAND [37]), where it is assumed that

$$\frac{\Delta m^2_{31}}{2E} L \simeq \frac{\Delta m^2_{32}}{2E} L \gg 1\,. \tag{1.127}$$

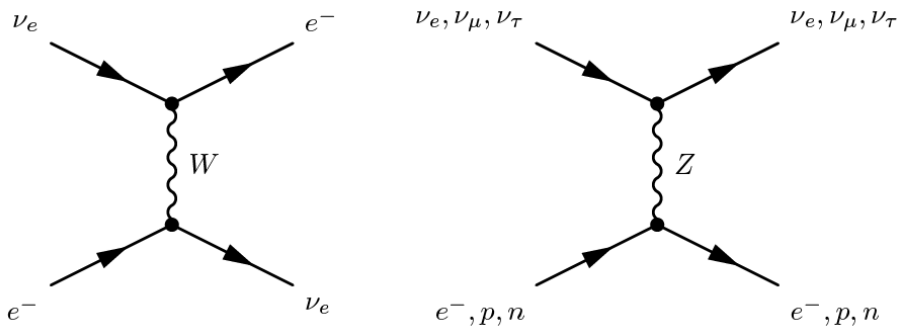

Figure 1.5: Feynman diagrams of neutrino interactions in matter.

In this case, the oscillations related to the large mass splittings, Δm^2_{31} and Δm^2_{32}, are very fast, so they can be averaged. Thus, the survival probability presents the following form [47]:

$$P_{\nu_e \to \nu_e}(L, E) \simeq \cos^4 \theta_{13} P_2 + \sin \theta^4_{13} \,, \tag{1.128}$$

where P_2 is the ν_e survival probability in the case of two neutrinos:

$$P_2 = 1 - \sin^2 2\theta_{12} \sin^2 \left(\frac{\Delta m^2_{21}}{4E} L \right) . \tag{1.129}$$

1.6 Neutrino oscillations in matter

Neutrinos propagating in matter are subject to interactions with particles in the medium. They can be absorbed by the matter constituents, or suffer coherent and incoherent scattering in their way through matter. These interactions are encoded in an effective potential which depends on the density of fermions in the medium and modifies the mixing of neutrinos, leading to an effective mixing angle in matter which can be large even for small values of the vacuum mixing angle. Thus, matter can enhance the flavor conversion of neutrinos, giving rise to a resonant effect under certain conditions of medium density and neutrino energy. This is known as the Mikheyev-Smirnov-Wolfenstein (MSW) effect [12, 48, 49] and it explains the so-called solar neutrino problem [47, 50–55]. We will be back to this effect in the following lines.

1.6.1 Neutrino evolution in matter

In their trip through matter, neutrinos interact with fermions by means of neutral-current weak interactions (NC) regardless of their flavor, but only electron-neutrinos do it with

electrons through charged-current weak interactions (CC), as we can see in Fig. 1.5.

In the case of electron-neutrinos interacting with electrons through CC, the effective hamiltonian has the following expression:

$$H_{CC} = \frac{G_F}{\sqrt{2}} \left[\bar{e}\gamma_\mu(1-\gamma_5)\nu_e\right] \left[\bar{\nu}_e\gamma^\mu(1-\gamma_5)e\right] , \tag{1.130}$$

where G_F is the Fermi constant [15]. After a Fierz transformation [11, 12, 57, 58] we obtain:

$$H_{CC} = \frac{G_F}{\sqrt{2}} \left[\bar{e}\gamma_\mu(1-\gamma_5)e\right] \left[\bar{\nu}_e\gamma^\mu(1-\gamma_5)\nu_e\right] . \tag{1.131}$$

The effective potential V_{CC} is given by

$$V_{CC} = \langle\nu_e| \int d\vec{x}\, H_{CC}(\vec{x}) |\nu_e\rangle \, . \tag{1.132}$$

After solving this integral [11, 12], we get

$$V_{CC} = \sqrt{2}\, G_F N_e \, , \tag{1.133}$$

with N_e being the electron number density in the medium. Similarly, we can proceed in order to calculate the NC contributions to the potential (V_{NC}), considering, in this case, all neutrino flavors in Fig. 1.5. Again, we start with the neutral-current effective hamiltonian,

$$H_{NC} = \frac{G_F}{\sqrt{2}} \sum_{\alpha=e,\mu,\tau} \left[\bar{\nu}_\alpha\gamma^\mu(1-\gamma_5)\nu_\alpha\right] \sum_{f=e,n,p} \left[\bar{f}\gamma_\mu(g_V^f - g_A^f\gamma_5)f\right] , \tag{1.134}$$

where g_V^f and g_A^f are the vector and axial coupling constants of the Standard Model respectively. In an electrically neutral medium, contributions coming from protons and electrons are canceled, so they have no influence on the potential V_{NC}:

$$\begin{aligned} g_V^e &= -\frac{1}{2} + 2\sin^2\theta_W \, , \\ g_V^p &= \frac{1}{2} - 2\sin^2\theta_W \, , \\ g_V^n &= -\frac{1}{2} \, . \end{aligned} \tag{1.135}$$

[15] Notice that Eq. (1.130) is related to Eqs. (1.16) and (1.19) considering $G_F \equiv \frac{\sqrt{2}}{8}\left(\frac{g}{M_W}\right)^2$ [56] in natural units.

Therefore, the matter potential due to neutral-current weak interactions is given by [11, 12]

$$V_{NC} = -\frac{1}{2}\sqrt{2}G_F N_n \,, \tag{1.136}$$

where N_n is the neutron number density. Then, considering all contributions, the matter potential for each type of neutrino will be expressed as follows:

$$V_{\nu_e} = V_{CC} + V_{NC} = \sqrt{2}G_F\left(N_e - \frac{N_n}{2}\right) , \tag{1.137}$$

$$V_{\nu_\mu} = V_{\nu_\tau} = V_{NC} = \sqrt{2}G_F\left(-\frac{N_n}{2}\right) . \tag{1.138}$$

Notice that, since antineutrinos have opposite isospin, we have to change $V_{\nu_\alpha} \to -V_{\bar{\nu}_\alpha}$.

Let us now consider the evolution of neutrinos in matter, starting with the most simple scheme of two neutrinos. The evolution equation for neutrinos in vacuum in the flavor basis [16] is given by

$$i\frac{d}{dt}\begin{pmatrix}\nu_e\\ \nu_\mu\end{pmatrix} = U\begin{pmatrix}E_1 & 0\\ 0 & E_2\end{pmatrix}U^\dagger\begin{pmatrix}\nu_e\\ \nu_\mu\end{pmatrix} , \tag{1.139}$$

$$i\frac{d}{dt}\begin{pmatrix}\nu_e\\ \nu_\mu\end{pmatrix} = \begin{pmatrix}-\frac{\Delta m^2}{4E}\cos 2\theta & \frac{\Delta m^2}{4E}\sin 2\theta\\ \frac{\Delta m^2}{4E}\sin 2\theta & \frac{\Delta m^2}{4E}\cos 2\theta\end{pmatrix}\begin{pmatrix}\nu_e\\ \nu_\mu\end{pmatrix} . \tag{1.140}$$

In order to derive the neutrino evolution in matter we have to introduce the matter potentials affecting ν_e and ν_μ:

$$i\frac{d}{dt}\begin{pmatrix}\nu_e\\ \nu_\mu\end{pmatrix} = \begin{pmatrix}-\frac{\Delta m^2}{4E}\cos 2\theta + V_{CC} & \frac{\Delta m^2}{4E}\sin 2\theta\\ \frac{\Delta m^2}{4E}\sin 2\theta & \frac{\Delta m^2}{4E}\cos 2\theta\end{pmatrix}\begin{pmatrix}\nu_e\\ \nu_\mu\end{pmatrix} . \tag{1.141}$$

Note that the neutral-current potential V_{NC} does not appear because it is common to electron-neutrinos and muon-neutrinos. Therefore, it does not modify the Schrödinger equation (Eq. (1.141)) and can be absorbed [17].

[16] For the case with matter, it is more convenient to use the flavor basis because the effective potentials are diagonal in this basis.

[17] Having $i\dot{\psi} = H\psi$, we can add a phase to each diagonal term of H, such that $H' = H + \alpha$. In this case, if we define $\psi' = e^{-i\alpha t}\psi$ we can find easily that $i\dot{\psi}' = H\psi' \iff i\dot{\psi} = H\psi$.

1.6.2 Oscillations in a medium of constant density

After deriving the hamiltonian in matter, further assumptions can be made in order to simplify the study of matter effects in neutrino oscillations. For instance, we can consider that the matter density is constant, i.e. $N_e = constant$.

After the diagonalization of the effective hamiltonian in matter, we find the following mass eigenstates:

$$\begin{aligned} \nu_1^m &= \nu_e \cos\theta_m + \nu_\mu \sin\theta_m \\ \nu_2^m &= -\nu_e \sin\theta_m + \nu_\mu \cos\theta_m \,, \end{aligned} \tag{1.142}$$

where θ_m is the mixing angle in matter, related with the vacuum mixing parameters by

$$\tan 2\theta_m = \frac{\frac{\Delta m^2}{2E}\sin 2\theta}{\frac{\Delta m^2}{2E}\cos 2\theta - \sqrt{2}\,G_F N_e} \,. \tag{1.143}$$

Finally, the oscillation probability in a medium of constant density has the following expression:

$$P^m_{\nu_e\to\nu_\mu} = \sin^2 2\theta_m \sin^2\left(\frac{\Delta m^2_{matt}}{4E}L\right) \,, \tag{1.144}$$

with the energy difference given by

$$E_1^m - E_2^m = \frac{\Delta m^2_{matt}}{2E} = \left[\left(\frac{\Delta m^2}{2E}\cos 2\theta - \sqrt{2}\,G_F N_e\right)^2 + \left(\frac{\Delta m^2}{2E}\right)^2 \sin^2 2\theta\right]^{1/2} \,. \tag{1.145}$$

Note that the probability in matter of constant density, Eq. (1.144), is analogous to the probability in vacuum, Eq. (1.116), considering the mixing parameters in matter, Eqs. (1.143) and (1.145).

Let us mention a special condition in a few lines. As it is derived from the oscillation amplitude,

$$\sin^2 2\theta_m = \frac{\left(\frac{\Delta m^2}{2E}\right)^2 \sin^2 2\theta}{\left(\frac{\Delta m^2}{2E}\cos 2\theta - \sqrt{2}\,G_F N_e\right)^2 + \left(\frac{\Delta m^2}{2E}\right)^2 \sin^2 2\theta} \,, \tag{1.146}$$

a resonance effect is produced when the condition

$$V_R \equiv \sqrt{2}\,G_F N_e^R = \frac{\Delta m^2}{2E}\cos 2\theta \tag{1.147}$$

is satisfied, being N_e^R the electron density at the resonance point and V_R the resonance

potential. This is known as the *Mikheyev-Smirnov-Wolfenstein (MSW) effect* [12, 48, 49] and it explains the behavior of neutrino oscillations inside a material medium, as the Earth or the Sun.

1.6.3 Oscillations in an adiabatic medium

Let us now consider a medium where the density is variable. With this condition, Eq. (1.141) is not easy to solve and, in general, it is not possible to find an analytic solution, so numerical techniques have to be applied. However, when the density changes slowly (adiabatic medium), Eq. (1.141) can be worked out, obtaining an approximate analytic solution.

For an adiabatic medium as we have described above, the mixing angle in matter θ_m, defined in Eq. (1.143), depends on the medium density, N_e. Therefore, as neutrino travels through the adiabatic medium, θ_m changes, acquiring a time dependence $\theta_m(t)$:

$$\begin{pmatrix} \nu_e \\ \nu_\mu \end{pmatrix} = \begin{pmatrix} \cos\theta_m & \sin\theta_m \\ -\sin\theta_m & \cos\theta_m \end{pmatrix} \begin{pmatrix} \nu_1^m \\ \nu_2^m \end{pmatrix} = U(\theta_m) \begin{pmatrix} \nu_1^m \\ \nu_2^m \end{pmatrix} , \tag{1.148}$$

The evolution equation in the mass basis [11] is

$$i \begin{pmatrix} \dot{\nu}_1^m \\ \dot{\nu}_2^m \end{pmatrix} = U^\dagger(\theta_m) M_W^m U(\theta_m) \begin{pmatrix} \nu_1^m \\ \nu_2^m \end{pmatrix} - iU^\dagger(\theta_m)\dot{U}(\theta_m) \begin{pmatrix} \nu_1^m \\ \nu_2^m \end{pmatrix} , \tag{1.149}$$

where we have used,

$$\frac{d}{dt} \begin{pmatrix} \nu_e \\ \nu_\mu \end{pmatrix} = \dot{U}(\theta_m) \begin{pmatrix} \nu_1^m \\ \nu_2^m \end{pmatrix} + U(\theta_m) \begin{pmatrix} \dot{\nu}_1^m \\ \dot{\nu}_2^m \end{pmatrix} . \tag{1.150}$$

Writing Eq. (1.149) in a more suitable way, we obtain

$$i \begin{pmatrix} \dot{\nu}_1^m \\ \dot{\nu}_2^m \end{pmatrix} = \begin{pmatrix} E_1^m(t) & -i\dot{\theta}_m(t) \\ i\dot{\theta}_m(t) & E_2^m(t) \end{pmatrix} \begin{pmatrix} \nu_1^m \\ \nu_2^m \end{pmatrix} , \tag{1.151}$$

where $E_{1,2}^m(t)$ are defined in Eq. (1.145), taking into account their dependence with the variation of N_e in the adiabatic medium and, as a consequence, their time dependence. As it can be observed, there is a significative difference with respect to Eq. (1.139) since the hamiltonian is not diagonal in this case. This is due to the time dependence of θ_m in a medium where the density is not constant, changing the mass basis too. Nevertheless,

in an adiabatic medium we find that

$$|\dot{\theta}_m| \ll |E_1^m - E_2^m| \,, \tag{1.152}$$

then the off-diagonal terms in the evolution equation, Eq. (1.151), are small and can be neglected. This is called the *adiabatic approximation*, and it can be used when the *adiabatic condition* [11, 47],

$$\frac{1}{\gamma} \equiv \frac{2|\dot{\theta}_m|}{|E_1^m - E_2^m|} = \frac{\frac{\Delta m^2}{2E}\sin 2\theta}{|E_1^m - E_2^m|^3}|\dot{V}_{CC}| \ll 1 \,, \tag{1.153}$$

is satisfied. Here, γ is the adiabaticity parameter, with $|E_1^m - E_2^m|$ and V_{CC} defined by Eqs. (1.145) and (1.133) respectively.

In order to achieve a better understanding of the adiabatic case, an illustrative example will be very useful. As starting point, we consider the usual description of neutrino mixing in a two flavor scheme:

$$\nu_e = \nu_1^m \cos\theta_m + \nu_2^m \sin\theta_m \,, \tag{1.154}$$

$$\nu_\mu = -\nu_1^m \sin\theta_m + \nu_2^m \cos\theta_m \,, \tag{1.155}$$

or their complementary expressions:

$$\nu_1^m = \nu_e \cos\theta_m - \nu_\mu \sin\theta_m \,, \tag{1.156}$$

$$\nu_2^m = \nu_e \sin\theta_m + \nu_\mu \cos\theta_m \,. \tag{1.157}$$

Under this description, an electron-neutrino ν_e is produced as initial state in a medium with very high density (the core of the Sun, for instance), which implies $V_{CC} \gg V_R$. We may redefine Eq. (1.143) as

$$\tan 2\theta_m = \frac{\tan 2\theta}{1 - \frac{V_{CC}}{V_R}} \,, \tag{1.158}$$

deriving that the matter mixing angle in the production point θ_m^i is approximately equal to $\pi/2$. Then, no neutrino mixing occurs due to the matter effect and therefore ν_e is a pure ν_2^m. As neutrino travels through matter, the density decreases, diminishing the related mixing angle in matter and giving rise to an increase in the neutrino mixing up its maximal value $\theta_m = \pi/4$, which is the value of the matter mixing angle at the resonance point ($V_{CC} = V_R$). Continuing its journey, the neutrino reaches zones with smaller density and, as a consequence, the mixing angle in matter keeps decreasing until a minimum identified with the vacuum mixing angle $\theta_m^f = \theta$, when $V_{CC} \ll V_R$. Summarizing this

example, we can say that the electron-neutrino ν_e, produced initially as ν_2^m, evolves to $\nu_e \sin\theta_0 + \nu_\mu \cos\theta_0$ during its propagation.

As it can be observed, there is no transition between the mass eigenstates ν_2^m and ν_1^m (the neutrino state remains as ν_2^m). On the other hand, a variation in the flavor composition is produced as neutrino propagates in matter because θ_m depends on the matter density, leading to the following transition probability between the two flavor eigenstates:

$$P(\nu_e \to \nu_\mu) = \cos^2\theta. \tag{1.159}$$

In a more general case, where no initial conditions are defined, we find the following expression for a newborn neutrino:

$$\nu(t_i) = \nu_e = \cos\theta_m^i \nu_1^m + \sin\theta_m^i \nu_2^m\,. \tag{1.160}$$

After propagation in matter, the final neutrino state becomes [47]

$$\nu(t_f) = \cos\theta_m^i e^{-i\int_{t_i}^{t_f} E_1^m(t')dt'} \nu_1^m + \sin\theta_m^i e^{-i\int_{t_i}^{t_f} E_2^m(t')dt'} \nu_2^m \tag{1.161}$$

at a time t_f. Keeping in mind the time dependence (due to density dependence) of θ_m, we find that the transition probability is expressed as

$$P_{\nu_e\to\nu_\mu} = \frac{1}{2} - \frac{1}{2}\cos 2\theta_m^i \cos 2\theta_m^f - \frac{1}{2}\sin 2\theta_m^i \sin 2\theta_m^f \cos\Phi\,, \tag{1.162}$$

with

$$\Phi = \int_{t_i}^{t_f} (E_1^m - E_2^m)dt'\,. \tag{1.163}$$

Notice that, if the high density initial condition and $\theta_m^f = \theta$ final condition are included in Eq. (1.162), the transition probability recovers the form of Eq. (1.159).

1.6.4 Oscillations in a non-adiabatic medium

As a final case, we will analyze the most generic case, when the adiabaticity condition is not fulfilled and the medium density does not vary softly. In this framework, where $|\dot{\theta}_m| \sim |E_1^m - E_2^m|$, transitions between the eigenstates ν_1^m and ν_2^m are allowed due to the violation of adiabaticity, giving rise to non-zero off-diagonal terms in Eq. (1.151). Under these requirements, the conversion probability in a non-adiabatic medium is given

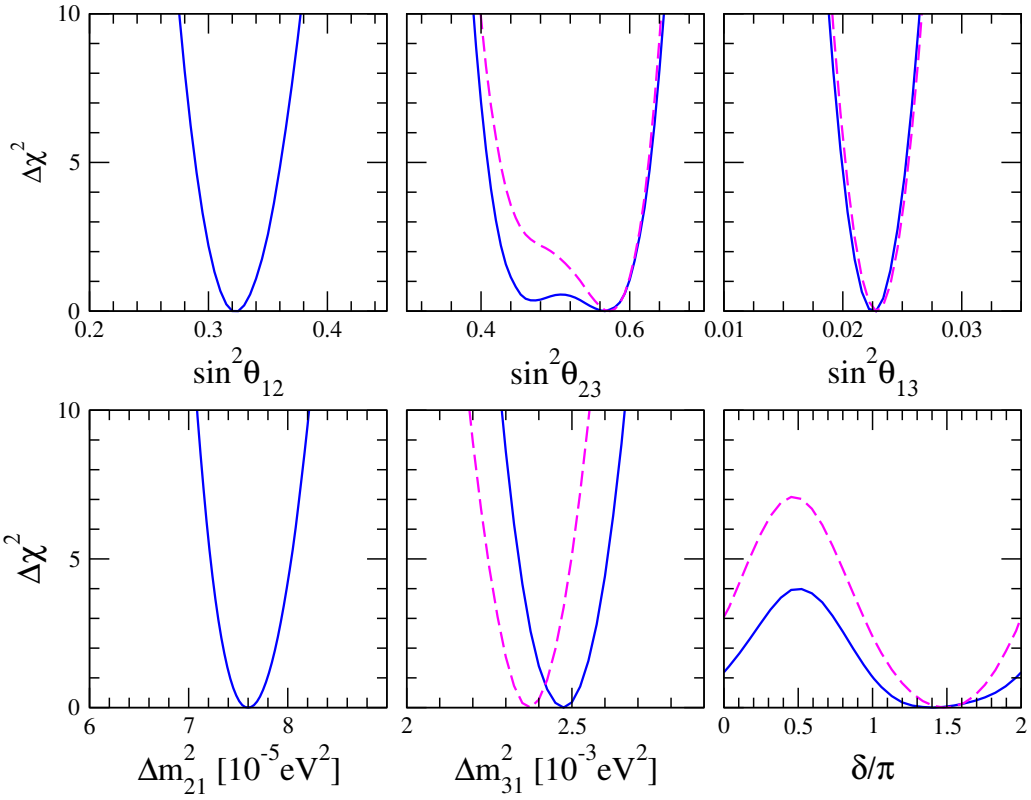

Figure 1.6: Plots stemming from the χ^2 analysis for the neutrino oscillation parameters [59].

by [11, 47]

$$P(\nu_e \to \nu_\mu) \simeq \frac{1}{2} - \frac{1}{2}\cos 2\theta_m^i \cos 2\theta_m^f (1 - 2P_{LZ})\,, \tag{1.164}$$

where P_{LZ} is the transition probability between ν_1^m and ν_2^m, known as Landau-Zener probability [11]. This probability is expressed as

$$P_{LZ} \simeq \exp\left(-\frac{\pi}{2}\gamma_r\right)\,. \tag{1.165}$$

In the above expression, γ_r stands for the adiabaticity parameter at the resonant point, given by the MSW condition Eq. (1.147), and it is presented as follows [11, 47]:

$$\gamma_r = \frac{\sin^2 2\theta}{\cos 2\theta}\frac{\Delta m^2}{2E}\left|\frac{V_{CC}}{\dot{V}_{CC}}\right|_{\rm res}\,. \tag{1.166}$$

In the adiabatic limit, $\gamma_r \gg 1$, when the Landau-Zener probability vanishes, the probability defined in Eq. (1.162) is recovered.

Table 1.3: Neutrino oscillation parameters from a global fit performed after Neutrino-2014 conference [59].

Parameter	Best fit $\pm$ 1σ	2σ range	3σ range
Δ^2_{21} $[10^{-5}\,\mathrm{eV}^2]$	$7.60^{+0.19}_{-0.18}$	$7.26 - 7.99$	$7.11 - 8.18$
Δ^2_{31} $[10^{-3}\,\mathrm{eV}^2]$ (NH)	$2.48^{+0.05}_{-0.07}$	$2.35 - 2.59$	$2.30 - 2.65$
Δ^2_{31} $[10^{-3}\,\mathrm{eV}^2]$ (IH)	$2.38^{+0.05}_{-0.06}$	$2.26 - 2.48$	$2.20 - 2.54$
$\sin^2\theta_{12}/10^{-1}$	3.23 ± 0.16	$2.92 - 3.57$	$2.78 - 3.75$
$\sin^2\theta_{23}/10^{-1}$ (NH)	$5.67^{+0.32}_{-1.15}$	$4.17 - 6.22$	$3.95 - 6.42$
$\sin^2\theta_{23}/10^{-1}$ (IH)	$5.73^{+0.25}_{-0.38}$	$4.38 - 6.20$	$4.05 - 6.39$
$\sin^2\theta_{13}/10^{-2}$ (NH)	$2.10^{+0.14}_{-0.09}$	$1.90 - 2.35$	$1.79 - 2.47$
$\sin^2\theta_{13}/10^{-2}$ (IH)	$2.16^{+0.10}_{-0.12}$	$1.93 - 2.38$	$1.82 - 2.50$
δ/π (NH)	$1.48^{+0.43}_{-0.39}$	$0.00 - 0.31\,\&\,0.72 - 2.00$	$0.00 - 2.00$
δ/π (IH)	$1.48^{+0.28}_{-0.29}$	$0.00 - 0.04\,\&\,0.89 - 2.00$	$0.00 - 2.00$

To finish this section, it is worth noting that the analysis performed above could be completed introducing a third neutrino. We can find works with a three-neutrino scheme in Refs. [11, 47], for example.

1.7 Oscillation data

In order to close this review of neutrino features in the Standard Model and beyond, we will summarize neutrino oscillation data coming from neutrino experiments. In particular, we will use [59] as reference [18], which includes an update of neutrino oscillation parameters performed after the Neutrino-2014 conference [62]. Specifically, a global analysis was done using the last data of Double Chooz [62, 63], Daya Bay [64–66] and RENO [66, 67] reactor experiments, together with T2K [39–41] and MINOS [42–44] results. The latest solar data from Super-Kamiokande (SK in what follows) [68, 69] and SNO [70, 71], as well as older solar data coming from Homestake [50], Gallex/GNO [72], SAGE [73], Borexino [74], SK-I [75] and SK-II [76] experiments are also included.

[18] We can find other compilations of neutrino oscillations data in Refs. [60] and [61], for instance.

The value of the most relevant neutrino oscillation parameters are compiled in Fig. 5.9 and Table 1.3. Notice that NH stands for *Normal Hierarchy*, where $\Delta m^2_{31} > 0$, and IH indicates *Inverted Hierarchy*, with $\Delta m^2_{31} < 0$.

Chapter 2

Non-Standard Interactions

The Standard Model is one of the most successful theories in particle physics, being confirmed in most of the existing experiments of high energy physics. However, the SM introduces neutrinos as massless particles (Sec. 1.2.3), contradicting the neutrino oscillation measurements [59]. Hence, the SM is not the end of the road and needs to be revised in order to introduce neutrino masses and mixings, giving rise to new physics beyond the Standard Model. Most of these models, which include mechanisms of neutrino mass generation (such as seesaw schemes, described in Sec. 1.4), imply extra interactions called Non-Standard Interactions (NSI). So far, there is no experimental evidence of the existence of interactions beyond those described within the framework of the SM plus oscillations, although their study is interesting from a phenomenological point of view, since their presence might indicate what type of physics beyond the Standard Model is favored.

These new interactions were used to explain the solar [50–54] and the atmospheric anomalies [1, 77–82], since NSI could induce neutrino conversions, as a resonant effect, even in the absence of the neutrino mass [83]. After the results of the KamLAND experiment it became clear that NSI can only play a sub-leading role [2, 84–86] and that neutrino oscillations is the main mechanism to explain neutrino data. Indeed, there exist in the literature several theoretical and phenomenological analyses of NSI involving accelerator, reactor, solar or supernova neutrino experiments. Combining data from all of these experiments it is possible to obtain bounds on NSI parameters, as we will see later in chapters 3 and 4.

Table 2.1: Coupling constants of fermions with the neutral-current weak boson Z.

NC couplings	g_L^f	g_R^f
ν_e, ν_μ, ν_τ	$\frac{1}{2}$	0
e, μ, τ	$-\frac{1}{2}+\sin^2\theta_W$	$\sin^2\theta_W$
u, c, t	$\frac{1}{2}-\frac{2}{3}\sin^2\theta_W$	$-\frac{2}{3}\sin^2\theta_W$
d, s, b	$-\frac{1}{2}+\frac{2}{3}\sin^2\theta_W$	$\frac{1}{3}\sin^2\theta_W$

2.1 Parameterization of NSI

At low-energy scales, the Standard Model interactions involving neutrinos are described by a four-fermion effective lagrangian:

$$\mathcal{L}_{eff} = -2\sqrt{2}\,G_F\left([\bar{\nu}_\alpha\gamma_\rho L\, l_\alpha][\bar{f}\gamma^\rho L f'] + h.c.\right) - 2\sqrt{2}\,G_F\sum_{P,f,\alpha} g_P^f[\bar{\nu}_\alpha\gamma_\rho L\nu_\alpha][\bar{f}\gamma^\rho P f]\,, \quad (2.1)$$

where G_F is the Fermi constant, $P = L, R$ correspond to the chirality operator, $L = (1-\gamma^5)/2$ and $R = (1-\gamma^5)/2$, l is a charged lepton, f is a fermion, with f' as its $SU(2)$ partner and g_P^f are the weak neutral-current couplings given in Table 2.1. The first term of Eq. (2.1) stands for the charged-current weak interaction mediated by the W boson, while the second one corresponds to the neutral-current weak interaction with Z as the gauge boson (Fig. 1.5).

If NSI are taken into account, they are introduced in theory as extra terms in the effective four-fermion lagrangian, where the strength of these extra interactions is given by the new couplings ε [87–90]:

$$\mathcal{L}_{NC}^{NSI} = -2\sqrt{2}\,G_F\sum_{P,f}\varepsilon_{\alpha\beta}^{f,P}[\bar{\nu}_\alpha\gamma_\rho L\nu_\beta][\bar{f}\gamma^\rho P f]\,, \quad (2.2)$$

where now, f is a first generation fermion (e, u or d). Notice that Eq. (2.2) is the neutral-current non-standard interaction lagrangian, in which this thesis will focus. For completeness, we describe the effective lagrangian involving charged-current non-standard interactions, which presents a similar structure to Eq. (2.1):

$$\mathcal{L}_{CC}^{NSI} = -2\sqrt{2}\,G_F\sum_{f,f',P}\varepsilon_{\alpha\beta}^{CC,f,f',P}[\bar{\nu}_\alpha\gamma_\rho L\, l_\beta][\bar{f}\gamma^\rho P f']\,. \quad (2.3)$$

2.2 NSI from extended models

NSI could appear in several extensions of SM as a consequence of the extra interactions following from neutrino mass as, for instance, in seesaw models (Sec. 1.4). In addition, extended models which include extra particles (additional fermions, neutral heavy leptons, Higgs triplet, etc) imply new physics interactions which can be parameterized using the NSI formalism described by the Eqs. (2.2) and (2.3). In order to illustrate how the NSI formalism parameterizes these models beyond SM, we will describe several of them in this section.

2.2.1 Models with extra neutral gauge bosons

Some extended models introduce extra gauge bosons in addition to those arising from the SM gauge symmetry $SU(2)_L \times U(1)_Y$. For instance, a neutral massive boson Z' is predicted in E_6 string-inspired models, coming from extra groups $U(1)_\chi$ and $U(1)_\psi$. In fact, one may take Z' as a combination of bosons of both groups with a β mixing angle. Another example is the left-right symmetric model, which is based on the gauge group $SU(2)_L \times SU(2)_R \times U(1)_{B-L}$ implying an expanded fermion sector (with right-lepton doublets) and new gauge bosons, Z' and W' for neutral-current and charged-current interactions respectively.

The existence of extra bosons introduces new interactions added to the standard ones. As an example, in a four-fermion description of the neutrino-quark scattering, the lagrangian is represented by the following expression:

$$\mathcal{L}^{NC}_{\nu q} = -\frac{G_F}{\sqrt{2}} \sum_{q=u,d} \left[\bar{\nu}_e \gamma_\mu (1-\gamma^5)\nu_e\right] \left(f^{qL}\left[\bar{q}\gamma^\mu(1-\gamma^5)q\right] + f^{qR}\left[\bar{q}\gamma^\mu(1+\gamma^5)q\right]\right) , \quad (2.4)$$

where f^{qP} are the SM coupling constants [6]

$$f^{uL} = \rho^{NC}_{\nu N}\left(\frac{1}{2} - \frac{2}{3}\hat{\kappa}_{\nu N}\hat{s}^2_Z\right) + \lambda^{uL} + \varepsilon^{uL} , \quad (2.5)$$

$$f^{dL} = \rho^{NC}_{\nu N}\left(-\frac{1}{2} + \frac{1}{3}\hat{\kappa}_{\nu N}\hat{s}^2_Z\right) + \lambda^{dL} + \varepsilon^{dL} , \quad (2.6)$$

$$f^{uR} = \rho^{NC}_{\nu N}\left(-\frac{2}{3}\hat{\kappa}_{\nu N}\hat{s}^2_Z\right) + \lambda^{uR} + \varepsilon^{uR} , \quad (2.7)$$

$$f^{dR} = \rho^{NC}_{\nu N}\left(\frac{1}{3}\hat{\kappa}_{\nu N}\hat{s}^2_Z\right) + \lambda^{dR} + \varepsilon^{dR} . \quad (2.8)$$

In these expressions, where we consider the $\overline{MS}$ scheme [6], $\hat{s}_Z^2$ stands for $\sin^2\theta_W$ (with θ_W as the Weinberg mixing angle) and $\rho_{\nu N}^{NC}$, $\hat{\kappa}_{\nu N}$, λ^{uL}, λ^{dL}, $\lambda^{dR} = 2\lambda^{uR}$ are the radiative corrections, whose values are given in [6]. The new interactions are included as ε^{qP} parameters which can be identified as NSI couplings. In particular for E_6 string inspired models, these NSI parameters are expressed as [91]

$$\varepsilon^{uL} = -4\frac{M_Z^2}{M_{Z'}^2}\sin^2\theta_W\rho_{\nu N}^{NC}\left(\frac{\cos\beta}{\sqrt{24}} - \frac{\sin\beta}{3}\sqrt{\frac{5}{8}}\right)\left(\frac{3\cos\beta}{2\sqrt{24}} + \frac{\sin\beta}{6}\sqrt{\frac{5}{8}}\right), \tag{2.9}$$

$$\varepsilon^{dR} = -8\frac{M_Z^2}{M_{Z'}^2}\sin^2\theta_W\rho_{\nu N}^{NC}\left(\frac{3\cos\beta}{2\sqrt{24}} + \frac{\sin\beta}{6}\sqrt{\frac{5}{8}}\right)^2, \tag{2.10}$$

$$\varepsilon^{dL} = \varepsilon^{uL} = -\varepsilon^{uR}, \tag{2.11}$$

with M_Z as the mass of the standard neutral gauge boson Z and $M_{Z'}$ denotes the mass of the heavier extra gauge boson Z', stemming from the combination of $U(1)_\chi$ and $U(1)_\psi$ gauge bosons.

From the lagrangian in Eq. (2.4) we may get the differential cross section of neutrino-nucleus scattering,

$$\frac{d\sigma}{dT} = \frac{G_F^2 M}{2\pi}\left[(G_V + G_A)^2 + (G_V - G_A)^2\left(1 - \frac{T}{E_\nu}\right)^2 - (G_V^2 - G_A^2)\frac{M\,T}{E_\nu^2}\right], \tag{2.12}$$

where M represents the nucleus mass, T is the recoil energy of the nucleus (going from 0 to $T_{max} = 2E_\nu^2/(M + 2E_\nu)$) and E_ν is the energy of the incident neutrino. The NSI contribution can be found in the vectorial and axial parameters G_V and G_A given by [91]

$$G_V = \left[(g_V^p + 2\varepsilon_{ee}^{uV} + \varepsilon_{ee}^{dV})\,Z + (g_V^n + \varepsilon_{ee}^{uV} + 2\varepsilon_{ee}^{dV})\,N\right]F_{nucl}^V(Q^2), \tag{2.13}$$

$$G_A = \left[(g_A^p + 2\varepsilon_{ee}^{uA} + \varepsilon_{ee}^{dA})(Z_+ - Z_-) + (g_A^n + \varepsilon_{ee}^{uA} + 2\varepsilon_{ee}^{dA})(N_+ - N_-)\right]F_{nucl}^A(Q^2). \tag{2.14}$$

Here, Z and N denote the number of protons and neutrons respectively, with a $\pm$ subscript indicating spin-up and spin-down, and $F_{nucl}^{V,A}(Q^2)$ are the vector and axial nuclear form factors. As can be seen from Eqs. (2.13) and (2.14), the NSI contribution is introduced through $\varepsilon_{ee}^{qV,A}$ parameters, but using the vectorial-axial description [1].

[1] Vectorial-axial NSI parameters are related with those coming from a left-right description through

For the sake of completeness, we show the influence of NSI in the neutrino-electron scattering characterized by the following lagrangian,

$$\mathcal{L}_{\nu e}^{NC} = -\frac{G_F}{\sqrt{2}} \sum_{\alpha,\beta=e,\mu,\tau} \left[\bar{\nu}_\alpha \gamma_\mu (1-\gamma^5)\nu_\beta\right] \left(f^{eL}\left[\bar{e}\gamma^\mu(1-\gamma^5)e\right] + f^{eR}\left[\bar{e}\gamma^\mu(1+\gamma^5)e\right]\right) , \tag{2.15}$$

with $f^{eL,R}$ identified with the coupling constants $g^e_{L,R}$ but including the NSI corrections $\varepsilon^{eL,R}$ [91]:

$$f^{eL,R} = g^e_{L,R} \pm \varepsilon^{eL,R} , \tag{2.16}$$

$$\varepsilon^{eL} = 2\frac{M_Z^2}{M_{Z'}^2} \sin^2\theta_W \rho_{\nu e}^{NC} \left(\frac{3\cos\beta}{2\sqrt{6}} + \frac{\sin\beta}{3}\sqrt{\frac{5}{8}}\right)^2 , \tag{2.17}$$

$$\varepsilon^{eR} = 2\frac{M_Z^2}{M_{Z'}^2} \sin^2\theta_W \rho_{\nu e}^{NC} \left(\frac{\cos\beta}{2\sqrt{6}} - \frac{\sin\beta}{3}\sqrt{\frac{5}{8}}\right)\left(\frac{3\cos\beta}{\sqrt{24}} + \frac{\sin\beta}{3}\sqrt{\frac{5}{8}}\right) . \tag{2.18}$$

Again, we may define the differential cross section as

$$\frac{d\sigma}{dT} = \frac{2G_F^2 m_e}{\pi}\left[(g_L^e)^2 + (g_R^e)^2\left(1-\frac{T}{E_\nu}\right)^2 - g_L^e\, g_R^e \frac{m_e\, T}{E_\nu^2}\right] , \tag{2.19}$$

with NSI parameters correcting the SM coupling constants $g^e_{L,R}$,

$$g_L^e = -\frac{1}{2} + \sin^2\theta_W + \varepsilon^{eL} , \tag{2.20}$$

$$g_R^e = \sin^2\theta_W + \varepsilon^{eR} . \tag{2.21}$$

2.2.2 Seesaw models

As we have seen in Sec. 1.4, seesaw models [9, 15, 92, 93] introduce extra neutral heavy leptons that it may imply a rich phenomenology to study. In these schemes, extra isosinglets are added to the standard $SU(2)_L \times U(1)_Y$ isodoublets giving rise to a possible mixing between them [9, 94]. This mixing is described by the rectangular matrix [2]

$$K = (K_L, K_H) , \tag{2.22}$$

the following relations: $\varepsilon_{ee}^{qL} = \frac{1}{2}\left(\varepsilon_{ee}^{qV} + \varepsilon_{ee}^{qA}\right)$ and $\varepsilon_{ee}^{qR} = \frac{1}{2}\left(\varepsilon_{ee}^{qV} - \varepsilon_{ee}^{qA}\right)$.

[2] Notice that this matrix comes from the truncation of the matrix $U^{n\times n}$ in a model with $n > 3$ neutrinos, where it is only considered the active ones.

where K_L describes the mixing between the standard light neutrinos, while K_H includes the mixture with neutral heavy leptons. In this framework, we can find new physics hints from this matrix as deviations from the standard charged-current interactions as a consequence of extra couplings in the lagrangian, or in neutral-current processes because K_L is no longer unitary [3]. Indeed, neutral-current interactions are described in the SM by the following lagrangian:

$$\begin{aligned} \mathcal{L} &= \frac{ig'}{2\sin\theta_W} Z_\mu \bar{\nu}_L \gamma_\mu U^\dagger U \nu_L \\ &= \frac{ig'}{2\sin\theta_W} Z_\mu \bar{\nu}_L \gamma_\mu \nu_L \,, \end{aligned} \tag{2.23}$$

where we have used the unitarity condition of U. After adding extra neutral heavy leptons the lagrangian presents a significant change:

$$\mathcal{L} = \frac{ig'}{2\sin\theta_W} Z_\mu \bar{\nu}_L \gamma_\mu K^\dagger K \nu_L \,. \tag{2.24}$$

Here, $K^\dagger K \neq I$ leading to the spontaneous appearance of NSI [9, 94]. These new interactions can be introduced in the theory using the ε parameters. For instance, considering only one extra heavy neutrino [4], NSI parameters could be expressed as

$$\varepsilon_{ee}^{eL} = -g_L \sin^2\theta_{14} \,, \quad \varepsilon_{ee}^{eR} = -g_R \sin^2\theta_{14} \,, \tag{2.25}$$

where θ_{14} is the mixing between the light neutrino and the neutral heavy lepton, and $g_{L,R}$ are the corresponding SM couplings.

On the other hand, certain seesaw models imply an extended Higgs sector too. In particular, for a Type-II seesaw model a Higgs triplet is introduced in order to provide mass to neutrinos, as we can observe in Fig. 2.1. In this case, the NSI parameters are related with the neutrino mass matrix as follows [95]:

$$\varepsilon_{\alpha\beta}^{\rho\sigma} = -\frac{m_\Delta^2}{8\sqrt{2}G_F v^4 \lambda_\phi^2} (m_\nu)_{\sigma\beta} (m_\nu^\dagger)_{\alpha\rho} \,, \tag{2.26}$$

where v denotes the vev of the SM Higgs, m_Δ stands for the Higgs triplet mass and λ_ϕ is related to the Higgs triplet coupling.

[3] We will explain this case more accurately in Chapter 5.

[4] One extra heavy neutrino implies a global extra factor in the effective lagrangian of electron-neutrino-electron scattering as a consequence of the non-unitarity of K_L [9, 94].

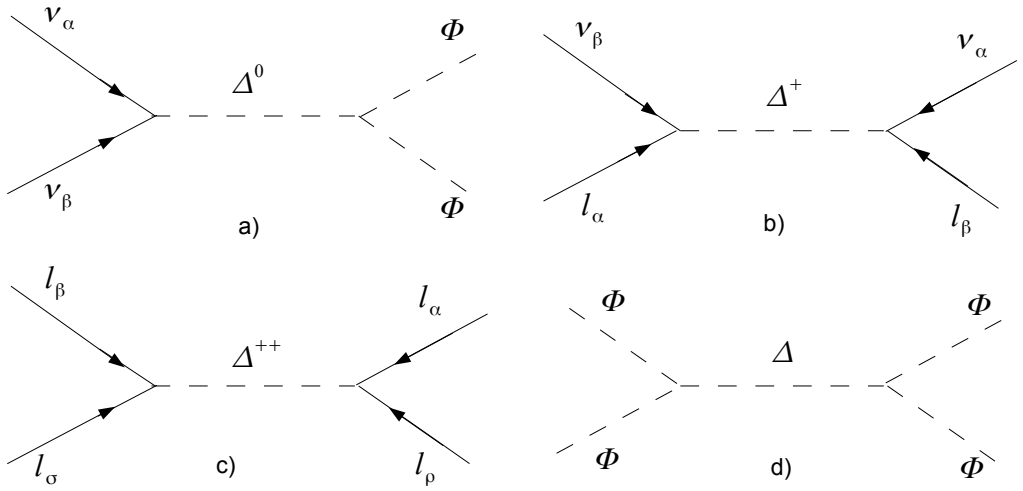

Figure 2.1: Diagrams for the exchange of a Higgs triplet in a Type-II seesaw model at tree-level [95].

2.2.3 SUSY with R-parity violation

In supersymmetric theories [96], the baryon number B and the lepton number L can be violated, implying that R-parity [5] is broken [97–99]. In the low-energy regime, these supersymmetric models may introduce NSI arising from extra violating L terms in the superpotential [30, 31, 100–102]

$$\lambda_{ijk}\, L_i\, L_j\, E^c_k\,, \tag{2.27}$$

$$\lambda^{'}_{ijk}\, L_i\, Q_j\, D^c_k\,, \tag{2.28}$$

where L and Q represent the super-fields containing the standard lepton and quark doublets, while E^c and D^c denote the super-fields including singlets, and i, j, k are generational indices.

In this kind of models, the R-violating interactions produced by the heavy supersymmetric particles can be described by a four-fermion effective lagrangian involving leptons and quarks. In the case where neutrinos interact with d-quarks we have:

$$\mathcal{L}_{eff} = -2\sqrt{2}G_F \sum_{\alpha,\beta} \varepsilon^{dR}_{\alpha\beta} \bar{\nu}_{L\alpha}\gamma^\mu \nu_{L\beta} \bar{d}_R \gamma^\mu d_R\,. \tag{2.29}$$

[5] R-parity is defined as $R = (-1)^{3B+L+2S}$, where B and L indicates the baryon and lepton number respectively, whereas that S stands for the spin.

In the above expression the NSI parameters are present, representing the strength of extra interactions. As an example, we can identify flavor-conserving NSI parameters [86, 103],

$$\varepsilon^{dR}_{\mu\mu} = \sum_j \frac{|\lambda'_{2j1}|^2}{4\sqrt{2}G_F m^2_{\tilde{q}jL}}\,, \tag{2.30}$$

$$\varepsilon^{dR}_{\tau\tau} = \sum_j \frac{|\lambda'_{3j1}|^2}{4\sqrt{2}G_F m^2_{\tilde{q}jL}}\,, \tag{2.31}$$

and flavor-changing NSI couplings,

$$\varepsilon^{dR}_{\mu\tau} = \sum_j \frac{\lambda'_{2j1}\lambda'_{3j1}}{4\sqrt{2}G_F m^2_{\tilde{q}jL}}\,. \tag{2.32}$$

In these equations, $m_{\tilde{q}L}$ indicates the masses of the squarks, identifying the subscripts $j = 1, 2, 3$ as $\tilde{d}_L, \tilde{s}_L, \tilde{b}_L$ respectively. These neutral NSI couplings lead to extra non-universal and flavor-changing terms relevant to solar [84, 85, 104, 105] and atmospheric propagation [86, 106, 107], as we will show in chapter 3.

2.2.4 Models with leptoquarks

In several extensions of the SM an exotic boson appears coupling indistinctly to a lepton and a quark: the leptoquark [108]. For example, the Pati-Salam model [109], grand unification theories based on $SU(5)$ [110–112] and $SO(10)$ groups [113] or extended technicolor models [114].

Due to the presence of these leptoquarks, NSI must be considered along with standard interactions, producing extra contributions to the four-fermion lagrangian given by the following NSI parameters [91, 115]:

$$\varepsilon^{uV} = \frac{\lambda_u^2}{m_{lq}^2}\frac{\sqrt{2}}{4G_F}\,, \tag{2.33}$$

$$\varepsilon^{dV} = \frac{\lambda_d^2}{m_{lq}^2}\frac{\sqrt{2}}{4G_F}\,, \tag{2.34}$$

where $\lambda_{u,d}$ are coupling constants and m_{lq} represents the leptoquark mass. We should note that Eqs. (2.33) and (2.34) are valid for vector leptoquarks. An extra 1/2 factor has to be added for the case of scalar leptoquarks [115].

2.3 NSI phenomenology

Studying NSI can be very attractive from a phenomenological point of view, since its existence would mean a new evidence of new physics. The effects of these new interactions could be observed in the production (ε^S), propagation (ε^m) and detection (ε^D) of neutrinos. In this section we will show how NSI influence each of these processes. Later we will introduce these new interactions in the data analysis of several kinds of neutrino experiments (Sec. 2.4).

2.3.1 NSI in the source and detector

Production and detection are charged-current processes, so extra contributions as in Eqs. (2.1) and (2.3) could be introduced in the presence of NSI, giving rise to an extra flavor component in both processes [89, 116–119]:

$$|\nu_\alpha^S\rangle = |\nu_\alpha\rangle + \sum_{\rho=e,\mu,\tau} \varepsilon^S_{\alpha\rho}|\nu_\rho\rangle = (1+\varepsilon^S)U|\nu_i\rangle\,, \tag{2.35}$$

$$\langle\nu_\beta^D| = \langle\nu_\beta| + \sum_{\gamma=e,\mu,\tau} \varepsilon^D_{\gamma\beta}\langle\nu_\beta| = \langle\nu_i|U^\dagger[1+(\varepsilon^D)^\dagger]\,, \tag{2.36}$$

where the superscripts S and D indicate "source" and "detector" respectively, and $|\nu_i\rangle$ is a mass eigenstate. Notice that the orthonormality between $|\nu_\alpha^S\rangle$ and $\langle\nu_\beta^D|$ is broken, because NSI matrices, ε^S and ε^D, are arbitrary and non-unitary (in general) due to different physical processes (related with NSI) that can take place at the source and at the detector of the experiment. Therefore, it is possible to detect a flavor transition at zero distance [83, 94, 120], as a consequence of the broken unitarity. Using Eqs (1.101), (2.35) and (2.36) we find that the transition probability is

$$\begin{aligned} P_{\nu_\alpha^S\to\nu_\beta^D}(L) &= \left|\sum_{\gamma,\rho,i}(1+\varepsilon^D)_{\gamma\beta}(1+\varepsilon^S)_{\alpha\rho}U_{\rho i}U^*_{\gamma i}e^{-i\frac{m_i^2 L}{2E}}\right|^2 \\ &= \sum_{i,j}\mathcal{J}^i_{\alpha\beta}\mathcal{J}^{j*}_{\alpha\beta} - 4\sum_{i>j}Re[\mathcal{J}^i_{\alpha\beta}\mathcal{J}^{j*}_{\alpha\beta}]\sin^2\left(\frac{\Delta m^2_{ij}L}{4E}\right) \\ &+ 2\sum_{i>j}Im[\mathcal{J}^i_{\alpha\beta}\mathcal{J}^{j*}_{\alpha\beta}]\sin\left(\frac{\Delta m^2_{ij}L}{2E}\right), \end{aligned} \tag{2.37}$$

where $\mathcal{J}^i_{\alpha\beta}$ contains the terms related with NSI,

$$\mathcal{J}^i_{\alpha\beta} = U^*_{\alpha i}U_{\beta i} + \sum_\gamma \varepsilon^S_{\alpha\gamma}U^*_{\gamma i}U_{\beta i} + \sum_\gamma \varepsilon^D_{\gamma\beta}U^*_{\alpha i}U_{\gamma i} + \sum_{\gamma,\rho} \varepsilon^S_{\alpha\gamma}\varepsilon^D_{\rho\beta}U^*_{\gamma i}U_{\rho i}\,. \tag{2.38}$$

As we can observe in Eq. (2.37), the first term is independent of the distance (L), so the flavor conversion could be produced at the source, i.e., at zero distance.

2.3.2 Neutrino propagation with NSI

On the journey of neutrinos through the Earth, NSI can contribute to coherent forward scattering processes in matter, which are neutral-current interactions parameterized by Eq. (2.2). Indeed, the presence of these NSI would modify the neutrino matter potential, adding a new term to the standard oscillation hamiltonian (Eq. (1.141)):

$$H_{mat+NSI} = \left[U \frac{1}{2E} \begin{pmatrix} m_1^2 & 0 & 0 \\ 0 & m_2^2 & 0 \\ 0 & 0 & m_3^2 \end{pmatrix} U^\dagger + \sum_f V_f \begin{pmatrix} \delta_{ef} + \varepsilon^f_{ee} & \varepsilon^f_{e\mu} & \varepsilon^f_{e\tau} \\ \varepsilon^{f\ *}_{e\mu} & \varepsilon^f_{\mu\mu} & \varepsilon^f_{\mu\tau} \\ \varepsilon^{f\ *}_{e\tau} & \varepsilon^{f\ *}_{\mu\tau} & \varepsilon_{\tau\tau} \end{pmatrix} \right], \tag{2.39}$$

where U is the lepton mixing matrix for three neutrinos (Eqs. (1.120) and (1.121)). The elements of the NSI matrix, $\varepsilon_{\alpha\beta}$, are related with those in Eq. (2.2) as

$$\varepsilon_{\alpha\beta} = \sum_{f,P} \frac{V_f}{V_e}\varepsilon^{f,P}_{\alpha\beta}\,, \tag{2.40}$$

representing the strength of NSI, m_i is the neutrino mass value, E stands for the neutrino energy, $V_f = \sqrt{2}G_F N_f$ denotes the interaction potential with fermions ($f = e, u\, or\, d$), where N_f is the fermion number density along the neutrino path throughout the matter. Note that $V_e = \sqrt{2}G_F N_e$ is the standard potential of neutrinos with matter, which produces the usual MSW effect (Eq. (1.133)).

Using this hamiltonian (Eq. (2.39)) we can write the evolution equation including NSI as

$$i\tfrac{d}{dt}\begin{pmatrix} \nu_e \\ \nu_\mu \\ \nu_\tau \end{pmatrix} = \left[U\, \tfrac{1}{2E} \begin{pmatrix} 0 & 0 & 0 \\ 0 & \Delta m^2_{21} & 0 \\ 0 & 0 & \Delta m^2_{31} \end{pmatrix} U^\dagger + \textstyle\sum_f V_f \begin{pmatrix} \delta_{ef} + \varepsilon^f_{ee} & \varepsilon^f_{e\mu} & \varepsilon^f_{e\tau} \\ \varepsilon^{f\ *}_{e\mu} & \varepsilon^f_{\mu\mu} & \varepsilon^f_{\mu\tau} \\ \varepsilon^{f\ *}_{e\tau} & \varepsilon^{f\ *}_{\mu\tau} & \varepsilon_{\tau\tau} \end{pmatrix} \right] \begin{pmatrix} \nu_e \\ \nu_\mu \\ \nu_\tau \end{pmatrix}. \tag{2.41}$$

Note that neutrinos, in their propagation, are only sensitive to vector currents [6] ($\varepsilon^V =$

[6] We will return to this property in Chap 3.

$\varepsilon^L + \varepsilon^R$), thus Eq. (2.40) may be written in a left-right notation as:

$$\varepsilon_{\alpha\beta} = \sum_f \frac{V_f}{V_e}(\varepsilon^{f,L}_{\alpha\beta} + \varepsilon^{f,R}_{\alpha\beta})\,. \tag{2.42}$$

Equation (2.41) provides the structure for the neutrino propagation in matter when NSI are present. Analyzing this expression we may find some interesting details concerning NSI couplings and their influence in neutrino propagation:

- The diagonal elements of NSI matrix, $\varepsilon_{\alpha\alpha}$, could induce extra resonance oscillation effects, additional to those following from the MSW matter potential, even if neutrinos were massless particles [83, 121].

- The off-diagonal elements, $\varepsilon_{\alpha\beta}$, could produce flavor transitions in matter, even if no neutrino mixing is present [83, 121, 122].

The observation of these phenomena would be considered an evidence for NSI and a signal of new physics.

In a similar procedure to the vacuum case, Sec. 1.5.1, we can diagonalize the hamiltonian $H_{mat+NSI}$ using a unitary matrix $\tilde{U}$,

$$\tilde{H} = H_{mat+NSI} = \tilde{U}\,\frac{1}{2E}\begin{pmatrix} \tilde{m}_1^2 & 0 & 0 \\ 0 & \tilde{m}_2^2 & 0 \\ 0 & 0 & \tilde{m}_3^2 \end{pmatrix}\,\tilde{U}^\dagger\,, \tag{2.43}$$

with $\tilde{m}_i^2$ as the effective neutrino mass-squared eigenvalues and $\tilde{U}$ is the effective mixing matrix when matter and NSI are taken into account.

The transition probability is the square of the probability amplitude, hence

$$P_{\nu_\alpha\to\nu_\beta}(L,E) = \left|\sum_{j=1}^{3}\tilde{U}^*_{\alpha j}\tilde{U}_{\beta j}e^{-i\frac{\tilde{m}_j L}{2E}}\right|^2\,. \tag{2.44}$$

So we get, after applying the same calculation as in Sec. 1.5.1,

$$\begin{aligned} P_{\nu_\alpha\to\nu_\beta}(L,E) = \delta_{\alpha\beta} \;&-\; 4\sum_{i>j} Re[\tilde{U}^*_{\alpha i}\tilde{U}_{\alpha j}\tilde{U}_{\beta i}\tilde{U}^*_{\beta j}]\sin^2\left(\frac{\Delta\tilde{m}^2_{ij}L}{4E}\right) \\ &+\; 2\sum_{i>j} Im[\tilde{U}^*_{\alpha i}\tilde{U}_{\alpha j}\tilde{U}_{\beta i}\tilde{U}^*_{\beta j}]\sin\left(\frac{\Delta\tilde{m}^2_{ij}L}{2E}\right)\,. \end{aligned} \tag{2.45}$$

Notice that Eq. (2.45) looks like the neutrino transition probability in vacuum, Eq. (1.124), but replacing the vacuum masses m_i^2 and the leptonic mixing matrix U, for those effective parameters which includes the interaction with matter (V_e) and NSI, $\tilde{m}_i^2$ and $\tilde{U}$ respectively. Therefore, in order to study the new physics behind NSI in propagation, it is useful to compare vacuum and effective parameters and relate them [123]. The effective masses with NSI have the following expressions:

$$\tilde{m}_1^2 \simeq \Delta m_{31}^2 \left(\tilde{V} + \alpha s_{12}^2 + \tilde{V}\varepsilon_{ee}\right) , \tag{2.46}$$

$$\tilde{m}_2^2 \simeq \Delta m_{31}^2 \left[\alpha c_{12}^2 - \tilde{V} s_{23}^2(\varepsilon_{\mu\mu} - \varepsilon_{\tau\tau}) - \tilde{V} s_{23} c_{23}(\varepsilon_{\mu\tau} + \varepsilon_{\mu\tau}^*) + \tilde{V}\varepsilon_{\mu\mu}\right] , \tag{2.47}$$

$$\tilde{m}_3^2 \simeq \Delta m_{31}^2 \left[1 + \tilde{V}\varepsilon_{\tau\tau} + \tilde{V} s_{23}^2(\varepsilon_{\mu\mu} - \varepsilon_{\tau\tau}) + \tilde{V} s_{23} c_{23}(\varepsilon_{\mu\tau} + \varepsilon_{\mu\tau}^*)\right] , \tag{2.48}$$

whereas the elements of the effective mixing matrix are given by

$$\tilde{U}_{e2} \simeq \frac{\alpha s_{12} c_{12}}{\tilde{V}} + c_{23}\varepsilon_{e\mu} - s_{23}\varepsilon_{e\tau} , \tag{2.49}$$

$$\tilde{U}_{e3} \simeq \frac{s_{13} e^{-i\delta} + \tilde{V}(s_{23}\varepsilon_{e\mu} + c_{23}\varepsilon_{e\tau})}{1 - \tilde{V}} , \tag{2.50}$$

$$\tilde{U}_{\mu 2} \simeq c_{23} + s_{23}^2 c_{23}\tilde{V}(\varepsilon_{\tau\tau} - \varepsilon_{\mu\mu}) + s_{23}\tilde{V}(s_{23}\varepsilon_{\mu\tau} - c_{23}^2\varepsilon_{\mu\tau}^*) , \tag{2.51}$$

$$\tilde{U}_{\mu 3} \simeq s_{23} + \tilde{V}\left[c_{23}\varepsilon_{\mu\tau} + s_{23} c_{23}^2(\varepsilon_{\mu\mu} - \varepsilon_{\tau\tau}) - s_{23}^2 c_{23}(\varepsilon_{\mu\tau} + \varepsilon_{\mu\tau}^*)\right] . \tag{2.52}$$

Here, $s_{ij} = \sin\theta_{ij}$, $c_{ij} = \cos\theta_{ij}$, $\alpha \equiv \Delta m_{21}^2/\Delta m_{31}^2$, $\tilde{V} \equiv V_e/\Delta m_{31}^2$ and δ stands for the CP violation phase.

It is worth noting that neutrino data is consistent with the oscillation mechanism. Thus, NSI will play only a sub-leading role in interpreting the results of neutrino experiments. NSI couplings have been constrained using solar and atmospheric neutrino oscillation experiments (Secs. 2.4.3 and 2.4.1 respectively), combining these data with those coming from laboratory experiments [7] [84–87, 124]. On the other hand, reactor neutrinos do not have relevance in constraining NSI in the propagation because the matter effect is negligible in this case. However, they can constrain NSI related with detection processes [125].

Two-neutrino propagation with NSI

As we have seen in Sec. 2.3.2, the expressions involving three-flavor neutrino propagation in matter including NSI, Eqs. (2.41) and (2.45), are quite complicated. Sometimes working

[7] We will present detailed constraint calculations in Chapter 3 and 4.

with a two-neutrino scheme is enough to illustrate the important features of NSI physics and simplifies tedious calculations. Hence, in order to shed light on neutrino oscillations with NSI, we will develop the conversion equations for the two-neutrino scheme (electron and tau-neutrino in this case, because muon-neutrino bounds are stronger) step by step [8].

The hamiltonian for a two-neutrino scheme is given as a combination of vacuum, matter and NSI hamiltonian,

$$\tilde{H} = H_{vac} + H_{mat} + H_{NSI}\,, \tag{2.53}$$

where

$$H_{vac} = \frac{1}{4E}\begin{pmatrix} -\Delta m^2\cos 2\theta & \Delta m^2 \sin 2\theta \\ \Delta m^2 \sin 2\theta & \Delta m^2 \cos 2\theta \end{pmatrix}, \tag{2.54}$$

$$H_{mat} = \begin{pmatrix} \sqrt{2}\,G_F N_e & 0 \\ 0 & 0 \end{pmatrix} \iff \begin{pmatrix} \frac{V_{CC}}{2} & 0 \\ 0 & -\frac{V_{CC}}{2} \end{pmatrix}, \tag{2.55}$$

$$H_{NSI} = \sqrt{2}\,G_F N_f \begin{pmatrix} \varepsilon_{ee} & \varepsilon_{e\tau} \\ \varepsilon_{e\tau} & \varepsilon_{\tau\tau} \end{pmatrix} \iff \begin{pmatrix} 0 & \varepsilon \\ \varepsilon & \varepsilon^{'} \end{pmatrix}, \tag{2.56}$$

with θ as the two-neutrino mixing angle, N_e and N_f represents the electron and fermion density respectively along neutrino trajectory in matter, G_F is the Fermi constant, $V_{CC} = \sqrt{2}G_F N_e$ indicates the standard charged-current weak interaction of neutrinos with electrons, and the strength of NSI is represented by the coupling constants, $\varepsilon = \sqrt{2}G_F N_f \varepsilon_{e\tau}$ and $\varepsilon^{'} = \sqrt{2}G_F N_f(\varepsilon_{\tau\tau} - \varepsilon_{ee})$. With all these ingredients, we can build the complete hamiltonian $\tilde{H}$,

$$\tilde{H} = \begin{pmatrix} -\frac{\Delta m^2}{4E}\cos 2\theta + V_{CC} & \frac{\Delta m^2}{4E}\sin 2\theta + \varepsilon \\ \frac{\Delta m^2}{4E}\sin 2\theta + \varepsilon & \frac{\Delta m^2}{4E}\cos 2\theta + \varepsilon^{'} \end{pmatrix} \tag{2.57}$$

$$\Leftrightarrow \begin{pmatrix} -\frac{\Delta m^2}{4E}\cos 2\theta + \frac{V_{CC}}{2} - \frac{\varepsilon^{'}}{2} & \frac{\Delta m^2}{4E}\sin 2\theta + \varepsilon \\ \frac{\Delta m^2}{4E}\sin 2\theta + \varepsilon & \frac{\Delta m^2}{4E}\cos 2\theta - \frac{V_{CC}}{2} + \frac{\varepsilon^{'}}{2} \end{pmatrix}. \tag{2.58}$$

Note that, in Eqs. (2.55), (2.56) and (2.57), we take again into account that the Schrödinger equation does not change if a common phase is introduced in the diagonal terms of the hamiltonian. Using this property, we can write the hamiltonian of Eq. (2.58) in a sym-

[8] We can find an accurate discussion about the two-neutrino scheme in presence of NSI in Ref. [126].

metrical way, leading to the following evolution equation:

$$i\frac{d}{dt}\begin{pmatrix}\nu_e\\ \nu_\tau\end{pmatrix}=\begin{pmatrix}-a & b\\ b & a\end{pmatrix}\begin{pmatrix}\nu_e\\ \nu_\tau\end{pmatrix}, \tag{2.59}$$

with

$$a = \frac{\Delta m^2}{4E}\cos 2\theta - \frac{V_{CC}}{2}+\frac{\varepsilon^{'}}{2}, \tag{2.60}$$

$$b = \frac{\Delta m^2}{4E}\sin 2\theta + \varepsilon\,. \tag{2.61}$$

From Eqs. (2.59), (2.60) and (2.61) we may obtain the parameters and equations that govern neutrino conversion in the presence of NSI. Specifically, the effective mixing angle φ in a two-neutrino scheme, propagating in matter with NSI is given by

$$\tan 2\varphi = \frac{2b}{a-(-a)} = \frac{\frac{\Delta m^2}{4E}\sin 2\theta+\varepsilon}{\frac{\Delta m^2}{4E}\cos 2\theta - \frac{V_{CC}}{2}+\frac{\varepsilon^{'}}{2}}, \tag{2.62}$$

and the transition probabilities are

$$P_{\nu_e\to\nu_e}(L,E) = 1-P_{\nu_e\to\nu_\tau}(L,E)\,, \tag{2.63}$$

$$P_{\nu_e\to\nu_\tau}(L,E) = \sin^2 2\varphi\sin^2(\omega L)\,, \tag{2.64}$$

with the oscillation parameter $\omega^2=a^2+b^2$. This parameter characterizes the neutrino transition, presenting the following form:

$$\omega^2=\left(\frac{\Delta m^2}{4E}\cos 2\theta-\frac{V_{CC}}{2}+\frac{\varepsilon^{'}}{2}\right)^2+\left(\frac{\Delta m^2}{4E}\sin 2\theta+\varepsilon\right)^2. \tag{2.65}$$

Notice that, if we consider antineutrinos instead of neutrinos, we should introduce $-N_e$ and $-N_f$ for the charged-current and neutral-current potential respectively, changing the sign of interactions with matter and NSI.

2.4 NSI and neutrino experiments

In this section we will review the impact of NSI in atmospheric, solar or laboratory neutrino experiments.

2.4.1 NSI in atmospheric neutrino experiments

The analysis of atmospheric neutrinos can be performed in a two-neutrino scheme, considering the non-universal $\nu_\mu + f \to \nu_\mu + f$ and flavor changing $\nu_\mu + f \to \nu_\tau + f$ processes, so that all the NSI parameters related with electron-neutrino, $\varepsilon_{e\alpha}$, are set to zero. In this approximation, the evolution equation is

$$i\frac{d}{dt}\begin{pmatrix}\nu_\mu\\ \nu_\tau\end{pmatrix} = \left[U\begin{pmatrix}0 & 0\\ 0 & \frac{\Delta m^2_{31}}{2E}\end{pmatrix}U^\dagger + \begin{pmatrix}V_f & \varepsilon\\ \varepsilon & \varepsilon^{'}\end{pmatrix}\right]\begin{pmatrix}\nu_\mu\\ \nu_\tau\end{pmatrix}, \tag{2.66}$$

noting that $\varepsilon = \sqrt{2}\,G_F N_f \varepsilon_{\mu\tau}$ and $\varepsilon^{'} = \sqrt{2}\,G_F N_f(\varepsilon_{\tau\tau} - \varepsilon_{\mu\mu})$. Assuming that neutrinos only interact with d quark and $\Delta m^2_{21}L/E \to 0$, the survival probability is given by [86, 89, 90, 106, 127–129]

$$P_{\nu_\mu\to\nu_\mu}(L,E) = 1 - P_{\nu_\mu\to\nu_\tau}(L,E) \simeq 1 - \sin^2 2\varphi \sin^2\left(\frac{\Delta m^2_{31}L}{4E}R\right), \tag{2.67}$$

where the effective parameters φ and R for the two-neutrino approximation with NSI are expressed as

$$\sin^2 2\varphi = \frac{1}{R^2}\left[\sin^2 2\theta + R_0^2 \sin^2 2\xi + 2R_0 \sin 2\theta \sin 2\xi\right], \tag{2.68}$$

$$R = \left[1 + R_0^2 + 2R_0(\cos 2\theta \cos 2\xi + \sin 2\theta \sin 2\xi)\right]^{\frac{1}{2}}. \tag{2.69}$$

The NSI couplings are introduced in the following parameters:

$$R_0 = \frac{4E}{\Delta m^2_{31}}\sqrt{|\varepsilon|^2 + \frac{\varepsilon^{'2}}{4}}, \tag{2.70}$$

$$\xi = \frac{1}{2}\arctan\left(\frac{2\varepsilon}{\varepsilon^{'}}\right). \tag{2.71}$$

Using the Super-Kamiokande (SK in what follows) experimental data within a two-neutrino framework, the SK Collaboration obtained the following bounds on NSI couplings at 90 % C.L. [128]:

$$|\varepsilon_{\mu\tau}| < 1.1 \times 10^{-2} \quad \text{and} \quad |\varepsilon_{\tau\tau} - \varepsilon_{\mu\mu}| < 4.9 \times 10^{-2}. \tag{2.72}$$

In a more recent analysis, considering IceCube-79 and DeepCore data [130], a more re-

strictive constraints have been found at 90 % C.L.:

$$|\varepsilon_{\mu\tau}| < 6.0 \times 10^{-3} \quad \text{and} \quad |\varepsilon_{\tau\tau} - \varepsilon_{\mu\mu}| < 3.0 \times 10^{-2}\,. \tag{2.73}$$

It is worth noting that NSI parameters involving electron-neutrinos cannot be constrained directly from atmospheric data, but they are related with atmospheric NSI parameters through the expression [131],

$$\varepsilon_{\tau\tau} \sim \frac{3|\varepsilon_{e\tau}|^2}{1+3\varepsilon_{ee}}\,. \tag{2.74}$$

2.4.2 NSI in accelerator neutrino experiments

In accelerator neutrino experiments the main channels are $\nu_\mu \to \nu_\mu$ and $\nu_{\bar{\mu}} \to \nu_{\bar{\mu}}$, so the relevant NSI parameters will be $\varepsilon_{\mu\mu}$, $\varepsilon_{\mu\tau}$ and $\varepsilon_{\tau\tau}$. For instance, from MINOS experiment [132–136] data, the NSI parameter $\varepsilon_{\mu\tau}$ has been constrained, assuming again two neutrinos and taking the survival probability as

$$P_{\nu_\mu\to\nu_\mu}(L,E) \simeq 1 - \sin^2\left(\left|\frac{\Delta m^2_{31}}{4E} - \varepsilon_{\mu\tau}\frac{V}{2E}\right| L\right). \tag{2.75}$$

The bound obtained on $\varepsilon_{\mu\tau}$ at 90 % C.L. from the MINOS Collaboration is [137]

$$-0.20 < \varepsilon_{\mu\tau} < 0.07\,. \tag{2.76}$$

2.4.3 NSI in solar neutrino experiments

There are several studies on NSI involving solar neutrinos [104, 138–145]. Collaborations such as Super-Kamiokande, SNO or Borexino [139, 145] have used their data in order to provide bounds on the NSI parameters. A recent updated work on solar NSI constraints is given in Ref. [146], where the two-neutrino approximation is again made [147],

$$i\frac{d}{dr}\begin{pmatrix}\nu'_e\\ \nu'_\mu\end{pmatrix} = \left[U_{\theta_{12}}\begin{pmatrix}0 & 0\\ 0 & \frac{\Delta m^2_{21}}{2E}\end{pmatrix}U^\dagger_{\theta_{12}} + \sum_f \begin{pmatrix}c^2_{13}\delta_{ef} - \varepsilon^f_D & \varepsilon^f_N\\ \varepsilon^{f\,*}_N & \varepsilon^f_D\end{pmatrix}\right]\begin{pmatrix}\nu'_e\\ \nu'_\mu\end{pmatrix} \tag{2.77}$$

with ν'_e and ν'_μ coming from

$$\begin{pmatrix}\nu'_e\\ \nu'_\mu\\ \nu'_\tau\end{pmatrix} = \begin{pmatrix}c_{12} & s_{12} & 0\\ -s_{12} & c_{12} & 0\\ 0 & 0 & 1\end{pmatrix}\begin{pmatrix}\nu_1\\ \nu_2\\ \nu_3\end{pmatrix} = \begin{pmatrix}c_{12} & s_{12} & 0\\ -s_{12} & c_{12} & 0\\ 0 & 0 & 1\end{pmatrix}U^\dagger\begin{pmatrix}\nu_e\\ \nu_\mu\\ \nu_\tau\end{pmatrix}. \tag{2.78}$$

Table 2.2: Bounds on NSI parameters at 90 % C.L. for the interaction of neutrinos with d-quark, following from oscillation experiments (propagation). Only one parameter is considered at a time [90].

NSI parameter	Bound	Reference
$\varepsilon^d_{ee} - \varepsilon^d_{\mu\mu}$	$(0.02,\ 0.51)$	[146]
$\varepsilon^d_{\tau\tau} - \varepsilon^d_{\mu\mu}$	$(-0.01,\ 0.03)$	[146]
$\varepsilon^d_{\tau\tau} - \varepsilon^d_{\mu\mu}$	$(-0.049,\ 0.049)$	[128]
$\varepsilon^d_{\tau\tau} - \varepsilon^d_{\mu\mu}$	$(-0.036,\ 0.031)$	[130]
$\varepsilon^d_{e\mu}$	$(-0.09,\ 0.04)$	[146]
$\varepsilon^d_{\mu\tau}$	$(-0.01,\ 0.01)$	[146]
$\varepsilon^d_{\mu\tau}$	$(-0.011,\ 0.011)$	[128]
$\varepsilon^d_{\mu\tau}$	$(-0.0061,\ 0.0056)$	[130]
$\varepsilon^d_{e\tau}$	$(-0.13,\ 0.14)$	[146]
$\varepsilon^d_{e\tau}$ (with $\varepsilon^{\rm d}_{\rm ee} = -0.5$)	$(-0.05,\ 0.05)$	[128]
$\varepsilon^d_{e\tau}$ (with $\varepsilon^{\rm d}_{\rm ee} = 0.5$)	$(-0.19,\ 0.13)$	[128]

The NSI parameters ε_D and ε_N are expressed as [146]

$$\begin{aligned}\varepsilon_D &= c_{13}s_{13}\,Re\left[e^{i\delta_{CP}}(s_{23}\varepsilon_{e\mu} + s_{23}\varepsilon_{e\tau})\right] - (1+s^2_{13})c_{23}s_{23}\,Re[\varepsilon_{\mu\tau}] \\ &- \frac{c^2_{13}}{2}(\varepsilon_{ee} - \varepsilon_{\mu\mu}) + \frac{s^2_{23} - s^2_{13}c^2_{23}}{2}(\varepsilon_{\tau\tau} - \varepsilon_{\mu\mu})\,, \qquad (2.79)\\ \varepsilon_N &= c_{13}(c_{23}\varepsilon_{e\mu} - s_{23}\varepsilon_{e\tau}) + s_{13}e^{-i\delta_{CP}}\left[s^2_{23}\varepsilon_{\mu\tau} - c^2_{23}\varepsilon^*_{\mu\tau} + c_{23}s_{23}(\varepsilon_{\tau\tau} - \varepsilon_{\mu\mu})\right]\,. \qquad (2.80)\end{aligned}$$

Note that, although we are working with a two-neutrino scheme, mixing parameters involving the third neutrino are present as $c_{13} = \cos\theta_{13}$, $s_{13} = \sin\theta_{13}$ or the CP violation phase δ_{CP}, characteristic of the three-neutrino setup. In addition, NSI parameters involving tau-neutrinos ($\varepsilon_{\tau\tau}$, $\varepsilon_{e\tau}$ and $\varepsilon_{\tau\mu}$) are also present in Eqs. (2.79) and (2.80) as a third neutrino effect.

Thus, taking into account the approximation given by Eq. (2.77), the disappearance probability is calculated as follows,

$$P_{\nu_e\to\nu_e} \simeq s^4_{13} + c^4_{13}P_2\,, \qquad (2.81)$$

where P_2 is the survival electron-neutrino probability, $P_{\nu'_e\to\nu'_e}$, arising from Eq. (2.77).

Table 2.3: Values of NSI constraints at 90 % C.L. for the neutrino-electron scattering considering one parameter at a time [90].

NSI	One parameter at a time	
ε_{ee}^{eL}	$(-0.021,\ 0.052)$ [140]	
ε_{ee}^{eR}	$(-0.07,\ 0.08)$ [148]	$(-0.08,\ 0.09)$ [90]
$\varepsilon_{\mu\mu}^{eL}$	$(-0.03,\ 0.03)$ [87]	$(-0.03,\ 0.03)$ [103]
$\varepsilon_{\mu\mu}^{eR}$	$(-0.03,\ 0.03)$ [87]	$(-0.03,\ 0.03)$ [103]
$\varepsilon_{\tau\tau}^{eL}$	$(-0.16,\ 0.11)$ [140]	$(-0.46,\ 0.24)$ [103]
$\varepsilon_{\tau\tau}^{eR}$		$(-0.25,\ 0.43)$ [103]
$\varepsilon_{e\mu}^{eL}$		$(-0.13,\ 0.13)$ [103]
$\varepsilon_{e\mu}^{eR}$	$(-0.19,\ 0.19)$ [148]	$(-0.13,\ 0.13)$ [103]
$\varepsilon_{e\tau}^{eL}$	$(-0.40,\ 0.40)$ [87]	$(-0.33,\ 0.33)$ [103]
$\varepsilon_{e\tau}^{eR}$	$(-0.28,\ -0.05)$ and $(-0.19,\ -0.19)$ [148]	$(0.05,\ 0.28)$ [103]
$\varepsilon_{\mu\tau}^{eL}$	$(-0.10,\ 0.10)$ [87]	$(-0.10,\ 0.10)$ [103]
$\varepsilon_{\mu\tau}^{eR}$	$(-0.10,\ 0.10)$ [87]	$(-0.10,\ 0.10)$ [103]

Considering NSI with d-quarks only, the bounds on NSI parameters are estimated in [146] at 90 % C.L.

$$-0.25 < \varepsilon_D < -0.02 \quad \text{and} \quad -0.14 < \varepsilon_N < 0.12\,. \tag{2.82}$$

The bounds on the NSI propagation parameters are compiled in Table 2.2. In the next section we discuss short baseline neutrino experiments, based at reactor and accelerators.

2.4.4 NSI in short baseline experiments

Up to now, we have considered experiments where the neutrino propagation is the most significant part of the experiment, but short baseline experiments, where the effects of propagation are not very important, have also been used to probe neutrino interactions with quarks and leptons. In this case, bounds on NSI couplings arise from comparing the experimental cross section with the SM cross section for the interaction of neutrinos with the corresponding lepton or quark. Note that such experiments are sensitive to the axial

Table 2.4: Values of NSI constraints at 90 % C.L. for the neutrino-electron scattering considering two parameters at a time [90].

NSI	Two parameters	
ε_{ee}^{eL}	$(-0.02,\ 0.09)$ [149]	$(-0.036,\ 0.063)$ [150]
ε_{ee}^{eR}	$(-0.11,\ 0.05)$ [149]	$(-0.10,\ 0.09)$ [90]
$\varepsilon_{\mu\mu}^{eL}$		$(-0.033,\ 0.055)$ [103]
$\varepsilon_{\mu\mu}^{eR}$		$(-0.040,\ 0.053)$ [103]
$\varepsilon_{\tau\tau}^{eL}$	$(-0.51,\ 0.34)$ [149]	$(-0.16,\ 0.11)$ [140]
$\varepsilon_{\tau\tau}^{eR}$	$(-0.35,\ 0.50)$ [149]	$(-0.40,\ 0.60)$ [103]
$\varepsilon_{e\mu}^{eL}$	$(-0.53,\ 0.53)$ [151]	
$\varepsilon_{e\mu}^{eR}$	$(-0.53,\ 0.53)$ [151]	
$\varepsilon_{e\tau}^{eL}$	$(-0.53,\ 0.53)$ [151]	
$\varepsilon_{e\tau}^{eR}$	$(-0.53,\ 0.53)$ [151]	
$\varepsilon_{\mu\tau}^{eL}$	$(-0.53,\ 0.53)$ [151]	
$\varepsilon_{\mu\tau}^{eR}$	$(-0.53,\ 0.53)$ [151]	

coupling [9], unlike propagation experiments.

As an example, we will consider the phenomenology related with short baseline experiments where electron-antineutrinos scatter off electrons. This is a neutral-current process, so corrections following from Eq. (2.2) must be introduced in the interaction cross section in order to study NSI. Therefore, the differential cross section including standard and new physics terms is written as

$$\begin{aligned}\frac{d\sigma}{dT_e} &= \frac{2G_F^2 m_e}{\pi}\left[(g_R^e+\varepsilon_{ee}^{eR})+\sum_{\alpha\neq e}|\varepsilon_{\alpha e}^{eR}|^2+\left[(g_L^e+\varepsilon_{ee}^{eL})^2+\sum_{\alpha\neq e}|\varepsilon_{\alpha e}^{eL}|^2\right]\left(1-\frac{T_e}{E_\nu}\right)^2\right. \\ &- \left.\left[(g_R^e+\varepsilon_{ee}^{eR})(g_L^e+\varepsilon_{ee}^{eL})\sum_{\alpha\neq e}|\varepsilon_{\alpha e}^{eR}||\varepsilon_{\alpha e}^{eL}|\right]\left(m_e\frac{T_e}{E_\nu^2}\right)\right]. \end{aligned} \tag{2.83}$$

In this expression, m_e stands for the electron mass, E_e represents the electron energy, $T_e = E_e - m_e$ is the electron recoil energy and g_L^e and g_R^e are the SM coupling constants, whose values can be found in Table 2.1.

Several experiments imply incoming electron-(anti)neutrino fluxes, as reactor exper-

[9] Translating to NSI couplings, this means $\varepsilon^A = \varepsilon^L - \varepsilon^R$.

iments, where we find TEXONO [152], MUNU [153], Rovno [154], Krasnoyarsk [155], Irvine [156], or accelerator experiments as LSND [157] and LAMPF [158]. An individual or combined analysis of their data can be performed in order to constrain NSI parameters. The results of these analyses are summarized in Tables 2.3 and 2.4.

Likewise, we may proceed for muon-(anti)neutrino scattering from CHARM-II data [159]. However, the tau-neutrino case presents a greater difficulty because there is no artificial source of these particles. Even so, it is possible study their interactions if one considers that tau-neutrinos take part in the process $e^+e^- \to \nu\bar{\nu}\gamma$ probed at LEP [151], or if it is a component of the solar neutrino flux [140]. Keeping these considerations in mind, we can find some bounds for muon and tau-neutrino NSI parameters, which are compiled in Tables 2.3 and 2.4.

In addition to the (anti)neutrino scattering off electrons, it is possible to study NSI with quarks. For this purpose, the data of accelerator experiments such as CHARM [160], CDHS [161] or NuTeV [162] have been analyzed, leading to bounds on NSI parameters for processes of neutrinos with d-quarks. It is worth noting that the NuTeV Collaboration found a discrepancy between the cross section measured by the experiment and the SM value. After this mismatch, new reinterpretations of NuTeV results were made [163, 164], reconciling the NuTeV results with SM predictions [10]. NSI constraints following from these experiments will be given in Chapters 3 and 4.

[10] We will go back to this puzzle in Chapter 4.

Chapter 3

Robustness of solar neutrino oscillations

The neutrino oscillation mechanism is the correct scenario to explain solar neutrino data, as we can infer from solar neutrino experiments [35, 36, 50, 70, 73, 75, 165–172], combining them with reactor data from the KamLAND experiment [37]. Solar neutrino experiments are affected by matter effects in a crucial way [173, 174], and the combination of both, solar and KamLAND data, determines the so-called Large Mixing Angle (LMA) solution, which has been considered as the correct explanation of data. It is however crucial to investigate whether this solution is robust against possible additional effects inside the Sun, for instance:

- Noise density fluctuations that are originated in the radiative zone by random magnetic fields [175–182].
- Spin-flavor precession [183, 184] that could be originated by magnetic fields in the convective region [185, 186].

For all these examples, the KamLAND experiment plays a decisive role, implying that any non-standard effect can only be considered as secondary [2].

Nevertheless, the possible existence of non-standard interactions still introduces an important exception to the robustness of the solar neutrino oscillation interpretation [84, 104, 187]. In this context, it has been found that NSI may produce a degeneracy in the solar neutrino parameter space, giving rise to the so-called LMA-Dark solution [84].

Given the precision expected in upcoming oscillation studies [188], one needs to scrutinize further the possible role of NSI [189]. As already mentioned in Chapter 2, NSI appears naturally in neutrino mass theories [4] and are a powerful phenomenological tool

to probe neutrino models. For example, NSI might give a guidance to distinguish between the simplest high-scale seesaw models [9, 17, 92, 190, 191] and other scenarios based on low scales, for instance, the inverse seesaw [18, 192] and the linear seesaw mechanisms [22], or radiative models of neutrino mass [23, 24, 108].

In order to study the robustness of the oscillation interpretation of solar neutrino data in the presence of non-standard interactions, we use data from Homestake [50], SAGE [73], GALLEX [165, 166], Super-Kamiokande I [75, 167], SNO [35, 36, 70, 168, 169] and Borexino [170, 171], in combination with the KamLAND reactor experiment [37]. We have used the solar fluxes and uncertainties from the updated Standard Solar Model (SSM) [193]. It has been found that the LMA solution becomes degenerate with a new "dark-side" solution in the presence of NSI [84]. So in this thesis, we have used new data such as SNO phase III [70], and the measurements of Borexino [170, 171] in order to further constrain and possibly lift the degeneracy. We have found however that the LMA-D solution still remains.

Besides the study of solar data, we also analyze data from the CHARM accelerator experiment [194]. The combination of both analyses plays a significant role in constraining the non-standard neutrino d-quark interactions. Although CHARM is sensitive only to electron-neutrino interactions, when combined with solar and KamLAND data, it allows to improve the restrictions on the tau-neutrino non-standard axial and vector couplings.

In our analysis of non-standard interactions we parametrize them in terms of the effective low-energy neutral-current operator for four fermions, as we have seen in Sec. 2.1:

$$\mathcal{L}_{NSI} = -\varepsilon_{\alpha\beta}^{fP} 2\sqrt{2} G_F \left(\bar{\nu}_\alpha \gamma_\mu L \nu_\beta\right) \left(\bar{f} \gamma^\mu P f\right). \tag{3.1}$$

Here, f is a first-generation fermion (e, u, d) and $P = L, R$ are the chiral projectors. The parameters $\varepsilon_{\alpha\beta}^{fP}$ account for the NSI couplings of a neutrino with α and β flavor and the left or right-handed component of a fermion f.

In this chapter, for simplicity we will consider f to be the down-type quark. It is plausible to extend this work to include also the coupling with up-type quarks. However, the computations are demanding. In the case of the interaction with electrons, this has been considered before in the literature [140, 195, 196]. In this part of the thesis, we also confine our discussion to NSI couplings of electron and tau-neutrinos, while the analysis for the muon-neutrino case will be covered in Chapter 4. This approach is motivated by the constraints on the ν_μ interactions, that are stronger than those for electron and tau-neutrinos, as discussed before in Refs. [87, 151, 197] and will be reanalyzed in the next chapter. Therefore, in the following analysis we will consider $\varepsilon_{\alpha\mu}^{dP} = 0$.

We will discuss in this chapter the impact of non-standard interactions in the neutrino propagation through matter as well as in their detection. The original neutrino fluxes are less likely to be modified by NSI, especially if we consider them as originating from new physics in the neutral-current interactions. For the case of solar and KamLAND neutrino experiments, we will obtain constraints for the vectorial NSI couplings [1]. This is the natural description for an analysis involving neutrino propagation since there is no sensitivity to the axial couplings in this case [2]. For the analysis of NSI in detectors (we will discuss this analysis in the case of SNO, for example) we will also obtain constraints for the axial coupling [3].

3.1 Solar and KamLAND restrictions on NSI

In this section, we carry out a detailed study of the robustness of the standard oscillation solution to the solar neutrino problem. To keep the number of parameters under control, we consider a two-neutrino picture, which is adequate to illustrate our results.

3.1.1 The solar and KamLAND data

In order to analyze the effect of non-standard interactions over the LMA solution, we include in our analysis the results from the radiochemical experiments as Homestake [50], SAGE [73] and GALLEX/GNO [165, 166], the zenith-spectra data set from Super-Kamiokande I [75, 167], as well as the results from the three phases of the SNO experiment [35, 36, 70, 168, 169] [4], and the measurement of the ^{7}Be solar neutrino ratio reported by the Borexino Collaboration [170, 171].

The latest version of the Solar Standard Model (SSM in what follows) [193] is used in this analysis as well, which implies an improved determination of the neutrino flux uncertainties, mainly thanks to the better accuracy on the ^{3}He-^{4}He cross section measurement and to the reduced systematic uncertainties in the determination of the surface composition of the Sun. There are two different solar models introduced in Ref. [193], that correspond to two different measurements of solar metal abundances. Our results are similar for both models and, for definiteness we show in this thesis the higher solar metallicity model, referred as BPS08(GS).

[1] Remember that $\varepsilon^{dV}_{\alpha\beta} = \varepsilon^{dL}_{\alpha\beta} + \varepsilon^{dR}_{\alpha\beta}$.

[2] We should point that SNO is sensitive to the NSI axial coupling as we will see in Sec. 3.1.4.

[3] Remember that $\varepsilon^{dA}_{\alpha\beta} = \varepsilon^{dL}_{\alpha\beta} - \varepsilon^{dR}_{\alpha\beta}$.

[4] In the third phase of the SNO experiment, ^{3}He proportional counters were used in order to measure the neutral-current signal of the solar neutrino flux.

Solar neutrino data are sensitive mainly to the neutrino oscillation parameters Δm^2_{12} and $\sin^2\theta_{12}$. A reactor experiment which is sensitive to the same sector of neutrino parameters is the KamLAND experiment. Hence, one can combine the results of both solar and KamLAND experiments, resulting in the Fig. 3.1. The KamLAND experiment measured the reactor antineutrino flux disappearance. It has an average baseline of 180 km and matter effects are nearly negligible because the antineutrinos travel over the most superficial layers of the Earth, parameterizing the terrestrial crust with a constant density profile ($\sim$ 2.6 g·cm^{-3}). This implies that the restrictions on NSI from the KamLAND experiment will be minimal, but it will be useful to restrict the standard oscillation parameters, as can be seen in Fig. 3.1. We have analyzed the results of a total exposure of 2881 ton·yr [37], considering the energy window above 2.6 MeV in order to avoid the geo-neutrino background.

3.1.2 Effects of NSI in neutrino propagation

The effects of non-standard interactions on neutrino propagation can be studied analyzing the hamiltonian describing solar neutrino evolution in the presence of NSI. These new interactions, in addition to the standard oscillation term,

$$H_{mat} = \begin{pmatrix} -\frac{\Delta m^2}{4E}\cos 2\theta + \sqrt{2}\,G_F N_e & \frac{\Delta m^2}{4E}\sin 2\theta \\ \frac{\Delta m^2}{4E}\sin 2\theta & \frac{\Delta m^2}{4E}\cos 2\theta \end{pmatrix}, \tag{3.2}$$

add an extra term H_{NSI}, accounting for an effective potential induced by the NSI with matter. It may be written as:

$$H_{NSI} = \sqrt{2}\,G_F N_d \begin{pmatrix} 0 & \varepsilon \\ \varepsilon & \varepsilon' \end{pmatrix}, \tag{3.3}$$

where ε and ε' are the NSI effective vectorial parameters. For the limit $\varepsilon^{fP}_{\alpha\mu} \sim 0$, they can be defined as [5]

$$\varepsilon = -\sin\theta_{23}\,\varepsilon^{dV}_{e\tau}\,, \qquad \varepsilon' = \sin^2\theta_{23}\,\varepsilon^{dV}_{\tau\tau} - \varepsilon^{dV}_{ee}\,. \tag{3.4}$$

The quantity N_d in Eq. (3.3) is the number density of the down-type quark along the neutrino path and θ_{23} is the atmospheric neutrino mixing angle. It is important to remark again that the neutrino propagation inside the Sun or the Earth is sensitive only to the vectorial component of NSI, $\varepsilon^{dV}_{\alpha\beta} = \varepsilon^{dL}_{\alpha\beta} + \varepsilon^{dR}_{\alpha\beta}$.

[5] The reader can find the calculation of this approximation in Appendix A.

Before introducing the numerical analysis of solar neutrino data, it is convenient to discuss the analytical formulas involving neutrino survival probabilities in the constant matter density case. In the two-neutrino picture where neutrinos evolve in an adiabatic regime, the survival probability can be approximated by Parke's formula [6] [198],

$$P(\nu_e \to \nu_e) = \frac{1}{2}\left[1 + \cos 2\theta \cos 2\theta_m\right], \tag{3.5}$$

where θ is the mixing angle in the two–neutrino scheme and θ_m is the effective mixing angle in the neutrino production point inside of the Sun. If we do not include the non-standard neutrino-matter interaction, the effective mixing angle may be calculated from the following expression:

$$\cos 2\theta_m = \frac{\Delta m^2 \cos 2\theta - 2\sqrt{2}\, EG_F N_e}{\sqrt{\left(\Delta m^2 \cos 2\theta - 2\sqrt{2}\, EG_F\, N_e\right)^2 + \left(\Delta m^2 \sin 2\theta\right)^2}}, \tag{3.6}$$

where N_e is the number density of electrons along the neutrino path and E is the neutrino energy.

To explain the deficit of the neutrino signal in detectors, the neutrino survival probability should satisfy $P_{ee} < 0.5$ which implies, according to Eqs. (3.5) and (3.6), $\cos 2\theta > 0$. Hence, only vacuum mixing angles between $0 < \theta < \frac{\pi}{4}$ are able to solve the solar neutrino problem, as we can see in Fig. 3.1.

However, this scenario changes in the presence of non-standard interactions. From Eqs. (3.2) and (3.3) one sees that the solar neutrino mixing angle in the presence of NSI is given by the following expression:

$$\cos 2\theta_m = \frac{\Delta m^2 \cos 2\theta - 2\sqrt{2}\, EG_F(N_e - \varepsilon' N_d)}{\left[\Delta m^2\right]_{matter}}, \tag{3.7}$$

where

$$\left[\Delta m^2\right]^2_{matter} = \left[\Delta m^2 \cos 2\theta - 2\sqrt{2}\, EG_F(N_e - \varepsilon' N_d)\right]^2 \tag{3.8}$$

$$+ \left[\Delta m^2 \sin 2\theta + 4\sqrt{2}\, \varepsilon\, EG_F N_d\right]^2. \tag{3.9}$$

As a result of the presence of non-standard parameters ε and ε' into the equations, we

[6] Notice that this is a particular case of Eq. (1.162) discussed in Sec. 1.6.3.

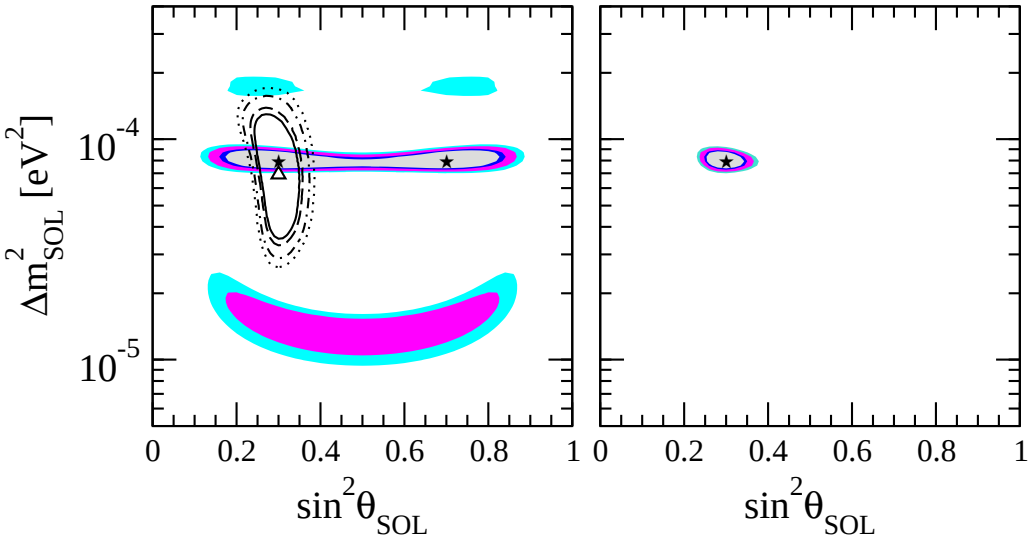

Figure 3.1: Regions at 90%, 95%, 99% and 99.73% C.L. for neutrino oscillation parameters. The left panel shows separately the result from the solar (empty regions) and from the KamLAND data (colored regions). The right panel shows the result for the combined analysis [84].

can obtain $P_{ee} < 0.5$ even for $\cos 2\theta < 0$, provided that

$$\varepsilon' > \frac{2\sqrt{2}\, EG_F N_e + \Delta m^2 |\cos 2\theta|}{2\sqrt{2}\, EG_F N_d} \,. \tag{3.10}$$

This makes possible to explain the solar neutrino data with values of the vacuum mixing angle larger than $\frac{\pi}{4}$ (in the so-called "dark side"), for large enough values of ε'. For instance, for neutrino energies and matter densities in the typical range of the solar regime one has $\varepsilon' \gtrsim 0.6$.

This degeneracy between the non-universal coupling ε' and the neutrino mixing angle θ, as a consequence of the effect of NSI on solar neutrino propagation, implies the presence of an additional solution to the solar neutrino problem, the LMA-D solution.

After this theoretical discussion, now we turn our attention to the experimental data. We perform a combined solar + KamLAND analysis using all the solar neutrino data available at the time, as discussed in Sec. 3.1.1, along with the KamLAND result [37]. For the solar neutrino data, we compute the survival probabilities for a wide range of $\Delta m^2_{\rm SOL}$, ε, and ε'. For the neutrino mixing angle, $\sin^2\theta_{\rm SOL}$ [7], we consider the whole range of values (from 0 to 1), which includes the dark-side region. Regarding the statistics, for

[7] We sholud remember that $\Delta m^2_{\rm SOL} = \Delta m^2_{21}$ and $\theta_{\rm SOL} = \theta_{12}$.

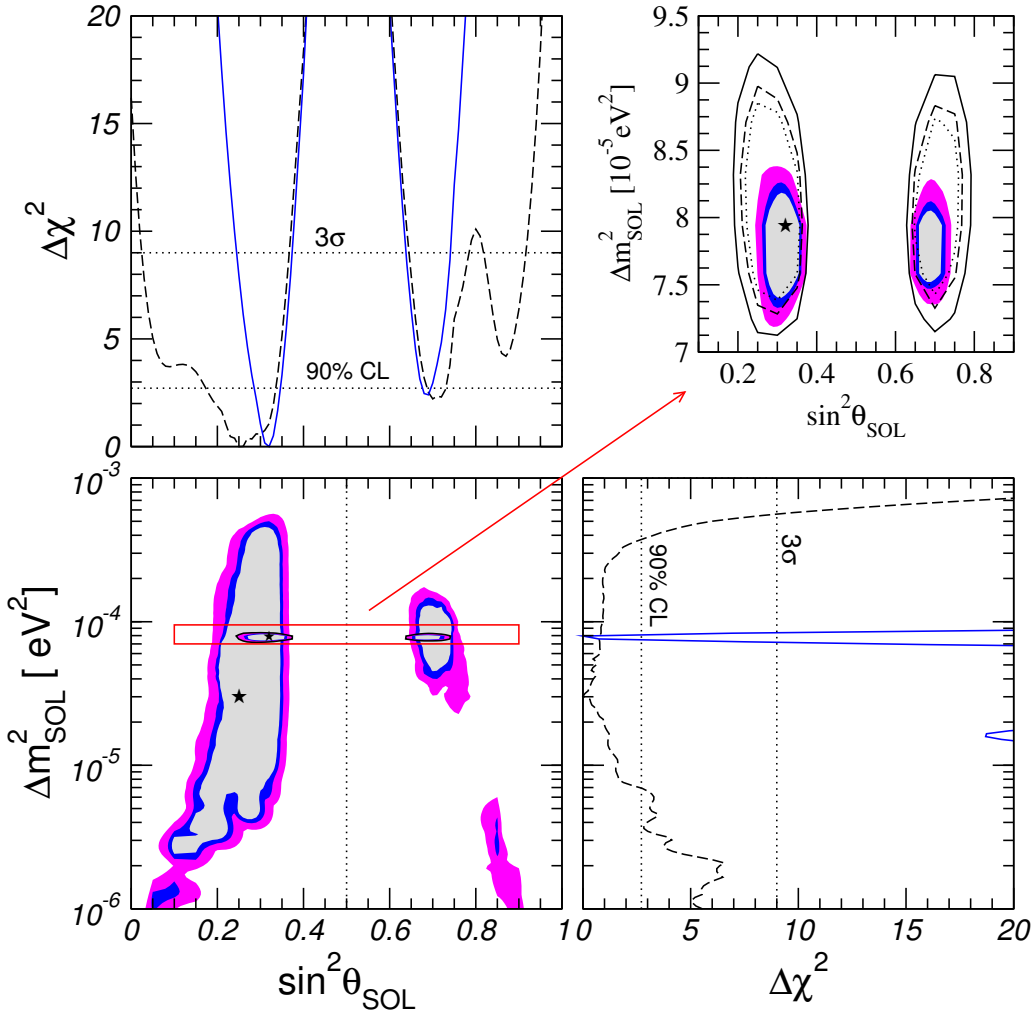

Figure 3.2: Regions at 90%, 95%, and 99% C.L. for neutrino oscillation parameters in the presence of NSI. The left-bottom panel shows the result from the combined analysis of solar and KamLAND data. The top-right panel presents the same result in more detail for the region of interest. In this case the current analysis (shaded regions) is compared with earlier results (empty regions) [84]. We also show the χ^2 in other two panels. We have marginalized over the NSI parameters in all panels.

the KamLAND analysis we use a Poisson statistics as in [199], while for the solar data we employ the pull method [200] in order to fit the results using the BPS08(GS) Standard Solar Model. The main result is shown in Fig. 3.2. There, we plot the allowed regions (90%, 95% and 99% C.L.) in the solar neutrino oscillation parameter space ($\sin^2\theta_{\rm SOL}$, $\Delta m^2_{\rm SOL}$) obtained in the analysis of solar and solar + KamLAND neutrino data. To obtain this result, a marginalization of the NSI 4-parameter $\chi^2(\sin^2\theta_{\rm SOL}, \Delta m^2_{\rm SOL}, \varepsilon, \varepsilon')$ analysis was necessary. The $\Delta\chi^2$ profiles, as a function of each parameter, are also shown. One can

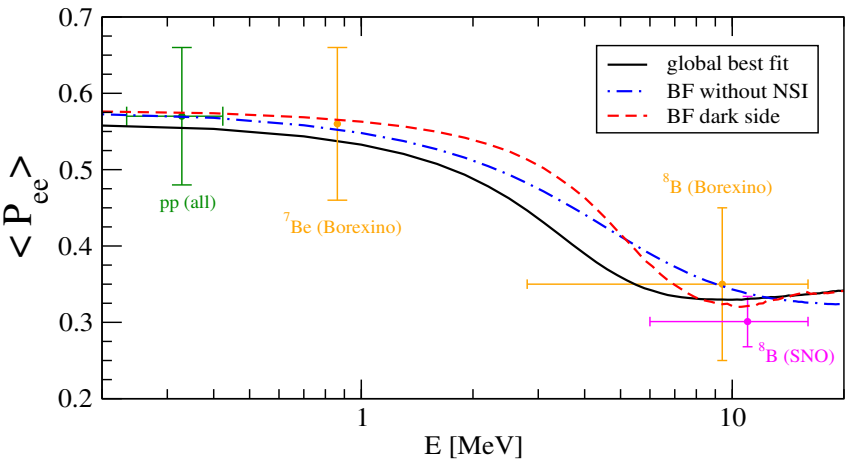

Figure 3.3: Predicted neutrino survival probabilities for three different reference points (details in the text). The probabilities have been averaged over the ^{8}B neutrino production region. We also show, for reference, the rates for the pp neutrino flux, for the ^{7}Be line, and for two different values for the ^{8}B neutrino flux, as reported from Borexino and from SNO (third phase). The vertical lines indicate the experimental errors. The horizontal lines show the energy range covered by the experiment.

see the presence of the dark-side region, which is a direct consequence of the NSI.

The best-fit points obtained for this χ^2 analysis are given by the following parameter values:

$$\sin^2\theta_{\rm SOL} = 0.32, \quad \Delta m^2_{\rm SOL} = 7.9\times10^{-5}\,{\rm eV}^2, \quad \varepsilon = -0.15, \quad \varepsilon' = -0.10. \tag{3.11}$$

We have also considered the best fit point in the absence of NSI, allowed with a $\Delta\chi^2 = 2.7$:

$$\sin^2\theta_{\rm SOL} = 0.30\,, \quad \Delta m^2_{\rm SOL} = 7.9\times10^{-5}\,{\rm eV}^2\,, \quad \varepsilon = 0.00\,, \quad \varepsilon' = 0.00\,. \tag{3.12}$$

Finally, the best fit point in the "dark-side" region of the oscillation parameters, which is allowed with a $\Delta\chi^2$= 2.9, gives rise to the values:

$$\sin^2\theta_{\rm SOL} = 0.70\,, \quad \Delta m^2_{\rm SOL} = 7.9\times10^{-5}\,{\rm eV}^2\,, \quad \varepsilon = -0.15\,, \quad \varepsilon' = 0.95\,. \tag{3.13}$$

In order to better understand the results obtained, we plot in Fig. 3.3 the neutrino survival probabilities for these reference points (Eqs. (3.11), (3.12) and (3.13) labeled as "global best fit", "BF without NSI" and "BF dark side" respectively.

Notice from Fig. 3.3 that the different survival probability predictions are in very good

agreement with the measurements in the low-energy neutrino region (*pp* and ^{7}Be). In the high-energy region, where the boron neutrino flux is predominant and matter effects are more significant, the presence of NSI gives a slightly better fit to the data, in comparison to the standard neutrino oscillation solution. This sensitivity in the high-energy region is due to the different spectrum shape at high energy for the NSI solution. In this region, a flatter spectrum is expected when NSI are introduced. The most important difference is found in the intermediate-energy region, above few MeV. A precise measurement in this region would break the degeneracy between these solutions. Therefore, a lower threshold boron solar experiment (such as in the proposals of Hyper-Kamiokande and SNO [201, 202]) would be of great interest for this type of physics. Precise measurements of the beryllium and *pep* fluxes may also help to break the degeneracy between the standard oscillation and the dark-side solution.

3.1.3 Constraints on vectorial NSI

In the previous section, we have considered the effects of NSI in solar neutrino propagation. We have shown how a new solution appears in the solar parameter space, in addition to the standard light-side solution. In this subsection, we focus on the allowed region for the vectorial NSI parameters, that we have defined for this case as ε and ε'. For this purpose, we can first obtain a restriction for either ε or ε' by marginalizing our four-parameter χ^2 analysis with respect to the other three-neutrino parameters. The results are shown in Fig. 3.4, allowing to obtain the following bounds at 90% C.L.:

$$-0.41 < \varepsilon < 0.06\,, \tag{3.14}$$

$$-0.50 < \varepsilon' < 0.19 \quad \& \quad 0.89 < \varepsilon' < 0.99\,. \tag{3.15}$$

As these constraints show, there is no degeneracy in the flavor changing parameter ε and we can constrain it to a single isolated region. However, we observe that for relatively large values of ε', the flavor conserving parameter, there is another solution in the "dark side" of the neutrino oscillation parameters. Thus, NSI still play a sub-leading (but significant) role for neutrino conversion in matter, making the determination of solar neutrino parameters, especially the solar mixing angle, still ambiguous.

Taking into account the value of the best fit for the atmospheric mixing angle in Ref. [203], we can use the bound obtained in Eq. (3.14) and the expression of ε (Eq. (3.4))

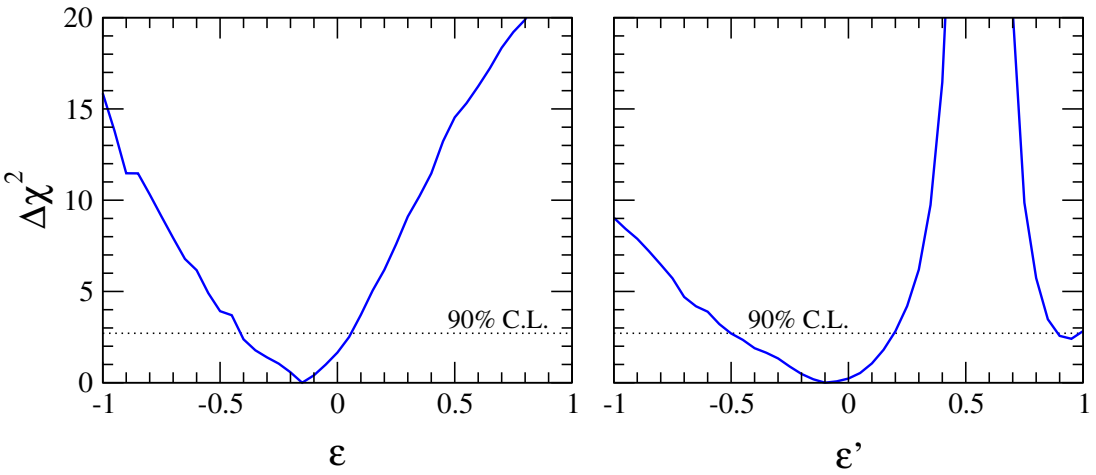

Figure 3.4: Constraints on ε and ε' effective NSI parameters. These constraints come from a global analysis of solar + KamLAND data. The ε parameter is constrained to one region, while for the ε' parameter we obtain two possible regions. One of these regions corresponds to the light-side solution while the other one (less favored) corresponds to the dark-side region.

in order to get a limit on the vectorial flavor changing coupling $\varepsilon^{dV}_{e\tau}$ at 90 % C.L.:

$$-0.08 < \varepsilon^{dV}_{e\tau} < 0.58\,. \tag{3.16}$$

Before our analysis, the strongest constraint on this parameter was $|\varepsilon^{dV}_{e\tau}| < 0.5$ [87]. We can see from our result that solar neutrino data give a certain preference for positive values of $\varepsilon^{dV}_{e\tau}$, henceforth improving the lower bound.

3.1.4 NSI effects in neutrino detection

The presence of non-standard interactions can also affect the detection processes. In particular, the axial component of the NSI could give rise to an extra contribution to the neutral-current cross section detection at the SNO experiment, as we will see in this subsection.

The neutral-current detection reaction at the SNO experiment is given by

$$\nu + d \to \nu + p + n\,, \tag{3.17}$$

being proportional to g_A^2, with g_A as the axial coupling of the neutrino current to the hadronic current [204]. Therefore, if there is a non-standard axial coupling, it will produce

an extra contribution in the NC signal of the SNO experiment. This non-standard axial contribution is parameterized as [87]

$$\phi_{NC} \sim f_B(1 + 2\varepsilon_A) \ , \tag{3.18}$$

where we have neglected the terms of order ε_A^2. In this expression, f_B stands for the boron neutrino flux and the effective axial parameter, ε_A, is defined as [87]:

$$\varepsilon_A = \sum_{\alpha=e,\mu,\tau} \langle P_{e\alpha} \rangle_{NC} \, (\varepsilon_{\alpha\alpha}^{uA} - \varepsilon_{\alpha\alpha}^{dA}) \ . \tag{3.19}$$

If we set to zero the non-standard axial couplings with up-type quarks we have

$$\varepsilon_A = - \sum_{\alpha=e,\mu,\tau} \langle P_{e\alpha} \rangle_{NC} \, \varepsilon_{\alpha\alpha}^{dA} \, . \tag{3.20}$$

Notice that

$$\varepsilon_{\alpha\alpha}^{dA} = \varepsilon_{\alpha\alpha}^{dL} - \varepsilon_{\alpha\alpha}^{dR} \tag{3.21}$$

denotes the couplings entering in the effective lagrangian shown in Eq. (3.1). Thus, ε_A is independent of the effective couplings ε and ε' defined in Eq. (3.4).

In the NSI analysis from previous sections, we have assumed that there is no influence of the axial component of NSI, i.e. $\varepsilon_A = 0$. This assumption was well justified, thanks to the good agreement between the SNO NC measurement [70]:

$$\phi_{NC}^{\rm SNO} = 5.54 \, ^{+0.33}_{-0.31} \, (\text{stat}) \, ^{+0.36}_{-0.34} \, (\text{syst}) \ \times 10^6 \, \text{cm}^{-2}\text{s}^{-1} \, , \tag{3.22}$$

and the SSM boron flux prediction [193]:

$$f_B = 5.94 \pm 0.65 \ \times \ 10^6 \, \text{cm}^{-2}\text{s}^{-1} \, . \tag{3.23}$$

We will now relax this hypothesis by considering the effect of the new NSI parameter ε_A in the analysis.

For this case, we perform a new χ^2 analysis which now includes five parameters, $\chi^2(\sin^2\theta_{\rm SOL}, \, \Delta m^2_{\rm SOL}, \, \varepsilon, \, \varepsilon', \, \varepsilon_A)$. The results for this generalized 5-parameter analysis are summarized in Fig. 3.5. In the left panel of this figure we show the regions at 90%, 95% and 99% C.L. obtained from the marginalization of the full 5-parameter analysis (filled colored regions). In the same panel we show, for comparison, the allowed areas obtained from the 4-parameter analysis, without the ε_A coupling, discussed in the previous section

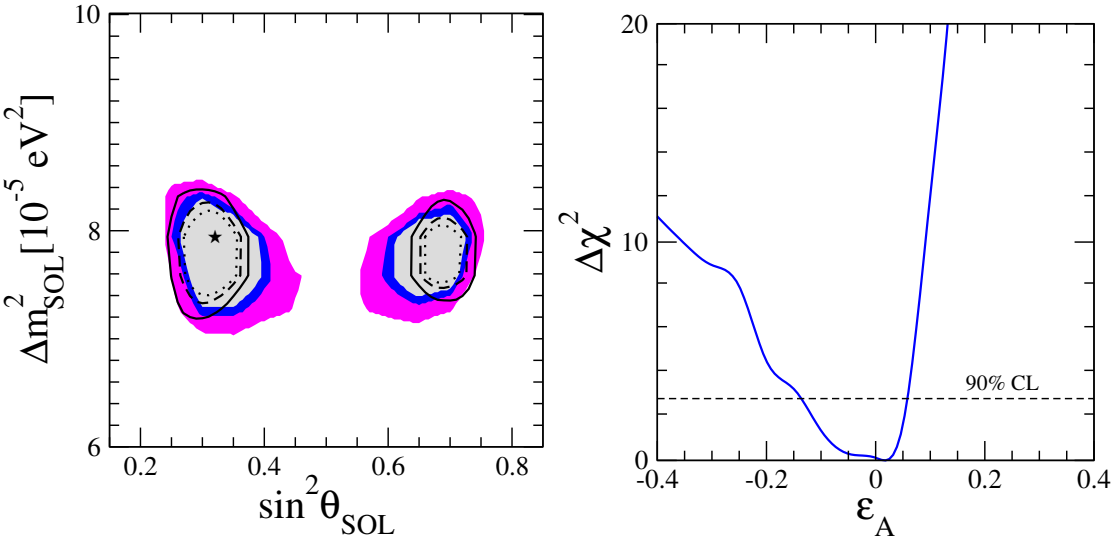

Figure 3.5: Combined five-parameter analysis, including axial couplings, of solar and KamLAND data. In the case of the solar data, we have also considered the presence of an axial NSI contribution in the SNO neutral-current channel for the detector. The left panel shows the neutrino oscillation parameters, marginalized over of all NSI parameters, while the right panel presents the χ^2 profile for the ε_A parameter, after marginalizing over all other parameters. The empty regions in the right panel show the case where the axial coupling has been set to zero. The data prefer $\varepsilon_A \sim 0$.

(empty regions). Both results are consistent, although, as expected, the inclusion of a new parameter increases slightly the allowed region. Using our analysis it is also possible to constrain the effective axial coupling ε_A. We show the $\Delta\chi^2$ analysis for this case, marginalized over the other four parameters, in the right panel of Fig. 3.5. It is clear that data prefer $\varepsilon_A \sim 0$, as expected from the good agreement between the predicted boron flux and the NC measurement reported by SNO. From this study, we report the constraint for ε_A at 90% C.L.

$$-0.14 < \varepsilon_A < 0.06\,. \tag{3.24}$$

We can attempt to translate this effective parameter into constraints for the NSI parameters that appear in the original lagrangian (Eq (3.1)), $\varepsilon^{dA}_{\alpha\alpha}$, through Eq. (3.20). From this equation, we can notice that neglecting muon-neutrino NSI, the effective parameter depends on four quantities: two averaged probabilities $\langle P_{ee}\rangle_{NC}$ and $\langle P_{e\tau}\rangle_{NC}$ and two NSI couplings ε^{dA}_{ee} and $\varepsilon^{dA}_{e\tau}$. The average values for the probabilities were reported by the SNO

Table 3.1: Sensitivity of neutrino experiments to non-universal NSI parameters.

Data	ε_{ee}^{dV}	$\varepsilon_{\tau\tau}^{dV}$	ε_{ee}^{dA}	$\varepsilon_{\tau\tau}^{dA}$
Solar propagation	✓	✓		
Solar NC detection			✓	✓
KamLAND propagation	✓	✓		
CHARM detection	✓		✓	

Collaboration [70]:

$$\langle P_{ee} \rangle_{NC} = 0.30 \pm 0.03\,, \tag{3.25}$$

$$\langle P_{e\tau} \rangle_{NC} = 0.35 \pm 0.02\,. \tag{3.26}$$

With these values for the average probabilities, we can compute restrictions for the parameters ε_{ee}^{dA} and $\varepsilon_{e\tau}^{dA}$. The allowed regions for this case will be presented and discussed in the next section, where we will see that a combined analysis with CHARM laboratory data will allow for additional constraints on the NSI couplings.

3.2 Analysis including CHARM data

Several laboratory experiments have also measured neutrino-nucleon scattering. Although some of them are insensitive to neutrino oscillations, they will be helpful to constrain neutrino NSI with d-quarks. In this section, we will focus on the results of the CHARM experiment. We will obtain additional bounds from this experiment and we will combine them with those already discussed in Sec. 3.1. Since the number of parameters involved in the analysis increases, we have limited ourselves to the case of flavor-conserving non-standard couplings. The relevant parameters for each experiment, in this approximation, are shown in Table 3.1.

3.2.1 Constraints on non-universal NSI from CHARM

CHARM was an accelerator experiment carried out at CERN. This experiment measured the neutral to charged-current cross section ratio for electron-(anti)neutrinos off quarks. We have used the results published by the CHARM Collaboration for the $\nu_e q \to \nu q$ [194],

which is

$$R^e = \frac{\sigma(\nu_e N \to \nu_e X) + \sigma(\bar{\nu}_e N \to \bar{\nu} X)}{\sigma(\nu_e N \to e X) + \sigma(\bar{\nu}_e N \to \bar{e} X)} = (\tilde{g}_{Le})^2 + (\tilde{g}_{Re})^2 = 0.406 \pm 0.140\,. \tag{3.27}$$

For the couplings $(\tilde{g}_{Le})^2$ and $(\tilde{g}_{Re})^2$, the most general expressions including all NSI parameters are given by

$$(\tilde{g}_{Le})^2 = (g_L^u + \varepsilon_{ee}^{uL})^2 + \sum_{\alpha \neq e} |\varepsilon_{\alpha e}^{uL}|^2 + (g_L^d + \varepsilon_{ee}^{dL})^2 + \sum_{\alpha \neq e} |\varepsilon_{\alpha e}^{dL}|\,, \tag{3.28}$$

$$(\tilde{g}_{Re})^2 = (g_R^u + \varepsilon_{ee}^{uR})^2 + \sum_{\alpha \neq e} |\varepsilon_{\alpha e}^{uR}|^2 + (g_R^d + \varepsilon_{ee}^{dR})^2 + \sum_{\alpha \neq e} |\varepsilon_{\alpha e}^{dR}|\,. \tag{3.29}$$

In order to render these Eqs. (3.28) and (3.29) more useful for our purpose, we introduce some simplifications:

- We neglect all flavor-changing non-standard contributions, implying that $\varepsilon_{\alpha e}^{qL} = 0$ for $\alpha \neq e$.

- The NSI parameters involving quark up are also omitted, implying that $\varepsilon_{ee}^{uP} = 0$.

In our analysis, the vectorial-axial notation is used to describe the coupling parameters, while the CHARM result is given in the left-right parametrization, so we transform Eqs. (3.28) and (3.29) employing the following relations:

$$\varepsilon_{ee}^{dL} = \frac{1}{2}(\varepsilon_{ee}^{dV} + \varepsilon_{ee}^{dA})\,, \tag{3.30}$$

$$\varepsilon_{ee}^{dR} = \frac{1}{2}(\varepsilon_{ee}^{dV} - \varepsilon_{ee}^{dA})\,. \tag{3.31}$$

With these conditions, we get our simplified expression for Eqs. (3.28) and (3.29) as

$$(\tilde{g}_{Le})^2 = (g_L^u)^2 + \left[g_L^d + \frac{1}{2}(\varepsilon_{ee}^{dV} + \varepsilon_{ee}^{dA})\right]^2\,, \tag{3.32}$$

$$(\tilde{g}_{Re})^2 = (g_R^u)^2 + \left[g_R^d + \frac{1}{2}(\varepsilon_{ee}^{dV} - \varepsilon_{ee}^{dA})\right]^2\,. \tag{3.33}$$

Then, we can perform the χ^2 for the CHARM data using the simplified form of the couplings given above (Eqs. (3.32) and (3.33)), which depends on two NSI parameters,

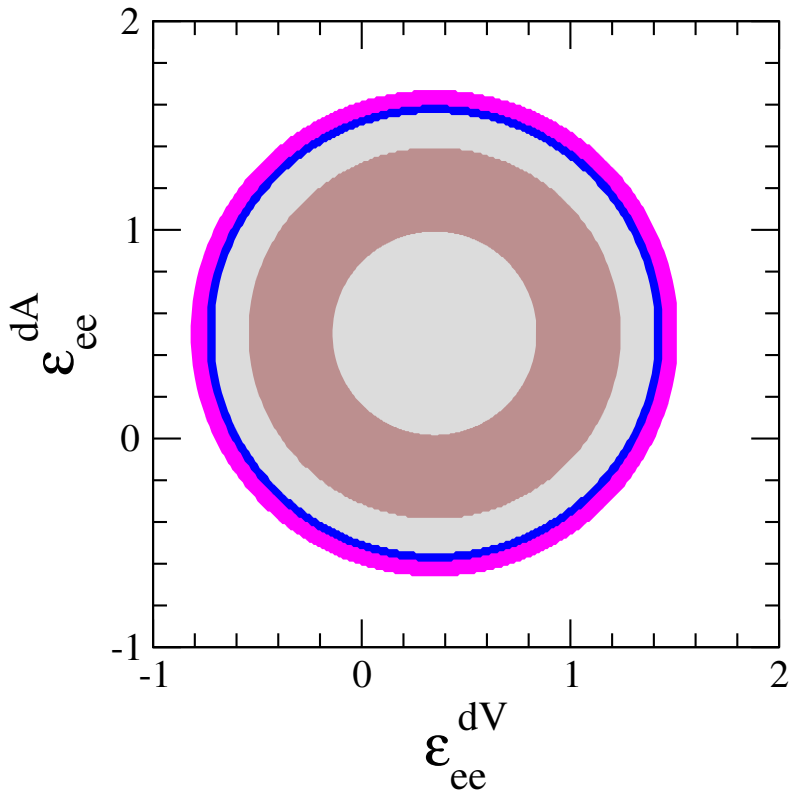

Figure 3.6: Constraints from the CHARM experiment, at 68%, 90%, 95% and 99% C.L., on the NSI couplings ε_{ee}^{dV} and ε_{ee}^{dA}.

ε_{ee}^{dV} and ε_{ee}^{dA}, through $R^{\text{theo}}(\varepsilon_{ee}^{dV}, \varepsilon_{ee}^{dA})$:

$$\chi^2 = \frac{\left[R^e - R^{\text{theo}}(\varepsilon_{ee}^{dV}, \varepsilon_{ee}^{dA})\right]^2}{(\sigma_R^e)^2} \,. \tag{3.34}$$

Here, R^e and σ_R^e are defined by the result given in Eq. (3.27) and R^{theo} corresponds to the theoretical prediction for R^e, which depends on the relevant NSI parameters ε_{ee}^{dV} and ε_{ee}^{dA} by means of $\tilde{g}_{Le}$ and $\tilde{g}_{Re}$. From this analysis, we obtain constraints in the (ε_{ee}^{dV}, ε_{ee}^{dA}) plane. These are shown in Fig. 3.6 and in Table 3.2 at 68%, 90%, 95% and 99% C.L.

3.2.2 Constraints on NSI from a combined analysis

In the previous sections, we have analyzed the sensitivity of CHARM, solar and KamLAND experiments to non-standard interactions. But, as the information obtained is complementary, we can combine the results from CHARM with the results from the analysis of solar and KamLAND data. This allows us to improve the constraints on the NSI

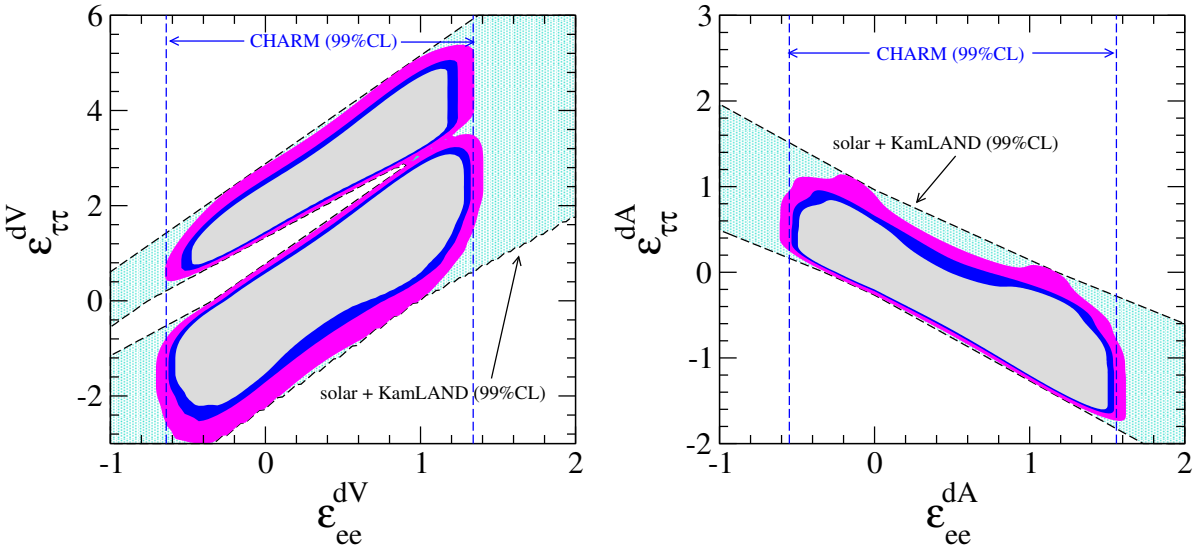

Figure 3.7: Constraints on the NSI parameters from a global analysis (colored regions), at 90, 95 and 99% C.L. The dashed lines show the restrictions from CHARM data only and solar + KamLAND. The left panel shows the limits for the vector NSI while the right one shows the axial case.

couplings. We show the outcome of this combination in Fig. 3.7. In this plot, we see the regions for the vector (left) and axial-vector (right) NSI couplings allowed by the global analysis. They are also compared with the constraints coming only from the CHARM data and that from the solar + KamLAND data.

The bounds obtained from the analysis of CHARM data are shown in Fig. 3.7 as vertical bands, after being translated into two independent bounds, ε^{dV}_{ee} and ε^{dA}_{ee}, coming from the χ^2 calculation. On the other hand, the allowed regions obtained from the solar + KamLAND combination (diagonal bands in the figure) have been derived from the limits on the non-universal NSI discussed in Sec. 3.1.

The constraints on the vectorial NSI parameters, ε^{dV}_{ee} and $\varepsilon^{dV}_{\tau\tau}$, arise from the allowed region of the effective coupling ε' in Eq. (3.14), after substituting the ε' definition in Eq. (3.4). The allowed region at 1σ for the mixing angle θ_{23} has also been used [203]. We should stress that there are two possible regions for the vector NSI parameters in this plot. This is a consequence of the existence of two allowed regions for the neutrino oscillation parameters when NSI are present (see Fig. 3.2, upper-right panel). The lower region is related to the standard LMA solution while the upper one corresponds to the dark-side solution.

We have also used the average probabilities in Eq. (3.26) to reanalyze the results for

Table 3.2: Limits on the vectorial and axial NSI parameters at 90% C.L. from the analysis of CHARM data only, and from a global analysis that combines CHARM, solar, and KamLAND data.

vectorial couplings		
Global	$-0.5 < \varepsilon_{ee}^{dV} < 1.2$	$-1.8 < \varepsilon_{\tau\tau}^{dV} < 4.4$
one parameter at a time		
CHARM	$-0.5 < \varepsilon_{ee}^{dV} < 1.2$	
Global	$-0.2 < \varepsilon_{ee}^{dV} < 0.5$	$-1.1 < \varepsilon_{\tau\tau}^{dV} < 0.4 \,\&\, 1.6 < \varepsilon_{\tau\tau}^{dV} < 2.2$

axial couplings		
Global	$-0.4 < \varepsilon_{ee}^{dA} < 1.4$	$-1.5 < \varepsilon_{\tau\tau}^{dA} < 0.7$
one parameter at a time		
CHARM	$-0.4 < \varepsilon_{ee}^{dA} < 1.4$	
Global	$-0.2 < \varepsilon_{ee}^{dA} < 0.3$	$-0.2 < \varepsilon_{\tau\tau}^{dA} < 0.4$

the effective NSI axial coupling ε_A (Eq. (3.24)). Thanks to this reanalysis we can obtain new bounds for the axial couplings ε_{ee}^{dA} and $\varepsilon_{\tau\tau}^{dA}$. We can see that for both NSI parameters (vector and axial), there is a degeneracy in the determination of the electron and tau-neutrino NSI couplings (solar + KamLAND regions in Fig. 3.2). This degeneracy has been restricted thanks to the addition of the CHARM data analysis.

We quote in Table 3.2 the allowed intervals at 90% C.L. that arise from the combined analysis for ε_{ee}^{dV}, $\varepsilon_{\tau\tau}^{dV}$, ε_{ee}^{dA} and $\varepsilon_{\tau\tau}^{dA}$. In the same table we also give the result of an analysis of one parameter at a time. We show both results, for CHARM data only and for the global analysis. We can compare these constraints with those of previous works (for instance Ref. [87]). In our case, the combination of CHARM results with solar and KamLAND data gives more restrictive bounds on the electron-neutrino NSI parameters. Concerning the tau-neutrino NSI, the previously existing limits were those coming from the measurement of the Z from LEP data and they have also been improved.

3.3 Summary

In this chapter, we have studied the role played by NSI in the explanation of solar neutrino data. For this purpose, we have performed an analysis of neutrino interactions with down-type quarks using the most recent solar and KamLAND data. We have found that, taking

into account NSI parameters, there is still room for large values of the NSI, allowing the so-called dark-side region of the neutrino parameter space found in Ref. [84]. Other secondary regions as LMA-0 and LMA-II, which were present in previous works, have now disappeared.

At this point, we asked how to remove this degeneracy in future studies. In the case of KamLAND, and other reactor experiments, we note that they are basically insensitive to matter effects. Therefore, they are not important in removing the degeneracy. Hence, for this purpose we have to consider the solar data. If we observe the shape of the neutrino survival probabilities in Fig. 3.3, we notice that the best region to discriminate the dark solution from the standard one is the intermediate energy. In this region, the relevant experiments would be, for instance, Borexino [170–172], solar + KamLAND [205] or the low-energy threshold analysis from Hyper-Kamiokande [206, 207]. Other experiments that could remove this degeneracy may be either atmospheric or laboratory data. The latter could rule out large NSI values. A possible future restriction from atmospheric and laboratory data was studied in Refs. [84, 107]. Based on the results discussed above, we conclude that the neutrino oscillation solution of solar neutrino data is still not robust enough in the presence of non-standard interactions.

We finish this chapter by noticing that we have obtained limits on the vector and axial non-standard neutrino interaction couplings with d-type quarks. In particular, we have set bounds for flavor-diagonal and flavor-changing couplings, for electron and tau-neutrinos, ε_{ee}^{dV}, $\varepsilon_{e\tau}^{dV}$, $\varepsilon_{\tau\tau}^{dV}$, ε_{ee}^{dA} and $\varepsilon_{\tau\tau}^{dA}$. The combination of the CHARM experiment with KamLAND and solar neutrino data has been very useful to obtain these constraints, improving previous results [84, 87].

Chapter 4

Probing ν_μ NSI with accelerator and atmospheric data

So far, we have concentrated on electron-neutrino NSI studies. For the study involving muon-neutrinos, collider experiments are very interesting because they produce a well-controlled and clean muon-neutrino beam, with just a small contamination of electron-neutrinos. Therefore, due to the precision of these experiments, it is expected that the muon-neutrino NSI parameters ($\varepsilon^{fP}_{\mu\beta}$) will be better constrained than for the case of other neutrino flavors. This occurs when we consider the interaction of muon-neutrinos with electrons [103, 140]. On the other hand, for neutrinos interacting with quarks, the situation is different. In the case of the NuTeV experiment, despite the accurate measurement of the $\nu_\mu - N$ interaction [162], there was a discrepancy between their results and the predicted Standard Model parameters. Besides, previous experiments, such as CDHS [161] and CHARM [160], did not have the same level of accuracy as the NuTeV result. Although these results could indicate the existence of new physics, introducing non-zero NSI for muon-neutrinos ($\varepsilon^{fP}_{\mu\alpha}$), it is important to notice that uncertainties arising from QCD corrections may have been underestimated [208]. We will make a detailed analysis on this point in this chapter, deriving new and reliable constraints on the NSI parameters coming from these experiments.

Before starting the discussion of our analysis, it is worth noting that the limits on NSI parameters, obtained from 1-loop dressing [87] of the effective four-fermion neutrino vertex, can not be expressed rigorously without specifying a model. Indeed, they will be highly model-dependent and a full analysis including all the diagrams needed to satisfy gauge-invariance, leads to rather weak constraints on the flavor changing NSI parameters, $\varepsilon^{qL,R}_{\mu\tau}$ and $\varepsilon^{qL,R}_{\mu e}$ [197].

After the NuTeV results were reported, several works introduced new corrections leading to higher systematic uncertainties. In particular, a new estimate of the electroweak mixing angle $\sin^2\theta_W$ was presented, using the NuTeV measurement and the newly calculated uncertainties [163, 164]. Since the NuTeV data give the most stringent model-independent constraints on the muon-neutrino NSI parameters ($\varepsilon_{\mu\alpha}$), it is important to reanalyze their results introducing the effect of the new systematic uncertainties on the NuTeV results. We will explain in this chapter how we made these computations. Besides, we will also review the status of the atmospheric neutrino constraints and we will perform a combined analysis with laboratory results.

In order to obtain these bounds, we will work with the following hypothesis:

- We carry out our analysis in a two-neutrino scheme.
- Only NSI parameters involving muon-neutrino are nonzero, $\varepsilon^{fP}_{\mu\beta} \neq 0$.

With these conditions, we will get relatively stringent constraints on the NSI interactions for muon-neutrinos, at the few 10^{-2} level, thanks mainly to the interplay between laboratory and atmospheric data.

4.1 Neutrino-nucleon scattering and measurements of $\sin^2\theta_W$

Neutrino scattering has been frequently used to probe different properties of the weak neutral-current, as well as to perform measurements of several parameters like the electroweak mixing angle $\sin^2\theta_W$. It is known that, for experiments with an isoscalar target, the uncertainties due to the QCD parton model cancel out, at least to a large extent [209]. If an interaction with an isoscalar target of up and down-type quarks is considered, isospin invariance relates the most important neutral and charged-current contributions. As a consequence, the ratio of both currents is related to the coupling constants g^P_μ:

$$R^\nu = \frac{\sigma(\nu_\mu N \to \nu_\mu X)}{\sigma(\nu_\mu N \to \mu^- X)} = (g^L_\mu)^2 + r(g^R_\mu)^2\,, \tag{4.1}$$

$$R^{\bar\nu} = \frac{\sigma(\bar\nu_\mu N \to \bar\nu_\mu X)}{\sigma(\bar\nu_\mu N \to \mu^+ X)} = (g^L_\mu)^2 + \frac{1}{r}(g^R_\mu)^2\,, \tag{4.2}$$

where r corresponds to the ratio between antineutrino and neutrino charged-current cross sections:

$$r = \frac{\sigma(\bar{\nu}_\mu N \to \mu^+ X)}{\sigma(\nu_\mu N \to \mu^- X)}\,. \tag{4.3}$$

The coupling constants have a contribution from both quarks, up and down:

$$(g_\mu^P)^2 = (g_\mu^{uP})^2 + (g_\mu^{dP})^2\,, \tag{4.4}$$

with $P = L, R$.

If we consider the presence of non-standard interactions, we have to introduce the (non-universal and flavor-changing) NSI parameters that couple muon-neutrinos with quarks, leading to the following expressions of the coupling constants (g_μ^P):

$$(\tilde{g}_\mu^L)^2 = (g_\mu^{uL} + \varepsilon_{\mu\mu}^{uL})^2 + (g_\mu^{dL} + \varepsilon_{\mu\mu}^{dL})^2 + \sum_{\alpha\neq\mu} |\varepsilon_{\mu\alpha}^{uL}|^2 + \sum_{\alpha\neq\mu} |\varepsilon_{\mu\alpha}^{dL}|^2\,, \tag{4.5}$$

$$(\tilde{g}_\mu^R)^2 = (g_\mu^{uR} + \varepsilon_{\mu\mu}^{uR})^2 + (g_\mu^{dR} + \varepsilon_{\mu\mu}^{dR})^2 + \sum_{\alpha\neq\mu} |\varepsilon_{\mu\alpha}^{uR}|^2 + \sum_{\alpha\neq\mu} |\varepsilon_{\mu\alpha}^{dR}|^2\,. \tag{4.6}$$

The values of R^ν and $R^{\bar{\nu}}$ parameters were measured by the CDHS [161] and CHARM experiments [160].

Another important observable in the study of deep inelastic neutrino scattering is the Paschos-Wolfenstein (PW) ratio, which is given by [210]

$$R_{PW} = \frac{\sigma(\nu_\mu N \to \nu_\mu X) - \sigma(\bar{\nu}_\mu N \to \bar{\nu}_\mu X)}{\sigma(\nu_\mu N \to \mu^- X) - \sigma(\bar{\nu}_\mu N \to \mu^+ X)} = \frac{R^\nu - r R^{\bar{\nu}}}{1 - r} = (g_\mu^L)^2 - (g_\mu^R)^2\,. \tag{4.7}$$

The PW ratio depends weakly on the nucleus target hadronic structure. Besides, this definition reduces the uncertainties coming from charm production and charm and strange sea distributions. On the negative side, it adds an extra difficulty: the simultaneous measurement of neutrino and antineutrino neutral-current cross sections makes necessary the use of two separate neutrino and antineutrino beams.

The "ratio" observables (Eqs. (4.1), (4.2) and (4.7)) could be used to calculate several neutral-current weak parameters. For instance, the NuTeV Collaboration uses these observables to report a measurement of the electroweak mixing angle, measuring the ratios R_ν and $R_{\bar{\nu}}$ experimentally and transforming them into the ratio R_{PW}. Once these ratios are computed, they can be related with $\sin^2\theta_W$ through [161, 210]

$$R^{\nu(\bar{\nu})} = \frac{1}{2} - \sin^2\theta_W + \frac{5}{4}\sin^4\theta_W\,(1 + r^{(-1)})\,. \tag{4.8}$$

4.2 The NuTeV data and constraints on NSI

Using intense neutrino and antineutrino beams, the NuTeV Collaboration measured the charged and neutral cross sections for neutrinos hitting an iron target. After separating the neutral and charged events, they reported their results for the values of R_ν and $R_{\bar{\nu}}$. With these parameters, a numerical analysis was performed by the NuTeV Collaboration, obtaining a measurement of the left and right-handed neutral couplings to the light quarks [162]:

$$(g_\mu^L)^2 = 0.30005 \pm 0.00137\,, \qquad (g_\mu^R)^2 = 0.03076 \pm 0.00110\,. \tag{4.9}$$

From these values it was possible to see a discrepancy with the Standard Model expectations [211]:

$$(g_\mu^L)^2_{\rm SM} = 0.30399 \pm 0.00017\,, \qquad (g_\mu^R)^2_{\rm SM} = 0.03001 \pm 0.00002\,, \tag{4.10}$$

being almost a 3σ discrepancy in the left-handed coupling. Similarly, the collaboration carried out a numerical fit getting a value for the electroweak mixing angle in the on-shell scheme [162]:

$$\sin^2\theta_W = 0.22773 \pm 0.00135(\text{stat}) \pm 0.00093(\text{syst})\,, \tag{4.11}$$

which is again 3σ away from the value predicted in global precise electroweak fits [211]:

$$\sin^2\theta_W = 0.22292 \pm 0.00082\,. \tag{4.12}$$

This discrepancy between the NuTeV calculations for the left (g_μ^L) and right (g_μ^R) couplings and their SM prediction could be ascribed to the existence of a non-zero NSI operator. Hence, it should take into account the $\varepsilon_{\mu\alpha}^{qP}$ parameters when the weak couplings are expressed, as we have already exposed in Eqs. (4.5) and (4.6). These considerations were borne in mind by the authors of Ref. [87], who obtained a positive hint for non-zero values of the left flavor-conserving NSI couplings, $\varepsilon_{\mu\mu}^{dL}$ and $\varepsilon_{\mu\mu}^{uL}$, as well as for the NSI parameters which involve flavor-changing interactions, $\varepsilon_{\mu\tau}^{qL;R}$.

However, before claiming the existence of non-standard interactions as possibly suggested by the NuTeV results, other more "conventional" corrections should be considered. For instance, corrections from nuclear effects and next-to-leading-order corrections which were neglected in the original NuTeV Collaboration analysis. As an example of inter-

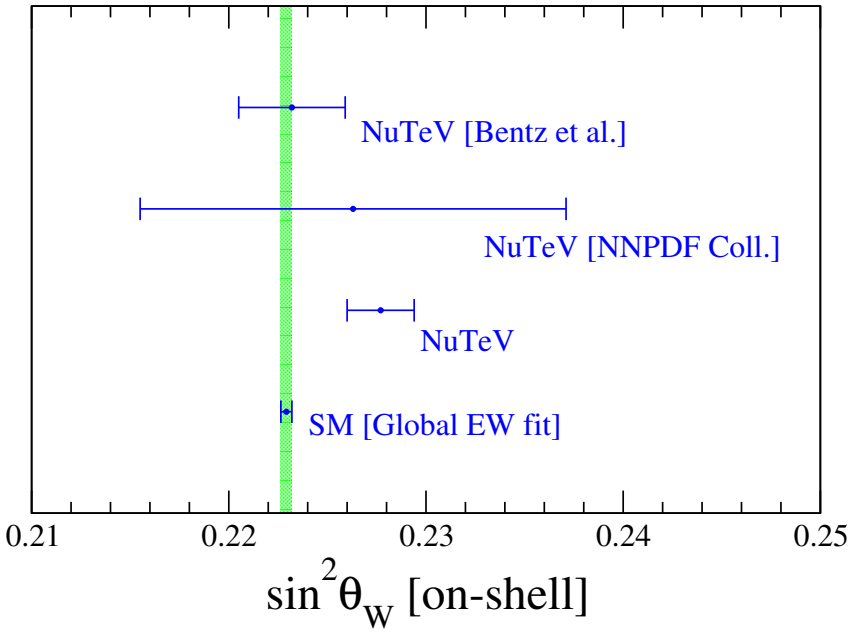

Figure 4.1: Measurements of $\sin^2\theta_W$ according to Refs. [162–164, 211].

pretations of the NuTeV anomaly in terms of conventional physics, the reader can see Refs. [208, 212].

Here, we have reanalyzed the NuTeV anomaly in terms of new physics, taking into account the new reported uncertainties from different theoretical groups [163, 164]. As we will see, we have obtained new constraints on the neutrino NSI parameters that can be considered as more reliable since they take into account this updated information.

One of the theoretical groups that has reanalyzed the uncertainties in the NuTeV experiment is the NNPDF Collaboration. They have obtained better estimates of the strange and antistrange parton distribution functions, introducing extra corrections to the NuTeV calculated parameters. With this analysis, the NNPDF Collaboration reported a new value for the weak mixing angle [163]:

$$\sin^2\theta_W = 0.2263 \pm 0.0014(\text{stat}) \pm 0.0009(\text{sys}) \pm 0.0107(\text{PDFs}). \tag{4.13}$$

In the case of Ref. [164], authors have considered corrections from nuclear effects such as the excess of neutrons in iron, the charge symmetry violation (which arises from the mass differences of the up and down-type quarks) and the strangeness. Including all these

corrections, the collaboration reported a value for the electroweak mixing angle [164]:

$$\sin^2\theta_W = 0.2232 \pm 0.0013(\text{stat}) \pm 0.0024(\text{sys})\,. \tag{4.14}$$

It can be seen from Eqs. (4.13) and (4.14), that the two new estimates for the electroweak mixing angle are very close to the SM prediction. Therefore, the inclusion of the new uncertainties has helped to understand this problem and agreement is found, within the error margin, as we can see in Fig. 4.1.

Having established that extra corrections to the NuTeV calculated parameters are needed in order to reconcile them with the SM predictions, we will use the results from NNPDF and Bentz et al. Collaborations [163, 164] to constrain the strength of the NSI couplings involving muon-neutrinos, $\varepsilon^{qP}_{\mu\alpha}$. For this purpose, we adopt the Paschos-Wolfenstein ratio R_{PW} because:

- It depends very weakly on the hadronic structure of the nucleus target.
- It is largely insensitive to the uncertainties resulting from charm production and up and down quark mass differences.
- It is only slightly affected by the charm and strange sea distribution.

After computing the prediction for the Paschos-Wolfenstein ratio for a particular value of the NSI parameters (obtained from Eqs. (4.5) and (4.6)), we calculate the corresponding χ^2 function and fit experimental data. We consider the two different recent results already discussed, Eqs. (4.13) and (4.14), and obtain constraints to $\varepsilon^{qP}_{\mu\mu}$ at 90% C.L. For the NNPDF case are:

$$-0.017 < \varepsilon^{dL}_{\mu\mu} < 0.025 \quad \& \quad 0.84 < \varepsilon^{dL}_{\mu\mu} < 0.88\,, \tag{4.15}$$

$$-0.24 < \varepsilon^{dR}_{\mu\mu} < 0.088\,, \tag{4.16}$$

$$-0.72 < \varepsilon^{uL}_{\mu\mu} < -0.67 \quad \& \quad -0.031 < \varepsilon^{uL}_{\mu\mu} < 0.020\,, \tag{4.17}$$

$$-0.058 < \varepsilon^{uR}_{\mu\mu} < 0.063 \quad \& \quad 0.24 < \varepsilon^{uR}_{\mu\mu} < 0.36\,. \tag{4.18}$$

On the other hand, when the results of Ref. [164] are used in our analysis we get:

$$-0.005 < \varepsilon^{dL}_{\mu\mu} < 0.005 \quad \& \quad 0.86 < \varepsilon^{dL}_{\mu\mu} < 0.87\,, \tag{4.19}$$

$$-0.17 < \varepsilon^{dR}_{\mu\mu} < -0.11 \quad \& \quad -0.042 < \varepsilon^{dR}_{\mu\mu} < 0.025\,, \tag{4.20}$$

$$-0.71 < \varepsilon^{uL}_{\mu\mu} < 0.70 \quad \& \quad -0.006 < \varepsilon^{uL}_{\mu\mu} < 0.006\,, \tag{4.21}$$

$$-0.014 < \varepsilon^{uR}_{\mu\mu} < 0.016 \quad \& \quad 0.28 < \varepsilon^{uR}_{\mu\mu} < 0.31\,. \tag{4.22}$$

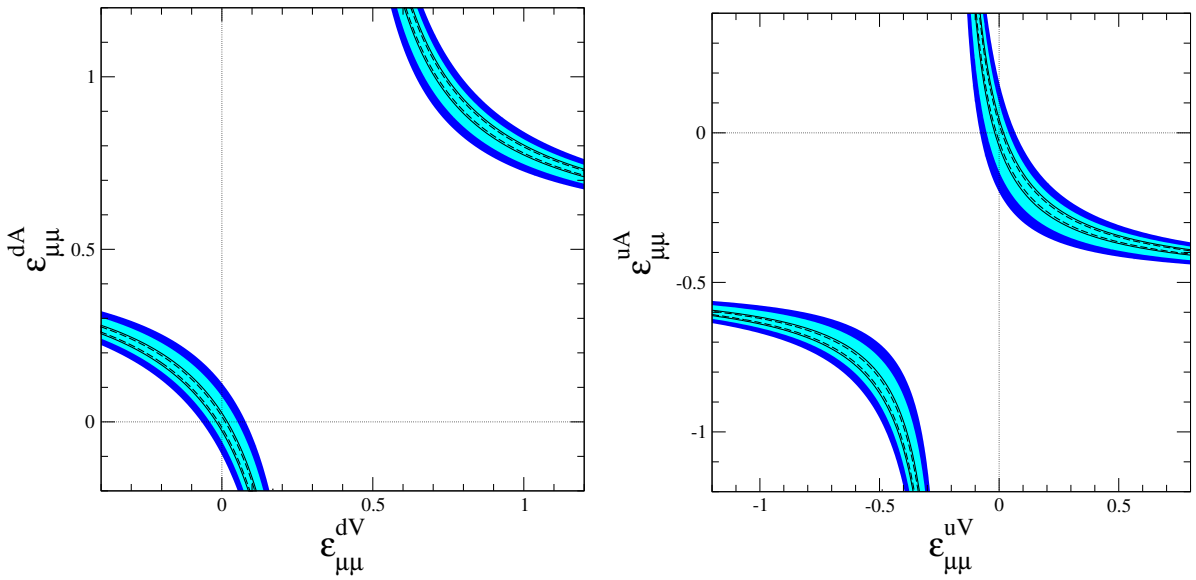

Figure 4.2: The left panel shows the allowed regions for vector and axial NSI of neutrinos with down-type quark, at 90% C.L. and 3σ. The up-type quark case is shown in the right panel. We show the results for the error analysis of the NNPDF Collaboration [163] (colored region) while the empty lines correspond to the error analysis performed by Bentz et al. [164].

In both results, two allowed regions have been obtained for most of the NSI couplings, reflecting the degeneracy shown in Fig. 4.2.

In a more general case, we increase the number of degrees of freedom implying the simultaneous presence of left and right-handed NSI neutrino couplings and obtaining a degenerate solution with hyperbolic shape, as we see in the Fig. 4.2. This degenerate solution in both cases, down and up quarks, is easily understood from Eq. (4.7). In the left panel of Fig. 4.2 we show the constraints for down-type quark NSI, while in the right one we show the corresponding restrictions on NSI for the up-type quark. We have assumed the presence of NSI with only one type of quark at a time. We present the constraints in terms of the vector and axial couplings, instead of using the left and right components. The reason for this is that we will combine these results with atmospheric data (see Sec. 4.4), that are sensitive to the vector couplings.

For the case of flavor-changing NSI, we show the allowed regions for the chiral components in Fig. 4.3. As in the previous figure, we show here the result for the two different updated error computations. In this case, only one plot is necessary since the constraints for the u and d-type quarks coincide. This time, the allowed region can be interpreted as a hyperbola centered in the origin $(\varepsilon^{qV}_{\mu\tau}, \varepsilon^{qA}_{\mu\tau}) = (0,0)$, that can be seen as a vestige of the

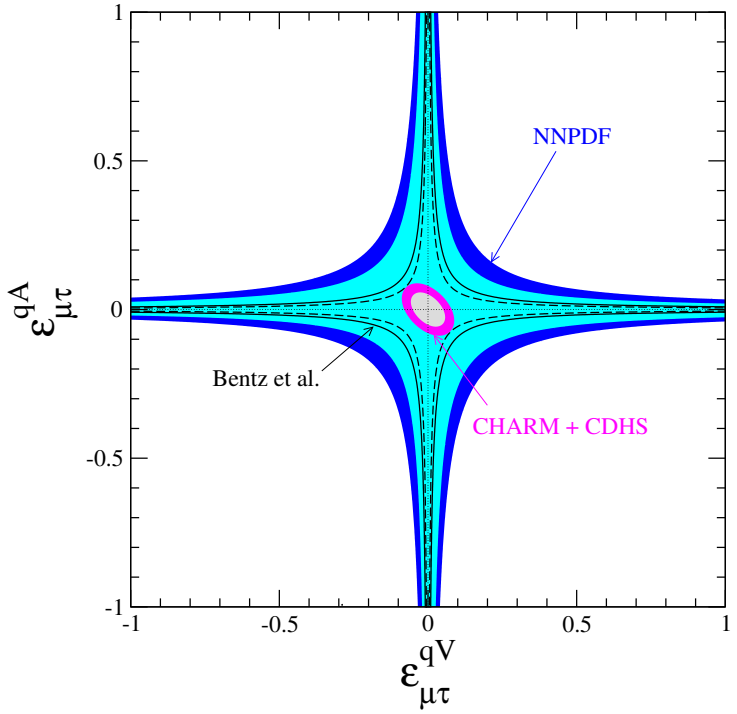

Figure 4.3: Allowed regions for vector and axial NSI of neutrinos with up and down-type quark, at 90% C. L. and 3σ. We show the results for the error analysis of the NNPDF Collaboration [163] using the colored region, while the empty lines correspond to the error analysis performed by Bentz et al. [164]. The central ellipse shows the analysis of CHARM and CDHS data, see discussion in Secs. 4.3 and 4.5.

two-fold degeneracy already discussed for the flavor-conserving case. It can be noticed, either from Fig. 4.3 or from Eqs. (4.5) and (4.7), that we constrain the product $\varepsilon^{qV}_{\mu\tau} \cdot \varepsilon^{qA}_{\mu\tau}$. This implies that one coupling may be of order one, as long as the other remains small.

4.3 NSI in the CHARM and CDHS experiments

CHARM [161] and CDHS [160] are two other experiments that measured semileptonic neutrino scattering cross sections. Their data are useful in a global fit, despite their sensitivity being lower than the one reached by the NuTeV experiment. In particular, they will play a role in the restrictions for the flavor-changing NSI. The measurements reported by these collaborations are summarized in Table 4.1.

Using the values of R^ν and $R^{\bar{\nu}}$ measured by CHARM and CDHS, we perform a χ^2 analysis taking into account the correlation between the neutrino and antineutrino ratios of neutral to charged-current given by the parameter r. With these considerations, our

Table 4.1: Neutral to charged-current ratios reported by CHARM and CDHS. We also show the SM prediction for comparison.

Experiment	Observable	Measurement	SM prediction
CDHS [161]	R^{ν}	0.3072 ± 0.0033	0.3208
	$R^{\bar{\nu}}$	0.382 ± 0.016	0.381
	r	0.393 ± 0.014	
CHARM [160]	R^{ν}	0.3093 ± 0.0031	0.3226
	$R^{\bar{\nu}}$	0.390 ± 0.014	0.371
	r	0.456 ± 0.011	

χ^2 function in this case is given by

$$\chi^2 = \sum_i \chi_i^2 = \sum_{j,k} (R_i^j - R_{i,NSI}^j)(\sigma^2)_{jk}^{-1}(R_i^k - R_{i,NSI}^k)\,, \tag{4.23}$$

where i refers to CHARM or CDHS and j, k run for R^{ν} and $R^{\bar{\nu}}$. The results of our fit analysis are shown in Fig. 4.3.

As we can observe in Fig. 4.3, the inclusion of CDHS and CHARM data provide strong constraints for the flavor changing NSI parameters. However, it is important to consider that the restriction follows from a discrepancy between the experimental and the theoretical value of R^{ν} and $R^{\bar{\nu}}$, as can be seen from Table 4.1. Therefore, as we mentioned previously, these constraints should be considered as less robust than those obtained for non-universal NSI discussed in Sec 4.1. Once we have pointed out this, for the sake of completeness, we report the 90% C.L. bounds from the CHARM/CDHS data, combined with the new analysis of the NuTeV data from the NNPDF (Bentz et al.) Collaboration:

$$-0.023(-0.023) < \varepsilon_{\mu\tau}^{qL} < 0.023(0.023), \qquad -0.039(-0.036) < \varepsilon_{\mu\tau}^{qR} < 0.039(0.036). \tag{4.24}$$

We should notice that these constraints in Eqs. (4.24) come mainly from CDHS and CHARM data, as we see in the central region of Fig. 4.3.

4.4 Combining with atmospheric neutrino data

After obtaining the bounds from laboratory experiments, we turn our attention to atmospheric neutrino data. The experimental results are in good agreement with standard neutrino oscillations [203, 213] and therefore, neutrino NSI with matter can only play a sub-leading role in these data. It is interesting to consider atmospheric data in our global analysis in order to "cut" the infinite branches of the hyperbola in Fig. 4.2. We will obtain better constraints on the NSI neutrino couplings, also including more than one NSI parameter at a time.

For this purpose, we consider NSI in matter in the context of atmospheric neutrinos for flavor-changing, as well as for flavor-diagonal contributions [86, 214, 215]. The main effect of NSI is the presence of an extra term in the hamiltonian that describes the atmospheric neutrino propagation. This will translate, for the two-neutrino approach, into the hamiltonian

$$H_{NSI} = \sqrt{2}\, G_F N_q \begin{pmatrix} \varepsilon^{qV}_{\mu\mu} & \varepsilon^{qV}_{\mu\tau} \\ \varepsilon^{qV}_{\mu\tau} & \varepsilon^{qV}_{\tau\tau} \end{pmatrix}, \tag{4.25}$$

where $\varepsilon^{qV}_{\alpha\beta} = \varepsilon^{qL}_{\alpha\beta} + \varepsilon^{qR}_{\alpha\beta}$ and $q = u, d$. Notice that we omit the axial NSI parameter, since the propagation effects are only sensitive to vectorial contributions.

Super-Kamiokande neutrino data have been analyzed under this assumption in Refs. [86, 214, 215]. But so far, no evidence of NSI has been found in the studied atmospheric data. Therefore, one gets upper bounds on the magnitude of the NSI coupling strengths. For our combined analysis, we include the full atmospheric SK-I and SK-II data sample [215] resulting in the bounds:

$$-0.007 < \varepsilon^{dV}_{\mu\tau} < 0.007\,, \tag{4.26}$$

$$|\varepsilon^{dV}_{\tau\tau} - \varepsilon^{dV}_{\mu\mu}| < 0.042\,, \tag{4.27}$$

at 90% C.L. and taking only one parameter at a time (1 d.o.f.). To obtain these limits, we have considered the following assumptions:

- NSI are present only in the neutrino interaction with down-type quarks.
- The Earth composition is the one specified by the PREM model [216].

Similarly, we can rewrite the bounds on Eq. (4.27) in terms of the neutrino NSI couplings with up-type quarks using the averaged ratio $N_d/N_u = 1.028$ [217]. In this case

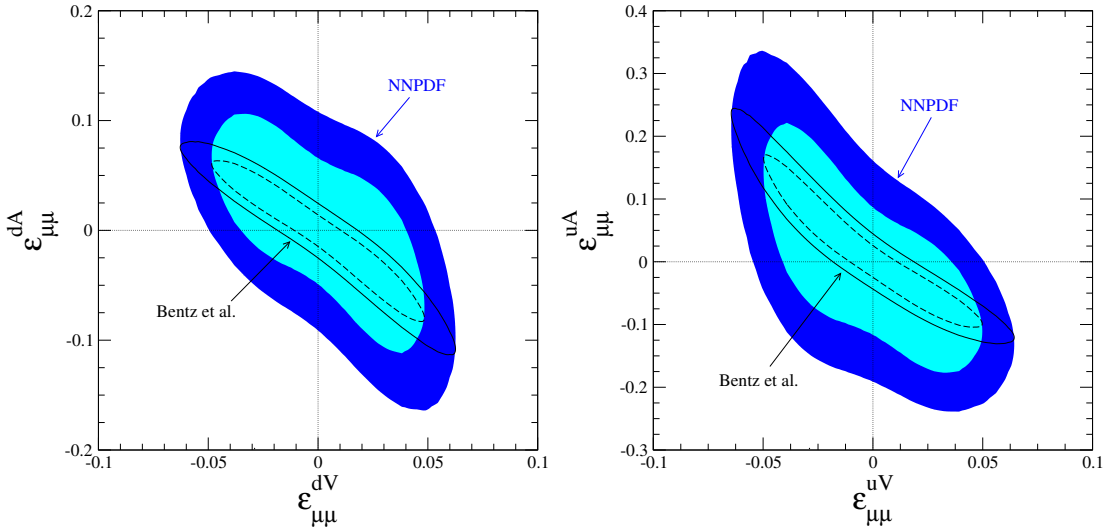

Figure 4.4: The left panel shows the allowed regions for vector and axial flavor-diagonal NSI of neutrinos with down-type quarks, at 90% C.L. and 3σ. The up-type quark case is shown in the right panel. Neutrino data from accelerator and atmospheric experiments have been combined to obtain this limit. Again, we show the results for the error analysis of the NNPDF Collaboration [163] (colored region) while the empty lines correspond to the error analysis performed by Bentz et al. [164].

we obtain:

$$-0.007 \;<\; \varepsilon^{uV}_{\mu\tau} < 0.007\,, \tag{4.28}$$

$$|\varepsilon^{uV}_{\tau\tau} - \varepsilon^{uV}_{\mu\mu}| < 0.043\,. \tag{4.29}$$

It is possible to go one step further and combine the results coming from atmospheric data with those from the previous accelerator analysis, reported in Secs. 4.2 and 4.3. With this combination we constrain the hyperbolic branches in Figs. 4.2 and 4.3, obtaining the allowed regions shown in Figs. 4.4 and 4.5 for the case of flavor-diagonal and flavor-changing NSI respectively. As in the previous section, the restrictions for flavor-changing couplings consider NuTeV, CHARM, and CDHS results. For the flavor-diagonal case, only the NuTeV data are considered. Again, for the combined result of NuTeV and accelerator data, we only show the down-type quark restrictions, since the bounds for the up-type case is nearly the same.

From Figs. 4.4 and 4.5 we can see the important role played by the atmospheric neutrino data, since now the degeneracy in the vector NSI coupling has been removed.

The two parameter analysis reported here can be translated into a one parameter

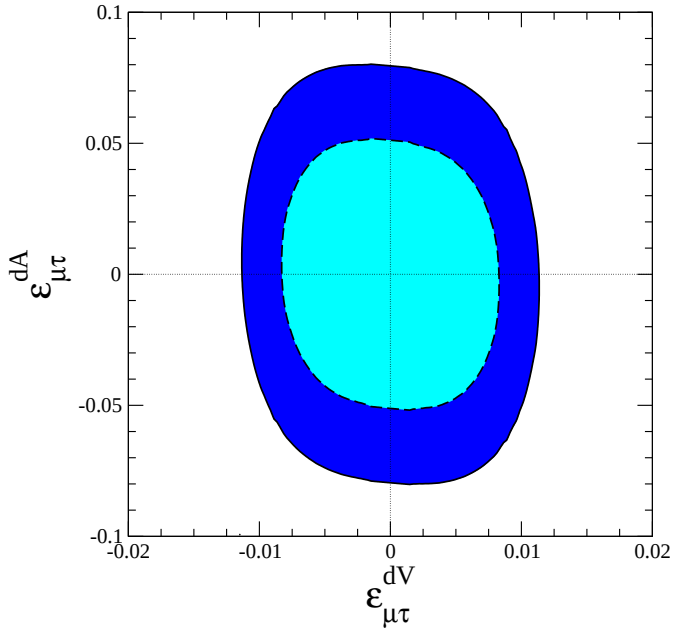

Figure 4.5: Allowed regions, at 90% C. L. and 3σ, for the flavor-changing NSI neutrino couplings with down-type quarks. In this case the result is dominated by CHARM + CDHS and the atmospheric data. This time, the two reanalyses of the NuTeV data give the same constraints. The constraints for the NSI with up-type quark are nearly the same.

constraint which, taking into account the reanalysis of Ref. [163] ([164]) at 90% C.L., is

$$-0.042(-0.042) < \varepsilon^{dV}_{\mu\mu} < 0.042(0.042)\,, \tag{4.30}$$

$$-0.091(-0.072) < \varepsilon^{dA}_{\mu\mu} < 0.091(0.057)\,, \tag{4.31}$$

$$-0.044(-0.044) < \varepsilon^{uV}_{\mu\mu} < 0.044(0.044)\,, \tag{4.32}$$

$$-0.15(-0.094) < \varepsilon^{uA}_{\mu\mu} < 0.18(0.140)\,. \tag{4.33}$$

We also report the one parameter constraints for the flavor-changing couplings. In this case, the atmospheric neutrino analysis plays the main role in the restriction of the vectorial couplings $\varepsilon^{qV}_{\mu\tau}$, while CHARM and CDHS dominate the restrictions for the axial couplings $\varepsilon^{qA}_{\mu\tau}$. The bounds for the down-type quark are

$$-0.007 < \varepsilon^{dV}_{\mu\tau} < 0.007\,, \qquad -0.039 < \varepsilon^{dA}_{\mu\tau} < 0.039\,, \tag{4.34}$$

$$-0.007 < \varepsilon^{uV}_{\mu\tau} < 0.007\,, \qquad -0.039 < \varepsilon^{uA}_{\mu\tau} < 0.039\,. \tag{4.35}$$

As a final comment in this section, we would like to point out that a detailed three-neutrino oscillation analysis combined with non-standard interactions will introduce the

Table 4.2: Summary of the constraints for the NSI parameters from the combined analysis of NuTeV and atmospheric data. The first rows show the constraints for the non-universal (NU) NSI parameters. The bottom row refers to the flavor-changing (FC) NSI were we have also included the CDHS and CHARM data.

Global with NuTeV reanal.	NSI with down	NSI with up
	NU	NU
NNPDF [163]	$-0.042 < \varepsilon^{dV}_{\mu\mu} < 0.042$	$-0.044 < \varepsilon^{uV}_{\mu\mu} < 0.044$
	$-0.091 < \varepsilon^{dA}_{\mu\mu} < 0.091$	$-0.15 < \varepsilon^{uA}_{\mu\mu} < 0.18$
Bentz at al. [164]	$-0.042 < \varepsilon^{dV}_{\mu\mu} < 0.042$	$-0.044 < \varepsilon^{uV}_{\mu\mu} < 0.044$
	$-0.072 < \varepsilon^{dA}_{\mu\mu} < 0.057$	$-0.094 < \varepsilon^{uA}_{\mu\mu} < 0.140$
	FC	FC
NNPDF/Bentz et al.	$-0.007 < \varepsilon^{dV}_{\mu\tau} < 0.007$	$-0.007 < \varepsilon^{uV}_{\mu\tau} < 0.007$
	$-0.039 < \varepsilon^{dA}_{\mu\tau} < 0.039$	$-0.039 < \varepsilon^{uA}_{\mu\tau} < 0.039$

three extra NSI couplings: ε_{ee}, $\varepsilon_{e\mu}$, and $\varepsilon_{e\tau}$, making the analysis more complex and the constraints weaker.

4.5 Summary

The original results reported by the NuTeV Collaboration suggested important deviations from the SM predictions. Considering that this could be a consequence of new physics effects, we have reanalyzed the constraints on non-standard neutrino interactions of muon-neutrinos with quarks. In particular, we have reanalyzed the results of the NuTeV experiment introducing systematic uncertainties which were not taken into account in the original analysis.

We have combined the restrictions obtained in this reanalysis with those coming from atmospheric data, that were useful to remove degeneracies in the NSI parameter space. Although we have found that muon-neutrino constraints are stronger than those for tau or electron-neutrinos, they are weaker than previously believed. While bounds of the order of few 10^{-3} are reported in the literature, when considering new uncertainties we found constraints of the order of few 10^{-2}. These results are summarized in Table 4.2. For the case of a general three-generation analysis, it is expected that even weaker constraints will be found.

It is not expected that data from the MINOS long baseline experiment [218] could

improve these results, since it has a reduced sensitivity to matter effects, especially when compared to the atmospheric neutrino data. Since the same would be expected for the OPERA experiment [219], we would need to wait for NOVA results [220] or the proposed DUNE experiment [221] for an improvement in this sector.

Another natural direction would be the NuSOnG proposal [222], a new high statistics neutrino scattering experiment [223], with the same goals as NuTeV. The experiment would be devoted to probe muon-neutrino couplings and the expectation would be that NuSOng would have twice the sensitivity of NuTeV. It is expected that NSI constraints would be improved by about the same amount.

Chapter 5

Non-unitary lepton mixing matrix

As we saw, the neutrino oscillation phenomenon cannot be explained without nonzero neutrino masses. The observed small neutrino mass differences can arise from an effective dimension-five operator $\mathcal{O}_5 \propto L\Phi L\Phi$ [16] (see Fig. 1.3) that violates the lepton number, which may stem from unknown physics beyond the Standard Model. In the operator, L denotes a lepton doublet while Φ is the SM scalar doublet. This operator generates Majorana neutrino masses after electroweak symmetry breaking. In this the case, neutrino mass appears in second order of $\langle\Phi\rangle$, and lepton number violation by two units ($\Delta L = 2$) can occur at large scale. This mechanism explains the small neutrino mass in comparison to the Standard Model charged fermion masses [1]. However, the mechanism that generates the operator $\mathcal{O}_5$ is still unknown and we cannot say much more about the interaction that produces the operator or its associated mass *scale*, nor the possible details of its *flavor structure*.

If there exist heavy "messenger" particles, the operator $\mathcal{O}_5$ could be induced through the exchange of them. They could be neutral heavy leptons (NHL), that arise naturally in several extensions of the Standard Model when $Y_\nu \sim 1$, playing a role as messengers of neutrino mass generation. This is one of their strongest motivations and a key ingredient of the Type-I seesaw mechanism [3] and variants. If this mechanism is realized at the Fermi scale [18, 19, 22, 224–228], the "seesaw messengers" might give rise to several interesting phenomenological implications, depending on the assumed gauge structure. If we consider the minimal $SU(3)_C \times SU(2)_L \times U(1)_Y$ structure, we could have several new states and potential signatures, for instance:

- Heavy isosinglet leptons. Below the Z mass, these particles have been searched

[1] Notice that it has been already discussed in Sec. 1.4. Here, we return to it in order to introduce this chapter properly.

for at LEP I [229–231]; if their mass is in the TeV range, they might be seen in the LHC experiments, although their rates are not expected to be large in the $SU(3)_C \times SU(2)_L \times U(1)_Y$ gauge structure.

- Light isosinglet leptons, usually called "sterile" neutrinos. If the mass of these particles is found in the eV range they could help to explain current neutrino oscillation anomalies [232, 233] since they will take part in the oscillations. If their mass is in the keV range or above, they might be relevant for cosmology [234] or appear as distortions in weak decay spectra [235].

- Universality violation. Due to the existence of NHL, weak decay rates would decrease if the NHL is not heavy enough to be emitted [236].

- Non-unitary lepton mixing matrix. Whenever NHL are too heavy to take part in neutrino oscillations, the admixture with light neutrino states will affect the current neutrino oscillation picture; in particular, the leptonic mixing matrix will be non-unitary [21].

- Neutrinoless double beta decay. If the NHL is a Majorana particle, lepton number violation processes would appear, including the well-known neutrinoless double beta decay. It could be generated through long-range (mass mechanism), or induce short-range contributions [237–239].

- Charged lepton flavor violation processes. They could be induced by NHL, although the rates and current constraints are model dependent [21, 240].

In this chapter we will consider the phenomenological consequences of a non-unitary lepton mixing matrix. We will consider that the non-unitarity is produced by the existence of NHL, for instance, from isosinglet neutrinos above 100 GeV. Therefore, these heavy particles will be too heavy to take part in oscillations or low-energy weak decay processes. We will show that the most general form of the mixing matrix is factorable, separating the mixing matrix in a "new physics part" and a "standard part". With this description, the current experiments described with a two-neutrino scheme (electron and muon-neutrinos for instance) can be expressed in terms of just four new parameters, three real mixing angles plus one new CP violation phase. We will show in this chapter how these new parameters affect oscillation probabilities, and we will discuss the main restrictions to the mixing structure that follows from oscillation data as well as from universality tests. We also present a compilation of several model-independent constraints on NHL mixing

parameters, translated into this new parametrization. We consider in this last case both low-energy searches and searches of direct NHL production at high-energy accelerator experiments.

5.1 A new way to describe extra heavy leptons

The existence of isosinglet neutral heavy leptons implies that they could mix with the standard isodoublet neutrinos. The mixing matrix including extra heavy leptons has been studied carefully and described in the symmetric parametrization in Refs. [9, 45]. In this thesis, we consider an equivalent presentation that manifestly factorizes out the parameters related with the extra heavy leptons and separate them from those describing the light neutrino mixing within the unitarity approximation. We will present here the main features of this parametrization and the more mathematical details will be shown in the appendix B.

If we consider three light neutrinos (the conventional number of neutrinos in the SM) and $(n-3)$ extra NHL, we have an $U^{n\times n}$ unitary mixing matrix. We can divide this mixing matrix in four different blocks [241]

$$U^{n\times n} = \begin{pmatrix} N & S \\ V & T \end{pmatrix}, \tag{5.1}$$

where N is a 3×3 non-unitary matrix describing the light neutrino sector. The matrix S describes the coupling of the isosinglet states, expected to be heavy [2]. We find that the 3×3 mixing matrix N can be decomposed most conveniently as a product of a standard matrix $U^{3\times 3}$ and a "new physics matrix" N^{NP}:

$$N = N^{NP}\, U^{3\times 3} = \begin{pmatrix} \alpha_{11} & 0 & 0 \\ \alpha_{21} & \alpha_{22} & 0 \\ \alpha_{31} & \alpha_{32} & \alpha_{33} \end{pmatrix} U^{3\times 3}, \tag{5.2}$$

where $U^{3\times 3}$ is the usual unitary 3×3 leptonic mixing matrix reported in neutrino oscillation searches. The submatrix $U^{3\times 3}$ may be expressed in the symmetric parametrization (Eq. (1.120)) or, equivalently, as prescribed by the Particle Data Group [6] [3] (Eq. (1.121)). In this thesis we prefer to use the symmetric parametrization. The reader can find a discussion on the advantages of each parametrization in Ref [45]. On the other hand, the

[2] See Ref. [17] for a perturbative expansion of $U^{n\times n}$.

[3] The factorization holds irrespective of which form is taken for light neutrino mixing matrix.

N^{NP} matrix in Eq. (5.2) contains all the new physics information through the α_{ij} parameters, which are complex in general. As we can see, this N^{NP} matrix induces the unitarity violation. More explicitly, we can calculate the mixing matrix N obtaining:

$$\begin{pmatrix} \alpha_{11}U_{e1} & \alpha_{11}U_{e2} & \alpha_{11}U_{e3} \\ \alpha_{21}U_{e1}+\alpha_{22}U_{\mu 1} & \alpha_{21}U_{e2}+\alpha_{22}U_{\mu 2} & \alpha_{21}U_{e3}+\alpha_{22}U_{\mu 3} \\ \alpha_{31}U_{e1}+\alpha_{32}U_{\mu 1}+\alpha_{33}U_{\tau 1} & \alpha_{31}U_{e2}+\alpha_{32}U_{\mu 2}+\alpha_{33}U_{\tau 2} & \alpha_{31}U_{e3}+\alpha_{32}U_{\mu 3}+\alpha_{33}U_{\tau 3} \end{pmatrix}. \tag{5.3}$$

Notice the convenience of using Eq. (5.2), since it gives a general and complete description of the current neutrino experiments when the unitarity condition is relaxed. An example will show the use of this notation. If we consider interactions involving electron-neutrinos and muon-neutrinos, we just need, with our description, four extra parameters which include all additional information beyond the SM: the two real parameters α_{11} and α_{22} plus a complex one, α_{21}, containing a single CP phase. For a discussion on the existence [242] and possible effects [243] of extra CP phases associated to the admixture of NHL in the charged leptonic weak interaction, the reader is referred to the original paper in [9]. The new point here is that, despite the proliferation of phase parameters, one can always stack them in a single physical parameter per non-diagonal entry, so only one combination enters in the "relevant" neutrino oscillation experiments. This interesting feature holds independently of the number of extra NHL.

We write below the explicit form of the elements of the new physics matrix, α_{ij}, for any number of extra NHL. They can be separated in:

- Diagonal elements, α_{ii}, which are real and expressed in a simple way as

$$\begin{aligned} \alpha_{11} &= c_{1\,n}\, c_{1\,n-1} c_{1\,n-2} \ldots c_{14}, \\ \alpha_{22} &= c_{2\,n}\, c_{2\,n-1} c_{2\,n-2} \ldots c_{24}, \\ \alpha_{33} &= c_{3\,n}\, c_{3\,n-1} c_{3\,n-2} \ldots c_{34}. \end{aligned} \tag{5.4}$$

  Notice that these diagonal terms depend only on the cosines of the mixing parameters, $c_{ij} = \cos\theta_{ij}$.

- Off diagonal term α_{31}. In this case the expression is more complicated; however, if we neglect quartic terms in $\sin\theta_{ij}$, with $j = 4, 5, \cdots$, we find:

$$\begin{aligned} \alpha_{31} \;=\; c_{3\,n}\, c_{3\,n-1} \ldots c_{3\,5}\, \eta_{34} c_{2\,4} \bar{\eta}_{14} \;+\; c_{3\,n}\, \ldots c_{3\,6}\, \eta_{35} c_{2\,5} \bar{\eta}_{15}\, c_{14} + \ldots \\ + \eta_{3n} c_{2\,n} \bar{\eta}_{1n}\, c_{1n-1}\, c_{1n-2}\, \ldots\, c_{14}\,, \end{aligned} \tag{5.5}$$

where $\eta_{ij} = e^{-i\phi_{ij}} \sin\theta_{ij}$ and its conjugate, $\bar{\eta}_{ij} = -e^{i\phi_{ij}} \sin\theta_{ij}$, contain all of the CP violating phases.

- Off-diagonal terms α_{21} and α_{32}, expressed as a sum of $n-3$ terms as

$$\begin{aligned}
\alpha_{21} &= c_{2\,n}\, c_{2n-1} \ldots c_{2\,5}\, \eta_{24}\bar{\eta}_{14} + c_{2\,n} \ldots c_{2\,6}\, \eta_{25}\bar{\eta}_{15}\, c_{14} + \ldots \\
&+ \eta_{2n}\bar{\eta}_{1n}\, c_{1n-1}\, c_{1n-2} \ldots c_{14}\,, \\
\alpha_{32} &= c_{3\,n}\, c_{3n-1} \ldots c_{3\,5}\, \eta_{34}\bar{\eta}_{24} + c_{3\,n} \ldots c_{3\,6}\, \eta_{35}\bar{\eta}_{25}\, c_{24} + \ldots \\
&+ \eta_{3n}\bar{\eta}_{2n}\, c_{2n-1}\, c_{2n-2} \ldots c_{24}\,.
\end{aligned} \tag{5.6}$$

In summary, by choosing a convenient ordering for the products of the complex rotation matrices ω_{ij}, one obtains a convenient parametrization that separates all the information relative to the additional leptons in a simple and compact form, with a matrix containing three zeroes and reducing the number of parameters related to new physics. In what follows, we will show the utility of this specific parametrization and we will also obtain the corresponding constraints.

5.2 NHL and non-unitary neutrino mixing

Keeping in mind the formalism described in the previous section and the chiral nature of the $SU(3)_C \times SU(2)_L \times U(1)_Y$ model, we describe the couplings of the n neutrino states in the charged-current weak interaction as part of a rectangular matrix K [9],

$$K = \begin{pmatrix} N & S \end{pmatrix}, \tag{5.7}$$

where the N block is the 3×3 matrix already discussed in Eq. (5.2), corresponding to the three light neutrinos matrix with contributions of new physics, and the S block is a $3 \times (n-3)$ matrix corresponding to the mixing of extra heavy leptons.

In a scenario with extra heavy fermions that mix with the active light neutrinos, the unitary mixing matrix is the complete matrix described by Eq. (5.1), so that the mixing matrix involving the standard neutrinos comes from a truncation of Eq. (5.1). Therefore, the 3×3 light neutrino mixing matrix N is not unitary and this fact modifies the SM observables. Note also that, in this case, the unitarity condition takes the form

$$KK^\dagger = NN^\dagger + SS^\dagger = I\,, \tag{5.8}$$

with

$$NN^\dagger = \begin{pmatrix} \alpha_{11}^2 & \alpha_{11}\alpha_{21}^* & \alpha_{11}\alpha_{31}^* \\ \alpha_{11}\alpha_{21} & \alpha_{22}^2 + |\alpha_{21}|^2 & \alpha_{22}\alpha_{32}^* + \alpha_{21}\alpha_{31}^* \\ \alpha_{11}\alpha_{31} & \alpha_{22}\alpha_{32} + \alpha_{31}\alpha_{21}^* & \alpha_{33}^2 + |\alpha_{31}|^2 + |\alpha_{32}|^2 \end{pmatrix} . \tag{5.9}$$

The parametrization shown here allows to concentrate all the information of the $(n-3)$ heavy states into the α_{ij} parameters, obtaining a more compact and simple notation. The parameters are totally general, include all the relevant CP phases and the parametrization is model independent. In the following sections, we will show the advantages of this parametrization by analyzing direct and indirect searches of the extra heavy leptons. We will rewrite the relevant observables and will obtain the corresponding constraints on the α_{ij} parameters.

5.3 Constraints from universality tests

Within the picture described in this chapter, the new extra heavy leptons will not participate in several weak processes [4], since they can not be emitted due to kinematical restrictions. As a consequence, the universality of certain weak processes will be broken and the effective value of the Fermi constant will change accordingly; this is the case of muon and beta decays, for example. Although the extra heavy leptons will not be kinematically emitted in various of these weak processes, they remain in the process as part of the admixture with the light particles. So we can use the formalism characterized by the α_{ij} parameters (Secs. 5.1 and 5.2) in order to describe various weak processes, translating their parameters in this compact formalism to derive the corresponding experimental sensitivities.

First we will discuss the universality constraints. Let us start considering the current bounds [236, 244–251], then we introduce them within the above formalism in order to prove its simplicity. Comparing muon and beta decays,

$$\begin{aligned} A(Z,N) &\rightarrow A(Z+1,N-1) + e^- + \bar{\nu}_e \,, \\ A(Z,N) &\rightarrow A(Z-1,N+1) + e^+ + \nu_e \,, \end{aligned} \tag{5.10}$$

$$\begin{aligned} \mu^+ &\rightarrow e^+ + \bar{\nu}_\mu + \nu_e \,, \\ \mu^- &\rightarrow e^- + \nu_\mu + \bar{\nu}_e \,, \end{aligned} \tag{5.11}$$

[4] Notice that neutral heavy leptons could participate virtually in weak processes.

for a model with just one extra heavy lepton, one finds the following corrections to the effective Fermi constant [244, 245, 249],

$$G_\mu = G_F \sqrt{(1-|S_{e4}|^2)(1-|S_{\mu 4}|^2)} = G_F \sqrt{\alpha_{11}^2(\alpha_{22}^2+|\alpha_{21}|^2)} \tag{5.12}$$

and

$$G_\beta = G_F \sqrt{(1-|S_{e4}|^2)}\,. \tag{5.13}$$

Relaxing this assumption and considering the presence of n extra heavy leptons, we can rewrite Eqs. (5.12) and (5.13) in terms of α_{ij} obtaining similar expressions,

$$G_\mu = G_F \sqrt{(NN^\dagger)_{11}(NN^\dagger)_{22}} = G_F \sqrt{\alpha_{11}^2(\alpha_{22}^2+|\alpha_{21}|^2)} \tag{5.14}$$

and

$$G_\beta = G_F \sqrt{(NN^\dagger)_{11}} = G_F \sqrt{\alpha_{11}^2}\,. \tag{5.15}$$

Notice that this change will affect all the observables related with the Fermi constant, for example the quark CKM matrix elements [244]. We focus on the two matrix elements V_{ud} and V_{us}. Their new expressions are obtained from the vector coupling in β, K_{e3} and hyperon decays, after scaling by the new constant G_μ. The unitarity relation for the first row of the CKM is now expressed as [244, 245]:

$$\sum_{i=1}^{3}|V_{ui}|^2 = \left(\frac{G_\beta}{G_\mu}\right)^2 = \left(\frac{G_F\sqrt{(NN^\dagger)_{11}}}{G_F\sqrt{(NN^\dagger)_{11}(NN^\dagger)_{22}}}\right)^2 = \frac{1}{(NN^\dagger)_{22}}, \tag{5.16}$$

From this equation one gets the following constraint [6]:

$$\sum_{i=1}^{3}|V_{ui}|^2 = \frac{1}{\alpha_{22}^2+|\alpha_{21}|^2} = 0.9999 \pm 0.0006\,, \tag{5.17}$$

which implies that $1-(NN^\dagger)_{22} = (SS^\dagger)_{22} = 1-\alpha_{22}^2-|\alpha_{21}|^2 < 0.0005$ at 1σ.

We can also get constraints on these α_{ij} parameters from other universality tests. In the absence of NHL the gauge bosons couple to the leptons with a flavor independent strength. But in the presence of heavy isosinglets this is no longer true, and the couplings will become flavor dependent because the unitarity of the mixing matrix has been broken and $NN^\dagger \neq I$. We can use the reported ratios for these couplings to obtain constraints from universality. As in the case of the CKM matrix elements, we may express them for

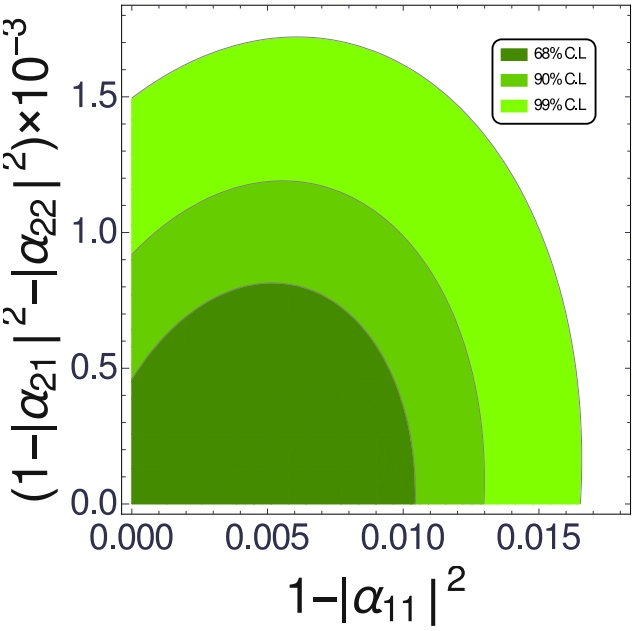

Figure 5.1: Constraints from universality test for the unitarity deviations.

one extra heavy lepton as [249]

$$\left(\frac{g_a}{g_\mu}\right)^2 = \frac{(1-|S_{a4}|)}{(1-|S_{\mu 4}|)} \quad a = e, \tau\,. \tag{5.18}$$

For a more general case they can be expressed as [244]

$$\left(\frac{g_a}{g_\mu}\right)^2 = \frac{(NN^\dagger)_{aa}}{(NN^\dagger)_{22}} \quad a = 1, 3\,. \tag{5.19}$$

We can consider the pion decay branching ratio [247]:

$$R_\pi = \frac{\Gamma(\pi^+ \to e^+\nu)}{\Gamma(\pi^+ \to \mu^+\nu)}. \tag{5.20}$$

Notice that this ratio will be proportional to the previous one, shown in Eq. (5.19), for the case $a = 1 \equiv e$. Then the current experimental value for the pion decay allows to obtain the constraint [247, 252]:

$$\begin{aligned} r_\pi &= \frac{R_\pi}{R_\pi^{SM}} = \frac{(NN^\dagger)_{11}}{(NN^\dagger)_{22}} = \frac{\alpha_{11}^2}{\alpha_{22}^2 + |\alpha_{21}|^2} \\ &= \frac{(1.2300 \pm 0.0040) \times 10^{-4}}{(1.2354 \pm 0.0002) \times 10^{-4}} = 0.9956 \pm 0.0040\,. \end{aligned} \tag{5.21}$$

This implies that $1-\alpha_{11}^2 < 0.0084$ at 1σ for the particular case of $\alpha_{22}^2 + |\alpha_{21}|^2 = 1$. This procedure was adopted in Ref. [249]. In general, $[(SS^\dagger)_{22}] \neq 0$.

We can obtain a more robust constraint if we consider the unitarity constraint on the CKM matrix already discussed. By combining the constraints from Eqs. (5.17) and (5.21) we get the bounds shown in Fig. 5.1. This result can be translated into the constraints

$$\begin{aligned} 1-\alpha_{11}^2 &< 0.0130\,, \\ 1-\alpha_{22}^2-|\alpha_{21}|^2 &< 0.0012\,, \end{aligned} \tag{5.22}$$

at 90% C.L. for 2 d.o.f. We can notice that another measurement is needed to break the degeneracy between the parameters α_{22} and $|\alpha_{21}|$. In the next section, we will study possible neutrino oscillation observables that could be of help for this analysis.

In order to complete this analysis, we can also find constraints from the $\mu-\tau$ universality, which give information on the τ mixing parameters. Using Eq. (5.19) and the corresponding experimental value [253], we obtain

$$\frac{(NN^\dagger)_{33}}{(NN^\dagger)_{22}} = 0.9850 \pm 0.0057\,. \tag{5.23}$$

From this result it is straightforward to notice that $1-(NN^\dagger)_{33} = (SS^\dagger)_{33} < 0.0207$ at 1σ for the least conservative case of $(SS^\dagger)_{22} = 0$.

As we have seen, the existence of extra heavy leptons implies variations in all observables related to the Fermi constant. We have expressed these corrections in terms of a few parameters that concentrate all the new physics information. In what follows we will apply this formalism to the important phenomenon of neutrino oscillations.

5.4 Neutrino oscillations with non-unitarity

The compact notation with α_{ij} may be useful to study new physics effects in neutrino oscillations. In this section we compute the expressions for this important case. Firstly we will obtain new formulae for the neutrino survival and conversion probabilities and then we will get restrictions for the new physics in terms of the α parameters. It should be noted that the general expressions have been calculated neglecting cubic products of α_{21}, $\sin\theta_{13}$ and $\sin\Delta_{21}$, where Δ_{ji} stands for $\Delta m_{ji}^2 L/4E$. This approximation is in a good agreement with the current experimental status.

First of all, we recall the most general expression for the neutrino oscillation probabilities in vacuum [12] (Sec. 1.5.1),

$$P_{\nu_\alpha\to\nu_\beta} = \sum_{i,j}^{3} U^*_{\alpha i}U_{\beta i}U_{\alpha j}U^*_{\beta j} \;-\; 4\sum_{j>i}^{3} Re\left[U^*_{\alpha j}U_{\beta j}U_{\alpha i}U^*_{\beta i}\right]\sin^2\left(\frac{\Delta m^2_{ji}L}{4E}\right) + \;2\sum_{j>i}^{3} Im\left[U^*_{\alpha j}U_{\beta j}U_{\alpha i}U^*_{\beta i}\right]\sin\left(\frac{\Delta m^2_{ji}L}{2E}\right), \tag{5.24}$$

where, if we introduce the unitarity condition of the mixing matrix, $UU^\dagger = I$, we obtain the usual expression in the literature,

$$P_{\nu_\alpha\to\nu_\beta} = \delta_{\alpha\beta} \;-\; 4\sum_{j>i}^{3} Re\left[U^*_{\alpha j}U_{\beta j}U_{\alpha i}U^*_{\beta i}\right]\sin^2\left(\frac{\Delta m^2_{ji}L}{4E}\right) + \;2\sum_{j>i}^{3} Im\left[U^*_{\alpha j}U_{\beta j}U_{\alpha i}U^*_{\beta i}\right]\sin\left(\frac{\Delta m^2_{ji}L}{2E}\right). \tag{5.25}$$

For the case with extra neutral heavy leptons, unitarity is broken, $NN^\dagger \neq I$ [5]. Although NHL will not participate in the oscillation because they are too heavy to be produced, they will mix with light neutrinos, so we have a similar expression as Eq. (5.24) but using N as the mixing matrix,

$$P_{\nu_\alpha\to\nu_\beta} = \sum_{i,j}^{3} N^*_{\alpha i}N_{\beta i}N_{\alpha j}N^*_{\beta j} \;-\; 4\sum_{j>i}^{3} Re\left[N^*_{\alpha j}N_{\beta j}N_{\alpha i}N^*_{\beta i}\right]\sin^2\left(\frac{\Delta m^2_{ji}L}{4E}\right) + \;2\sum_{j>i}^{3} Im\left[N^*_{\alpha j}N_{\beta j}N_{\alpha i}N^*_{\beta i}\right]\sin\left(\frac{\Delta m^2_{ji}L}{2E}\right). \tag{5.26}$$

If we consider the muon-neutrino conversion into an electron-neutrino, the probability is:

[5] Notice again that N is the mixing matrix following from the truncation of the general matrix U, Eq. (5.1).

$$P_{\nu_\mu\to\nu_e} = \sum_{i,j}^{3} N^*_{\mu i}N_{ei}N_{\mu j}N^*_{ej} \;-\; 4\sum_{j>i}^{3} Re\left[N^*_{\mu j}N_{ej}N_{\mu i}N^*_{ei}\right]\sin^2\left(\frac{\Delta m^2_{ji}L}{4E}\right) + \; 2\sum_{j>i}^{3} Im\left[N^*_{\mu j}N_{ej}N_{\mu i}N^*_{ei}\right]\sin\left(\frac{\Delta m^2_{ji}L}{2E}\right). \tag{5.27}$$

Using the condition given in Eqs. (5.8) and (5.9) for the 3×3 matrix N, instead of the usual unitarity condition, we observe how the unitarity is broken. The Dirac delta disappears and instead of it we have the new α_{ij} terms:

$$P_{\nu_\mu\to\nu_e} = \alpha^2_{11}|\alpha_{21}|^2 \;-\; 4\sum_{j>i}^{3} Re\left[N^*_{\mu j}N_{ej}N_{\mu i}N^*_{ei}\right]\sin^2\left(\frac{\Delta m^2_{ji}L}{4E}\right) + \; 2\sum_{j>i}^{3} Im\left[N^*_{\mu j}N_{ej}N_{\mu i}N^*_{ei}\right]\sin\left(\frac{\Delta m^2_{ji}L}{2E}\right). \tag{5.28}$$

In order to obtain a more explicit expression of Eq. (5.28), we may use Eq. (5.3) and substitute the values of $N_{\alpha i}$ in terms of $U_{\alpha i}$ and α_{ij}, arriving to the expression:

$$\begin{aligned} P_{\nu_\mu\to\nu_e} &= \alpha^2_{11}|\alpha_{21}|^2\left(1-4\sum_{j>i}^{3}|U_{ej}|^2|U_{ei}|^2\sin^2\left(\frac{\Delta m^2_{ji}L}{4E}\right)\right) \\ &- (\alpha_{11}\alpha_{22})^2\,4\sum_{j>i}^{3} Re\left[U^*_{\mu j}U_{ej}U_{\mu i}U^*_{ei}\right]\sin^2\left(\frac{\Delta m^2_{ji}L}{4E}\right) \\ &+ (\alpha_{11}\alpha_{22})^2\,2\sum_{j>i}^{3} Im\left[U^*_{\mu j}U_{ej}U_{\mu i}U^*_{ei}\right]\sin\left(\frac{\Delta m^2_{ji}L}{2E}\right) \\ &- 4\alpha^2_{11}\alpha_{22}\sum_{j>i}^{3} Re\left[\alpha_{21}|U_{ei}|^2U^*_{\mu j}U_{ej}+\alpha^*_{21}|U_{ej}|^2U_{\mu i}U^*_{ei}\right]\sin^2\left(\frac{\Delta m^2_{ji}L}{4E}\right) \\ &+ 2\alpha^2_{11}\alpha_{22}\sum_{j>i}^{3} Im\left[\alpha_{21}|U_{ei}|^2U^*_{\mu j}U_{ej}+\alpha^*_{21}|U_{ej}|^2U_{\mu i}U^*_{ei}\right]\sin\left(\frac{\Delta m^2_{ji}L}{2E}\right). \end{aligned} \tag{5.29}$$

We can now use the standard parametrization for the mixing matrix entries ($U_{\alpha i}$) in this equation. We remind the reader that we neglect cubic products of α_{21}, $\sin\theta_{13}$, and $\sin\Delta_{21}$.

With this approximation one obtains

$$P_{\nu_\mu\to\nu_e} = (\alpha_{11}\alpha_{22})^2 P^{3\times3}_{\nu_\mu\to\nu_e} + \alpha_{11}^2\alpha_{22}|\alpha_{21}|P^{I}_{\nu_\mu\to\nu_e} + \alpha_{11}^2|\alpha_{21}|^2, \tag{5.30}$$

where $P^{3\times3}_{\nu_\mu\to\nu_e}$ denotes the standard neutrino conversion probability for the three active species [189, 254, 255],

$$\begin{aligned} P^{3\times3}_{\nu_\mu\to\nu_e} &= 4\Bigg[\cos^2\theta_{12}\cos^2\theta_{23}\sin^2\theta_{12}\sin^2\left(\frac{\Delta m^2_{21}L}{4E}\right) \\ &+ \cos^2\theta_{13}\sin^2\theta_{13}\sin^2\theta_{23}\sin^2\left(\frac{\Delta m^2_{31}L}{4E}\right)\Bigg] \\ &+ \sin(2\theta_{12})\sin\theta_{13}\sin(2\theta_{23})\sin\left(\frac{\Delta m^2_{21}L}{2E}\right) \\ &\times \sin\left(\frac{\Delta m^2_{31}L}{4E}\right)\cos\left(\frac{\Delta m^2_{31}L}{4E} - I_{123}\right), \end{aligned} \tag{5.31}$$

with $\mathrm{I}_{123} = -\delta_{CP} = \phi_{12} - \phi_{13} + \phi_{23}$. On the other hand, $P^{I}_{\nu_\mu\to\nu_e}$ denotes a new physics term which depends on an extra CP phase, $\mathrm{I}_{\mathrm{NP}} = \phi_{12} - \mathrm{Arg}(\alpha_{21})$, along with the usual mixing angles and the standard CP phase through I_{123},

$$\begin{aligned} P^{I}_{\nu_\mu\to\nu_e} &= -2\Bigg[\sin(2\theta_{13})\sin\theta_{23}\sin\left(\frac{\Delta m^2_{31}L}{4E}\right)\sin\left(\frac{\Delta m^2_{31}L}{4E} + I_{NP} - I_{123}\right)\Bigg] \\ &- \cos\theta_{13}\cos\theta_{23}\sin(2\theta_{12})\sin\left(\frac{\Delta m^2_{21}L}{2E}\right)\sin(I_{NP})\,. \end{aligned} \tag{5.32}$$

We would like to remark again that the neutrino conversion probability in this channel depends on two CP phases. Besides the standard CP phase, there is a new phase that comes from the existence of the NHL, denoted as I_{NP}. This "new physics" phase condensates (for this channel) the impact of all the additional phases from NHL and appears in our formalism as the phase of the parameter α_{21}. I_{NP} appears in both terms of Eq. (5.32), in the first one as a difference with the standard phase, $I_{123} - I_{NP}$, being proportional to $\sin\theta_{13}$. In the second one, I_{NP} is not accompanied by the standard phase and the term depends on the solar mass difference Δm^2_{21}. Both terms are expected to give small corrections to the standard probability.

The contribution of the extra neutral heavy lepton to the neutrino oscillation data can be shown qualitatively by giving specific values to the new parameters introduced here. For this purpose, we consider the case where $\alpha_{11} = 1$, $\alpha_{22} = 0.9939$, $|\alpha_{21}| = 0.078$, and I_{NP} is equal to $\pi/2$, $3\pi/2$, π or 0. We have chosen the standard phase $\delta = -I_{123} = 3\pi/2$, close

to its best fit [59]. With these values, the conversion probability takes the form shown in Fig. 5.2 which shows that the new CP phase could be interesting in future neutrino experiments.

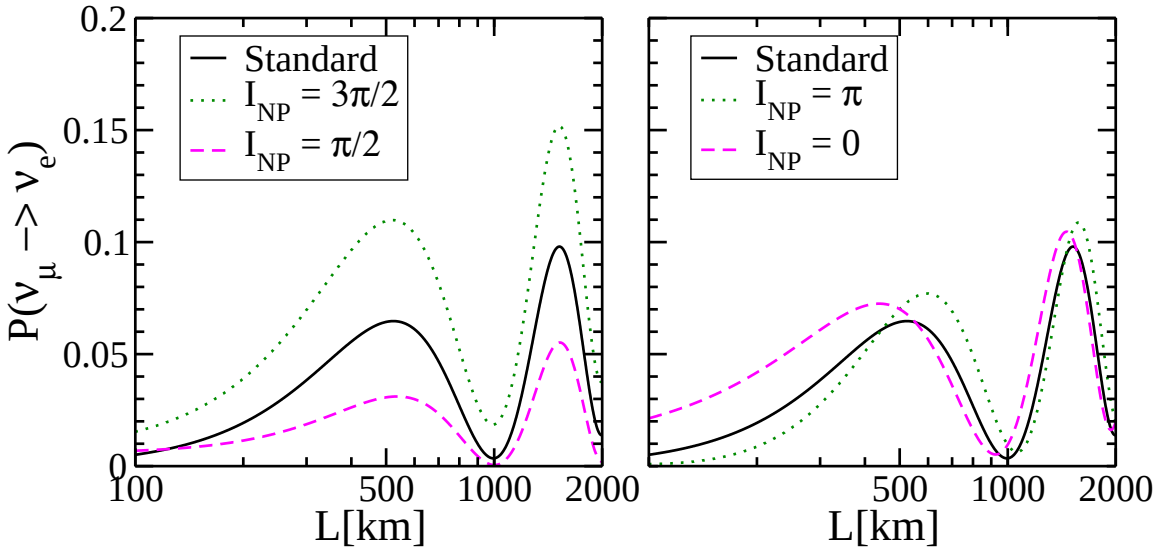

Figure 5.2: Neutrino conversion probability for $E_\nu = 1$ GeV. We show in this plot the standard conversion probability (black) for the CP phase $\delta = -I_{123} = 3\pi/2$. The non-unitary cases are illustrated for the particular values $\alpha_{11} = 1$, $\alpha_{22} = 0.9939$, and $|\alpha_{21}| = 0.078$. In the left panel we consider the following values for the new CP phase, $I_{NP} = \pi/2$ (magenta line) and $I_{NP} = 3\pi/2$ (green line). The cases $I_{NP} = 0$ (magenta line) and $I_{NP} = \pi$ (green line) are shown in the right panel.

For the muon neutrino survival probability, we proceed in a similar way as we did in the $P_{\nu_\mu \to \nu_e}$ case, getting the expression

$$P_{\nu_\mu \to \nu_\mu} = \sum_{i,j}^{3} N^*_{\mu i} N_{\mu i} N_{\mu j} N^*_{\mu j} - 4 \sum_{j>i}^{3} Re\left[N^*_{\mu j} N_{\mu j} N_{\mu i} N^*_{\mu i}\right] \sin^2\left(\frac{\Delta m^2_{ji} L}{4E}\right) . \qquad (5.33)$$

Substituting again the values of $N_{\alpha i}$ from Eq. (5.3), we can appreciate once more a decrease

in the probability before neutrinos have a chance to oscillate, the zero distance effect [83]:

$$P_{\nu_\mu\to\nu_\mu} = (|\alpha_{21}|^2+\alpha_{22}^2)^2 - 4\sum_{j>i}^{3}|N_{\mu j}|^2|N_{\mu i}|^2\sin^2\left(\frac{\Delta m^2_{ji}}{4E}L\right), \tag{5.34}$$

$$\begin{aligned} P_{\nu_\mu\to\nu_\mu} &= (|\alpha_{21}|^2+\alpha_{22}^2)^2 \\ &- 4\sum_{j>i}^{3}|\alpha_{21}U_{ej}+\alpha_{22}U_{\mu j}|^2|\alpha_{21}U_{ei}+\alpha_{22}U_{\mu i}|^2\sin^2\left(\frac{\Delta m^2_{ji}}{4E}L\right). \end{aligned} \tag{5.35}$$

As we did previously, we neglect for simplicity cubic products of α_{21}, $\sin\theta_{13}$, and $\sin\Delta_{21}$, obtaining the following expression:

$$P_{\nu_\mu\to\nu_\mu} = \alpha_{22}^4 P^{3\times3}_{\nu_\mu\to\nu_\mu} + \alpha_{22}^3|\alpha_{21}|P^{I_1}_{\nu_\mu\to\nu_\mu} + 2|\alpha_{21}|^2\alpha_{22}^2 P^{I_2}_{\nu_\mu\to\nu_\mu}, \tag{5.36}$$

where $P^{3\times3}_{\nu_\mu\to\nu_\mu}$ corresponds to the standard oscillation formula,

$$\begin{aligned} P^{3\times3}_{\nu_\mu\to\nu_\mu} &\approx 1 - 4\left[\cos^2\theta_{23}\sin^2\theta_{23} - \cos(2\theta_{23})\sin^2\theta_{23}\sin^2\theta_{13}\right]\sin^2\left(\frac{\Delta m^2_{31}L}{4E}\right) \\ &+ 2\left[\cos^2\theta_{12}\cos^2\theta_{23}\sin^2\theta_{23} - \cos(\mathrm{I}_{123})\cos\theta_{23}\sin(2\theta_{12})\sin^3\theta_{23}\sin\theta_{13}\right] \\ &\times \sin\left(\frac{\Delta m^2_{31}L}{2E}\right)\sin\left(\frac{\Delta m^2_{21}L}{2E}\right) \\ &- 4\Bigg[\cos^2\theta_{12}\cos^2\theta_{23}\sin^2\theta_{23}\cos\left(\frac{\Delta m^2_{31}L}{2E}\right) \\ &+ \cos^2\theta_{12}\cos^4\theta_{23}\sin^2\theta_{12}\Bigg]\sin^2\left(\frac{\Delta m^2_{21}L}{4E}\right). \end{aligned} \tag{5.37}$$

The two extra contributions to the standard probability are given by:

$$\begin{aligned} P^{I_1}_{\nu_\mu\to\nu_\mu} &\approx - 8\left[\sin\theta_{13}\sin\theta_{23}\cos(2\theta_{23})\cos(\mathrm{I}_{123}-\mathrm{I}_{\mathrm{NP}})\right]\sin^2\left(\frac{\Delta m^2_{31}L}{4E}\right) \\ &\quad + 2\left[\cos\theta_{23}\sin(2\theta_{12})\sin^2\theta_{23}\cos(\mathrm{I}_{\mathrm{NP}})\right]\sin\left(\frac{\Delta m^2_{31}L}{2E}\right)\sin\left(\frac{\Delta m^2_{21}L}{2E}\right), \\ P^{I_2}_{\nu_\mu\to\nu_\mu} &\approx 1 - 2\sin^2\theta_{23}\sin^2\left(\frac{\Delta m^2_{31}L}{4E}\right). \end{aligned} \tag{5.38}$$

We show graphically this probability in Fig. 5.3.

Since the contribution in this case is very small and, therefore, difficult to appreciate, we have decided to plot the difference between the probability including new physics and

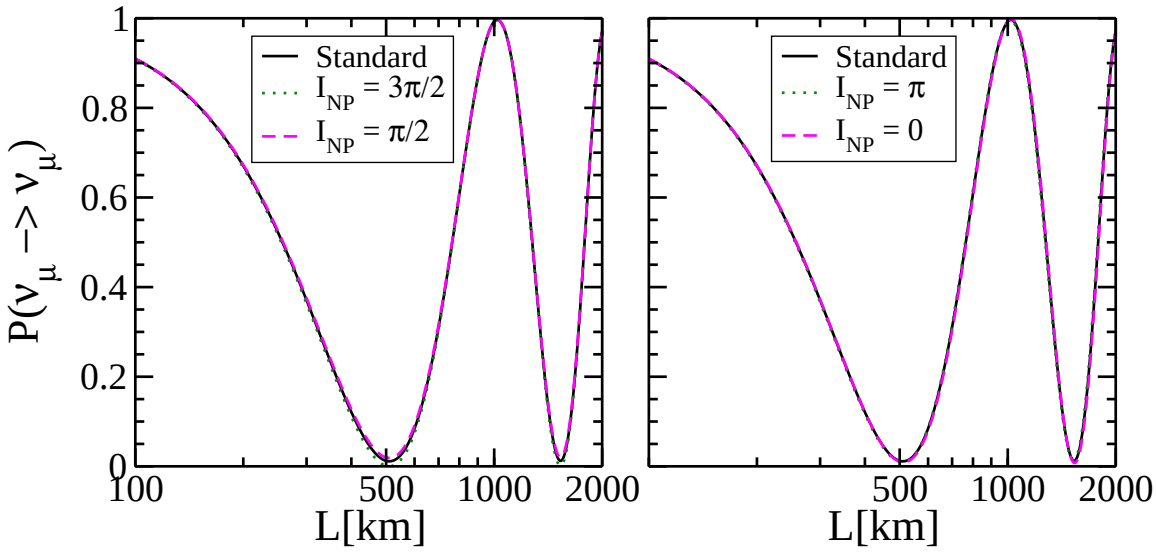

Figure 5.3: Survival probability for a fixed neutrino energy of $E_\nu = 1$ GeV. We show the standard survival probability, with $\delta = -I_{123} = 3\pi/2$ in the black curve. The non-unitary case is also given for the same parameter values of Fig. 5.2.

the standard probability $(P^{NP}_{\nu_\mu\to\nu_\mu} - P^{3\times3}_{\nu_\mu\to\nu_\mu})$ in Fig. 5.4.

One can see from these plots that the disappearance channel has worse sensitivity to the extra CP phase I_{NP} than the appearance channel. The computations in these plots were done for the same values of the appearance case: $\alpha_{11} = 1$, $\alpha_{22} = 0.9939$, $|\alpha_{21}| = 0.078$, $\delta = -I_{123} = 3\pi/2$, and I_{NP} equal to either $\pi/2$ or $3\pi/2$.

We turn now to terrestrial experiments using reactors or radioactive sources, and discuss oscillations of electron-neutrinos or antineutrinos. They are relevant in the description of solar neutrino experiments. The electron-(anti)neutrino survival probability in vacuum is given by the following expression:

$$P_{\nu_e\to\nu_e} = \sum_{i,j}^{3} N^*_{ei}N_{ei}N_{ej}N^*_{ej} - 4\sum_{j>i}^{3} Re\left[N^*_{ej}N_{ej}N_{ei}N^*_{ei}\right]\sin^2\left(\frac{\Delta m^2_{ji}L}{4E}\right). \tag{5.39}$$

For this case, it is easy to notice that $N_{ei} = \alpha_{11}U_{ei}$ (see for example Eq. (5.3)) and, therefore,

$$P_{\nu_e\to\nu_e} = \alpha^4_{11}\left[\sum_{i}^{3}|U_{ei}|^2|U_{ei}|^2 - 4\sum_{j>i}^{3}|U_{ej}|^2|U_{ei}|^2\sin^2\left(\frac{\Delta m^2_{ji}}{4E}L\right)\right]. \tag{5.40}$$

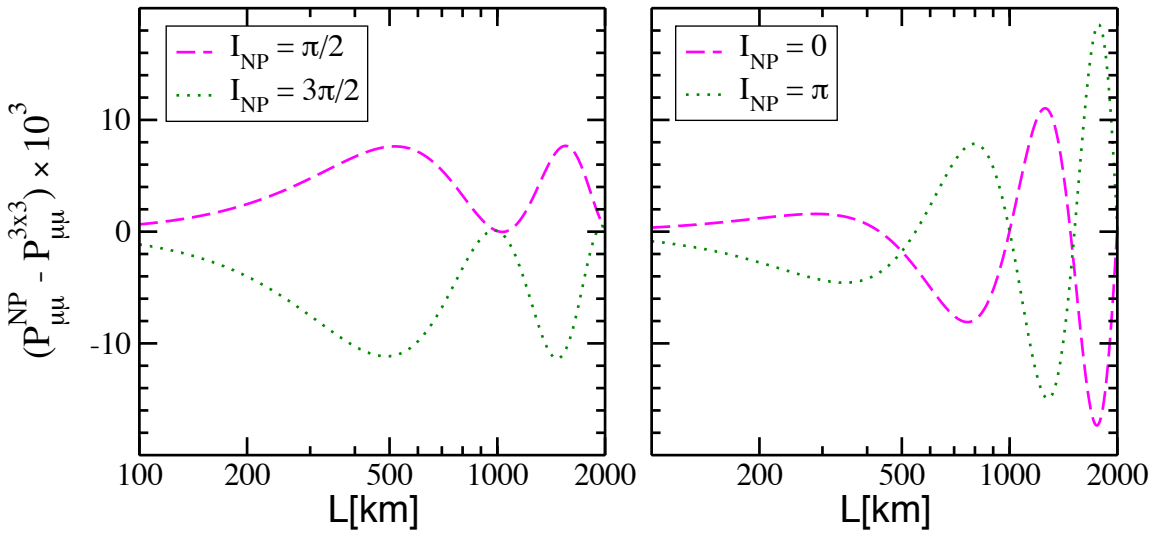

Figure 5.4: Difference between the standard muon-neutrino survival probability and the corresponding new physics probability for some values of the additional CP phase I_{NP}. The remaining parameters have been fixed to be the same as in Fig. 5.2.

Using Eq. (1.120), this expression can be rewritten as

$$P_{\nu_e \to \nu_e} = \alpha_{11}^4 \left[1 - \cos^4 \theta_{13} \sin^2(2\theta_{12}) \sin^2 \left(\frac{\Delta m^2_{21}}{4E} L \right) - \sin^2 (2\theta_{13}) \sin^2 \left(\frac{\Delta m^2_{31}}{4E} L \right) \right]. \tag{5.41}$$

Notice that, for this last probability, the existence of neutral heavy leptons produces a correction given simply by an overall factor α_{11}^4. This parameter will contain the effects of unitarity violation. Unfortunately, due to the strong restrictions on universality, the expected modifications to the probability will be limited.

To conclude this section, we point out that this formalism can easily be applied to the case of extra light neutrinos. They will take part in oscillations and may play a role [256, 257] in the well-known anomalies reported by reactor neutrino experiments [258] and the MiniBooNE Collaboration [233].

5.5 Neutrino oscillations and universality

As a consequence of the effective non-unitarity of the 3×3 leptonic mixing matrix, one may observe neutrino flavor change even though neutrinos have not traveled yet [83], a phenomenon known in the literature as the zero distance effect. The survival and conversion probabilities differ from one and zero respectively, as can be seen from Eqs.

(5.29), (5.34) and (5.40). In those equations, instead of the usual Dirac delta ($\delta_{\alpha\beta}$) we find α terms, which are independent of the distance (L). Therefore, for zero distance we express these probabilities in terms of α_{ij} as

$$\begin{aligned} P_{\nu_e\to\nu_e} &= [\alpha_{11}]^4 = [(NN^\dagger)_{11}]^2 = [1-(SS^\dagger)_{11}]^2\,, \\ P_{\nu_\mu\to\nu_\mu} &= [|\alpha_{21}|^2+\alpha_{22}^2]^2 = [(NN^\dagger)_{22}]^2 = [1-(SS^\dagger)_{22}]^2\,, \\ P_{\nu_\mu\to\nu_e} &= \alpha_{11}^2|\alpha_{21}|^2 = [(NN^\dagger)_{21}]^2 = [(SS^\dagger)_{21}]^2\,. \end{aligned} \tag{5.42}$$

From these expressions we can make an estimate of the constraints for the new parameters. We first notice that it is possible to express these equations in a similar way to the case of a light sterile neutrino in the limit $\Delta m_{ij}^2 L/(4E) \gg 1$ ($\left\langle \sin^2(\Delta m_{ij}^2 l/(4E))\right\rangle = 1/2$). Analogous expressions are obtained [259]:

$$\begin{aligned} P_{\nu_e\to\nu_e} &= 1-\frac{1}{2}\left[\sin^2(2\theta_{ee})\right]_{\rm eff}\,, \\ P_{\nu_\mu\to\nu_\mu} &= 1-\frac{1}{2}\left[\sin^2(2\theta_{\mu\mu})\right]_{\rm eff}\,, \\ P_{\nu_\mu\to\nu_e} &= \frac{1}{2}\left[\sin^2(2\theta_{\mu e})\right]_{\rm eff}\,, \end{aligned} \tag{5.43}$$

with

$$\begin{aligned} \left[\sin^2(2\theta_{ee})\right]_{\rm eff} &= 2(1-\alpha_{11}^4), \\ \left[\sin^2(2\theta_{\mu\mu})\right]_{\rm eff} &= 2[1-(|\alpha_{21}|^2+\alpha_{22}^2)^2], \\ \left[\sin^2(2\theta_{\mu e})\right]_{\rm eff} &= 2\alpha_{11}^2|\alpha_{21}|^2. \end{aligned} \tag{5.44}$$

Although the MiniBooNE experiment reports an anomaly that might be interpreted as new physics [233], there are strong constraints on light sterile neutrinos at 3σ [257] given by:

$$\begin{aligned} \left[\sin^2(2\theta_{ee})\right]_{\rm eff} &\leq 0.2\,, \\ \left[\sin^2(2\theta_{\mu\mu})\right]_{\rm eff} &\leq 0.06\,, \\ \left[\sin^2(2\theta_{\mu e})\right]_{\rm eff} &\leq 1\times10^{-3}\,. \end{aligned} \tag{5.45}$$

Even stronger constraints on the existence of a fourth neutrino are derived from ν_μ to ν_e oscillation experiments such as NOMAD [260]:

$$\left[\sin^2(2\theta_{\mu e})\right]_{\text{eff}} \leq 1.4 \times 10^{-3}\,. \tag{5.46}$$

Translated into the parametrization under discussion we have

$$\alpha_{11}^2 |\alpha_{21}|^2 \leq 0.007 \;\; (90\%\,\text{C.L.})\,. \tag{5.47}$$

Finally, we can obtain bounds at 90 % C.L. on the individual α_{ij} parameters, by combining this limit with those coming from universality (Eq. (5.22)):

$$\alpha_{11}^2 \geq 0.987, \qquad \alpha_{22}^2 \geq 0.9918, \qquad |\alpha_{21}|^2 \leq 0.0071. \tag{5.48}$$

5.6 Current constraints on NHL

The unitarity violation discussed in this chapter could point to new physics as the one responsible for neutrino mass. For example, the possible existence of neutral heavy leptons could give an explanation of the neutrino mass generation mechanism in seesaw schemes. They might be the messengers in this mechanism. However, in these schemes very heavy right-handed neutrinos are predicted, restricting their expected signatures. Nevertheless, several low-scale seesaw realizations do not introduce these high-scale masses [18, 19, 22, 224–226]. For this reason, we consider useful to give a compilation of model-independent NHL searches. These results are based only on a phenomenological analysis without taking into account any particular seesaw scheme.

For many years, experiments have been searching for isosinglet neutrinos without any positive signal up to now. The range of masses already covered is wide, between 10 MeV and 100 GeV, looking for:

- A peak in leptonic decays of pions and kaons. It could imply a mixing of heavy neutrinos with electron or muon-neutrinos [249, 261]. The signal of a neutral heavy lepton would be a monochromatic line at

$$E_l = \frac{m_M^2 + m_l^2 - m_{NHL}^2}{2m_M}\,, \tag{5.49}$$

  where E_l and m_l are the energy and mass of the lepton respectively, m_M is the mass of the meson and m_{NHL} corresponds to the mass of the heavy neutrino.

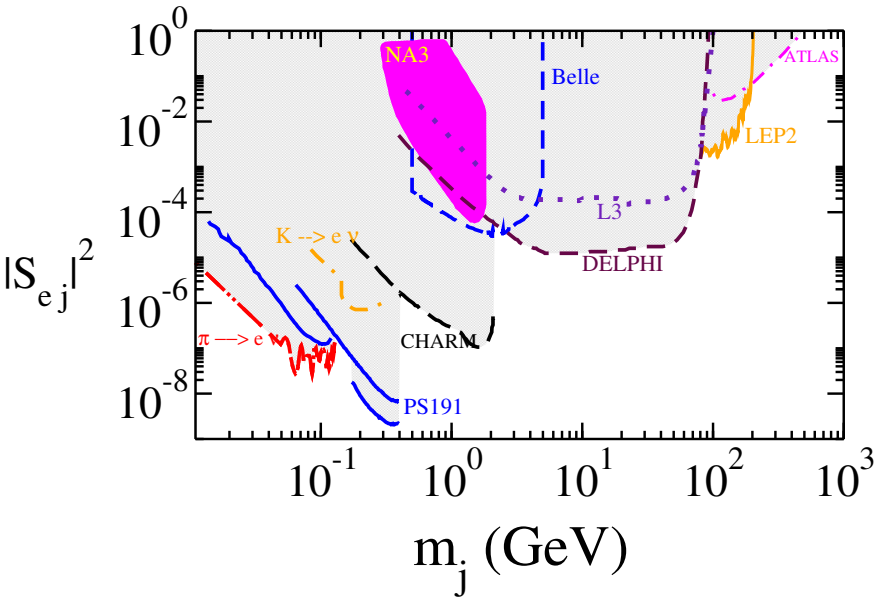

Figure 5.5: Bounds on the mixing between the electron-neutrino and neutral heavy leptons, $|S_{ej}|$, depending on the NHL mass, m_j.

- A signature coming from a possible heavy neutrino decay in electrons, muons and pions.

In particular, for the couplings of heavy neutrinos with electron and muon-neutrinos, the mixing parameters $|S_{ej}|^2$ and $|S_{\mu j}|^2$ can be tested (between 10 MeV and 100 GeV) in:

- Peak searches in the energy spectrum of leptons (electron or muon) in meson decays:
  - $\pi \to e\nu$ and $K \to e\nu$ for the coupling with electron-neutrino.
  - $\pi \to \mu\nu$ and $K \to \mu\nu$ for the muon-neutrino case.
- NHL decays in reactor and accelerator neutrino experiments. If they were heavy enough but lighter than the Z boson, they would have been copiously produced in the first phase of the LEP experiment (the coupling should be appreciable [229, 230]). Searches have been negative, including those performed in the second phase of LEP with higher energies [231] or in LHC [262–264].

We show the constraints coming from direct production of NHL in Fig. 5.5 and Fig. 5.6.

In Fig. 5.5 we show the wide range of energy that has been scanned in the search for neutral heavy leptons coupled to the electron-neutrino. The constraints on $|S_{ej}|^2$ are given as a function of m_j and can be interpreted as bounds on the $m_4 - U_{e4}$ plane. Figure 5.5 shows the results from nine different experiments [194, 231, 262, 265–273], since

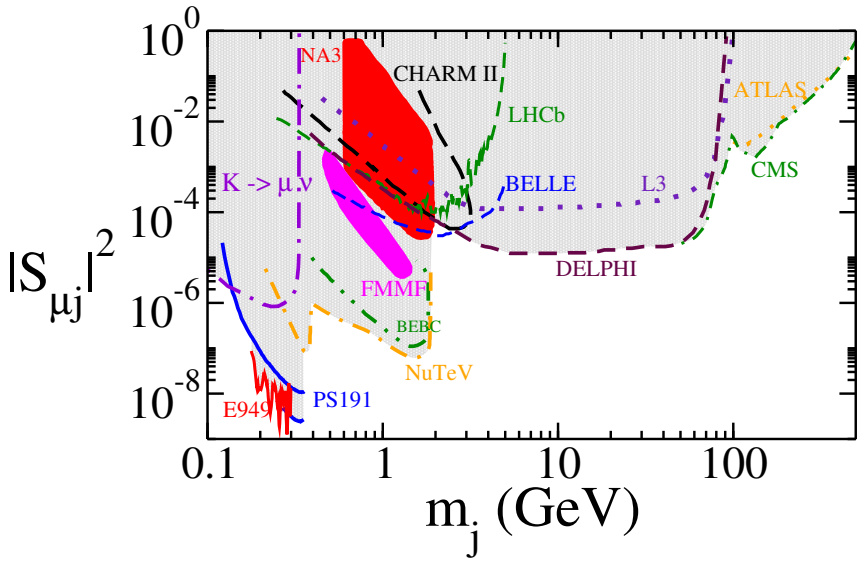

Figure 5.6: Bounds on the mixing between the muon-neutrino and neutral heavy leptons, $|S_{\mu j}|$, depending on the NHL mass, m_j.

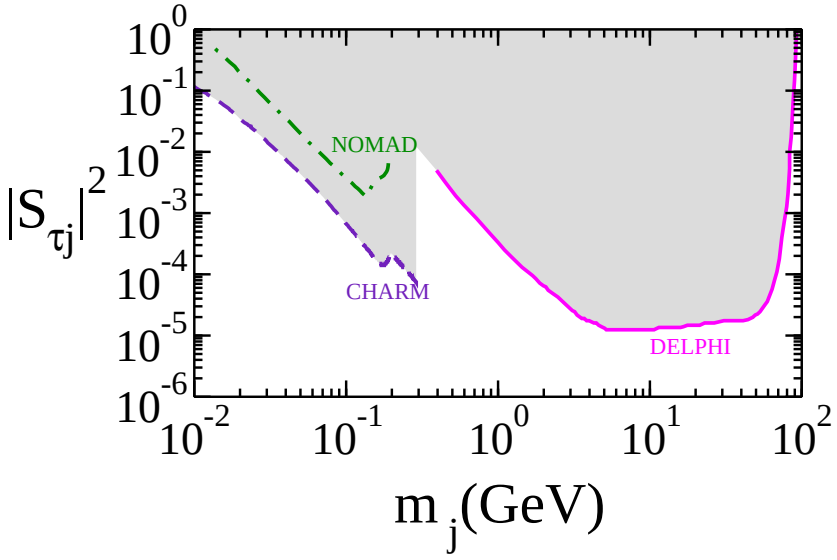

Figure 5.7: Bounds on the mixing between the tau-neutrino and neutral heavy leptons, $|S_{\tau j}|$, depending on the NHL mass, m_j.

the CHARM Collaboration up to the recent LHC results from ATLAS. A brief description of all these experiments is given in the appendix C. Future experiments will also search for this heavy lepton [274]. That is the case, for instance, of DUNE [221], ILC [275] and FCC-ee [276, 277] proposals.

We show in Fig. 5.6 the constraints for the mixing of extra neutral heavy leptons with the muon-neutrino. The constraints also cover a wide region of energy as result of several experimental searches [263, 264, 278–284]. Again, a short description of the experiments that have constrained this coupling is given in the appendix C.

For the sake of completeness, we also show in Fig. 5.7 the restrictions for the neutral heavy lepton mixing with the tau-neutrino [231, 285, 286]. By comparing with previous figures, one can see that, as expected, the tau-neutrino sector has been less explored.

Colliders such as the LHC can set more stringent constraints thanks to the ATLAS and CMS detectors. However, it should also be noticed that for the $SU(3)_C \times SU(2)_L \times U(1)_Y$ gauge structure, extra heavy leptons will be isosinglets and, therefore, their production rate will be scaled by small mixing factors. In order to avoid this limitation, one can consider extended models, such as the left-right symmetric models (Sec. 1.4.4). In this type of schemes extra right-handed gauge bosons could be produced at high energies, opening the door to lepton flavour violation signatures [287, 288].

5.6.1 Neutrinoless double beta decay

It is expected, based on theoretical grounds, that neutrinos have a Majorana nature which implies lepton number violation. In particular, neutrinoless double beta decay ($0\nu\beta\beta$) may take place at some level [237].

We begin this section by recalling that the effective Majorana neutrino mass [289] is given by

$$\langle m \rangle = |\sum_j (U_{ej}^{n\times n})^2 m_j|, \tag{5.50}$$

where the j index indicates the light neutrinos couplings to the electron and the W-boson.

This dependence on the mixing matrix $U^{n\times n}$ implies that the presence of the heavy neutrinos would change the charged-current couplings to $U_{ej}^{n\times n} = \alpha_{11} U_{ej}$. This is derived from Eqs. (5.2) and (5.3), modifying Eq. (5.50) to

$$\langle m \rangle = |\sum_j (\alpha_{11} U_{ej})^2 m_j|, \tag{5.51}$$

with the index j running for the three light neutrino species.

The presence of an extra heavy neutrino in the neutrinoless double beta decay will induce an extra amplitude contribution to this process, that will depend on the mixing with the electron component. The amplitude will involve the exchange of the heavy

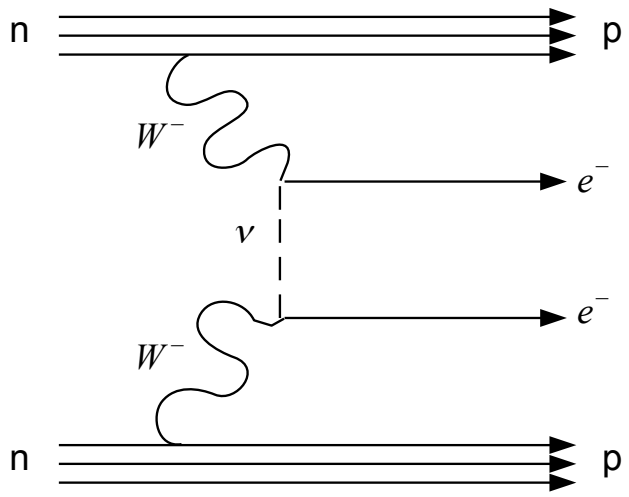

Figure 5.8: Diagram of neutrinoless double beta decay. A virtual Majorana neutrino is exchanged.

Majorana neutrinos Fig. 5.8 and it will be proportional to

$$\mathcal{A} \propto \frac{m_j}{q^2 - m_j^2}, \tag{5.52}$$

where q is the virtual momentum transfer ($q \sim 100\,\mathrm{MeV}$). It is well known that there are two different regimes for this amplitude [45]; if the virtual neutrino particle is light, we can consider $q^2 \gg m_j^2$ and we have

$$\mathcal{A}_{\mathrm{light}} \propto m_j. \tag{5.53}$$

On the other hand, for the exchange of a heavier neutrino we have $q^2 \ll m_j^2$, leading to

$$\mathcal{A}_{\mathrm{heavy}} \propto \frac{1}{m_j}\,. \tag{5.54}$$

From current constraints on neutrinoless double beta decay it is possible to obtain a restriction on the effect of an extra heavy lepton with a mass m_j and a mixing S_{ej}. Using, for instance, the data from ^{76}Ge searches and assuming an isosinglet neutrino of mass m_j [290], it is possible to obtain constraints as shown in Fig. 5.9. In this figure we may see the change of slope when the mass of the NHL approaches the nuclear momentum transfer, $m_j \simeq 100$ MeV, as expected from the previous discussion. Although the restrictions

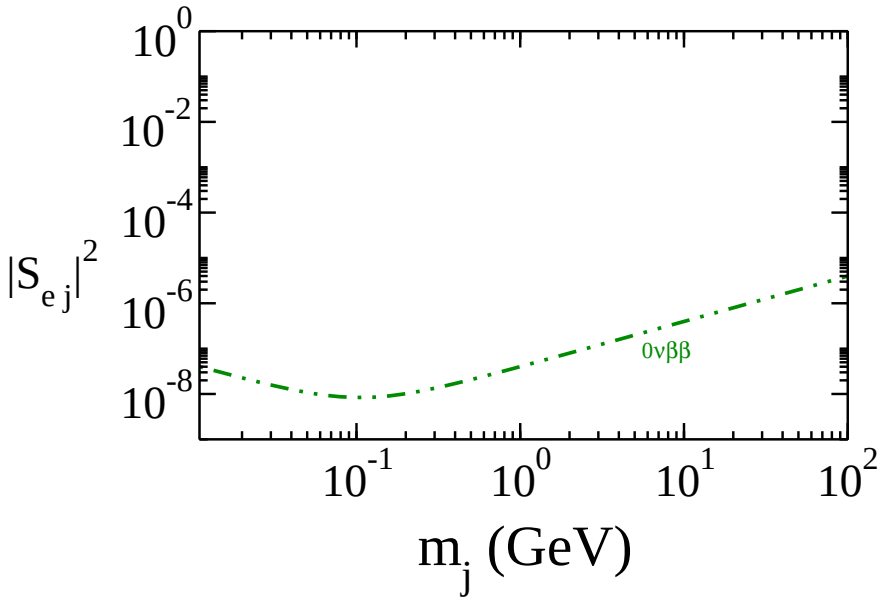

Figure 5.9: Constraints from neutrinoless double beta decay to an isosinglet of mass m_j, depending on its electron neutrino component $|S_{ej}|$.

coming from this process are tighter than those shown in Figs. 5.5, 5.6 and 5.7, it should be reminded that neutrinoless double beta decay takes place only if the neutrinos are Majorana particles.

5.6.2 Charged lepton flavor violation

For the sake of completeness, we comment the charged lepton flavor violation processes. These processes could be induced by the exchange of a virtual NHL, either at low-energies [21] or at the high-energy scale of accelerator experiments [240]. They could be seen at hadronic colliders, such as the LHC, especially if we consider well motivated low-scale seesaw models [287, 288, 291, 292]. However, the rates of these processes would depend on additional flavor parameters as well as upon details on the seesaw mechanism providing masses to neutrinos, being very model-dependent. Since we have performed a general model-independent analysis we have not considered charged lepton flavor violation in this thesis.

5.7 Summary

Extensions of the Standard Model, such as models employing the seesaw mechanism, predict the breaking of weak universality and a non-trivial leptonic mixing matrix. This can be generated by the admixture of heavy isosinglet neutrinos in leptonic charged-currents. These models are well motivated and most of them are successful in generating neutrino mass and mixing, thanks to the presence of the NHL. These heavy particles acts as messengers that generate the small neutrino masses. The scale of such heavy right-handed neutrinos is huge, but other realizations of these models exist, like the low-scale seesaw models. These low-scale models suggest that such NHL may be light enough to be accessible at high-energy colliders such as the LHC, or indirectly induce sizeable unitarity deviations in the "effective" lepton mixing matrix.

When we study extended models where extra heavy neutrinos are included, we work with many parameters, making it difficult to describe the model and their implications. Using our parameterization (Eq. (5.2)) simplifies the description of such models, since it involves only a set of effective parameters (three real plus a single CP phase) that concentrate all the new physics information. With this parameterization we have described the impact of non-unitary lepton mixing on weak decay processes and neutrino oscillations. Finally, for completeness, we have shown the up-to-date status of direct searches for extra heavy leptons, translated into this notation.

Chapter 6

Conclusions

Particle physics is going through an interesting epoch, with important discoveries in the past two decades. As a confirmation of this, we find the recent recognition to this field through the Nobel prizes awarded to the Higgs boson discovery (2013) and the detection of neutrino oscillations (2015). Particle physics is in an era of precision, prepared to solve new challenges raised in our understanding of the universe.

At these crossroads of knowledge is situated a little and seemingly inoffensive particle, the neutrino. It may seem insignificant but it has great news to tell us, new physics is here! Neutrino oscillations are a solid evidence of physics beyond Standard Model. But it is not an isolated phenomenon since it is accompanied by another prodigy, neutrinos are massive particles! This implies the necessity to develop mechanisms and models to induce neutrino mass. From most of these models we have non-conventional neutrino properties like Non-Standard Interactions (NSI) or the magnetic moment of neutrino. Also processes such as neutrinoless double beta decay, since typically neutrinos are Majorana. This thesis has tried to derive information on NSI and their implications, using the experimental data from oscillation searches.

For this purpose, we have started with two introductory chapters:

- In chapter 1 we have reviewed the most interesting features of neutrinos in the Standard Model and beyond.
- In chapter 2 we have introduced the physics of Non-Standard Interactions, reviewing how NSI theoretically arise and their effects in neutrino experiments.

After these introductory chapters we continue with the original part of this thesis where the NSI effect on oscillation experiments has been discussed. In particular, a global analysis of solar data including KamLAND reactor data has been performed in order to

check how robust is the LMA solution to the solar neutrino problem in presence of NSI. After introducing NSI, an extra solution appears, the so-called LMA-D (Large Mixing Angle-Dark). It implies that solar neutrino data can also be accounted for $\theta_{12} > \pi/4$ if the NSI strength is large enough. Therefore, although NSI play a sub-leading role in the explanation of the solar neutrino problem, they still have influence over the neutrino oscillation solution. Thus a question arises immediately: how is it possible to eliminate the degeneracy of LMA? This a challenge for solar experiments like Borexino, SNO or Super-Kamiokande and for new proposals as DUNE [221], LENA [293] or another LBNE (Long Baseline Neutrino Experiments) [188, 294]. Atmospheric and laboratory experiments such as Hyper-Kamiokande [206, 207] IceCube and DeepCore [295, 296] will be help in ruling out the "dark" region.

Following with the study of NSI effects on neutrino experiments, a new analysis of NuTeV results has been performed in this thesis. NuTeV results present a discrepancy with the Standard Model parameters, taken as a possible hint of NSI. Since several uncertainties from QCD were omitted, we have carried out a reanalysis of NuTeV results in this thesis. Several bounds on NSI couplings involving muon-neutrinos and quarks ($\varepsilon^q_{\mu\alpha}$) have been derived from our discussion. Our conclusion is that, although these NSI parameters are much smaller than those involving electron and tau-neutrinos, they need not be as small as previously believed.

These studies have allowed us to obtain limits on vectorial and axial components of NSI parameters in processes of neutrinos with quarks ($\varepsilon^{qV,A}_{\alpha\alpha}$). In particular, NSI couplings involving electron and tau-neutrinos have been studied by combining solar, reactor (KamLAND) and accelerator (CHARM) data; whereas muon-neutrino NSI parameters have been analyzed using the results from the NuTeV reanalysis, combining them with accelerator (CHARM and CDHS) and atmospheric data (Super-Kamiokande) in order to lift the degeneracy. The most relevant results are compiled in Table 6.1 at 90% of C.L.

In the last chapter of this thesis we have assumed the existence of neutral heavy leptons and studied their implications. These heavy particles arise in most extended models as exchange particles in the mechanism generating neutrino masses. As a consequence, NSI could appear directly or indirectly through the non-unitarity of the light neutrino mixing matrix, as we expressed in Eqs. (6.1). These models beyond the SM usually imply a very large number of parameters, making it difficult to work with them. In order to facilitate the study of these models, we have presented a model-independent formalism which provides a very useful way to separate the light mixing matrix ($N^{3\times3}$) in two parts: the standard one ($U^{SM} \equiv U^{3\times3}$) and another one which concentrates the new physics

Table 6.1: Limits on NSI parameters of neutrino with quark interactions at 90 % C.L. following from several combined analysis. The information on this table corresponds to original results derived in this thesis.

NSI with down	NSI with up	Experiments
NU	NU	
$-0.5 < \varepsilon_{ee}^{dV} < 1.2$		Sol+KamL+CHARM
$-0.4 < \varepsilon_{ee}^{dA} < 1.4$		Sol+KamL+CHARM
$-1.8 < \varepsilon_{\tau\tau}^{dV} < 4.4$		Sol+KamL+CHARM
$-1.5 < \varepsilon_{\tau\tau}^{dA} < 0.7$		Sol+KamL+CHARM
$-0.042 < \varepsilon_{\mu\mu}^{dV} < 0.042$	$-0.044 < \varepsilon_{\mu\mu}^{uV} < 0.044$	NuTeV(NNPDF)+SK
$-0.091 < \varepsilon_{\mu\mu}^{dA} < 0.091$	$-0.15 < \varepsilon_{\mu\mu}^{uA} < 0.18$	NuTeV(NNPDF)+SK
$-0.042 < \varepsilon_{\mu\mu}^{dV} < 0.042$	$-0.044 < \varepsilon_{\mu\mu}^{uV} < 0.044$	NuTeV(Bentz et al.)+SK
$-0.072 < \varepsilon_{\mu\mu}^{dA} < 0.057$	$-0.094 < \varepsilon_{\mu\mu}^{uA} < 0.140$	NuTeV(Bentz et al.)+SK
FC	FC	
$-0.08 < \varepsilon_{e\tau}^{dV} < 0.58$		Sol+KamL
$-0.007 < \varepsilon_{\mu\tau}^{dV} < 0.007$	$-0.007 < \varepsilon_{\mu\tau}^{uV} < 0.007$	NuTeV+SK+CHARM+CDHS
$-0.039 < \varepsilon_{\mu\tau}^{dV} < 0.039$	$-0.039 < \varepsilon_{\mu\tau}^{uA} < 0.039$	NuTeV+SK+CHARM+CDHS

information (N^{NP}). This formalism has been applied to:

- obtain bounds on the relevant α_{ij} parameters from universality tests,
- describe the oscillation probabilities, observing interesting features, such as zero-distance effects and the appearance of a new phase I_{NP} which could affect the oscillation probability,
- describe $(3+1)$ and $(3+3)$ neutrino schemes [1].

These applications show explicitly the simplicity of this method. As a future project, it would be very convenient to rewrite NSI couplings in terms of the α_{ij} parameters, for instance:

$$\varepsilon_{ee}^{eL} = -g_L \frac{|\alpha_{21}||\alpha_{31}|}{|\alpha_{32}|\alpha_{22}}\,, \quad \varepsilon_{ee}^{eR} = -g_R \frac{|\alpha_{21}||\alpha_{31}|}{|\alpha_{32}|\alpha_{22}}\,, \tag{6.1}$$

where a scenario with an extra heavy neutrino is considered.

[1] See appendix B.

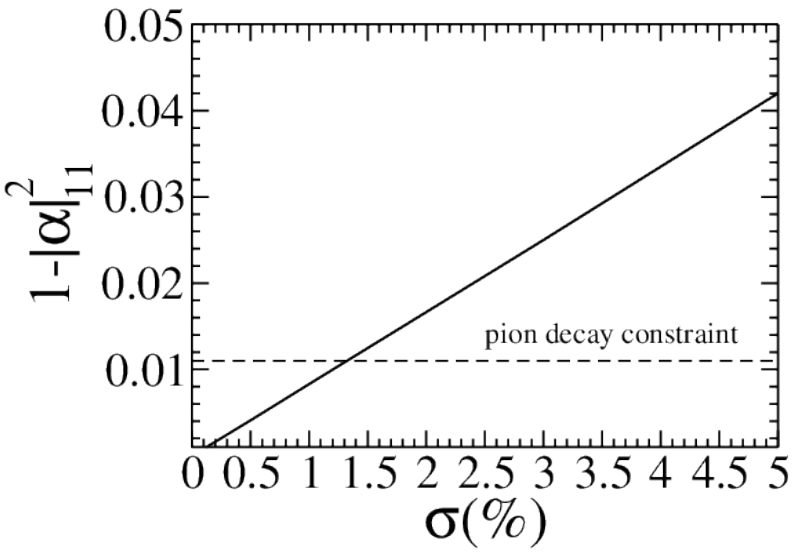

Figure 6.1: Estimated LENA sensitivity to the non-unitary parameters [297].

For the sake of completeness, a compilation of the mixing parameters $|S_{\alpha j}|^2$ of heavy neutrinos with the light ones from several laboratory experiments has been carried out. We want to stress that studying these bounds could be very useful in order to elucidate the neutrino mass generation mechanism and the energy scale of new physics. But it is not possible from current experiments to get very strong bounds on these parameters, so new experimental proposals must be considered, such as the aforementioned LENA. As an example, an estimate of the LENA sensitivity to the non-unitarity of the mixing matrix is shown in Fig. 6.1 in terms of α_{11}.

Summarizing in a couple of sentences: Neutrinos have opened the door to new physics, involving non-standard effects and new extra particles among other features. Faced with these prospects, we should be aware that a very interesting neutrino era is waiting for us.

Conclusions

La física de partícules es troba ara mateix en una època interessant, amb importants descobriments durant les dues dècades passades. Com a prova d'açò, trobem el recent reconeixement als premis Nobel, atorgant aquesta distinció al descobriment del bosó de Higgs (2013) i a la detecció de les oscil·lacions de neutrins (2015). La física de partícules es troba immersa en una era de precisió, preparada per resoldre els nous reptes plantejats en el nostre intent d'entendre l'univers.

En meitat d'aquesta cruïlla de coneixements es troba una diminuta i aparentment inofensiva partícula, el neutrí. Sembla insignificant però té notícies importants per a nosaltres, la nova física està ja ací! Les oscil·lacions de neutrins són una sòlida evidència de física més enllà del Model Estàndard. Però aquest no és un fenomen aïllat sinó que ve acompanyat d'altre prodigi, els neutrins són partícules amb massa! Aquest fet implica la necessitat de desenvolupar mecanismes i models que indueixin la massa del neutrí. De la gran majoria d'aquests models sorgeixen propietats no convencionals dels neutrins com les Interaccions No Estàndard (NSI) o el moment magnètic. També processos com la desintegració doble beta sense neutrins, ja que els neutrins són típicament partícules de Majorana. Com el lector haurà comprovat, aquesta tesi ha intentat aportar informació sobre les NSI i les seves implicacions, utilitzant les dades experimentals provinents de la cerca d'oscil·lació de neutrins.

Per a aquest comès, hem començat la tesi amb dos capítols recopilatoris:

- El capítol 1 ha sigut una revisió de les propietats més importants dels neutrins dins del Model Estàndard i més enllà d'aquest.

- El capítol 2 ens ha endinsat en la física de les Interaccions No Estàndard, revisant el seu origen a la teoria i la seva influència als experiments de neutrins.

Després d'aquests dos capítols introductoris hem continuat amb la part original d'aquesta tesi, on l'efecte de les NSI sobre experiments d'oscil·lació de neutrins ha sigut discutit. En concret, s'ha realitzat una anàlisi global utilitzant les dades provinents d'experiments

amb neutrins solars i incloent els resultats de l'experiment de reactor KamLAND, per tal de dilucidar com de robusta és la solució LMA al problema dels neutrins solars en presència de NSI. Després d'introduir les NSI apareix una solució extra no contemplada anteriorment, la anomenada LMA-D (Large Mixing Angle-Dark). Aquesta nova solució implica que les dades de neutrins solars poden ser explicades inclús per a angles de mescla grans ($\theta > \pi/4$), sempre que els valors dels paràmetres de NSI siguen lo suficientment grans també. Per tant, malgrat que les NSI tenen un paper secundari en l'explicació dels fluxos de neutrins solars, encara tenen influència a l'hora de determinar una solució. Així doncs, una qüestió sorgeix immediatament: com és possible eliminar la degeneració de la solució LMA? Aquest és un repte per experiments de neutrins solars com Borexino, SNO o Super-Kamiokande i per a noves propostes com DUNE [221] LENA [293] o altres LBNE (Long Baseline Neutrino Experiments) [188, 294]. Així mateix, els experiments de neutrins atmosfèrics i de laboratori com Hyper-Kamiokande [206, 207], IceCube i DeepCore [295, 296] seran de gran ajuda per tal de descartar la regió "dark".

Seguint amb l'estudi dels efectes de les NSI sobre els experiments de neutrins, una nova anàlisi dels resultats de NuTeV s'ha dut a terme en aquesta tesi. Com és ben conegut, NuTeV presentà una discrepància amb els paràmetres del Model Estàndard, sent utilitzada com a possible indici de NSI. Però, ja que certes incerteses relacionades amb QCD foren omeses, hem realitzat una reanàlisi dels resultats de NuTeV en aquesta tesi. D'aquesta discussió hem obtingut diversos límits en els acoblaments de NSI del neutrí muònic amb quarks ($\varepsilon^q_{\mu\alpha}$). La nostra conclusió ha estat que, encara que aquests paràmetres de NSI són més menuts que aquells que impliquen neutrins del electró i del tau, no ho són tant com s'esperava.

Aquests estudis ens han permet obtindre límits en les components vectorial i axial dels paràmetres de NSI en processos d'interacció de neutrins amb quarks ($\varepsilon^{qV,A}_{\alpha\alpha}$). En concret, els acoblaments relacionats amb els neutrins de l'electró i el tau han sigut aconseguits combinant dades d'experiments solars, de reactor (KamLAND) i d'accelerador (CHARM); mentre que els paràmetres que impliquen neutrins muònics han sigut obtinguts utilitzant els resultats de la reanàlisi de NuTeV juntament amb dades d'accelerador (CHARM i CDHS) i d'atmosfèric (Super-Kamiokande). Els resultats més rellevants es troben recopilats a la Taula 6.1 al 90% de C.L.

En l'últim capítol d'aquesta tesi hem assumit l'existència de leptons pesats i neutres (NHL) i hem estudiat les implicacions de la seva existència. Aquestes partícules pesades apareixen en la gran majoria de models estesos com a partícules d'intercanvi dins del mecanisme que genera la massa del neutrí. Com a conseqüència, les NSI podrien aparèixer

directament o de forma indirecta, producte de la no unitarietat de la matriu de mescla dels neutrins lleugers, com mostrem en les Eqs. (6.1). Aquests models més enllà del SM normalment impliquen una gran quantitat de paràmetres dificultant el treball amb ells. Per tal de facilitar l'estudi d'aquests models, hem presentat un formalisme (independent del model) que ens proporciona una forma molt útil de separar la matriu de mescla dels neutrins lleugers ($N^{3\times3}$) en dos: l'estàndard ($U^{SM} \equiv U^{3\times3}$) i un altra que concentra tota la informació de nova física (N^{NP}). Aquest formalisme ha sigut aplicat a:

- obtindre límits als paràmetres α_{ij} a partir de tests d'universalitat,
- descriure les probabilitats d'oscil·lació, observant efectes interessants com l'oscil·lació de neutrins a distància zero i l'aparició d'una nova fase I_{NP} la qual podria variar les probabilitats d'oscil·lació,
- descriure esquemes amb $(3+1)$ i $(3+3)$ neutrins [2].

Aquestes aplicacions posen de manifest la simplicitat d'aquest mètode. Com a un projecte futur, seria molt convenient escriure els acoblaments de NSI en funció dels paràmetres α_{ij}, per exemple:

$$\varepsilon_{ee}^{eL} = -g_L \frac{|\alpha_{21}||\alpha_{31}|}{|\alpha_{32}|\alpha_{22}}\,, \quad \varepsilon_{ee}^{eR} = -g_R \frac{|\alpha_{21}||\alpha_{31}|}{|\alpha_{32}|\alpha_{22}}\,,$$

on s'ha considerat un escenari amb només un neutrí extra.

Buscant la completesa d'aquest treball, s'ha realitzat una compilació del valor dels paràmetres d'acoblament $|S_{\alpha j}|^2$ dels neutrins pesats amb els lleugers a partir de diferent experiments de laboratori. Ens agradaria assenyalar que estudiar aquests límits podria ser de gran utilitat per tal de dilucidar quin és el mecanisme generador de la massa del neutrí així com el valor de l'escala d'energia de nova física. Però no és possible trobar cotes determinants en aquests paràmetres, així doncs s'han de considerar noves propostes experimentals, com la ja mencionada de LENA. Com a exemple, una estimació de la sensitivitat de LENA a la no unitarietat de la matriu de mescla, en funció de α_{11}, pot trobar-se a la Fig. 6.1.

Per resumir aquest treball en un parell de frases podríem dir: Els Neutrins han obert la porta a la nova física, que implica efectes no estàndard i partícules extra entre altres característiques. Davant aquestes perspectives, deuríem d'estar ben atents al que ens envolta perquè una etapa molt interessant en física de neutrins ens espera.

[2] Veure apèndix B.

Appendix A

NSI in a two-neutrino scheme

It is obvious that working with less parameters simplifies calculations and makes easier to understand the consequences derived from them. This is obtained when we pass from a description with three neutrinos to a two-neutrino scheme. The benefits of this approximation were already discussed in Sec. 1.5.2 and it is usually done because reproduces quite accurately the scenario to study. In fact, it was carried out in Sec. 3.1.2, in particular when the NSI matrix was defined in Eq. (3.3). Thus, it is worth showing step by step how this simple calculation is performed, in order to provide rigor to our results obtained in chapter 3.

In a three-neutrino scheme, the NSI matrix is defined as a 3×3 matrix containing all the NSI couplings:

$$\begin{pmatrix} \varepsilon_{ee} & \varepsilon_{e\mu} & \varepsilon_{e\tau} \\ \varepsilon_{\mu e} & \varepsilon_{\mu\mu} & \varepsilon_{\mu\tau} \\ \varepsilon_{\tau e} & \varepsilon_{\tau\mu} & \varepsilon_{\tau\tau} \end{pmatrix} . \tag{A.1}$$

This matrix can be rotated in the $\mu - \tau$ plane thanks to the ω_{23} rotation matrix [1]:

$$\begin{pmatrix} 1 & 0 & 0 \\ 0 & \cos\theta_{23} & -\sin\theta_{23} \\ 0 & \sin\theta_{23} & \cos\theta_{23} \end{pmatrix} \begin{pmatrix} \varepsilon_{ee} & \varepsilon_{e\mu} & \varepsilon_{e\tau} \\ \varepsilon_{\mu e} & \varepsilon_{\mu\mu} & \varepsilon_{\mu\tau} \\ \varepsilon_{\tau e} & \varepsilon_{\tau\mu} & \varepsilon_{\tau\tau} \end{pmatrix} \begin{pmatrix} 1 & 0 & 0 \\ 0 & \cos\theta_{23} & \sin\theta_{23} \\ 0 & -\sin\theta_{23} & \cos\theta_{23} \end{pmatrix} , \tag{A.2}$$

[1] Here, we are using the Okubo's notation [46] as in the Appendix B.

getting explicitly

$$\begin{pmatrix} \varepsilon_{ee} & c_{23}\varepsilon_{e\mu} - s_{23}\varepsilon_{e\tau} & s_{23}\varepsilon_{e\mu} + c_{23}\varepsilon_{e\tau} \\ c_{23}\varepsilon_{\mu e} - s_{23}\varepsilon_{\tau e} & c_{23}^2\varepsilon_{\mu\mu} - s_{23}c_{23}\varepsilon_{\tau\mu} - s_{23}c_{23}\varepsilon_{\mu\tau} + s_{23}^2\varepsilon_{\tau\tau} & c_{23}s_{23}\varepsilon_{\mu\mu} - s_{23}^2\varepsilon_{\tau\mu} + c_{23}^2\varepsilon_{\mu\tau} - s_{23}c_{23}\varepsilon_{\tau\tau} \\ s_{23}\varepsilon_{\mu e} + c_{23}\varepsilon_{\tau e} & c_{23}^2\varepsilon_{\tau\mu} + s_{23}c_{23}\varepsilon_{\mu\mu} - s_{23}^2\varepsilon_{\mu\tau} - s_{23}c_{23}\varepsilon_{\tau\tau} & s_{23}^2\varepsilon_{\mu\mu} + s_{23}c_{23}\varepsilon_{\tau\mu} + s_{23}c_{23}\varepsilon_{\mu\tau} + c_{23}^2\varepsilon_{\tau\tau} \end{pmatrix}, \tag{A.3}$$

with $c_{23} = \cos\theta_{23}$ and $s_{23} = \sin\theta_{23}$. In this point we make the approximation from three to two neutrinos, neglecting NSI couplings related with muon-neutrinos ($\varepsilon_{\mu\mu} = \varepsilon_{\mu e} = \varepsilon_{\mu\tau} = 0$) [2] and truncating the matrix in Eq. (A.3) to a 2×2 matrix. After these considerations, we get the following expression for the NSI hamiltonian:

$$H_{NSI} = \pm\sqrt{2}G_F N_f \begin{pmatrix} \varepsilon_{ee} & -s_{23}\varepsilon_{e\tau} \\ -s_{23}\varepsilon_{e\tau} & s_{23}^2\varepsilon_{\tau\tau} \end{pmatrix}. \tag{A.4}$$

As the Schrödinger equation does not change if an extra element is introduced in the diagonal entries of the hamiltonian, we can rewrite Eq. (A.4) as

$$H_{NSI} = \pm\sqrt{2}G_F N_f \begin{pmatrix} 0 & -s_{23}\varepsilon_{e\tau} \\ -s_{23}\varepsilon_{e\tau} & s_{23}^2\varepsilon_{\tau\tau} - \varepsilon_{ee} \end{pmatrix}, \tag{A.5}$$

where it is possible identify

$$\varepsilon = -\sin\theta_{23}\varepsilon_{e\tau}\,, \qquad \varepsilon' = \sin^2\theta_{23}\varepsilon_{\tau\tau} - \varepsilon_{ee}\,, \tag{A.6}$$

as we wanted to prove.

[2] We neglect these parameters because we do not take into account muon-neutrinos in the scenario considered in chapter 3. Obviously, we could cancel other NSI couplings if the situation requires it.

Appendix B

Neutrino mixing and heavy isosinglets

Neutral heavy leptons are included in several extensions of the Standard Model, giving rise to new interactions (NSI) or non-unitary effects of the lepton mixing matrix, as we have already discussed in Secs. 1.4 and 2.2. In these models the neutrino mixing matrix includes extra terms involving neutral heavy leptons [9], with effects on the light neutrino sector since the light mixing matrix [1] is not longer unitary. In this appendix we will show explicitly how the light mixing matrix loses its unitarity and we will develop, step by step, the α-formalism till we arrive to the α_{ij} expressions, Eqs. (5.4), (5.6) and (5.5).

Let us start constructing the mixing matrix for n neutrinos $U^{n\times n}$ from Okubo's notation [46]:

$$U^{n\times n} = \omega_{n-1\,n}\,\omega_{n-2\,n}\,\ldots\,\omega_{1\,n}\,\omega_{n-2\,n-1}\,\omega_{n-3\,n-1}\,\ldots\,\omega_{1\,n-1}\,\ldots\,\omega_{2\,3}\,\omega_{1\,3}\,\omega_{1\,2}\,, \tag{B.1}$$

where each ω_{ij} $(i<j)$ represents the common complex rotation matrix in the ij plane [9, 45]:

$$\omega_{13} = \begin{pmatrix} c_{13} & 0 & e^{-i\phi_{13}}s_{13} \\ 0 & 1 & 0 \\ -e^{i\phi_{13}}s_{13} & 0 & c_{13} \end{pmatrix}, \tag{B.2}$$

with $s_{ij}=\sin\theta_{ij}$ and $c_{ij}=\cos\theta_{ij}$. In a more compact form, it can be written as:

$$(\omega_{ij})_{\alpha\beta} = \delta_{\alpha\beta}\sqrt{1-\delta_{\alpha i}\delta_{\beta j}s_{ij}^2-\delta_{\alpha j}\delta_{\beta i}s_{ij}^2}+\eta_{ij}\delta_{\alpha i}\delta_{\beta j}+\bar{\eta}_{ij}\delta_{\alpha j}\delta_{\beta i}, \tag{B.3}$$

[1] We call light mixing matrix, to the mixing matrix corresponding to the three light neutrinos.

where $i < j$ and $s_{ij}^2 = \sin^2\theta_{ij}$, $\eta_{ij} = e^{-i\phi_{ij}}\,\sin\theta_{ij}$ and $\bar{\eta}_{ij} = -e^{i\phi_{ij}}\,\sin\theta_{ij}$. For a general treatment, Eq. (B.2) can be expressed in a n-neutrino case as:

$$\omega_{ij} = \begin{pmatrix} 1 & 0 & & \cdots & 0 & \cdots & & & 0 \\ 0 & 1 & & & & & & & \vdots \\ \vdots & & c_{ij} & \cdots & 0 & \cdots & \eta_{ij} & & \\ & & \vdots & \ddots & & & \vdots & & \\ & & 0 & & 1 & & 0 & & \\ & & \vdots & & & \ddots & \vdots & & \\ & & \bar{\eta}_{ij} & \cdots & 0 & \cdots & c_{ij} & & \vdots \\ \vdots & & & & & & & 1 & 0 \\ 0 & & & \cdots & 0 & \cdots & & 0 & 1 \end{pmatrix}. \tag{B.4}$$

As we will see later, it is very useful to separate Eq. (B.1) in a product of two matrices,

$$U^{n\times n} = U^{n-N}\,U^{N}\,, \tag{B.5}$$

with

$$U^{N} = \omega_{N-1\,N}\,\omega_{N-2\,N}\,\ldots\,\omega_{1\,N}\,, \tag{B.6}$$

$$U^{n-N} = \omega_{n-1\,n}\,\omega_{n-2\,n}\,\ldots\,\omega_{1\,n}\,\omega_{n-1\,n-1}\,\omega_{n-2\,n-1}\,\ldots\,\omega_{1\,N+1}\,. \tag{B.7}$$

In a matrix form, Eq. (B.5) can be written as:

$$\begin{pmatrix} \alpha_{11} & 0 & \cdots & 0 & \vdots & & & \\ \alpha_{21} & \alpha_{22} & \ddots & \vdots & \vdots & & & \\ \vdots & & \ddots & 0 & \vdots & & S & \\ \alpha_{N1} & \cdots & & \alpha_{NN} & \vdots & & & \\ \cdots & \cdots & \cdots & \cdots & \vdots & \cdots & \cdots & \cdots \\ & & & & \vdots & & & \\ & & V' & & \vdots & & T & \\ & & & & \vdots & & & \end{pmatrix} \begin{pmatrix} U_{11}^N & U_{12}^N & \cdots & U_{1N}^N & \vdots & & \\ U_{21}^N & U_{22}^N & & \vdots & \vdots & & \\ \vdots & & \ddots & & \vdots & 0 & \\ U_{N1}^N & \cdots & & U_{NN}^N & \vdots & & \\ \cdots & \cdots & \cdots & \cdots & \vdots & \cdots & \cdots \\ & & & & \vdots & & \\ & & 0 & & \vdots & I & \\ & & & & \vdots & & \end{pmatrix}, \tag{B.8}$$

which will be very convenient in order to separate new physics and the Standard Model.

The standard neutrino mixing matrix $U^{3\times3}$ (Eq. (1.120) or (1.121)) is unitary in the

usual description of three neutrinos. But if we consider an extended lepton sector with n neutrinos, it is a non-unitary (in general) submatrix of the total mixing matrix $U^{n\times n}$ given by Eq. (B.1). Using the property represented by Eq. (B.5), the extended mixing matrix $U^{n\times n}$ can be divided in a more appropriate way as a matrix U^{NP}, which contains the new physics information, and the usual lepton mixing matrix $U^{SM} \equiv U^{3\times 3}$:

$$U^{n\times n} = U^{NP}\, U^{SM}\,, \tag{B.9}$$

defining each matrix as

$$U^{NP} = \omega_{n-1\,n}\omega_{n-2\,n}\ldots\omega_{3\,n}\omega_{2\,n}\omega_{1\,n}\omega_{n-2\,n-1}\ldots\omega_{3\,n-1}\omega_{2\,n-1}\omega_{1\,n-1}\ldots\omega_{3\,4}\omega_{2\,4}\omega_{1\,4}\,, \tag{B.10}$$

$$U^{SM} = \omega_{2\,3}\,\omega_{1\,3}\,\omega_{1\,2}\,. \tag{B.11}$$

The total mixing matrix for n neutrinos $U^{n\times n}$ can be also expressed in a description of four blocks as [241]

$$U^{n\times n} = \begin{pmatrix} N & S \\ V & T \end{pmatrix}\,, \tag{B.12}$$

where $N \equiv N^{3\times 3}$ stands for the mixing matrix of the three light neutrinos, which includes the standard oscillation parameters together with those related with the extra heavy neutrinos, breaking the unitarity given in a three-neutrino scenario. The terms of this submatrix N are those that can be observed in oscillation experiments, that is why N is considered the most important part of $U^{n\times n}$. The submatrix N can be also decomposed, as in Eqs. (B.5) and (B.9), in a more convenient form as

$$N = N^{NP}\, U^{3\times 3} = \begin{pmatrix} \alpha_{11} & 0 & 0 \\ \alpha_{21} & \alpha_{22} & 0 \\ \alpha_{31} & \alpha_{32} & \alpha_{33} \end{pmatrix} U^{3\times 3}\,. \tag{B.13}$$

This division is characterized by the zero triangle submatrix, that depends on the arbitrary order of the ω_{ij} matrices product.

As we have already mentioned, it is interesting to show how the α_{ij} components of the N matrix can be obtained. In order to explain this calculation more accurately, we should denote that $\omega_{ij}\omega_{kl}$ commutes when $i \neq k, l$ and $j \neq k, l$; so the new physics part

of the total mixing matrix, Eq. (B.10), can be split as follows:

$$\begin{aligned} U^{NP} &= \omega_{n-1\,n}\,\omega_{n-2\,n}\,\ldots\,\omega_{4\,n}\,\omega_{n-2\,n-1}\,\ldots\,\omega_{4\,n-1}\,\ldots\omega_{4\,5}\,\times \\ &\quad \omega_{3\,n}\,\omega_{2\,n}\,\omega_{1\,n}\;\omega_{3\,n-1}\,\omega_{2\,n-1}\,\omega_{1\,n-1}\,\ldots\,\omega_{3\,4}\;\omega_{2\,4}\,\omega_{1\,4}\,. \end{aligned} \tag{B.14}$$

This decomposition of Eq. (B.10) is very suitable because, as it can be observed, the first line of Eq. (B.14) has no influence in the relevant submatrix N. However, the second line components introduce the new physics in the light mixing matrix N, being a set of products of three matrices in the form $\omega_{3j}\omega_{2j}\omega_{1j}$. Each product will be identified with a parameter α^j with the following explicit form:

$$\begin{aligned} \alpha^j = \omega_{3j}\omega_{2j}\omega_{1j} &= \begin{pmatrix} c_{1j} & 0 & 0 & \vdots & 0 & \eta_{1j} & 0 \\ \eta_{2j}\bar{\eta}_{1j} & c_{2j} & 0 & \vdots & 0 & \eta_{2j}c_{1j} & 0 \\ \eta_{3j}c_{2j}\bar{\eta}_{1j} & \eta_{3j}\bar{\eta}_{2j} & c_{3j} & \vdots & 0 & \eta_{3j}c_{2j}c_{1j} & 0 \\ \cdots & \cdots & \cdots & \cdots & \cdots & \cdots & \cdots \\ 0 & 0 & 0 & \vdots & I & 0 & 0 \\ c_{3j}c_{2j}\bar{\eta}_{1j} & c_{3j}\bar{\eta}_{2j} & \bar{\eta}_{3j} & \vdots & 0 & c_{3j}c_{2j}c_{1j} & 0 \\ 0 & 0 & 0 & \vdots & 0 & 0 & I \end{pmatrix} \\ &= \begin{pmatrix} \alpha^j_{11} & 0 & 0 & \vdots & 0 & \alpha^j_{1j} & 0 \\ \alpha^j_{21} & \alpha^j_{22} & 0 & \vdots & 0 & \alpha^j_{2j} & 0 \\ \alpha^j_{31} & \alpha^j_{32} & \alpha^j_{33} & \vdots & 0 & \alpha^j_{3j} & 0 \\ \cdots & \cdots & \cdots & \cdots & \cdots & \cdots & \cdots \\ 0 & 0 & 0 & \vdots & I & 0 & 0 \\ \alpha^j_{j1} & \alpha^j_{2j} & \alpha^j_{j3} & \vdots & 0 & \alpha^j_{jj} & 0 \\ 0 & 0 & 0 & \vdots & 0 & 0 & I \end{pmatrix}. \end{aligned} \tag{B.15}$$

We can see that each α^j parameter contains the new physics information introduced by the i-neutral heavy lepton, but the relevant parameters for N^{NP} are those coming from the 3×3 submatrix located in the upper left side, which presents a triangle submatrix as we expected. After solving the multiplication given by $\alpha^n\alpha^{n-1}\cdots\alpha^5\alpha^4$, we can find the

explicit value of the α_{ij} entries in Eq. (B.13):

$$\begin{aligned}
\alpha_{11} &= \alpha_{11}^{n}\,\alpha_{11}^{n-1}\,\alpha_{11}^{n-2}\,\cdots\,\alpha_{11}^{4} = c_{1\,n}\,c_{1\,n-1}c_{1\,n-2}\ldots c_{14}\,,\\
\alpha_{22} &= \alpha_{22}^{n}\,\alpha_{22}^{n-1}\,\alpha_{22}^{n-2}\,\cdots\,\alpha_{22}^{4} = c_{2\,n}\,c_{2\,n-1}c_{2\,n-2}\ldots c_{24}\,,\\
\alpha_{33} &= \alpha_{33}^{n}\,\alpha_{33}^{n-1}\,\alpha_{33}^{n-2}\,\cdots\,\alpha_{33}^{4} = c_{3\,n}\,c_{3\,n-1}c_{3\,n-2}\ldots c_{34}
\end{aligned} \tag{B.16}$$

stand for the diagonal elements α_{ii}, while the off-diagonal parameters α_{ij} are expressed as follows:

$$\begin{aligned}
\alpha_{21} &= \alpha_{21}^{n}\,\alpha_{11}^{n-1}\,\cdots\,\alpha_{11}^{4} + \alpha_{22}^{n}\,\alpha_{21}^{n-1}\,\cdots\,\alpha_{11}^{4} + \cdots + \alpha_{22}^{n}\,\alpha_{22}^{n-1}\,\alpha_{22}^{n-2}\,\cdots\,\alpha_{21}^{4}\,,\\
\alpha_{32} &= \alpha_{32}^{n}\,\alpha_{22}^{n-1}\,\cdots\,\alpha_{22}^{4} + \alpha_{33}^{n}\,\alpha_{32}^{n-1}\,\cdots\,\alpha_{22}^{4} + \cdots + \alpha_{33}^{n}\,\alpha_{33}^{n-1}\,\alpha_{33}^{n-2}\,\cdots\,\alpha_{32}^{4}\,,\\
\alpha_{31} &= \alpha_{31}^{n}\,\alpha_{11}^{n-1}\,\cdots\,\alpha_{11}^{4} + \alpha_{33}^{n}\,\alpha_{31}^{n-1}\,\cdots\,\alpha_{11}^{4} + \cdots + \alpha_{33}^{n}\,\alpha_{33}^{n-1}\,\alpha_{33}^{n-2}\,\cdots\,\alpha_{31}^{4}\\
&+ \alpha_{32}^{n}(\,\alpha_{21}^{n-1}\,\alpha_{11}^{n-2}\,\cdots\,\alpha_{11}^{4} + \alpha_{22}^{n-1}\alpha_{21}^{n-2}\,\cdots\,\alpha_{11}^{4} + \cdots + \alpha_{22}^{n-1}\alpha_{22}^{n-2}\,\cdots\,\alpha_{21}^{4})\\
&+ \alpha_{33}^{n}\,\alpha_{32}^{n-1}(\,\alpha_{21}^{n-2}\,\alpha_{11}^{n-3}\,\cdots\alpha_{11}^{4} + \cdots + \alpha_{22}^{n-2}\,\alpha_{22}^{n-3}\,\cdots\alpha_{21}^{4}) + \cdots\\
&+ \alpha_{33}^{n}\,\alpha_{33}^{n-1}\,\alpha_{32}^{n-2}(\,\alpha_{21}^{n-3}\,\alpha_{11}^{n-4}\,\cdots\alpha_{11}^{4} + \cdots + \alpha_{22}^{n-3}\,\alpha_{22}^{n-4}\,\cdots\alpha_{21}^{4}) + \cdots\\
&+ \alpha_{33}^{n}\,\alpha_{33}^{n-1}\,\alpha_{33}^{n-2}\,\cdots\,\alpha_{32}^{5}\,\alpha_{21}^{4}\,,
\end{aligned} \tag{B.17}$$

or using a more explicit notation,

$$\begin{aligned}
\alpha_{21} &= c_{2\,n}\,c_{2\,n-1}\ldots c_{2\,5}\,\eta_{24}\bar{\eta}_{14} + c_{2\,n}\,\ldots c_{2\,6}\,\eta_{25}\bar{\eta}_{15}\,c_{14} + \ldots\\
&+ \eta_{2n}\bar{\eta}_{1n}\,c_{1n-1}\,c_{1n-2}\,\ldots\,c_{14}\,,\\
\alpha_{32} &= c_{3\,n}\,c_{3\,n-1}\ldots c_{3\,5}\,\eta_{34}\bar{\eta}_{24} + c_{3\,n}\,\ldots c_{3\,6}\,\eta_{35}\bar{\eta}_{25}\,c_{24} + \ldots\\
&+ \eta_{3n}\bar{\eta}_{2n}\,c_{2n-1}\,c_{2n-2}\,\ldots\,c_{24}\,,\\
\alpha_{31} &= c_{3\,n}\,c_{3\,n-1}\ldots c_{3\,5}\,\eta_{34}c_{2\,4}\bar{\eta}_{14} + c_{3\,n}\ldots c_{3\,6}\,\eta_{35}c_{2\,5}\bar{\eta}_{15}\,c_{14} + \ldots\\
&+ \eta_{3n}c_{2\,n}\,\bar{\eta}_{1n}\,c_{1n-1}\,c_{1n-2}\ldots c_{14} + c_{3\,n}\,c_{3n-1}\ldots c_{3\,5}\,\eta_{35}\bar{\eta}_{25}\eta_{24}\bar{\eta}_{14}\\
&+ c_{3\,n}\,\ldots c_{3\,6}\,\eta_{36}\bar{\eta}_{26}c_{2\,5}\,\eta_{24}\bar{\eta}_{14} + \ldots + \eta_{3n}\bar{\eta}_{2n}\eta_{2n-1}\bar{\eta}_{1n-1}c_{1n-2}\ldots c_{14}\,.
\end{aligned} \tag{B.18}$$

To summarize this appendix, we may say that the α_{ij} parameters agglutinate all the new physics information. These parameters along with the known entries of the standard mixing matrix $U^{3\times3}$ construct the light mixing matrix N in Eq. (B.13), whose terms could be observed experimentally. Notice that if there is no extra neutrino, $\alpha_{ij} = 0$ and the Standard Model description is recovered.

The form of N^{NP}, with an upper right triangular submatrix, has been chosen on

purpose. This structure gives rise to the most convenient form of the mixing matrix N in order to study the most interesting scenarios from a phenomenological point of view. Therefore, if another order of the ω_{ij} products is chosen, we can find the zeros located at different entries of N^{NP}, being interesting to analyze a particular situation.

Losing the unitarity

In the Standard Model, the neutrino sector is described with three neutrinos (and their corresponding antineutrinos) as we have discussed in Sec. 1.5.1. The mixing matrix connecting flavor and mass eigenstates is a 3×3 unitary matrix (Eq. (1.119)) with the following generic form:

$$U^{SM} \equiv U^{3\times 3} = \begin{pmatrix} U_{e1} & U_{e2} & U_{e3} \\ U_{\mu 1} & U_{\mu 2} & U_{\mu 3} \\ U_{\tau 1} & U_{\tau 2} & U_{\tau 3} \end{pmatrix} . \tag{B.19}$$

In a most general case, where n neutrinos are taken into account (including, of course, the three light neutrinos among them) the unitary mixing matrix have n rows and n columns:

$$U^{n\times n} = \begin{pmatrix} N^{3\times 3} & S^{3\times n-3} \\ T^{n-3\times 3} & V^{n-3\times n-3} \end{pmatrix} . \tag{B.20}$$

Therefore, a mixing matrix including all neutrinos is unitary, Eq. (1.93). On the other hand, in models with extended lepton sector, the light mixing matrix $N^{3\times 3}$ follows from the truncation of $U^{n\times n}$, so it has not to be unitary in general. It has the following generic structure in our α-formalism:

$$\begin{pmatrix} \alpha_{11}\, U_{e1} & \alpha_{11}\, U_{e2} & \alpha_{11}\, U_{e3} \\ \alpha_{21}\, U_{e1} + \alpha_{22}\, U_{\mu 1} & \alpha_{21}\, U_{e2} + \alpha_{22}\, U_{\mu 2} & \alpha_{21}\, U_{e3} + \alpha_{22}\, U_{\mu 3} \\ \alpha_{31}\, U_{e1} + \alpha_{32}\, U_{\mu 1} + \alpha_{33}\, U_{\tau 1} & \alpha_{31}\, U_{e2} + \alpha_{32}\, U_{\mu 2} + \alpha_{33}\, U_{\tau 2} & \alpha_{31}\, U_{e3} + \alpha_{32}\, U_{\mu 3} + \alpha_{33}\, U_{\tau 3} \end{pmatrix} . \tag{B.21}$$

The inclusion of the α_{ij} parameters, where the new physics is encoded, breaks the unitarity:

$$N N^\dagger \neq 1 \,, \qquad N^\dagger N \neq 1 \,, \qquad \sum_i N_{\alpha i} N^*_{\beta i} \neq \delta_{\alpha\beta} \,, \qquad \sum_\alpha N_{\alpha i} N^*_{\alpha j} \neq \delta_{ij} \,. \tag{B.22}$$

For instance we have:

$$N^*_{e1}N_{e1} + N^*_{e2}N_{e2} + N^*_{e3}N_{e3} = \alpha^2_{11}\,, \tag{B.23}$$

$$N^*_{\mu 1}N_{e1} + N^*_{\mu 2}N_{e2} + N^*_{\mu 3}N_{e3} = \alpha_{11}\alpha^*_{21}\,, \tag{B.24}$$

instead of 1 or 0 as they should be respectively, if the unitarity condition was accomplished.

3 + 1 seesaw scheme with α parameters

In order to illustrate the convenience of the α-formalism we will apply it to a 3+1 scheme, where an extra right-handed singlet is added to the SM description:

$$\Psi_L = \begin{pmatrix} \nu_L \\ l_L \end{pmatrix} \quad , \quad \mathcal{N}_4\,, \tag{B.25}$$

giving rise to the following relation among flavor and mass eigenstates [5],

$$\nu_{\alpha L} = \sum_{k=1}^{3} N_{\alpha k}\,\nu_{kL} + S_{\alpha\,4}\,\mathcal{N}^c_{4\,L}\,. \tag{B.26}$$

In this scenario, the complete mixing matrix $U^{4\times4}$ is given by

$$U^{4\times4} = \begin{pmatrix} N^{3\times3} & S^{3\times1} \\ T^{1\times3} & V^{1\times1} \end{pmatrix} = \begin{pmatrix} N_{e1} & N_{e2} & N_{e3} & S_{e4} \\ N_{\mu 1} & N_{\mu 2} & N_{\mu 3} & S_{\mu 4} \\ N_{\tau 1} & N_{\tau 2} & N_{\tau 3} & S_{\tau 4} \\ T_{41} & T_{42} & T_{43} & V \end{pmatrix}\,, \tag{B.27}$$

where $N^{3\times3}$ is again the submatrix related with the standard neutrinos, Eq. (B.13). It is important to remember that $U^{4\times4}$ is unitary because includes extra and standard neutrinos, while $N^{3\times3}$ is not since it comes from the $U^{4\times4}$ truncation.

The light mixing matrix has the form given in Eq. (B.21), and the α_{ij} parameters are obtained from Eqs. (B.17) and (B.18), being expressed as follows:

$$\begin{aligned} \alpha_{11} = c_{14}\,, \qquad \alpha_{22} &= c_{24}\,, \qquad \alpha_{33} = c_{34}\,, \\ \alpha_{21} &= \eta_{24}\,\bar{\eta}_{14}\,, \\ \alpha_{32} &= \eta_{34}\,\bar{\eta}_{24}\,, \\ \alpha_{31} &= \eta_{34}\,c_{24}\,\bar{\eta}_{14}\,. \end{aligned} \tag{B.28}$$

Application to the 3 + 3 seesaw scheme

In general, the lepton sector is enlarged with more than one extra neutrino in order to produce the neutrino mass. As we have seen in Sec. 1.4, models including three extra singlets (as standard seesaw) or more (as inverse or linear seesaw) are common in the literature. In particular, for a 3 + 3 description the full mixing matrix will have the following structure,

$$U^{6\times 6} = \begin{pmatrix} N_{3\times 3} & S_{3\times 3} \\ T_{3\times 3} & V_{3\times 3} \end{pmatrix} , \tag{B.29}$$

with these expressions for the α_{ij} parameters:

$$\begin{aligned}
\alpha_{11} &= c_{16}\, c_{15}\, c_{14} \,, \\
\alpha_{22} &= c_{26}\, c_{25}\, c_{24} \,, \\
\alpha_{33} &= c_{36}\, c_{35}\, c_{34} \,, \\
\alpha_{21} &= \eta_{26}\, \bar{\eta}_{16}\, c_{15}\, c_{14} \;+\; c_{26}\, \eta_{25}\, \bar{\eta}_{15}\, c_{14} \;+\; c_{26}\, c_{25}\, \eta_{24}\, \bar{\eta}_{14} \,, \\
\alpha_{32} &= c_{36}\, c_{35}\, \eta_{34}\, \bar{\eta}_{24} \;+\; c_{36}\, c_{35}\, \bar{\eta}_{25}\, c_{24} \;+\; \eta_{36}\, \bar{\eta}_{26}\, c_{25}\, c_{24} \,, \\
\alpha_{31} &= c_{36}\, c_{35}\, c_{34}\, \eta_{34}\, c_{24}\, \bar{\eta}_{14} \;+\; c_{36}\, \eta_{35}\, c_{24}\, \bar{\eta}_{15}\, c_{14} \;+\; \eta_{36}\, c_{26}\, \bar{\eta}_{16}\, c_{15}\, c_{14} \\
&+\; c_{36}\, \eta_{35}\, \bar{\eta}_{25}\, \eta_{24}\, \bar{\eta}_{14} \;+\; \eta_{36}\, \bar{\eta}_{26}\, c_{25}\, \eta_{24}\, \bar{\eta}_{14} \;+\; \eta_{36}\, \bar{\eta}_{26}\, \eta_{25}\, \bar{\eta}_{15}\, c_{14} \,.
\end{aligned} \tag{B.30}$$

Appendix C

Relevant neutrino experiments

In this thesis, several neutrino experiments have been mentioned and their data have been used to perform our calculations. Therefore, we consider that it is worth dedicating this appendix to explain briefly their features.

C.1 Reactor experiments

Reactor neutrino experiments analyze the number of antineutrino events placing neutrino detectors around nuclear power plants. This study is performed in order to search for differences between the expected and the observed antineutrino signal, since this could be a hint of neutrino oscillations.

In this kind of experiments, antineutrinos are detected through inverse β-decay process on protons: $\bar{\nu}_e + p \rightarrow e^+ + n$. In particular, when an antineutrino travels through the detector it interacts with a proton giving rise to a positron and a neutron. The produced positron annihilates with an electron generating photons, whereas the neutron is absorbed by the liquid scintillator in the detector leading to more photons as a signal of the process. In the Fig. C.1 we can find a diagram of this detection process.

Double Chooz

Double Chooz [63] is a reactor neutrino experiment with the main goal of measuring the θ_{13} mixing angle. It is located at the border between France and Belgium near the Chooz nuclear plant.

Double Chooz uses two detectors of electron-antineutrinos in order to measure the number and energy of antineutrinos coming from a pair of nuclear reactors. The near

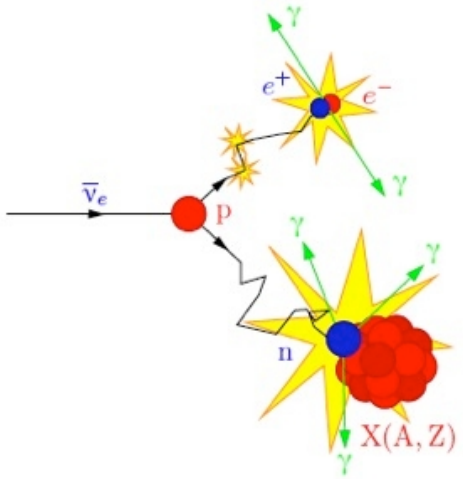

Figure C.1: Detection process in a reactor experiment [298].

detector is located 400 m away from reactors, while the far detector is 1.1 km away from the nuclear cores.

In these detectors, the innermost volume is filled with liquid scintillator doped with gadolinium. A schematic description of the detectors is given in Fig. C.2.

A difference between the number of events detected in near and far detectors would imply that some electron-antineutrinos have oscillated in their path towards the detector. The best-fit value of θ_{13} measured in Ref. [63] is

$$\sin^2 2\theta_{13} = 0.090^{+0.032}_{-0.029}\,. \tag{C.1}$$

Daya Bay

The Daya Bay neutrino experiment [64, 65] is a neutrino oscillation experiment. It is located in Daya Bay (China) where we find two nuclear power plants: Daya Bay NPP and Ling Ao NPP (Fig. C.3), having 6 nuclear reactors in total.

In the Daya Bay Complex we find three experimental underground halls (EH) where 8 antineutrinos detectors (AD) are placed. Each detector is filled with a liquid scintillator doped with gadolinium. They are protected against ambient radiation with high-purity water. A detailed description of these detectors can be found in Refs. [64, 65, 299, 300].

As in Double Chooz, antineutrinos are detected via the inverse β-decay process (Fig. C.1), showing oscillation events if the ratio between the number of expected and observed antineutrinos is smaller than 1. In a three-neutrino framework, the following results are

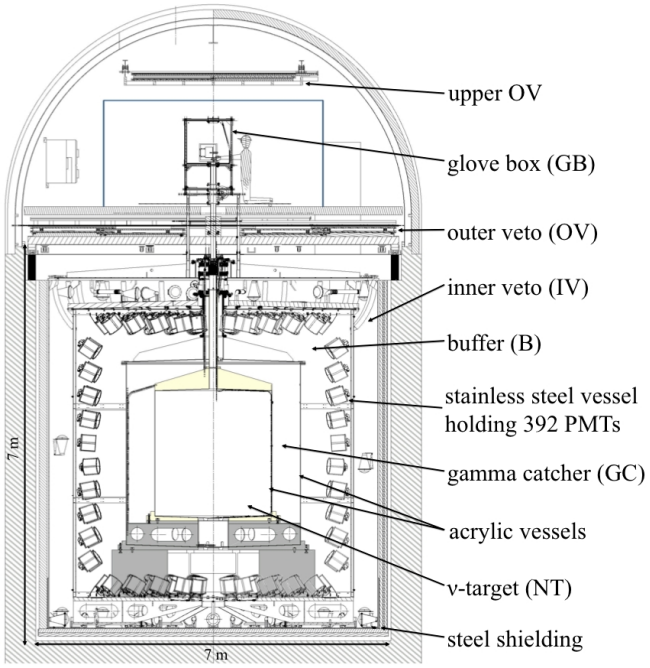

Figure C.2: Schematic view of the Double Chooz detector [63].

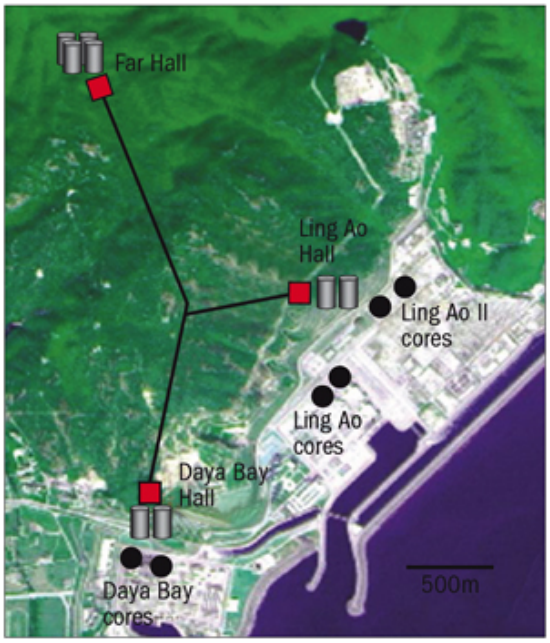

Figure C.3: Schematic view of Daya Bay experiment. [301].

derived from Daya Bay data [65]:

$$\sin^2 2\theta_{13} = 0.090^{+0.008}_{-0.009}\,, \qquad |\Delta m^2_{ee}| = (2.59^{+0.19}_{-0.20}) \times 10^{-3}\,\mathrm{eV}^2\,. \tag{C.2}$$

RENO

RENO (Reactor Experiment for Neutrino Oscillations) [67, 302] is a short baseline reactor experiment placed at South Korea. It has two identical antineutrino detectors, situated at 294 m and 1383 m from the Hanbit nuclear power plant, composed by six reactors. Each detector consists of four coaxial layers of cylindrical vessels containing different liquids depending on the layer purposes (target, gamma-catcher, buffer and veto).

Again, comparing the number of events in the near and far detector, the RENO Collaboration found the following value for θ_{13} [302]:

$$\sin^2 2\theta_{13} = 0.100 \pm 0.010\,(\mathrm{stat}) \pm 0.015\,(\mathrm{syst})\,. \tag{C.3}$$

KamLAND

The Kamioka Liquid Scintillator Antineutrino Detector (KamLAND) [37, 303] is an experiment that was located at the Kamioka mine in Japan. The antineutrino flux comes from 53 nuclear reactors surrounding the zone. These reactors are placed, on average, at 180 km away from the Kamioka mine, making it sensitive to the neutrino mixing related with the Large Mixing Angle (LMA), the solar neutrino solution with $\Delta m^2 \sim 10^{-5}\,\mathrm{eV}^2$.

The KamLAND detector consists in a 18 m sphere of stainless steel divided in several layers. The outer layer is plenty of photomultiplier tubes, while the second inner layer is a 13 m balloon filled with a scintillating liquid (mineral oil, benzene and fluorescent chemicals). Finally, a cylindrical water Cherenkov detector is placed around the containment vessel with two purposes: muon veto counter and protect the detector from cosmic rays and radioactivity.

The KamLAND Collaboration found the following best-fit values for the mixing parameters [37]:

$$\begin{aligned} \Delta m^2_{21} &= 7.58^{+0.14}_{-0.013}\,(\mathrm{stat})^{+0.15}_{-0.15}\,(\mathrm{syst}) \times 10^{-5}\,\mathrm{eV}^2\,, \\ \tan^2\theta_{12} &= 0.56^{+0.10}_{-0.07}\,(\mathrm{stat})^{+0.10}_{-0.86}\,(\mathrm{syst})\,. \end{aligned} \tag{C.4}$$

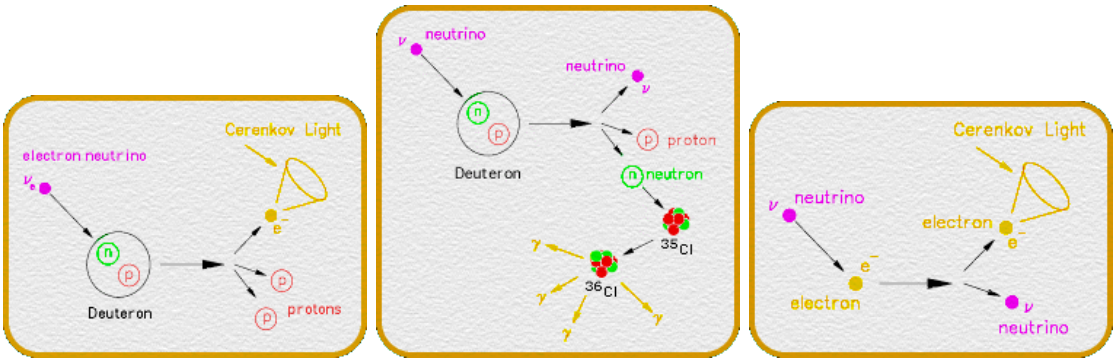

Figure C.4: The detection processes in the SNO experiment [304]. From left to right, the panels show CC, NC and neutrino-electron scattering respectively.

Combining the results in Eq. (C.4) with solar neutrino data, it was obtained

$$\Delta m^2_{21} = 7.59^{+0.21}_{-0.21} \times 10^{-5}\,\mathrm{eV}^2\,, \qquad \tan^2\theta_{12} = 0.47^{+0.06}_{-0.05}\,. \tag{C.5}$$

C.2 Solar experiments

Solar neutrino experiments study neutrinos produced in the Sun. They measure the number of neutrino events in a detector comparing it with the SSM prediction in order to constrain neutrino oscillation parameters. As an example of detection processes in solar neutrino experiments, we show those produced in SNO experiment in Fig. C.4.

SNO

The Sudbury Neutrino Observatory (SNO) [35, 36, 70, 71, 168, 169] was placed in the Creighton mine, in Sudbury (Canada), 2070 m underground.

The experiment was built to detect the energy and direction of ^{8}B neutrino flux produced in the Sun, distinguishing between electron-neutrinos and other flavors.

Neutrinos coming from the Sun interact with the detector via charged-current weak interactions, neutral-current weak interactions and neutrino-electron elastic scattering, as we can see in Fig. C.4. These interactions are registered by 9600 photomultipliers distributed around the detector (Fig. C.5).

The SNO Collaboration reported an evidence of flavor changing in the solar neutrino flux [35, 36]. Along with this, the SNO experiment measured a ^{8}B neutrino flux of [71]

$$\Phi_{^8B} = 5.046^{+0.159}_{-0.152}\,(\mathrm{stat})^{+0.107}_{-0.123}\,(\mathrm{syst})\,, \tag{C.6}$$

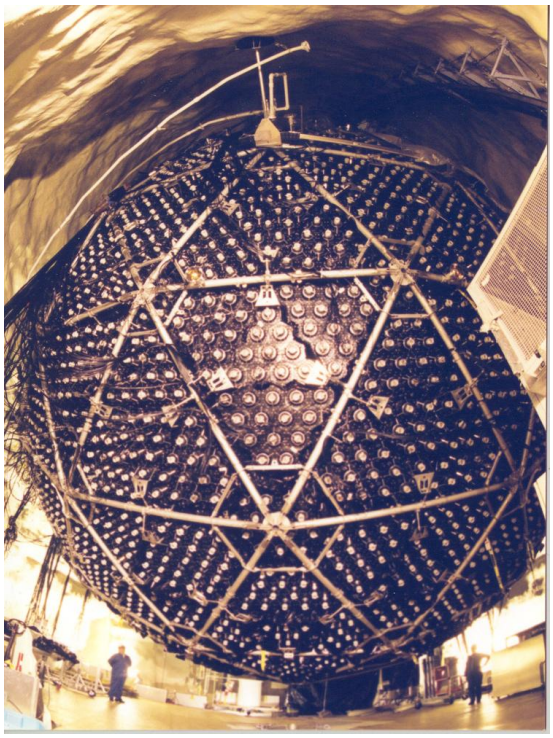

Figure C.5: Picture of SNO detector [304].

leading, in combination with all other solar data and KamLAND, to the following best-fit values for θ_{12} and Δm^2_{21}:

$$\theta_{12}\,(^\circ) = 34.06^{+1.16}_{-0.84}\,, \qquad \Delta m^2_{21} = 7.59^{+0.20}_{-0.21} \times 10^{-5}\,\mathrm{eV}^2\,. \tag{C.7}$$

Super-Kamiokande

The Super-Kamiokande experiment [68, 69, 75, 167] is a collaboration between 30 institutions of several countries (Japan, United States, Korea, China Poland and Spain). The detector is placed 1000 m underground in the Kamioka mine in Japan. This experiment observes neutrinos stemming from the Sun, atmospheric neutrinos as well as neutrinos produced artificially. Neutrino oscillations were observed for the first time in Super-Kamiokande in 1998.

Super-Kamiokande is a large water Cherenkov detector (Fig. C.6), which consists in a spherical stainless steel tank of 39 m of diameter, filled with 50.000 tons of ultra-pure water. 13.000 photomultipliers are installed in the inner surface of the tank wall, in order to register the Cherenkov radiation produced after neutrino scattering with electrons

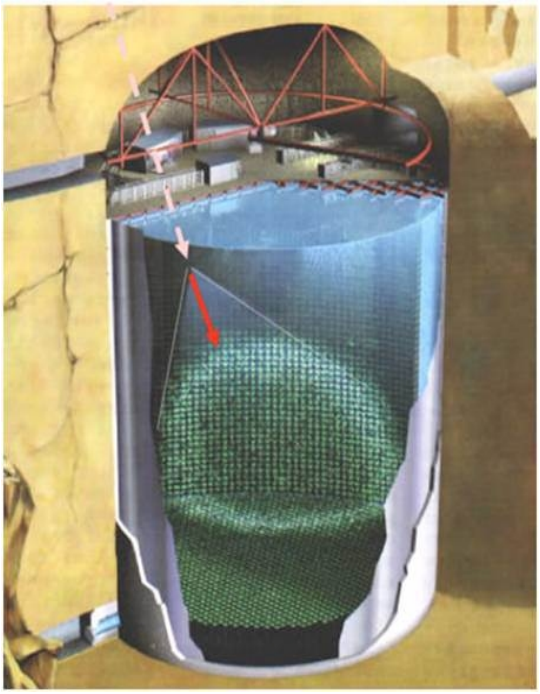

Figure C.6: Schematic image of the Super-Kamiokande detector [305].

(Fig. C.4).

From a global analysis including all current solar neutrino data (incorporating even SK-IV) together with KamLAND results, the Super-Kamiokande Collaboration published the following values for the oscillation parameters [69]:

$$\Delta m^2_{21} = 7.49^{+0.19}_{-0.17} \times 10^{-5}\,\mathrm{eV}^2\,, \qquad \sin^2\theta_{12} = 0.305 \pm 0.013\,. \tag{C.8}$$

Borexino

Borexino [74, 170, 171] is an experiment which studies low-energy neutrinos coming from the Sun, with the particular goal of measuring ^{7}Be solar neutrino flux and compare it with the Standard Model prediction. It is located at the Laboratori Nazionali del Gran Sasso near of L'Aquila (Italy).

The detector is a liquid scintillator, where the neutrino interactions are registered by 2200 photomultipliers that surround it. The liquid scintillator is inside a stainless steel sphere, being protected by a water tank. For a schematic view of the detector, see Fig. C.7.

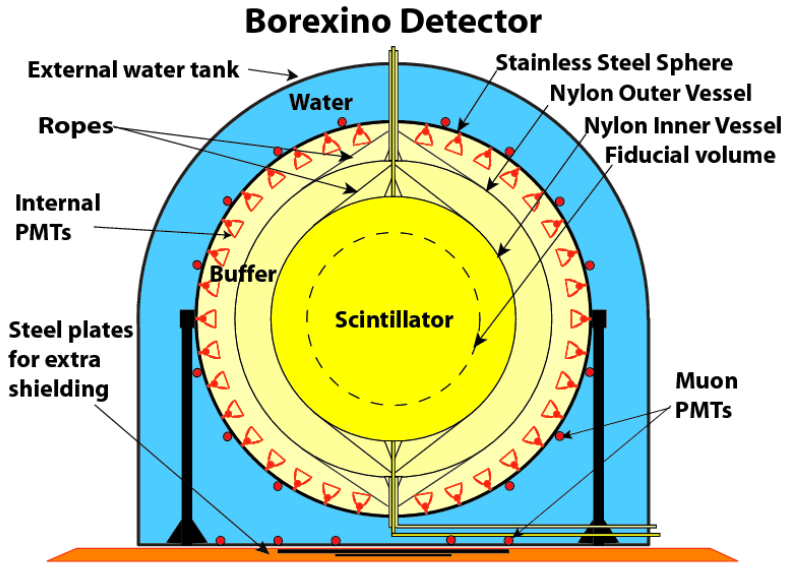

Figure C.7: Schematic view of the Borexino detector [306].

From the analysis of Borexino data, it was found that [74]

$$\Delta m^2_{21} = 5.2^{+1.5}_{-0.24} \times 10^{-5}\,\mathrm{eV}^2\,, \qquad \tan^2\theta_{12} = 0.468^{+0.039}_{-0.030}\,. \tag{C.9}$$

After including the KamLAND results, the oscillation parameters became

$$\Delta m^2_{21} = 7.50^{+0.16}_{-0.9} \times 10^{-5}\,\mathrm{eV}^2\,, \qquad \tan^2\theta_{12} = 0.457^{+0.033}_{-0.025}\,. \tag{C.10}$$

C.3 Accelerator experiments

Accelerator neutrino experiments are experimental devices using neutrinos produced at accelerators as source. In particular, neutrinos come from hadron decays as, for instance,

$$\begin{aligned} K^+ &\to e^+\nu\,, \\ K^+ &\to \mu^+\nu\,, \\ \pi^+ &\to e^+\nu\,, \\ \pi^+ &\to \mu^+\nu\,. \end{aligned} \tag{C.11}$$

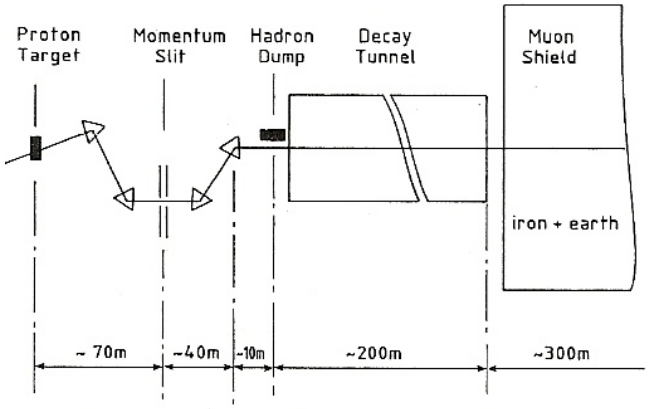

Figure C.8: Schematic view of the CHARM detector [160].

CHARM

CHARM (Cern Hamburg Rome Moscow) [160, 194, 307] was a collaboration which tried to shed some light on some aspects of electroweak theory as the Weinberg angle or the universality of the weak couplings. The experiment measured the ratios

$$R^e = \frac{\sigma(\nu_e N \to \nu_e X)}{\nu_e N \to e X}, \qquad R^\mu = \frac{\sigma(\nu_\mu N \to \nu_\mu X)}{\nu_\mu N \to \mu X}, \tag{C.12}$$

using accelerator neutrinos produced in SPS (CERN). In particular, electron-neutrinos were obtained from K^0 decay, whereas muon-neutrinos were produced at π decay.

The CHARM detector was a calorimeter surrounded by a muon spectrometer. This calorimeter consisted in 72 marble plates connected through scintillating plates. An image of this detector is given in Fig. C.8. The calorimeter recorded neutrino events produced from neutral-current or charged-current weak interactions.

NuTeV

NuTeV [162] was a detector designed to observe the interactions of neutrinos produced in the Tevatron accelerator at Fermilab, after the collision of 800 GeV protons on a BeO target. The detector was built with three types of layers (Fig. C.9).

The results obtained by NuTeV were quite controversial because they were far from the SM predictions, as we discussed in chapter 4.

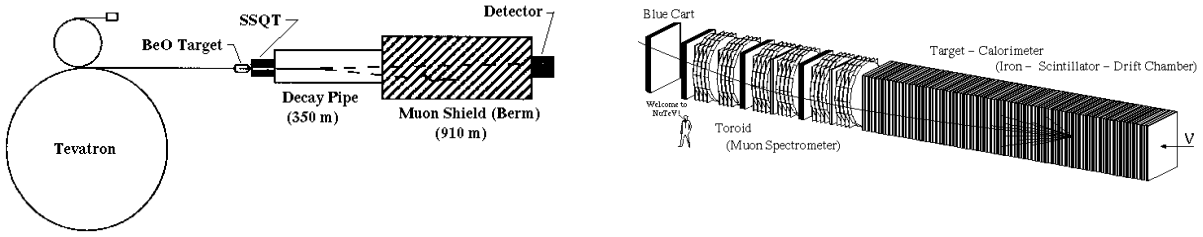

Figure C.9: The left panel shows neutrino production at Fermilab. The right: scheme of the NuTeV detector [308].

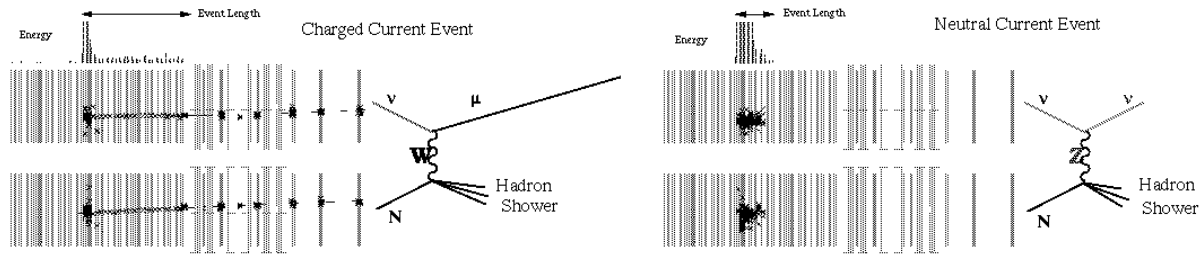

Figure C.10: Signals registered in the NuTeV detector: CC signal and the NC signal respectively [308].

C.4 Experiments giving constraints on NHL

$\pi \to \mathrm{e}\,\nu$ (TRIUMF)

This experiment [265, 266] tested the universality from studying the branching ratio of $\pi \to e\,\nu$ with respect to the common decay $\pi \to \mu\,\nu$ obtaining [265]:

$$R_{\pi e\nu} = \frac{\Gamma(\pi \to e\,\nu + \pi \to e\,\nu\,\gamma)}{\Gamma(\pi \to \mu\,\nu + \pi \to \mu\,\nu\,\gamma)} = 1.2265 \pm 0.0034(\mathrm{stat}) \pm 0.0044(\mathrm{syst}) \times 10^{-4}\,. \quad \text{(C.13)}$$

The experiment was performed in the M13 channel at TRIUMF, using a π^+ beam of momentum $P = 83\,\mathrm{MeV}/c$ and $\Delta P/P = 1$. The incoming beam was detected in a scintillator and stopped close to the target counter with a rate of $7 \times 10^4\,\mathrm{s}^{-1}$. Then, the produced positrons were detected with two $203\,\mathrm{mm} \times 203\,\mathrm{mm}$ wire chambers, before being analyzed in a 460 mm diam $\times$ 510 mm long NaI crystals, "TINA."

The mixing with extra heavy neutrinos should produce additional peaks in the positron energy spectrum from decays like $\pi^+ \to e^+\,\nu$ and $K^+ \to e^+\,\nu$, leading to the following

ratio which can be related to a heavy state [266]:

$$R_{ei} = \frac{\Gamma(\pi \to e\,\nu_i)}{\Gamma(\pi \to e\,\nu_1)} = |U_{ei}|^2 \rho_e\,, \tag{C.14}$$

with ν_1 being a massless neutrino.

PS191

PS191 [267] was an experiment located at CERN, which was expressly designed to search for neutrino decays in a low-energy neutrino beam. The apparatus consisted in a ~ 10 m long decay volume, built with eight pairs of flash chambers and a shower detector, including also a scintillator hodoscope for triggering purposes.

Several channels were studied, as $K^+ \to e^+\,\nu$ and $\nu_H \to e^+\,e^-\,\nu$, being used to find bounds on the matrix elements $|U_e|^2$ and $|U_e^*\,U_\mu|$ as a function of m_H.

NA3

NA3 [268] was a spectrometer used in SPS at CERN in order to search new and long-lived particles. The experiment used a beam of $300\,\mathrm{GeV}/c$ of π^-, colliding on an hadron iron absorber of 2 m long.

The device had to be able to detect neutrinos heavy enough to decay in a final states, which could be: $e^+e^-\nu$, $\mu^+\mu^-\nu$, π^+e^-, $\mu^+e^-\nu$ or $\mu^+\mu^-$. Such heavy neutrinos may be produced in rare decays of π, K, D, F or B mesons. The branching ratio of these mesons decaying into a heavy a neutrino ν_h has the following expression related with the mixing matrix element U_{ih}:

$$B.R. = c\,|U_{ih}|\,, \tag{C.15}$$

with $c = 0.1 \times 10^{-3}$ depending on de mass of ν_h.

CHARM

In the CHARM experiment [269, 286] (described above), the heavy neutrino production was searched in decays of the charmed D meson. Heavy neutrinos should have $e^+e^-\nu_e$, $\mu^+e^-\nu_e$, $e^+\mu^-\nu_\mu$ or $\mu^+\mu^-\nu_\mu$ as decaying signature, but no evidence was found.

This experiment was prepared to detect decays of neutrinos with masses in the range

$0.5 - 2.8\,\mathrm{GeV}$, finding two upper limits [269]:

$$|U_{ei}|^2\,|U_{\mu i}|^2 \;<\; 10^{-7} \text{ for masses around } 1.5\,\mathrm{GeV}\,, \tag{C.16}$$

$$|U_{\mu i}|^2 \;<\; 3\times 10^{-4} \text{ for masses around } 2.5\,\mathrm{GeV}\,. \tag{C.17}$$

DELPHI

DELPHI [231] was a detector of LEP, collecting data from 3.3×10^6 hadronic Z^0 decays ($e^+e^- \to Z^0 \to \nu_H\bar{\nu}$) coming from a total sample of 12.3×10^6 events. From the data analysis, an upper limit was obtained [231],

$$B.R.(Z^0 \to \nu_H\bar{\nu}) = B.R.(Z^0 \to \nu\bar{\nu})\,|U|^2\left(1-\frac{m^2_{\nu_H}}{m^2_{Z^0}}\right)\left(1+\frac{1}{2}\frac{m^2_{\nu_H}}{m^2_{Z^0}}\right) < 1.3\times 10^{-6} \tag{C.18}$$

at 95% C.L., leading to

$$|U|^2 < 2.1\times 10^{-5}\,. \tag{C.19}$$

L3

L3 [271] was a device of LEP, which was composed by a central vertex chamber (TEC) with inner radius of 9 cm and outer of 47 cm, a high resolution electromagnetic calorimeter of BGO crystals, a ring of scintillation counters, an uranium and brass hadron calorimeter and a precise muon chamber system. These detectors were placed around a 12 m diameter magnet which produced an uniform field of 0.5 Tesla along the beam axis.

As in DELPHI, the search was performed through Z^0 decay ($e^+e^- \to Z^0 \to \nu_H\bar{\nu}$), obtaining the following values at 95% C.L.:

$$B.R.(e^+e^- \to Z^0 \to \nu_H\bar{\nu}) \;<\; 3\times 10^{-5}\,, \tag{C.20}$$

$$|U|^2 \;<\; 10^{-4}\,. \tag{C.21}$$

$K \to \mu\,\nu$ (KEK)

As we have already said, a discrete muon peak in the muon momentum spectrum produced in K^+ decays could imply a heavy neutrino emission. This special production could be possible due to the mixing of heavy neutrinos with the light ones.

In order to look for the emission of a heavy neutrino, a high resolution magnetic spectrograph was built at the K3 beam channel of the 12 GeV proton synchrotron at the

National Laboratory for High Energy Physics (KEK) [278, 279]. It used a 550 MeV/c K^+ beam crossing through ten layers of plastic scintillators (seven $8 \times 20 \times 0.6\,\mathrm{cm}^3$, two $8 \times 20 \times 0.2\,\mathrm{cm}^3$ and one $8 \times 20 \times 0.1\,\mathrm{cm}^3$). Although, the number of stopped K^+ was high (about 5000 per beam) no heavy neutrino was found.

BEBC

BEBC [282] was a bubble chamber filled with a mixture of Ne/H_2, giving rise to a fiducial mass of 11.5 t. This material was exposed to a neutrino flux produced by 1.9×10^{18} protons colliding on a solid copper target and 0.18×10^{18} protons hitting a laminated copper target. BEBC was equipped with an External Muon Identifier. The most relevant results of BEBC are compiled in Ref. [282].

FMMF

FMMF [281] was a detector designed for studying high-energy neutrino interactions. It was used at Fermilab Tevatron, being placed 1599 m downstream of the neutrino target. It consisted of two parts; a calorimeter with alternating planes of target material (sand and steel) interleaved with flash chamber planes and proportional tube planes, and a muon spectrometer which measured the momentum and polarity of any high-energy muons coming from the calorimeter.

CHARM-II

CHARM-II [280, 309] was a neutrino detector at CERN. It consisted of a large target calorimeter equipped with streamer tubes and a muon spectrometer. It was constructed in order to look for heavy neutrinos in the muon-neutrino-nucleon scattering and the subsequent decay into $\mu^+\mu^-\nu_\mu$.

The analysis was based on 2×10^7 NC neutrino events collected between 1987-1991, searching heavy neutrinos in the mass range $0.3 - 2.4\,\mathrm{GeV}/c^2$. The best limit for the mixing parameter with muon-neutrino was [280]

$$|U_{\mu i}|^2 < 3 \times 10^{-5} \tag{C.22}$$

for a mass around $2\,\mathrm{GeV}/c^2$.

This new analysis improved by an order of magnitude previous results stemming from CHARM.

NOMAD

A search for heavy neutrinos (ν_h) was performed studying the decay $D \to \tau\nu_h$ at the SPS proton target. After this decay, another process, with signature $\nu_h \to \nu_\tau e^+ e^-$, could be produced and detected in NOMAD [285], proving the existence of heavy neutrinos. It must be said that no evidence was found.

Bibliography

[1] Y. Fukuda et al. Evidence for oscillation of atmospheric neutrinos. *Phys. Rev. Lett.*, 81:1562–1567, 1998.

[2] S. Pakvasa and J. W. F. Valle. Neutrino properties before and after KamLAND. *Proc. Indian Natl. Sci. Acad.*, 70A:189–222, 2004.

[3] Jose W. F. Valle and Jorge C. Romao. *Neutrinos in high energy and astroparticle physics*. Physics textbook, ISBN: 978-3-527-41197-9, 978-3-527-67102-1. Wiley-VCH, Weinheim, 2015.

[4] J. W. F. Valle. Neutrino physics overview. *J. Phys. Conf. Ser.*, 53:473–505, 2006. These review lectures were given at Corfu, 2005 and contain extensive references to the early papers on the seesaw mechanism.

[5] R. N. Mohapatra and P. B. Pal. *Massive neutrinos in physics and astrophysics. Second edition*. Physics textbook. World Sci. Lect. Notes Phys. 397 p., 1998.

[6] K. A. Olive et al. Review of Particle Physics. *Chin. Phys.*, C38:090001, 2014.

[7] J. Beringer et al. Review of Particle Physics (RPP). *Phys.Rev.*, D86:010001, 2012.

[8] S. Schael et al. Precision electroweak measurements on the Z resonance. *Phys. Rept.*, 427:257–454, 2006.

[9] J. Schechter and J.W.F. Valle. Neutrino Masses in SU(2) x U(1) Theories. *Phys.Rev.*, D22:2227, 1980.

[10] K. Zuber. *Neutrino physics*. Physics textbook, ISBN: 9780750307505. Boca Raton: USA: CRC Pr. 448 p., 2004.

[11] C.W. Kim and A. Pevsner. *Neutrinos in Physics and Astrophysics*. Physics textbook. Harwood Academic: 429 p., 1993.

[12] Carlo Giunti and Chung W. Kim. *Fundamentals of Neutrino Physics and Astrophysics*. Physics textbook. Oxford UK: Univ.Pr. 710 p., 2007.

[13] Walter Grimus. Neutrino Physics - Models for Neutrino Masses and Lepton Mixing. Proceedings, School on Particle Physics, Gravity and Cosmology. *ArXiv*, 0612311 [hep-ph]:001, 2006.

[14] Robert Foot, H. Lew, X. G. He, and Girish C. Joshi. Seesaw neutrino masses induced by a triplet of leptons. *Z. Phys.*, C44:441, 1989.

[15] Peter Minkowski. $\mu \to e\gamma$ at a Rate of One Out of 10^9 Muon Decays? *Phys. Lett.*, B67:421, 1977.

[16] Steven Weinberg. Varieties of baryon and lepton nonconservation. *Phys. Rev.*, D22:1694, 1980.

[17] J. Schechter and J. W. F. Valle. Neutrino Decay and Spontaneous Violation of Lepton Number. *Phys. Rev.*, D25:774, 1982.

[18] R. N. Mohapatra and J. W. F. Valle. Neutrino mass and baryon-number nonconservation in superstring models. *Phys. Rev.*, D34:1642, 1986.

[19] M.C. Gonzalez-Garcia and J.W.F. Valle. Fast Decaying Neutrinos and Observable Flavor Violation in a New Class of Majoron Models. *Phys.Lett.*, B216:360, 1989.

[20] Edward Witten. Symmetry breaking patterns in superstring models. *Nucl. Phys.*, B258:75, 1985.

[21] D.V. Forero, S. Morisi, M. Tórtola, and J. W. F. Valle. Lepton flavor violation and non-unitary lepton mixing in low-scale type-I seesaw. *JHEP*, 1109:142, 2011.

[22] Michal Malinsky, J.C. Romao, and J.W.F. Valle. Novel supersymmetric SO(10) seesaw mechanism. *Phys.Rev.Lett.*, 95:161801, 2005.

[23] A. Zee. A theory of lepton number violation, neutrino majorana mass, and oscillation. *Phys. Lett.*, B93:389, 1980.

[24] K. S. Babu. Model of 'calculable' majorana neutrino masses. *Phys. Lett.*, B203:132, 1988.

[25] J. T. Peltoniemi and J. W. F. Valle. Massive neutrinos and electroweak baryogenesis. *Phys. Lett.*, B304:147–151, 1993.

[26] M. Hirsch and J. W. F. Valle. Supersymmetric origin of neutrino mass. *New J. Phys.*, 6:76, 2004.

[27] A. Masiero and J. W. F. Valle. A model for spontaneous R parity breaking. *Phys. Lett.*, B251:273–278, 1990.

[28] J. C. Romao, C. A. Santos, and J. W. F. Valle. How to spontaneously break R-parity. *Phys. Lett.*, B288:311–320, 1992.

[29] J. C. Romao, A. Ioannisian, and J. W. F. Valle. Supersymmetric unification with radiative breaking of R-parity. *Phys. Rev.*, D55:427–430, 1997.

[30] M. Hirsch et al. Neutrino masses and mixings from supersymmetry with bilinear R-parity violation: A theory for solar and atmospheric neutrino oscillations. *Phys. Rev.*, D62:113008, 2000. Err-ibid. **D65**:119901,2002.

[31] M. A. Diaz et al. Solar neutrino masses and mixing from bilinear R-parity broken supersymmetry: Analytical versus numerical results. *Phys. Rev.*, D68:013009, 2003.

[32] B. Pontecorvo. Mesonium and anti-mesonium. *Sov. Phys. JETP*, 6:429, 1957. [Zh. Eksp. Teor. Fiz.33,549(1957)].

[33] B. Pontecorvo. Inverse beta processes and nonconservation of lepton charge. *Sov. Phys. JETP*, 7:172–173, 1958. [Zh. Eksp. Teor. Fiz.34,247(1957)].

[34] T. Futagami et al. Observation of the east - west anisotropy of the atmospheric neutrino flux. *Phys. Rev. Lett.*, 82:5194–5197, 1999.

[35] Q. R. Ahmad et al. Direct evidence for neutrino flavor transformation from neutral-current interactions in the Sudbury Neutrino Observatory. *Phys. Rev. Lett.*, 89:011301, 2002.

[36] Q. R. Ahmad et al. Measurement of day and night neutrino energy spectra at SNO and constraints on neutrino mixing parameters. *Phys. Rev. Lett.*, 89:011302, 2002.

[37] S. Abe et al. Precision Measurement of Neutrino Oscillation Parameters with KamLAND. *Phys.Rev.Lett.*, 100:221803, 2008.

[38] M. H. Ahn et al. Measurement of Neutrino Oscillation by the K2K Experiment. *Phys. Rev.*, D74:072003, 2006.

[39] K. Abe et al. Indication of Electron Neutrino Appearance from an Accelerator-produced Off-axis Muon Neutrino Beam. *Phys.Rev.Lett.*, 107:041801, 2011.

[40] K. Abe et al. Observation of Electron Neutrino Appearance in a Muon Neutrino Beam. *Phys. Rev. Lett.*, 112:061802, 2014.

[41] K. Abe et al. Precise Measurement of the Neutrino Mixing Parameter θ_{23} from Muon Neutrino Disappearance in an Off-Axis Beam. *Phys. Rev. Lett.*, 112(18):181801, 2014.

[42] P. Adamson et al. Improved search for muon-neutrino to electron-neutrino oscillations in MINOS. *Phys.Rev.Lett.*, 107:181802, 2011.

[43] P. Adamson et al. Electron neutrino and antineutrino appearance in the full MINOS data sample. *Phys. Rev. Lett.*, 110(17):171801, 2013.

[44] P. Adamson et al. Measurement of Neutrino and Antineutrino Oscillations Using Beam and Atmospheric Data in MINOS. *Phys.Rev.Lett.*, 110:251801, 2013.

[45] W. Rodejohann and J. W. F. Valle. Symmetrical Parametrizations of the Lepton Mixing Matrix. *Phys.Rev.*, D84:073011, 2011.

[46] S. Okubo. Note on Unitary Symmetry in Strong Interaction. II Excited States of Baryons. *Prog.Theor.Phys.*, 28:24–32, 1962.

[47] Evgeny K. Akhmedov. Neutrino physics. Particle physics. Proceedings, Summer School, Trieste, Italy, June 21-July 9, 1999. *ArXiv*, 0001264 [hep-ph], 1999.

[48] L. Wolfenstein. Neutrino Oscillations in Matter. *Phys.Rev.*, D17:2369–2374, 1978.

[49] S. P. Mikheev and A. Yu. Smirnov. Resonant amplification of neutrino oscillations in matter and solar neutrino spectroscopy. *Nuovo Cim.*, C9:17–26, 1986.

[50] Bruce T. Cleveland et al. Measurement of the solar electron neutrino flux with the homestake chlorine detector. *Astrophys. J.*, 496:505–526, 1998.

[51] Y. Fukuda et al. Solar neutrino data covering solar cycle 22. *Phys. Rev. Lett.*, 77:1683–1686, 1996.

[52] W. Hampel et al. Gallex solar neutrino observations: Results for gallex iv. *Phys. Lett.*, B447:127–133, 1999.

[53] J. N. Abdurashitov et al. Measurement of the solar neutrino capture rate by sage and implications for neutrino oscillations in vacuum. *Phys. Rev. Lett.*, 83:4686, 1999.

[54] Y. Fukuda et al. Measurements of the solar neutrino flux from Super- Kamiokande's first 300 days. *Phys. Rev. Lett.*, 81:1158–1162, 1998.

[55] John N. Bahcall. Standard solar models. *Nucl. Phys. Proc. Suppl.*, 77:64–72, 1999.

[56] David Griffiths. *Introduction to elementary particles*. Physics textbook, ISBN: 9783527406012. Weinheim, Germany: Wiley-VCH (2008) 454 p., 2008.

[57] Jose F. Nieves and Palash B. Pal. Generalized Fierz identities. *Am. J. Phys.*, 72:1100–1108, 2004.

[58] Samoil M. Bilenky. *Introduction to Feynman diagrams and electroweak interactions physics*. Physics textbook. Gif-sur-Yvette, France: Ed. Frontieres (1994) 368 p., 1995.

[59] D. V. Forero, M. Tórtola, and J. W. F. Valle. Neutrino oscillations refitted. *Phys. Rev.*, D90(9):093006, 2014.

[60] F. Capozzi, G. L. Fogli, E. Lisi, Marrone A., D. Montanino, and A. Palazzo. Status of three-neutrino oscillation parameters, circa 2013. *Phys. Rev.*, D89:093018, 2014.

[61] M. C. Gonzalez-Garcia, Michele Maltoni, and Thomas Schwetz. Updated fit to three neutrino mixing: status of leptonic CP violation. *JHEP*, 11:052, 2014.

[62] Ed Kearns, editor. *Proceedings, 26th International Conference on Neutrino Physics and Astrophysics (Neutrino 2014)*, volume 1666, ISBN: 978-0-7354-1313-9, 2015.

[63] Y. Abe et al. Improved measurements of the neutrino mixing angle θ_{13} with the Double Chooz detector. *JHEP*, 10:086, 2014. [Erratum: JHEP02,074(2015)].

[64] F.P. An et al. Observation of electron-antineutrino disappearance at Daya Bay. *Phys.Rev.Lett.*, 108:171803, 2012.

[65] F. P. An et al. Spectral measurement of electron antineutrino oscillation amplitude and frequency at Daya Bay. *Phys. Rev. Lett.*, 112:061801, 2014.

[66] Proceedings, 13th International Conference on Topics in Astroparticle and Underground Physics (TAUP 2013). *Phys. Procedia*, 61:pp.1–838, 2015.

[67] J.K. Ahn et al. Observation of Reactor Electron Antineutrino Disappearance in the RENO Experiment. *Phys.Rev.Lett.*, 108:191802, 2012.

[68] K. Abe et al. Solar neutrino results in Super-Kamiokande-III. *Phys.Rev.*, D83:052010, 2011.

[69] Andrew Renshaw. Solar Neutrino Results from Super-Kamiokande. *Phys. Procedia*, 61:345–354, 2015.

[70] B. Aharmim et al. An Independent Measurement of the Total Active 8B Solar Neutrino Flux Using an Array of 3He Proportional Counters at the Sudbury Neutrino Observatory. *Phys. Rev. Lett.*, 101:111301, 2008.

[71] B. Aharmim et al. Low Energy Threshold Analysis of the Phase I and Phase II Data Sets of the Sudbury Neutrino Observatory. *Phys. Rev.*, C81:055504, 2010.

[72] F. Kaether, W. Hampel, G. Heusser, J. Kiko, and T. Kirsten. Reanalysis of the GALLEX solar neutrino flux and source experiments. *Phys.Lett.*, B685:47–54, 2010.

[73] J. N. Abdurashitov et al. Measurement of the solar neutrino capture rate with gallium metal. III: Results for the 2002–2007 data-taking period. *Phys. Rev.*, C80:015807, 2009.

[74] G. Bellini, J. Benziger, D. Bick, S. Bonetti, G. Bonfini, et al. Precision measurement of the ^7Be solar neutrino interaction rate in Borexino. *Phys.Rev.Lett.*, 107:141302, 2011.

[75] J. Hosaka et al. Solar neutrino measurements in Super-Kamiokande-I. *Phys. Rev.*, D73:112001, 2006.

[76] J.P. Cravens et al. Solar neutrino measurements in Super-Kamiokande-II. *Phys.Rev.*, D78:032002, 2008.

[77] Y. Fukuda et al. Measurement of the flux and zenith-angle distribution of upward through-going muons by Super-Kamiokande. *Phys. Rev. Lett.*, 82:2644–2648, 1999.

[78] Y. Fukuda et al. Atmospheric muon-neutrino / electron-neutrino ratio in the multi-gev energy range. *Phys. Lett.*, B335:237–245, 1994.

[79] R. Becker-Szendy et al. Neutrino measurements with the imb detector. *Nucl. Phys. Proc. Suppl.*, 38:331–336, 1995.

[80] W. W. M. Allison et al. The atmospheric neutrino flavor ratio from a 3.9 fiducial kiloton-year exposure of soudan 2. *Phys. Lett.*, B449:137, 1999.

[81] M. Ambrosio et al. Measurement of the atmospheric neutrino-induced upgoing muon flux using macro. *Phys. Lett.*, B434:451–457, 1998.

[82] Takaaki Kajita and Yoji Totsuka. Observation of atmospheric neutrinos. *Rev. Mod. Phys.*, 73:85–118, 2001.

[83] J. W. F. Valle. Resonant oscillations of massless neutrinos in matter. *Phys. Lett.*, B199:432, 1987.

[84] O.G. Miranda, M.A. Tórtola, and J.W.F. Valle. Are solar neutrino oscillations robust? *JHEP*, 0610:008, 2006.

[85] F. J. Escrihuela, O. G. Miranda, M. A. Tórtola, and J. W. F. Valle. Constraining nonstandard neutrino-quark interactions with solar, reactor and accelerator data. *Phys. Rev.*, D80:105009, 2009.

[86] N. Fornengo et al. Probing neutrino non-standard interactions with atmospheric neutrino data. *Phys. Rev.*, D65:013010, 2002.

[87] S. Davidson, C. Peña-Garay, N. Rius, and A. Santamaria. Present and future bounds on non-standard neutrino interactions. *JHEP*, 03:011, 2003.

[88] Joachim Kopp, Manfred Lindner, Toshihiko Ota, and Joe Sato. Non-standard neutrino interactions in reactor and superbeam experiments. *Phys. Rev.*, D77:013007, 2008.

[89] Tommy Ohlsson. Status of non-standard neutrino interactions. *Rept. Prog. Phys.*, 76:044201, 2013.

[90] O. G. Miranda and H. Nunokawa. Non standard neutrino interactions: current status and future prospects. *New J. Phys.*, 17(9):095002, 2015.

[91] J. Barranco, O. G. Miranda, and T. I. Rashba. Low energy neutrino experiments sensitivity to physics beyond the Standard Model. *Phys. Rev.*, D76:073008, 2007.

[92] Murray Gell-Mann, Pierre Ramond, and Richard Slansky. Complex Spinors and Unified Theories. *Conf. Proc.*, C790927:315–321, 1979.

[93] Rabindra N. Mohapatra and Goran Senjanovic. Neutrino Mass and Spontaneous Parity Violation. *Phys. Rev. Lett.*, 44:912, 1980.

[94] F. J. Escrihuela, D. V. Forero, O. G. Miranda, M. Tórtola, and J. W. F. Valle. On the description of non-unitary neutrino mixing. *Phys. Rev.*, D92(5):053009, 2015.

[95] Michal Malinsky, Tommy Ohlsson, and He Zhang. Non-Standard Neutrino Interactions from a Triplet Seesaw Model. *Phys. Rev.*, D79:011301, 2009.

[96] M. Drees, R. Godbole, and P. Roy. *Theory and phenomenology of sparticles: An account of four-dimensional N=1 supersymmetry in high energy physics.* Physics book. Hackensack, USA: World Scientific (2004) 555 p, 2004.

[97] Lawrence J. Hall and Mahiko Suzuki. Explicit R parity breaking in supersymmetric models. *Nucl. Phys.*, B231:419, 1984.

[98] A. Santamaria and J. W. F. Valle. Spontaneous R parity violation in supersymmetry: a model for solar neutrino oscillations. *Phys. Lett.*, B195:423, 1987.

[99] G. G. Ross and J. W. F. Valle. Supersymmetric models without R parity. *Phys. Lett.*, B151:375, 1985.

[100] Vernon D. Barger, G. F. Giudice, and Tao Han. Some new aspects of supersymmetry R parity violating interactions. *Phys. Rev.*, D40:2987, 1989.

[101] Marco A. Diaz, Jorge C. Romao, and J. W. F. Valle. Minimal supergravity with R-parity breaking. *Nucl. Phys.*, B524:23–40, 1998.

[102] Asmaa Abada, Sacha Davidson, and Marta Losada. Neutrino masses and mixings in the MSSM with soft bilinear R(p) violation. *Phys. Rev.*, D65:075010, 2002.

[103] J. Barranco et al. Constraining Nonstandard Neutrino-Electron Interactions. *Phys. Rev.*, D77:093014, 2008.

[104] M. M. Guzzo, P. C. de Holanda, and O. L. G. Peres. Effects of non-standard neutrino interactions on MSW-LMA solution. *Phys. Lett.*, B591:1–6, 2004.

[105] Sven Bergmann and Alex Kagan. Z-induced fcncs and their effects on neutrino oscillations. *Nucl. Phys.*, B538:368–386, 1999.

[106] M. C. Gonzalez-Garcia et al. Atmospheric neutrino observations and flavor changing interactions. *Phys. Rev. Lett.*, 82:3202–3205, 1999.

[107] Alexander Friedland, Cecilia Lunardini, and Michele Maltoni. Atmospheric neutrinos as probes of neutrino matter interactions. *Phys. Rev.*, D70:111301, 2004.

[108] D. Aristizabal Sierra, M. Hirsch, and S. G. Kovalenko. Leptoquarks: Neutrino masses and accelerator phenomenology. *Phys. Rev.*, D77:055011, 2008.

[109] Jogesh C. Pati and Abdus Salam. Lepton number as the fourth color. *Phys. Rev.*, D10:275–289, 1974.

[110] H. Georgi and S.L. Glashow. Unity of All Elementary Particle Forces. *Phys.Rev.Lett.*, 32:438–441, 1974.

[111] Ilja Dorsner and Pavel Fileviez Perez. Unification without supersymmetry: Neutrino mass, proton decay and light leptoquarks. *Nucl. Phys.*, B723:53–76, 2005.

[112] Ilja Dorsner, Pavel Fileviez Perez, and Ricardo Gonzalez Felipe. Phenomenological and cosmological aspects of a minimal GUT scenario. *Nucl. Phys.*, B747:312–327, 2006.

[113] Harald Fritzsch and Peter Minkowski. Unified Interactions of Leptons and Hadrons. *Annals Phys.*, 93:193–266, 1975.

[114] Edward Farhi and Leonard Susskind. Technicolor. *Phys. Rept.*, 74:277, 1981.

[115] Sacha Davidson, David C. Bailey, and Bruce A. Campbell. Model independent constraints on leptoquarks from rare processes. *Z. Phys.*, C61:613–644, 1994.

[116] Yuval Grossman. Nonstandard neutrino interactions and neutrino oscillation experiments. *Phys. Lett.*, B359:141–147, 1995.

[117] M. C. Gonzalez-Garcia, Y. Grossman, A. Gusso, and Y. Nir. New CP violation in neutrino oscillations. *Phys. Rev.*, D64:096006, 2001.

[118] Samoil M. Bilenky and C. Giunti. Seesaw type mixing and $\nu_\mu \to \nu_\tau$ oscillations. *Phys. Lett.*, B300:137–140, 1993.

[119] Davide Meloni, Tommy Ohlsson, Walter Winter, and He Zhang. Non-standard interactions versus non-unitary lepton flavor mixing at a neutrino factory. *JHEP*, 04:041, 2010.

[120] Paul Langacker and David London. Lepton Number Violation and Massless Nonorthogonal Neutrinos. *Phys. Rev.*, D38:907, 1988.

[121] M. M. Guzzo, A. Masiero, and S. T. Petcov. On the MSW effect with massless neutrinos and no mixing in the vacuum. *Phys. Lett.*, B260:152, 1991.

[122] Esteban Roulet. Mikheyev-Smirnov-Wolfenstein effect with flavor-changing neutrino interactions. *Phys. Rev.*, D44:935–938, 1991.

[123] D. Meloni, T. Ohlsson, and H. Zhang. Exact and Approximate Formulas for Neutrino Mixing and Oscillations with Non-Standard Interactions. *JHEP*, 04:033, 2009.

[124] F. J. Escrihuela, M. Tórtola, J. W. F. Valle, and O. G. Miranda. Global constraints on muon-neutrino non-standard interactions. *Phys. Rev.*, D83:093002, 2011.

[125] Sanjib Kumar Agarwalla, Partha Bagchi, David V. Forero, and Mariam Tórtola. Probing Non-Standard Interactions at Daya Bay. *JHEP*, 07:060, 2015.

[126] Mattias Blennow and Tommy Ohlsson. Approximative two-flavor framework for neutrino oscillations with non-standard interactions. *Phys. Rev.*, D78:093002, 2008.

[127] M. C. Gonzalez-Garcia and Michele Maltoni. Atmospheric neutrino oscillations and new physics. *Phys. Rev.*, D70:033010, 2004.

[128] G. Mitsuka et al. Study of Non-Standard Neutrino Interactions with Atmospheric Neutrino Data in Super-Kamiokande I and II. *Phys. Rev.*, D84:113008, 2011.

[129] A. M. Gago, M. M. Guzzo, H. Nunokawa, W. J. C. Teves, and R. Zukanovich Funchal. Probing flavor changing neutrino interactions using neutrino beams from a muon storage ring. *Phys. Rev.*, D64:073003, 2001.

[130] Arman Esmaili and Alexei Yu. Smirnov. Probing Non-Standard Interaction of Neutrinos with IceCube and DeepCore. *JHEP*, 06:026, 2013.

[131] Alexander Friedland and Cecilia Lunardini. A test of tau neutrino interactions with atmospheric neutrinos and K2K. *Phys. Rev.*, D72:053009, 2005.

[132] Noriaki Kitazawa, Hiroaki Sugiyama, and Osamu Yasuda. Will MINOS see new physics? *ArXiv: 0606013, [hep-ph]*, 2006.

[133] Joachim Kopp, Pedro A. N. Machado, and Stephen J. Parke. Interpretation of MINOS data in terms of non-standard neutrino interactions. *Phys. Rev.*, D82:113002, 2010.

[134] W. Anthony Mann, Daniel Cherdack, Wojciech Musial, and Tomas Kafka. Apparent multiple Δm^2_{32} in muon anti-neutrino and muon neutrino survival oscillations from non-standard interaction matter effect. *Phys. Rev.*, D82:113010, 2010.

[135] Alexander Friedland and Cecilia Lunardini. Two modes of searching for new neutrino interactions at MINOS. *Phys. Rev.*, D74:033012, 2006.

[136] Zeynep Isvan. Search for Non-standard Interactions with the MINOS Experiment. *Particles and fields. Proceedings, Meeting of the Division of the American Physical Society, DPF 2011, Providence, USA, August 9-13, 2011*. *ArXiv*, 1110.1900 [hep-ex], 2011.

[137] P. Adamson et al. Search for flavor-changing non-standard neutrino interactions by MINOS. *Phys. Rev.*, D88(7):072011, 2013.

[138] S. Bergmann, M. M. Guzzo, P. C. de Holanda, P. I. Krastev, and H. Nunokawa. Status of the solution to the solar neutrino problem based on nonstandard neutrino interactions. *Phys. Rev.*, D62:073001, 2000.

[139] Zurab Berezhiani, R. S. Raghavan, and Anna Rossi. Probing non-standard couplings of neutrinos at the borexino detector. *Nucl. Phys.*, B638:62–80, 2002.

[140] A. Bolaños, O. G. Miranda, A. Palazzo, M. A. Tórtola, and J. W. F. Valle. Probing non-standard neutrino-electron interactions with solar and reactor neutrinos. *Phys. Rev.*, D79:113012, 2009.

[141] A. Palazzo and J. W. F. Valle. Confusing non-zero θ_{13} with non-standard interactions in the solar neutrino sector. *Phys. Rev.*, D80:091301, 2009.

[142] C. R. Das and Joao Pulido. Improving LMA predictions with non-standard interactions: Neutrino decay in solar matter? *Phys. Rev.*, D83:053009, 2011.

[143] Antonio Palazzo. Hint of non-standard dynamics in solar neutrino conversion. *Phys. Rev.*, D83:101701, 2011.

[144] E.A. Garces, O.G. Miranda, M.A. Tórtola, and J. W. F. Valle. Low-energy neutrino-electron scattering as a Standard Model probe: the potential of LENA as case study. *Phys.Rev.*, D85:073006, 2012.

[145] Sanjib Kumar Agarwalla, Francesco Lombardi, and Tatsu Takeuchi. Constraining Non-Standard Interactions of the Neutrino with Borexino. *JHEP*, 12:079, 2012.

[146] M. C. Gonzalez-Garcia and Michele Maltoni. Determination of matter potential from global analysis of neutrino oscillation data. *JHEP*, 09:152, 2013.

[147] Tzee-Ke Kuo and James T. Pantaleone. Three Neutrino Oscillations and the Solar Neutrino Experiments. *Phys. Rev.*, D35:3432, 1987.

[148] M. Deniz et al. Constraints on Non-Standard Neutrino Interactions and Unparticle Physics with Neutrino-Electron Scattering at the Kuo-Sheng Nuclear Power Reactor. *Phys. Rev.*, D82:033004, 2010.

[149] D. V. Forero and M. M. Guzzo. Constraining nonstandard neutrino interactions with electrons. *Phys. Rev.*, D84:013002, 2011.

[150] Stefan Antusch, Jochen P. Baumann, and Enrique Fernandez-Martinez. Non-Standard Neutrino Interactions with Matter from Physics Beyond the Standard Model. *Nucl. Phys.*, B810:369–388, 2009.

[151] Zurab Berezhiani and Anna Rossi. Limits on the non-standard interactions of neutrinos from e+ e- colliders. *Phys. Lett.*, B535:207–218, 2002.

[152] M. Deniz et al. Measurement of Neutrino-Electron Scattering Cross-Section with a CsI(Tl) Scintillating Crystal Array at the Kuo-Sheng Nuclear Power Reactor. *Phys. Rev.*, D81:072001, 2010.

[153] Z. Daraktchieva et al. Limits on the neutrino magnetic moment from the MUNU experiment. *Phys. Lett.*, B564:190–198, 2003.

[154] A. I. Derbin et al. Experiment on anti-neutrino scattering by electrons at a reactor of the Rovno nuclear power plant. *JETP Lett.*, 57:768–772, 1993.

[155] G. S. Vidyakin, V. N. Vyrodov, I. I. Gurevich, Yu. V. Kozlov, V. P. Martemyanov, S. V. Sukhotin, V. G. Tarasenkov, E. V. Turbin, and S. Kh. Khakhimov. Limitations on the magnetic moment and charge radius of the electron-anti-neutrino. *JETP Lett.*, 55:206–210, 1992. [Pisma Zh. Eksp. Teor. Fiz.55,212(1992)].

[156] F. Reines, H. S. Gurr, and H. W. Sobel. Detection of anti-electron-neutrino e scattering. *Phys. Rev. Lett.*, 37:315–318, 1976.

[157] L. B. Auerbach et al. Measurement of electron-neutrino electron elastic scattering. *Phys. Rev.*, D63:112001, 2001.

[158] R. C. Allen et al. Study of electron-neutrino electron elastic scattering at LAMPF. *Phys. Rev.*, D47:11–28, 1993.

[159] P. Vilain et al. Precision measurement of electroweak parameters from the scattering of muon-neutrinos on electrons. *Phys. Lett.*, B335:246–252, 1994.

[160] J. V. Allaby et al. A Precise Determination of the Electroweak Mixing Angle from Semileptonic Neutrino Scattering. *Z. Phys.*, C36:611, 1987.

[161] A. Blondel, P. Bockmann, .H. Burkhardt, F. Dydak, A.L. Grant, et al. Electroweak Parameters From a High Statistics Neutrino Nucleon Scattering Experiment. *Z.Phys.*, C45:361–379, 1990.

[162] G. P. Zeller et al. A Precise determination of electroweak parameters in neutrino nucleon scattering. *Phys. Rev. Lett.*, 88:091802, 2002. [Erratum: Phys. Rev. Lett.90,239902(2003)].

[163] Richard D. Ball et al. Precision determination of electroweak parameters and the strange content of the proton from neutrino deep-inelastic scattering. *Nucl.Phys.*, B823:195–233, 2009.

[164] W. Bentz, I. C. Cloet, J. T. Londergan, and A. W. Thomas. Reassessment of the NuTeV determination of the Weinberg angle. *Phys. Lett.*, B693:462–466, 2010.

[165] M. Altmann et al. Complete results for five years of GNO solar neutrino observations. *Phys. Lett.*, B616:174–190, 2005.

[166] Florian Kaether. *Datenanalyse der Sonnenneutrinoexperiments Gallex*. PhD thesis, Heidelberg U., 2007.

[167] S. Fukuda et al. Determination of solar neutrino oscillation parameters using 1496 days of Super-Kamiokande-I data. *Phys. Lett.*, B539:179–187, 2002.

[168] S. N. Ahmed et al. Measurement of the total active B-8 solar neutrino flux at the Sudbury Neutrino Observatory with enhanced neutral current sensitivity. *Phys. Rev. Lett.*, 92:181301, 2004.

[169] B. Aharmim et al. Electron energy spectra, fluxes, and day-night asymmetries of B-8 solar neutrinos from the 391-day salt phase SNO data set. *Phys. Rev.*, C72:055502, 2005.

[170] C. Arpesella et al. Direct Measurement of the Be-7 Solar Neutrino Flux with 192 Days of Borexino Data. *Phys.Rev.Lett.*, 101:091302, 2008.

[171] C. Galbiati et al. New results on solar neutrino fluxes from 192 days of Borexino data. *J. Phys. Conf. Ser.*, 136:022001, 2008.

[172] G. Bellini et al. Measurement of the solar ^8B neutrino rate with a liquid scintillator target and 3 MeV energy threshold in the Borexino detector. *Phys. Rev.*, D82:033006, 2010.

[173] L. Wolfenstein. Neutrino oscillations in matter. *Phys. Rev.*, D17:2369, 1978.

[174] S. P. Mikheev and A. Yu. Smirnov. Resonance enhancement of oscillations in matter and solar neutrino spectroscopy. *Sov. J. Nucl. Phys.*, 42:913–917, 1985.

[175] A. Schaefer and S. E. Koonin. Influence of Density Fluctuations on Solar Neutrino Conversion. *Phys. Lett.*, B185:417–420, 1987.

[176] P. I. Krastev and A. Yu. Smirnov. Density perturbations and resonant conversion of neutrinos. *Mod. Phys. Lett.*, A6:1001–1009, 1991.

[177] F. N. Loreti and A. B. Balantekin. Neutrino oscillations in noisy media. *Phys. Rev.*, D50:4762–4770, 1994.

[178] H. Nunokawa et al. The effect of random matter density perturbations on the MSW solution to the solar neutrino problem. *Nucl. Phys.*, B472:495–517, 1996.

[179] C. P. Burgess et al. Resonant origin for density fluctuations deep within the sun: helioseismology and magneto-gravity waves. *Mon. Not. Roy. Astron. Soc.*, 348:609, 2004.

[180] C. Burgess et al. Large mixing angle oscillations as a probe of the deep solar interior. *Astrophys. J.*, 588:L65, 2003.

[181] C. P. Burgess et al. Cornering solar radiative-zone fluctuations with KamLAND and SNO salt. *JCAP*, 0401:007, 2004.

[182] G. L. Fogli, E. Lisi, A. Marrone, D. Montanino, and A. Palazzo. Probing non-standard decoherence effects with solar and KamLAND neutrinos. *Phys. Rev.*, D76:033006, 2007.

[183] J. Schechter and J. W. F. Valle. Majorana neutrinos and magnetic fields. *Phys. Rev.*, D24:1883, 1981. Err. D25, 283 (1982).

[184] E. Kh. Akhmedov. Resonant amplification of neutrino spin rotation in matter and the solar-neutrino problem. *Phys. Lett.*, B213:64–68, 1988.

[185] O. G. Miranda et al. The simplest resonant spin-flavour solution to the solar neutrino problem. *Nucl. Phys.*, B595:360–380, 2001.

[186] O. G. Miranda, T. I. Rashba, A. I. Rez, and J. W. F. Valle. Constraining the neutrino magnetic moment with anti- neutrinos from the sun. *Phys. Rev. Lett.*, 93:051304, 2004.

[187] Alexander Friedland, Cecilia Lunardini, and Carlos Peña-Garay. Solar neutrinos as probes of neutrino - matter interactions. *Phys. Lett.*, B594:347, 2004.

[188] A. Bandyopadhyay et al. Physics at a future Neutrino Factory and super-beam facility. *Rept.Prog.Phys.*, 72:106201, 2009.

[189] Hiroshi Nunokawa, Stephen J. Parke, and Jose W.F. Valle. CP Violation and Neutrino Oscillations. *Prog.Part.Nucl.Phys.*, 60:338–402, 2008.

[190] T. Yanagida. *KEK lectures*. Ed. O. Sawada and A. Sugamoto (KEK, 1979), 1979.

[191] Rabindra N. Mohapatra and Goran Senjanovic. Neutrino mass and spontaneous parity nonconservation. *Phys. Rev. Lett.*, 44:91, 1980.

[192] F. Bazzocchi, D.G. Cerdeno, C. Munoz, and J. W. F. Valle. Calculable inverse-seesaw neutrino masses in supersymmetry. *Phys.Rev.*, D81:051701, 2010.

[193] Carlos Peña-Garay and Aldo Serenelli. Solar neutrinos and the solar composition problem. *ArXiv*, 0811.2424 [astro-ph], 2008.

[194] J. Dorenbosch et al. Experimental Verification of the Universality of ν_e and ν_μ Coupling to the Neutral Weak Current. *Phys. Lett.*, B180:303, 1986.

[195] Andre de Gouvea and James Jenkins. What can we learn from neutrino electron scattering? *Phys. Rev.*, D74:033004, 2006.

[196] J. Barranco and others. Constraining non-standard interactions in nu/e e or anti-nu/e e scattering. *Phys. Rev.*, D73:113001, 2006.

[197] Carla Biggio, Mattias Blennow, and Enrique Fernandez-Martinez. Loop bounds on non-standard neutrino interactions. *JHEP*, 03:139, 2009.

[198] Stephen J. Parke. Nonadiabatic Level Crossing in Resonant Neutrino Oscillations. *Phys.Rev.Lett.*, 57:1275–1278, 1986.

[199] G.L. Fogli, E. Lisi, A. Marrone, D. Montanino, A. Palazzo, et al. Solar neutrino oscillation parameters after first KamLAND results. *Phys.Rev.*, D67:073002, 2003.

[200] G. L. Fogli, E. Lisi, A. Marrone, D. Montanino, and A. Palazzo. Getting the most from the statistical analysis of solar neutrino oscillations. *Phys. Rev.*, D66:053010, 2002.

[201] Yasuo Takeuchi. Low-energy neutrino observation at Super-Kamiokande-III. *J. Phys. Conf. Ser.*, 120:052008, 2008.

[202] Joshua R. Klein. Results and Prospects for SNO. *Proceedings, 24th International Conference on Neutrino physics and astrophysics (Neutrino 2010). Nucl. Phys. Proc. Suppl.*, 229-232:68–73, 2012.

[203] Thomas Schwetz, M.A. Tórtola, and Jose W.F. Valle. Three-flavour neutrino oscillation update. *New J.Phys.*, 10:113011, 2008.

[204] John N. Bahcall, K. Kubodera, and S. Nozawa. Neutral Current Reactions of Solar and Supernova Neutrinos on Deuterium. *Phys. Rev.*, D38:1030, 1988.

[205] K. Nakamura. Solar neutrino results, KamLAND and prospects. *AIP Conf. Proc.*, 721:12–19, 2004.

[206] K. Abe et al. Letter of Intent: The Hyper-Kamiokande Experiment — Detector Design and Physics Potential —. *ArXiv*, 1109.3262 [hep-ex], 2011.

[207] K. Abe et al. A Long Baseline Neutrino Oscillation Experiment Using J-PARC Neutrino Beam and Hyper-Kamiokande. *ArXiv*, 1412.4673, 2014.

[208] S. Davidson, S. Forte, P. Gambino, N. Rius, and A. Strumia. Old and new physics interpretations of the NuTeV anomaly. *JHEP*, 0202:037, 2002.

[209] C.H. Llewellyn Smith. On the Determination of $\sin^2\theta_w$ in Semileptonic Neutrino Interactions. *Nucl.Phys.*, B228:205, 1983.

[210] E.A. Paschos and L. Wolfenstein. Tests for neutral currents in neutrino reactions. *Phys.Rev.*, D7:91–95, 1973.

[211] K. Nakamura et al. Review of particle physics. *J.Phys.*, G37:075021, 2010.

[212] Kevin Scott McFarland and Sven-Olaf Moch. Conventional physics explanations for the NuTeV $sin^2\theta_W$. *Electroweak precision data and the Higgs mass. Proceedings, Workshop, Zeuthen, Germany, February 28-March 1, 2003*. *ArXiv*, hep-ph/0306052:61–83, 2003.

[213] M. Maltoni, T. Schwetz, M.A. Tórtola, and J.W.F. Valle. Status of global fits to neutrino oscillations. *New J.Phys.*, 6:122, 2004.

[214] M. C. Gonzalez-Garcia and Michele Maltoni. Phenomenology with Massive Neutrinos. *Phys. Rept.*, 460:1–129, 2008.

[215] Gaku Mitsuka. Limit on non-standard interactions from the atmospheric neutrino data. *PoS*, NUFACT08:059, 2008.

[216] A. M. Dziewonski and D. L. Anderson. Preliminary reference earth model. *Phys. Earth Planet. Interiors*, 25:297–356, 1981.

[217] Eligio Lisi and Daniele Montanino. Earth regeneration effect in solar neutrino oscillations: An analytic approach. *Phys. Rev.*, D56:1792–1803, 1997.

[218] D. G. Michael et al. Observation of muon neutrino disappearance with the MINOS detectors and the NuMI neutrino beam. *Phys. Rev. Lett.*, 97:191801, 2006.

[219] Mattias Blennow, Davide Meloni, Tommy Ohlsson, Francesco Terranova, and Mattias Westerberg. Non-standard interactions using the OPERA experiment. *Eur.Phys.J.*, C56:529–536, 2008.

[220] R. B. Patterson. Oscillation measurements with the NuMI beam. *Nucl. Part. Phys. Proc.*, 265-266:153–158, 2015.

[221] C. Adams et al. The Long-Baseline Neutrino Experiment: Exploring Fundamental Symmetries of the Universe. *ArXiv*, 1307.7335 [hep-ex].

[222] J. M. Conrad. Neutrino scattering on Glass: NuSOnG. *AIP Conf. Proc.*, 981:243–246, 2008.

[223] T. Adams et al. Terascale Physics Opportunities at a High Statistics, High Energy Neutrino Scattering Experiment: NuSOnG. *Int.J.Mod.Phys.*, A24:671–717, 2009.

[224] Evgeny K. Akhmedov, Manfred Lindner, Erhard Schnapka, and J.W.F. Valle. Left-right symmetry breaking in NJL approach. *Phys.Lett.*, B368:270–280, 1996.

[225] Evgeny K. Akhmedov, Manfred Lindner, Erhard Schnapka, and J.W.F. Valle. Dynamical left-right symmetry breaking. *Phys.Rev.*, D53:2752–2780, 1996.

[226] Sofiane M. Boucenna, Stefano Morisi, and José W.F. Valle. The low-scale approach to neutrino masses. *Adv.High Energy Phys.*, 2014:831598, 2014.

[227] P.S. Bhupal Dev and R.N. Mohapatra. TeV Scale Inverse Seesaw in SO(10) and Leptonic Non-Unitarity Effects. *Phys.Rev.*, D81:013001, 2010.

[228] Chang-Hun Lee, P.S. Bhupal Dev, and R.N. Mohapatra. Natural TeV-scale left-right seesaw mechanism for neutrinos and experimental tests. *Phys.Rev.*, D88(9):093010, 2013.

[229] M. Dittmar, A. Santamaria, M. C. Gonzalez-Garcia, and J. W. F. Valle. Production mechanisms and signatures of isosinglet neutral heavy leptons in Z0 decays. *Nucl. Phys.*, B332:1, 1990.

[230] M.Z. Akrawy et al. Limits on neutral heavy lepton production from Z0 decay. *Phys.Lett.*, B247:448–457, 1990.

[231] P. Abreu et al. Search for neutral heavy leptons produced in Z decays. *Z.Phys.*, C74:57–71, 1997.

[232] A. Aguilar et al. Evidence for neutrino oscillations from the observation of anti-nu/e appearance in a anti-nu/mu beam. *Phys. Rev.*, D64:112007, 2001.

[233] A.A. Aguilar-Arevalo et al. Improved Search for $\bar{\nu}_\mu \to \bar{\nu}_e$ Oscillations in the MiniBooNE Experiment. *Phys.Rev.Lett.*, 110:161801, 2013.

[234] Takehiko Asaka, Steve Blanchet, and Mikhail Shaposhnikov. The nuMSM, dark matter and neutrino masses. *Phys.Lett.*, B631:151–156, 2005.

[235] Robert E. Shrock. General Theory of Weak Leptonic and Semileptonic Decays. 1. Leptonic Pseudoscalar Meson Decays, with Associated Tests For, and Bounds on, Neutrino Masses and Lepton Mixing. *Phys.Rev.*, D24:1232, 1981.

[236] Michael Gronau, Chung Ngoc Leung, and Jonathan L. Rosner. Extending Limits on Neutral Heavy Leptons. *Phys.Rev.*, D29:2539, 1984.

[237] J. Schechter and J.W.F. Valle. Neutrinoless Double beta Decay in SU(2) x U(1) Theories. *Phys.Rev.*, D25:2951, 1982.

[238] Martin Hirsch. Phenomenology of neutrinoless double beta decay. *Nucl. Phys. Proc. Suppl.*, 221:119–124, 2011.

[239] Werner Rodejohann. Neutrino-less Double Beta Decay and Particle Physics. *Int.J.Mod.Phys.*, E20:1833–1930, 2011.

[240] J. Bernabeu et al. Lepton flavor nonconservation at high-energies in a superstring inspired standard model. *Phys. Lett.*, B187:303, 1987.

[241] Hans Hettmansperger, Manfred Lindner, and Werner Rodejohann. Phenomenological Consequences of sub-leading Terms in See-Saw Formulas. *JHEP*, 1104:123, 2011.

[242] G. C. Branco, M. N. Rebelo, and J. W. F. Valle. Leptonic CP violation with massless neutrinos. *Phys. Lett.*, B225:385, 1989.

[243] N. Rius and J. W. F. Valle. Leptonic CP violating asymmetries in Z0 decays. *Phys. Lett.*, B246:249–255, 1990.

[244] Enrico Nardi, Esteban Roulet, and Daniele Tommasini. Limits on neutrino mixing with new heavy particles. *Phys.Lett.*, B327:319–326, 1994.

[245] Paul Langacker and David London. Mixing Between Ordinary and Exotic Fermions. *Phys.Rev.*, D38:886, 1988.

[246] M.C. Gonzalez-Garcia, A. Santamaria, and J.W.F. Valle. Isosinglet Neutral Heavy Lepton Production in Z Decays and Neutrino Mass. *Nucl.Phys.*, B342:108–126, 1990.

[247] A. Abada, D. Das, A.M. Teixeira, A. Vicente, and C. Weiland. Tree-level lepton universality violation in the presence of sterile neutrinos: impact for R_K and R_π. *JHEP*, 1302:048, 2013.

[248] A. Abada, A.M. Teixeira, A. Vicente, and C. Weiland. Sterile neutrinos in leptonic and semileptonic decays. *JHEP*, 1402:091, 2014.

[249] Anupama Atre, Tao Han, Silvia Pascoli, and Bin Zhang. The Search for Heavy Majorana Neutrinos. *JHEP*, 0905:030, 2009.

[250] A. Abada, V. De Romeri, and A.M. Teixeira. Effect of steriles states on lepton magnetic moments and neutrinoless double beta decay. *JHEP*, 1409:074, 2014.

[251] Stefan Antusch and Oliver Fischer. Non-unitarity of the leptonic mixing matrix: Present bounds and future sensitivities. *JHEP*, 1410:94, 2014.

[252] G. Czapek et al. Branching ratio for the rare pion decay into positron and neutrino. *Phys. Rev. Lett.*, 70:17–20, 1993.

[253] Bernard Aubert et al. Measurements of Charged Current Lepton Universality and —V(us)— using Tau Lepton Decays to e- nu(e)-bar nu(tau), mu-bar nu(mu)-bar nu(tau), pi- nu(tau) and K- nu(tau). *Phys.Rev.Lett.*, 105:051602, 2010.

[254] Martin Freund. Analytic approximations for three neutrino oscillation parameters and probabilities in matter. *Phys. Rev.*, D64:053003, 2001.

[255] Evgeny K. Akhmedov, Robert Johansson, Manfred Lindner, Tommy Ohlsson, and Thomas Schwetz. Series expansions for three flavor neutrino oscillation probabilities in matter. *JHEP*, 04:078, 2004.

[256] C. Giunti, M. Laveder, Y.F. Li, Q.Y. Liu, and H.W. Long. Update of Short-Baseline Electron Neutrino and Antineutrino Disappearance. *Phys.Rev.*, D86:113014, 2012.

[257] C. Giunti, M. Laveder, Y.F. Li, and H.W. Long. Pragmatic View of Short-Baseline Neutrino Oscillations. *Phys.Rev.*, D88:073008, 2013.

[258] G. Mention et al. The Reactor Antineutrino Anomaly. *Phys. Rev.*, D83:073006, 2011.

[259] Tzee-Ke Kuo and James T. Pantaleone. Neutrino oscillations in matter. *Rev. Mod. Phys.*, 61:937, 1989.

[260] P. Astier et al. Search for $\nu_\mu \to \nu_e$ oscillations in the NOMAD experiment. *Phys. Lett.*, B570:19–31, 2003.

[261] Marco Cirelli, Guido Marandella, Alessandro Strumia, and Francesco Vissani. Probing oscillations into sterile neutrinos with cosmology, astrophysics and experiments. *Nucl. Phys.*, B708:215–267, 2005.

[262] ATLAS Collaboration. Search for Majorana neutrino production in pp collisions at sqrt(s)=7 TeV in dimuon final states with the ATLAS detector. *ATLAS-CONF-2012-139, ATLAS-COM-CONF-2012-165*, 2012.

[263] Vardan Khachatryan et al. Search for heavy Majorana neutrinos in $\mu^{\pm}\mu^{\pm}$+ jets events in proton-proton collisions at $\sqrt{s} = 8$ TeV. *Phys. Lett.*, B748:144–166, 2015.

[264] Roel Aaij et al. Search for Majorana neutrinos in $B^- \to \pi^+\mu^-\mu^-$ decays. *Phys.Rev.Lett.*, 112(13):131802, 2014.

[265] D.I. Britton, S. Ahmad, D.A. Bryman, R.A. Burnbam, E.T.H. Clifford, et al. Measurement of the $\pi^+ \to e^+$ neutrino branching ratio. *Phys.Rev.Lett.*, 68:3000–3003, 1992.

[266] D.I. Britton, S. Ahmad, D.A. Bryman, R.A. Burnham, E.T.H. Clifford, et al. Improved search for massive neutrinos in $\pi^+ \to e^+$ neutrino decay. *Phys.Rev.*, D46:885–887, 1992.

[267] G. Bernardi, G. Carugno, J. Chauveau, F. Dicarlo, M. Dris, et al. Further limits on heavy neutrino couplings. *Phys.Lett.*, B203:332, 1988.

[268] J. Badier et al. Mass and Lifetime Limits on New Longlived Particles in 300-GeV/$c\pi^-$ Interactions. *Z.Phys.*, C31:21, 1986.

[269] F. Bergsma et al. A Search for Decays of Heavy Neutrinos in the Mass Range 0.5-GeV to 2.8-GeV. *Phys.Lett.*, B166:473, 1986.

[270] D. Liventsev et al. Search for heavy neutrinos at Belle. *Phys.Rev.*, D87(7):071102, 2013.

[271] O. Adriani et al. Search for isosinglet neutral heavy leptons in Z0 decays. *Phys.Lett.*, B295:371–382, 1992.

[272] P. Achard et al. Search for heavy isosinglet neutrino in e^+e^- annihilation at LEP. *Phys.Lett.*, B517:67–74, 2001.

[273] J. Klinger. Search for heavy majorana neutrinos in pp collisions at $\sqrt{s} = 8$ tev with the atlas detector. *University of Manchester, Ph D thesis*, B388:81–112, 2014.

[274] Frank F. Deppisch, P. S. Bhupal Dev, and Apostolos Pilaftsis. Neutrinos and Collider Physics. *New J. Phys.*, 17(7):075019, 2015.

[275] Strahinja Lukić. Physics highlights at ILC and CLIC. *12th International School-Seminar on The Actual Problems of Microworld Physics Gomel, Belarus, July 22-August 2, 2013*. *ArXiv*, 1406.4313, 2014.

[276] Frank Zimmermann et al. FCC-ee Overview. *Proceedings, 55th ICFA Advanced Beam Dynamics Workshop on High Luminosity Circular e+e- Colliders – Higgs Factory (HF2014)*. THP3H1, 2015.

[277] A. Abada, V. De Romeri, S. Monteil, J. Orloff, and A. M. Teixeira. Indirect searches for sterile neutrinos at a high-luminosity Z-factory. *JHEP*, 04:051, 2015.

[278] R.S. Hayano, T. Taniguchi, T. Yamanaka, T. Tanimori, R. Enomoto, et al. Heavy neutrino search using K(mu2) decay. *Phys.Rev.Lett.*, 49:1305, 1982.

[279] Alexander Kusenko, Silvia Pascoli, and Dmitry Semikoz. New bounds on MeV sterile neutrinos based on the accelerator and Super-Kamiokande results. *JHEP*, 0511:028, 2005.

[280] P. Vilain et al. Search for heavy isosinglet neutrinos. *Phys.Lett.*, B343:453–458, 1995.

[281] E. Gallas et al. Search for neutral weakly interacting massive particles in the Fermilab Tevatron wide band neutrino beam. *Phys.Rev.*, D52:6–14, 1995.

[282] Amanda M. Cooper-Sarkar et al. Search for Heavy Neutrino Decays in the BEBC Beam Dump Experiment. *Phys.Lett.*, B160:207, 1985.

[283] A. Vaitaitis et al. Search for neutral heavy leptons in a high-energy neutrino beam. *Phys.Rev.Lett.*, 83:4943–4946, 1999.

[284] A.V. Artamonov et al. Search for heavy neutrinos in $K^+ \to \mu^+ \nu_H$ decays. *Phys.Rev.*, D91(5):052001, 2015.

[285] P. Astier et al. Search for heavy neutrinos mixing with tau neutrinos. *Phys.Lett.*, B506:27–38, 2001.

[286] J. Orloff, Alexandre N. Rozanov, and C. Santoni. Limits on the mixing of tau neutrino to heavy neutrinos. *Phys.Lett.*, B550:8–15, 2002.

[287] J.A. Aguilar-Saavedra, F. Deppisch, O. Kittel, and J. W. F. Valle. Flavour in heavy neutrino searches at the LHC. *Phys.Rev.*, D85:091301, 2012.

[288] S.P. Das, F.F. Deppisch, O. Kittel, and J. W. F. Valle. Heavy Neutrinos and Lepton Flavour Violation in Left-Right Symmetric Models at the LHC. *Phys.Rev.*, D86:055006, 2012.

[289] Frank F. Deppisch, Martin Hirsch, and Heinrich Pas. Neutrinoless Double Beta Decay and Physics Beyond the Standard Model. *J.Phys.*, G39:124007, 2012.

[290] Manimala Mitra, Goran Senjanovic, and Francesco Vissani. Neutrinoless Double Beta Decay and Heavy Sterile Neutrinos. *Nucl.Phys.*, B856:26–73, 2012.

[291] Frank F. Deppisch, Nishita Desai, and Jose W. F. Valle. Is charged lepton flavour violation a high energy phenomenon? *Phys.Rev.*, D89:051302(R), 2014.

[292] Chien-Yi Chen, P. S. Bhupal Dev, and R.N. Mohapatra. Probing Heavy-Light Neutrino Mixing in Left-Right Seesaw Models at the LHC. *Phys.Rev.*, D88:033014, 2013.

[293] Michael Wurm et al. The next-generation liquid-scintillator neutrino observatory LENA. *Astropart. Phys.*, 35:685–732, 2012.

[294] T. Patzak. LAGUNA-LBNO: Large apparatus studying grand unification and neutrino astrophysics and long baseline neutrino oscillations. *J. Phys. Conf. Ser.*, 375:042056, 2012.

[295] Irina Mocioiu and Warren Wright. Non-standard neutrino interactions in the mu–tau sector. *Nucl. Phys.*, B893:376–390, 2015.

[296] J. P. Yanez. Results from atmospheric neutrino oscillations with IceCube DeepCore. *AIP Conf. Proc.*, 1666:100002, 2015.

[297] F. J. Escrihuela, D. V. Forero, O. G. Miranda, M. Tórtola, and J. W. F. Valle. Constraining right-handed neutrinos. *International Conference on High Energy Physics 2014 (ICHEP 2014) Valencia, Spain, July 2-9, 2014*. *ArXiv*, 1505.01097 [hep-ph], 2015.

[298] Double Chooz Experiment webpage. http://www.physics.drexel.edu/ wkushner/index.php.

[299] Xinheng Guo et al. A precision measurement of the neutrino mixing angle θ_{13} using reactor antineutrinos at Daya Bay. *ArXiv*, 0701029 [hep-ex], 2007.

[300] F. P. An et al. A side-by-side comparison of Daya Bay antineutrino detectors. *Nucl. Instrum. Meth.*, A685:78–97, 2012.

[301] CERN Courier webpage. http://cerncourier.com/cws/article/cern/31840.

[302] Seon-Hee Seo. New Results from RENO. *Proceedings of the 15th International Workshop on Neutrino Telescopes (Neutel 2013). ArXiv*, 1312.4111, 2014.

[303] A. Suzuki. Results from KamLAND reactor neutrino detection. *Phys. Scripta*, T121:33–38, 2005.

[304] SNO Experiment webpage. http://www.sno.phy.queensu.ca/.

[305] Super-Kamiokande webpage. http://www-sk.icrr.u-tokyo.ac.jp/.

[306] G. Bellini, L. Ludhova, G. Ranucci, and F. L. Villante. Neutrino oscillations. *Adv. High Energy Phys.*, 2014:191960, 2014.

[307] J. V. Allaby et al. A Precise Determination of the Electroweak Mixing Angle from Semileptonic Neutrino Scattering. *Phys. Lett.*, B177:446, 1986.

[308] NuTeV Experiment webpage. http://www-e815.fnal.gov/.

[309] D. Geiregat et al. Calibration and performance of the CHARM-II detector. *Nucl. Instrum. Meth.*, A325:92–108, 1993.